Targeting Kcnn4 for Treatment of Autosomal Dominant Polycystic Kidney Disease

Guanhan Yao

Department of Experimental Medicine
McGill University, Montreal, Canada
May 2023

A thesis submitted to McGill University in partial fulfillment of requirements of the degree of Doctor of Philosophy

ABSTRACT

Autosomal dominant polycystic kidney disease (ADPKD) is the most prevalent genetic kidney disorder caused mainly by mutations in the *PKD1* gene. ADPKD is characterized by progressive bilateral renal cyst formation and enlargement, driven by dysregulated processes such as cAMP-mediated hyperproliferation and excessive fluid secretion, culminating in renal insufficiency by mid-life. The only approved drug treatment for ADPKD, Tolvaptan, is effective but only in a subset of patients. Therefore, additional therapeutic candidates remain to be explored. As cyst growth in ADPKD is largely driven by uncontrolled fluid secretion and proliferation, great effort has been put into identifying potential therapeutic targets within the fluid secretory pathway. The currently accepted model requires active chloride secretion through apical Cftr into cyst lumen. Replenishment of chloride occurs through sustained stimulation of basolateral Nkcc1 which cotransports sodium and potassium. Sodium is likely balanced by Na^+-K^+-ATPase. How potassium is recycled is not completely understood. We speculated that the calcium activated potassium ion channel Kcnn4, a known regulator of proliferation and fluid transport, could be a potential candidate to fulfill this role. We hypothesized that inhibition of Kcnn4 could block potassium recycling and consequently reduce cyst fluid secretion, delaying cyst growth. To evaluate Kcnn4's potential as a therapeutic target for treatment of ADPKD, we targeted Kcnn4 *ex vivo* and *in vivo* using genetic and pharmacologic approaches and assessed key indicators of disease progression such as cystic indices, renal cAMP level and proliferative status. We found that *Kcnn4* expression is consistently upregulated by 2- to 6-fold in four *Pkd1* orthologous mouse models and by ~20-fold in human ADPKD kidneys. *Ex vivo* analysis demonstrated that *Pkd1*$^{-/-}$ metanephroi treated with Kcnn4 activator not only exacerbated cyst growth but even induced cysts in the otherwise non-cystic Pkd1$^{+/+}$ metanephroi. *Pkd1*$^{-/-}$*; Kcnn4*$^{-/-}$

metanephroi showed marked reduction in cyst formation and growth in comparison to *Pkd1*$^{-/-}$. Moreover, a nontoxic Kcnn4 inhibitor substantially suppressed cyst growth and even promoted regression of established *Pkd1*$^{-/-}$ cysts. In parallel to *Kcnn4* upregulation, *in vivo* analysis also revealed 4- to 16-fold elevation in renal cAMP that hyperactivated MAPK/ERK/c-Myc pathway and ciliary elongation. *Kcnn4* genetic inactivation markedly suppressed cyst growth as determined by pronounced reduction or normalization of kidney weight, cyst number and area, cAMP levels, renal epithelial cell proliferation, fibrosis, ciliary length, and MAPK/ERK/c-Myc signaling. Importantly, kidney function and survival were strikingly improved in an adult-onset *Pkd1* model upon *Kcnn4* inactivation. Our drug repurposing trial of a Kcnn4 inhibitor, Senicapoc, revealed significant suppression of global cystic indices consistent with the results of *in vivo Kcnn4* genetic inactivation. Overall, our study uncovered a hyperactive, cAMP-dependent Cftr/Nkcc1/Na^+-K^+-ATPase/Kcnn4 pro-secretory network that, when disrupted by targeting Kcnn4, severely limits disease progression. Our data strongly support Kcnn4 as a major regulator of *Pkd1*-associated cystogenesis through modulation of cyst-driven processes such as fluid secretion, proliferation, and fibrosis. These preclinical findings are highly promising toward repurposing Senicapoc for ADPKD clinical trial.

RÉSUMÉ

La polykystose rénale autosomique dominante (ADPKD) est la maladie rénale génétique la plus répandue, causée principalement par des mutations du gène *PKD1*. L'ADPKD se caractérise par la formation et l'élargissement progressifs de kystes rénaux bilatéraux, processus provoqués par des mécanismes cellulaires dérégulés tels que l'hyperprolifération médiée par l'AMPc et la sécrétion excessive de liquide. La croissance progressive des kystes about à l'insuffisance rénale à l'âge moyen de 50 ans. Le seul traitement médicamenteux approuvé pour l'ADPKD, le Tolvaptan, est efficace seulement chez un sous-ensemble de patients. D'autres candidats thérapeutiques restent donc à explorer. Comme la croissance des kystes dans l'ADPKD est en grande partie due à la sécrétion incontrôlée de liquide et à la prolifération cellulaire, de grands efforts ont été déployés pour identifier des cibles thérapeutiques potentielles dans la voie de sécrétion du liquide. Le modèle actuellement accepté exige une sécrétion active de chlorure par le canal ionique Cftr apical dans lumen du kyste. Le réapprovisionnement intracellulaire en chlorure s'effectue par une stimulation soutenue de la Nkcc1 basolatérale qui co-transporte le sodium et le potassium. Le sodium est probablement équilibré par la Na^+-K^+-ATPase. La façon dont le potassium est recyclé n'est pas complètement comprise. Nous avons supposé que le canal ionique de potassium activé par le calcium Kcnn4, un régulateur connu de la prolifération et du transport des fluides, pourrait être un candidat potentiel pour remplir ce rôle. Nous avons émis l'hypothèse que l'inhibition de Kcnn4 pourrait bloquer le recyclage du potassium et, par conséquent, réduire la sécrétion de liquide dans les kystes, retardant ainsi leur croissance. Pour évaluer le potentiel de Kcnn4 en tant que cible thérapeutique pour le traitement de l'ADPKD, nous avons ciblé Kcnn4 *ex vivo* et *in vivo* en utilisant des approches génétiques et pharmacologiques et nous avons évalué les indicateurs clés de la progression de la maladie tels

que les indices kystiques, le niveau d'AMPc rénale et l'état prolifératif. Nous avons constaté que l'expression de *Kcnn4* est systématiquement augmentée de 2 à 6 fois dans quatre modèles de souris orthologues de *Pkd1* et d'environ 20 fois dans les reins humains atteints d'ADPKD. L'analyse *ex vivo* a démontré que les métanéphroi *Pkd1*$^{-/-}$ traités avec l'activateur Kcnn4 non seulement exacerbaient la croissance des kystes mais induisaient même des kystes dans les métanéphroi Pkd1$^{+/+}$, par ailleurs non kystiques. Les métanéphroi *Pkd1*$^{-/-}$ *; Kcnn4*$^{-/-}$ ont montré une réduction marquée de la formation et de la croissance des kystes par rapport aux métanéphroïdes *Pkd1*$^{-/-}$. De plus, un inhibiteur non toxique de Kcnn4 a considérablement diminué la croissance des kystes et a même favorisé la régression des kystes *Pkd1*$^{-/-}$ établis. Parallèlement à l'augmentation de *Kcnn4*, l'analyse *in vivo* a également révélé une augmentation de 4 à 16 fois de l'AMPc rénale responsable de l'hyperactivation de la voie MAPK/ERK/c-Myc et de l'élongation ciliaire. *In vivo* l'inactivation génétique de *Kcnn4* réduit nettement la croissance des kystes, comme le montre la réduction prononcée ou la normalisation du poids des reins, du nombre et de la surface des kystes, des niveaux d'AMPc, de la prolifération des cellules épithéliales rénales, de la fibrose, de la longueur ciliaire et de la signalisation MAPK/ERK/c-Myc. Il est important de noter que la fonction rénale et la survie ont été améliorées de façon frappante dans un modèle *Pkd1* adulte après l'inactivation de *Kcnn4*. Notre essai de reconversion d'un inhibiteur de Kcnn4, le Senicapoc, a révélé une suppression significative des indices kystiques globaux, en accord avec les résultats de l'inactivation génétique de *Kcnn4 in vivo*. Dans l'ensemble, notre étude a mis en évidence un réseau pro-sécrétoire Cftr/Nkcc1/Na^+-K^+-ATPase/Kcnn4 hyperactif et dépendant de l'AMPc qui, lorsqu'il est perturbé par le ciblage de Kcnn4, limite considérablement la progression de la maladie. Nos données confirment que Kcnn4 est un régulateur majeur de la cystogenèse associée à *Pkd1* par la modulation des

processus induits par les kystes tels que la sécrétion de liquide, la prolifération et la fibrose. Ces résultats précliniques sont très prometteurs pour la réorientation du Senicapoc vers des essais cliniques sur l'ADPKD.

TABLE OF CONTENTS

LIST OF ABBREVIATIONS

AC	adenylyl cyclase
AD	Alzheimer's Disease
ADPKD	autosomal dominant polycystic kidney disease
AE1	anion exchanger type I
AMPK	5'AMP-activated protein kinase
AP-1	Activation Protein-1
AQP2	aquaporin 2
BCA	bicinchoninic acid
BK	large conductance calcium-activated potassium
BSA	bovine serum albumin
BUN	blood urea nitrogen
cAMP	cyclic Adenosine Monophosphate
CDCA	cilia dependent cyst activation
CF	cystic fibrosis
CFTR	cystic fibrosis transmembrane conductance regulator
C-MYC	cellular myelocytomatosis oncogene
CRAC	calcium release-activated calcium
CYP	cytochrome P450
DBA	Dolichos biflorus agglutinin
DCEBIO	dichloro-EBIO
DN	diabetic nephropathy
Dvl	Dishevelled
ECM	extracellular matrix
EGF	epidermal growth factor
eGFR	glomerular filtration rate
EMT	epithelial-mesenchymal transition
ENaC	epithelial sodium channel
ERK	extracellular-regulated kinase
ESRD	end stage renal disease
FFPE	formalin-fixed paraffin-embedded
GAIN	G-protein-coupled receptor Autoproteolysis-inducing domain
GPS	G-protein-coupled receptor proteolytic site
H&E	hematoxylin and eosin
Hh	Hedgehog

HKC	human kidney cortex
hIK1	human intermediate-conductance potassium channel
hPSC	human pluripotent stem cells
IFT	intraflagellar transport
IK	intermediate conductance calcium-activated potassium
Ik-2	Ikaros-2
IP_3	inositol triphosphate
IPA	ingenuity pathway analysis
IPF	idiopathic pulmonary fibrosis
JAK/STAT	Janus Kinase and Signal Transducers of Transcription
Jbn	Jouberin
KBW	kidney weight to body weight ratio
KCNN4 or K_{Ca}	calcium-activated potassium channel
KLF1	krüppel-like factor 1
KLF2	krüppel-like factor 2
K_v	voltage-gated potassium channel
LEL	lycopersicon esculentum lectin
LTL	lotus tetragonolobus lectin
LRR	leucine-rich repeats
M-1	murine wildtype principal
MAPK	mitogen-activated protein kinase
MCP-1	monocyte chemoattractant protein 1
MEK	MAPK kinase
MDCK	Madin-Darby canine kidney
MMPs	matrix metalloproteinases
NAFLD	non-alcoholic fatty liver disease
NDPK-B	nucleoside diphosphate kinase B
NKCC1	Na^+K^+-Cl^- cotransporter
OCT	optimal cutting temperature
PaO_2/FiO_2	arterial-to-inspired oxygen
PBS	phosphate buffered saline
PC1	polycystin-1
PC2	polycystin-2
PDE	phosphodiesterase
PI3P	phosphoinositol-3-phosphate
PKA	protein kinase A

PKD1	polycystic kidney disease 1
PKD2	polycystic kidney disease 2
Ptc1	Patched1
PROPKD	Predicting Renal Outcomes in Polycystic Kidney Disease
REST	Repressor Element 1-Silencing Transcription factor
RVD	regulatory volume decrease
S16	ribosomal protein subunit 16
SAD	transgenic mouse of sickle cell disease
SEM	standard error of the mean
Shh	Sonic Hedgehog
SK	small conductance calcium-activated potassium
Smo	Smoothened
TBS	tris buffered saline
TCF/LEF	T-cell factor/lymphoid enhancer factor
TGFa	transforming growth factor a
TGFb	transforming growth factor beta
TIMPs	tissue inhibitor of metalloproteinases
TKV	total kidney volume
TMEM16A	anoctamin 1
TRP	transient receptor potential
U-AQP2	urinary-AQP2
U-AQP2/Cr	urinary-AQP2 per milligram of urinary creatinine
UHPLC-ESI-MS/MS	ultra-high-performance liquid chromatography-tandem mass spectrometry
UUO	unilateral ureteral obstruction
V2R	vasopressin 2 receptor

LIST OF FIGURES

LIST OF TABLES

ACKNOWLEDGEMENTS

This thesis officially closes my chapter at McGill U and Montreal. With over six years of sweat, pain, determination, and hard work, this day finally arrived. Like all of us living the dream, I could not have survived without the endless love and support of my family and friends in Toronto and Montreal. I am dedicating this work to my loving parents and my late grandparents.

I thank my supervisor Dr. Marie Trudel for this interesting project and for all the critical advice. I thank my committee members Dr. Tomoko Takano, Dr. Reza Sharif, Dr. Nicole Francis, Dr. William Tsang, and our collaborator Dr. Seth L. Alper, for their time and valuable scientific inputs. I am thankful for having had many wonderful colleagues: Josepha-Clara Sedzro, Jennifer Lake, Camila Parrot, Monica Pata, Almira Kurbegovic, Rey Christian Pacis, Marie-Lorna Paul, Kevin Loayza-Vega, Laurence Gingras-Perron, Catherine Wang, William Boudreau, and Svenja Koslowski. I want to thank Dominic Filion for all the help with microscopy and Manon Laprise for teaching me drug administration techniques. I am also grateful for having supportive family and friends during my thesis writing. Your encouragements kept me going.

I am very thankful for having Ashely Chin accompanying me on this ride. You are a great role model and friend, and I am glad to have been a part of yours. The many late nights and weekends we spent working together at IRCM (Institut de recherches cliniques de Montreal) made the work more manageable. There were times when I thought I couldn't see the light at the end of the tunnel, but I am truly blessed to be surrounded by supportive family members and friends who never cease to encourage me, lifting me up from the swamp of darkness. I am grateful for this experience; however difficult it was. I sincerely thank everyone at McGill U and

at IRCM who has helped and supported me to get through those difficult times, especially Leah at McGill U and my friends Ashley, Ying, Svenja and Will, you are the best that has happened to me. I look forward to making new memories with you.

Thank you for reading this. May God bless you. I hope for a better world.

CONTRIBUTION TO ORIGINAL KNOWLEDGE

The research presented in this thesis constitutes original work towards understanding of the implication of KCNN4 in ADPKD progression. By targeting *Kcnn4 ex vivo* and *in vivo*, we demonstrated that the pro-secretive, proliferative, and pro-fibrotic roles of KCNN4 previously identified in other pathophysiological conditions are actively promoting cyst growth in ADPKD. The improvements in ADPKD phenotypes following Kcnn4 genetic inactivation or pharmacologic inhibition suggest KCNN4 to be a potential therapeutic candidate for treatment of ADPKD. The detailed key contributions are the following:

1. This is the first study to investigate the role of Kcnn4 in ADPKD disease progression where both *ex vivo* and *in vivo Pkd1* models are utilized.
2. Our data revealed for the first time that *KCNN4* expression in human ADPKD kidneys and in *Pkd1* mouse kidneys are highly elevated compared to controls.
3. This is the first study to simultaneously analyze the expression of multiple components of the secretory pathway in *Pkd1* mouse kidneys.
4. Results from *Pkd1*$^{-/-}$ metanephroi studies showed that Kcnn4 can modulate cyst initiation and enlargement. For the very first time, we introduced an activator to the *ex vivo* setting, administered an inhibitor to established cysts rather than at the time of cyst induction, and tested combined drug inhibition on *Pkd1*$^{-/-}$ cyst growth.
5. Synergy between Kcnn4 and Cftr is demonstrated in *Pkd1*$^{-/-}$ metanephroi.
6. This is the first study where renal cAMP levels are analyzed in multiple *Pkd1* orthologous mouse models, whereas most *in vivo* studies to date utilize *Pkd* non-orthologous mouse models for this analysis.

7. Our *in vivo* results revealed a positive feedback loop, whereby elevated cAMP leads to upregulation of Kcnn4 mRNA, which in turn promotes upregulation of cAMP. In addition to the conventionally accepted one way relationship where cAMP upregulates Kcnn4, we showed that modulation of Kcnn4 also alters cAMP level.
8. Our *in vivo* results showed that genetically targeting *Kcnn4* delays cyst growth in both early- and adult-onset *Pkd1* mouse models, in part by limiting fluid secretion, proliferation and fibrosis.
9. We uncovered Kcnn4 as a novel modulator of renal primary cilia length *in vivo*.
10. This is the first study where Senicapoc is given to *Pkd1* mouse models for treatment of ADPKD. We compared different means of administration and found the oral route to be most safe and tolerable.

PREFACE TO THE THESIS

In accordance with the guidelines of the Faculty of Graduate and Postdoctoral Studies of McGill University, this thesis is presented in a traditional format consisting of 6 chapters.

Chapter 1 reviews the literature background of ADPKD and KCNN4 that are relevant to this thesis, outlines the link between ADPKD and CFTR, the primary chloride transporter responsible for cyst fluid secretion, and concludes by providing the objective and rationale.

Chapter 2 describes all materials and methods employed for completion of experiments within this thesis.

Chapter 3 summaries all obtained results and is divided into 5 sections:

1- Characterization of Kcnn4-related pathways in 2 orthologous *Pkd1* mouse models.

2- Modulation of Kcnn4 in the embryonic kidney model.

3- Kcnn4 genetic inactivation causes delay in disease progression in 2 *Pkd1* mouse models of different disease onset and severity.

4- Administration of Kcnn4 pharmacologic inhibitor Senicapoc in 4 *Pkd1* mouse models induces an improvement in disease status.

5- Evaluation of combined channel inhibition versus single treatment on *ex vivo* $Pkd1^{-/-}$ cyst growth.

Chapter 4 interprets the results and highlights the major findings.

Chapter 5 is the conclusion and consists of a scheme of how KCNN4 may be implicated in ADPKD.

Chapter 6 lists all references.

The **appendix** lists the licence numbers for permission to use Fig. 2-7.

CONTRIBUTIONS OF AUTHORS

This thesis was written by Guanhan Yao. Guanhan Yao was responsible for all primary analysis of data from experiments that she performed that were included in the figures. She also reviewed and re-analyzed all data from others that have been included in the figures. With the exception of those contributions outlined below, Guanhan Yao was responsible for 100% of all data acquisition, experimentation, analysis, and preparation of figures.

The contribution of others to data used for figures in this thesis are stated below. In those experiments, Guanhan Yao contributed through either sample preparation, experimentation, and/or data analysis.

- Dr. Almira Kurbegovic performed the qPCR experiments for Figures 8A, 8B, 9A, 9B and 10, assisted with image acquisition of cultured embryonic kidneys for Figures 17B, 19B, 42-45 and 47, and performed mouse necropsy for Figures 42-45 and 47.
- Noushine Sadeghi performed the qPCR experiment for Figure 8B and the western blots for Figure 12B.
- Dr. Camila Parrot contributed to the cAMP assays for Figures 11, 24A and 32A, and performed the c-Myc western blot in Figure 12D.
- Simone Terouz at IRCM Histology core performed the Sirius Red IHC experiment for Figure 25.
- Delphine Cotteverte performed the primary cilia experiment for Figure 26.
- Olivier Cote contributed to the primary cilia experiment for Figure 34.
- Guanhan Yao contributed over 70% for Figures 11, 12C, 12D, 20, 24, 31, 32A and 32B.

Finally, Guanhan Yao would also like to acknowledge previous undergraduate students whom she did not meet but who contributed to laying the groundwork for some of these experiments, even though their data does not appear in this thesis.

CHAPTER 1: INTRODUCTION AND LITERATURE REVIEW

1.1 Overview and rationale of the study

Over the last three decades, significant progress has been made towards our understanding of ADPKD pathogenesis, the most prevalent genetic kidney disorder that affects 1 in 500 worldwide. From the initial observation of the secretive nature of excised ADPKD cyst by Ye and Grantham in 1993, to the approval of Tolvaptan in 2018 for treatment of ADPKD by limiting the increase in total kidney volume, there is ongoing effort to elucidate the underlying mechanism driving cyst growth to identify therapeutic targets that would be effective in a larger proportion of patients with fewer adverse effects.

Cyst growth in ADPKD requires sustained epithelial cell proliferation and active fluid secretion, which is largely dependent on apical chloride secretion through CFTR. The currently accepted model of cyst fluid secretion (Fig. 1) describes basolateral NKCC1 as the transporter that replenishes chloride that is depleted by CFTR, while co-transporting sodium and potassium. Sodium could exit the cell through Na^+-K^+-ATPase, which also allows additional potassium to enter the cell. The excess potassium needs to be recycled through a basolateral potassium channel to maintain the electrochemical gradient to favour this pathway. We propose that the calcium-activated potassium channel KCNN4 is well-suited for this role. The implications of KCNN4 in proliferation, fluid transport, and fibrosis, all known processes involved in progression of ADPKD, have been well documented in other pathophysiological contexts. As our lab has previously identified *KCNN4* to be downstream of *MYC*, the *MYC* overexpression that is typical of ADPKD can potentially upregulate *KCNN4* and favour cyst fluid secretion, driving ADPKD cyst growth.

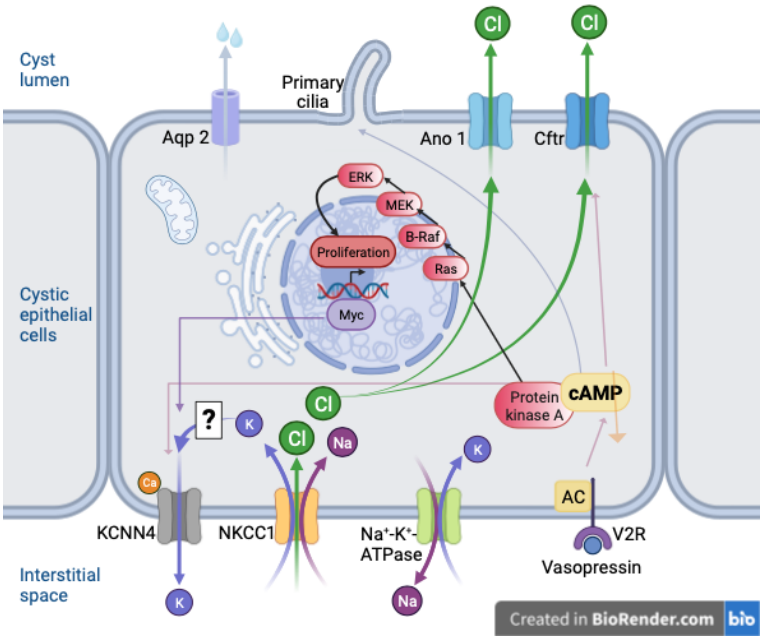

Fig. 1 Schematic representation of cAMP-mediated Kcnn4-relevant cystogenic processes. cAMP drives cyst growth by stimulating proliferation through activation of mitogen-activated protein kinase/extracellular-regulated kinase (MAPK/ERK) signaling and enhancing cyst fluid secretion by activating members of the pathway. Additionally, cAMP has been demonstrated to stimulate primary cilia elongation as well as activating calcium-activated potassium channel KCNN4 *in vitro.* The elevated vasopressin frequently observed in ADPKD binds to vasopressin 2 receptor (V2R) and causes elevated production of cAMP by adenylyl cyclase (AC). Elevation in cAMP causes hyperactivation of MAPK/ERK signaling, increasing c-Myc level and contributing to hyper proliferation that is typical of ADPKD. cAMP also activates members of the secretory pathway such as cystic fibrosis transmembrane conductance regulator (CFTR). Hyperactivated CFTR drives increased chloride secretion. Chloride is replenished by Na^+K^+-Cl^- cotransporter (NKCC1) which cotransports sodium and potassium. Sodium can be recycled by Na^+-K^+-ATPase but at the same time, causes even more accumulation of potassium. We propose that KCNN4 could be a potential candidate to recycle the potassium brought in by NKCC1 and Na^+-K^+-ATPase to maintain ionic balance. There exist apical potassium channels, basolateral chloride channels and basolateral potassium-chloride cotransporters that mediate ion transport, but in the context of cyst fluid secretion in ADPKD, the currently accepted involved components are depicted in this figure. Created with Biorender.com

1.2 Autosomal Dominant Polycystic Kidney Disease (ADPKD)

1.2.1 Human ADPKD

Autosomal dominant polycystic kidney disease (ADPKD) is the most common genetic kidney disorder with an incidence of 1 in 500 (Pei & Watnick, 2010). ADPKD is caused mainly by mutations in the *PKD1* or *PKD2* genes, and accounts for approximately 5% to 10% of

individuals who develop end stage renal disease (ESRD) by age 60 and requiring renal replacement therapy (dialysis or kidney transplantation) (Chebib & Torres, 2016). Individuals affected by ADPKD invariably develop cystic kidneys (Fig. 2) that enlarge with time due to an increase in number and size of fluid-filled cysts, despite the widely varied severity of renal phenotypes and variations in the age of disease onset, even within the same family (Lanktree et al., 2021; Rossetti et al., 2002; Torres et al., 2007). This gradual cystogenesis leads to a progressive loss in kidney function, gross hematuria, frequent urinary tract infections and urolithiasis (Chebib & Torres, 2016). Furthermore, patients frequently develop a spectrum of extrarenal manifestations which, notably consist of extrarenal cysts, particularly in the liver, that may cause further complications such as increased abdominal mass or chronic back pain (Luciano & Dahl, 2014). ADPKD is a fully penetrant disease; individuals who inherit a mutated *PKD* gene will develop renal cysts that can be detected sonographically by age 30 (Igarashi & Somlo, 2002). The molecular mechanisms underlying cystogenesis are continually being studied. Contribution of dysregulated cellular processes, such as uncontrolled fluid secretion, hyper-proliferation, and extracellular matrix remodeling, to ADPKD progression, are well documented (Reif & Wallace, 2019; Wallace, 2011). With only one FDA approved medication, namely the vasopressin 2 receptor antagonist Tolvaptan (Jinarc®), that is effective in only a subset of patients, there remains an urgent need to identify further therapeutic avenues (Muller et al., 2022; Wulfmeyer et al., 2019). A better understanding of ADPKD pathobiology is crucial to achieve this goal.

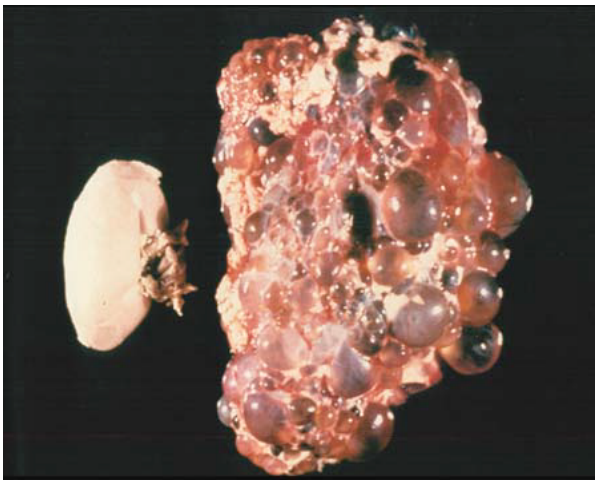

Fig. 2 End stage human autosomal polycystic kidneys are significantly enlarged compared to healthy human kidneys. A healthy kidney is about the size of a human fist (left), while cyst fluid-filled end-stage human ADPKD kidneys can enlarge to the size of a football (right). From *"Ciliary signaling goes down the tubes," Nature Genetics,* permission obtained (Calvet, 2003).

1.2.1.1 Genetics of ADPKD and affected proteins

1.2.1.1.1 *PKD1* and polycystin-1

The *PKD1* gene is on chromosome 16 and is developmentally regulated. The *PKD1* gene is expressed at high levels during embryonic and early kidney development and is lowered and maintained at baseline levels thereafter (Chauvet et al., 2002; Paul & Vanden Heuvel, 2014; Ward et al., 1996). Mutations in *PKD1* are responsible for 75-80% of all ADPKD cases and include truncating (frameshift, splicing, nonsense) and non-truncating (missense, in-frame insertion/deletion) mutations that can be found throughout the gene (Audrezet et al., 2012; Harris, 1999; Igarashi & Somlo, 2002; Schonauer et al., 2020; Torres et al., 2007). The position of *PKD1* mutation was thought to confer onset of ESRD such that mutations in the 5' end associate with more severe and earlier disease onset than mutations in the 3' end (Rossetti et al., 2002). With advancement of mutational analysis, scientists found that it is the type of *PKD1* mutation, and not the position, that correlate with disease severity determined by estimated glomerular filtration rate (eGFR), total kidney volume (TKV), and age of ESRD onset (Cornec-Le Gall et al., 2019; Cornec-Le Gall et al., 2013; Heyer et al., 2016; Hwang et al., 2016). Patients

harboring a truncating mutation generally have more likelihood (~3-fold) to develop ESRD and experience earlier ESRD onset (~12 years) than those with non-truncating mutations (Chebib & Torres, 2016; Cornec-Le Gall et al., 2013). These studies led to the development of a robust prognostic model by Cornec-Le Gall and colleagues, the Predicting Renal Outcomes in Polycystic Kidney Disease (PROPKD) score, that accurately predicts renal outcomes (eGFR decline and ESRD progression) in ADPKD patients based on genetic and clinical data (Cornec-Le Gall et al., 2016; Cornec-Le Gall, Blais, et al., 2018).

PKD1 is a large gene with 46 exons and encodes for polycystin-1 (PC1), an integral membrane protein composed of 4302 amino acids that can be found in many tissues including kidney, liver, pancreas, brain, heart, and bone (Chauvet et al., 2002; Fedeles et al., 2014; Ward et al., 1996). Within the kidney, PC1 is expressed in all nephron segments (Bycroft et al., 1999; Ong et al., 1999; Ward et al., 1996). Subcellularly, PC1 is localized to the apical and/or basolateral plasma membranes, at cell junctions, and in the primary cilia (Fedeles et al., 2014; Geng et al., 1996; Gilder et al., 2018; Yoder et al., 2002). PC1 contains 11 transmembrane segments, a large extracellular amino-terminal domain, and a carboxyl-terminal domain in the cytoplasm (Bycroft et al., 1999; Harris, 1999; Hughes et al., 1995). The extracellular amino-terminal domain consists of a unique array of distinct protein motifs (Fig. 3) including two leucine-rich repeats (LRR) flanked by cysteine-rich domains, a C-type lectin domain, a WSC domain (named after the cell wall integrity and stress component proteins), and 16 immunoglobin-like PKD repeats, many of which are involved in protein-protein or protein-carbohydrate interactions (Babich et al., 2004; Hughes et al., 1995; Maser et al., 2022; Moy et al., 1996; Paul & Vanden Heuvel, 2014; Sandford et al., 1997). Closer to the membrane, post translational cis-autoproteolytic cleavage occurs at the G-protein-coupled receptor proteolytic

site (GPS) within the G-protein-coupled receptor autoproteolysis-inducing domain (GAIN); this cleavage is essential for maturation of PC1 in humans and mice (Kurbegovic et al., 2014; Wei et al., 2007; Yu et al., 2007). The intracellular carboxyl-terminal domain consists of a coiled-coil domain that mediates protein-protein interactions and contains several potential sites of phosphorylation (Bycroft et al., 1999; Cornec-Le Gall et al., 2019).

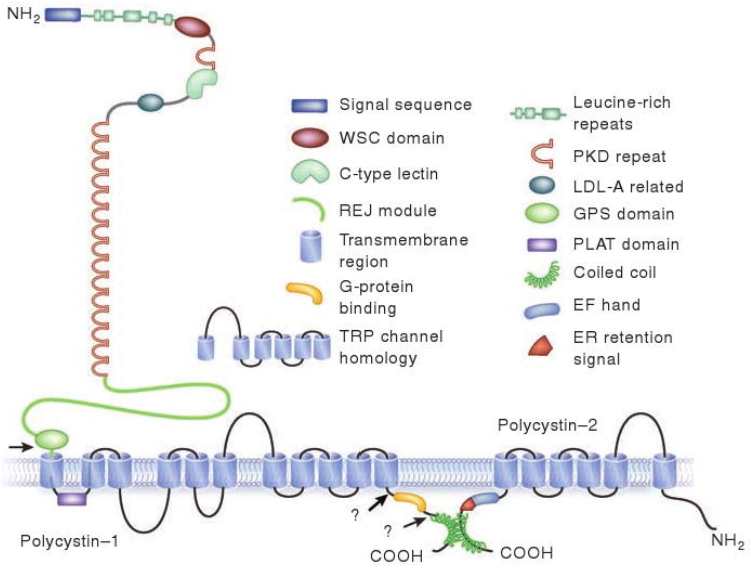

Fig. 3 Schematic representation of structural domains of polycystin-1 and polycystin-2. Polycystin-1 and polycystin-2 are integral membrane proteins that can interact through carboxyl termini. The large extracellular amino terminal domain of polycystin-1 consists of a multitude of protein motifs that facilitate protein-protein and protein-carbohydrate interactions, while polycystin-2 is thought to function as a calcium activated nonselective cation channel. From *"Autosomal dominant polycystic kidney disease: the last 3 years," Kidney International,* permission obtained (Torres & Harris, 2009).

Although the function of PC1 is still under investigation, its structure resembles cell surface receptors such as G-protein coupled receptors (Hama & Park, 2016; Maser et al., 2022; Parnell et al., 1998). This structural similarity and the numerous motifs for protein-protein interactions within PC1 suggest it may function as a receptor and regulate signaling like the G protein coupled receptors (Maser & Calvet, 2020). In fact, the cytoplasmic carboxyl-terminal domain of PC1 can directly bind to heterotrimeric G proteins and to RGS7, the regulator of G

protein signaling (Hama & Park, 2016; Kim, Arnould, Sellin, Benzing, Comella, et al., 1999; Parnell et al., 1998). This coupling allows activation of intracellular signaling pathways such as Wnt via stabilization of b-catenin and activation of TCF/LEF transcription factors (Kim, Arnould, Sellin, Benzing, Fan, et al., 1999; Nichols et al., 2013). Interestingly, one of the downstream targets of this pathway is the *PKD1* gene itself (Rodova et al., 2002). This proposed pathway not only positively regulates *PKD1* gene transcription, but more importantly in the context of ADPKD, the G protein signaling pathway can regulate processes that drive cyst formation including fluid secretion, proliferation, cell polarity and differentiation (Arnould et al., 1998; Grantham, 2001; Maser et al., 2022; Parnell et al., 2002).

The structure of PC1 also resembles a family of cell surface receptors (sea urchin sperm receptor for egg jelly) that are involved in the acrosome reaction, an essential step in fertilization that requires ligand binding for activation, further supporting PC1 may function as a cell surface receptor (Darszon et al., 2020; Gunaratne et al., 2007; Mengerink et al., 2002; Moy et al., 1996). Numerous motifs are conserved, including lectin C-type domain, GPS domain and PKD repeats, suggesting similar signaling pathways may be shared (Gunaratne et al., 2007; Hughes et al., 1999; Mengerink et al., 2002; Moy et al., 1996).

1.2.1.1.2 *PKD2* and polycystin-2

The *PKD2* gene is on chromosome 4 and its expression is more constant during development than *PKD1* (Chauvet et al., 2002; Paul & Vanden Heuvel, 2014). Mutations in *PKD2* are responsible for 10-15% of ADPKD cases (Chang et al., 2006; Cornec-Le Gall et al., 2019; Schonauer et al., 2020). *PKD2* mutations lead to similar renal and extrarenal manifestations as *PKD1* mutations, suggesting both genes affect common regulatory pathways in the kidneys (Harris & Hopp, 2013; Igarashi & Somlo, 2002; Koptides et al., 2000; Nobakht et

al., 2020). However, *PKD2*-induced ADPKD is generally milder with a slower progression to ESRD than in patients presenting with *PKD1* mutations: *PKD2* patients survive approximately 20 years longer than *PKD1* patients and experience later onset of ESRD (median age 79.7 versus 58.1 years) with fewer complications (Chebib & Torres, 2016; Cornec-Le Gall et al., 2013; Igarashi & Somlo, 2002). Like *PKD1* mutations, *PKD2* mutations have been identified throughout the gene, vast majority being truncating mutations (Audrezet et al., 2016; Kataoka et al., 2020). Additionally, trans-heterozygous mutations have been documented in a minority of patients in which individuals carrying a germline mutation of *PKD1* and *PKD2* acquire more severe phenotypes with faster progression than in patients affected by either mutation alone (Elisakova et al., 2018; Koptides et al., 2000; Losekoot et al., 2020; Pei et al., 2012; Pei et al., 2001; Watnick et al., 2000). This is also demonstrated in mouse studies in which trans-heterozygous mutations ($Pkd1^{+/-}$; $Pkd2^{+/-}$) led to noticeably greater cyst formation than simple additive effect of $Pkd1^{+/-}$ and $Pkd2^{+/-}$, whereas homozygous mutations ($Pkd1^{-/-}$ or $Pkd2^{-/-}$) causes embryonic lethality (Wu et al., 2002). Understandably, no humans with homozygous germline mutations of either *PKD1* or *PKD2* have been documented.

PKD2 encodes for polycystin-2 (PC2) which is composed of 968 amino acids and is also predicted to be an integral membrane protein like PC1 (Mochizuki et al., 1996; Yang & Ehrlich, 2016). Tissue distribution largely overlaps with, but is not identical to, PC1 expression. PC2 is primarily found in the kidney, heart, ovary, testis, vascular smooth muscle, and small intestine. Subcellularly, PC2 is mainly localize to the endoplasmic reticulum, and is also found at the plasma membrane and in primary cilia, where interactions with PC1 may occur (Cai et al., 1999; Chauvet et al., 2002; Cornec-Le Gall et al., 2019). Within the kidney, PC2 is expressed in all nephron segments apart from the thin limbs and glomeruli (Chauvet et al., 2002). Structurally,

PC2 consists of six transmembrane segments with intracellular amino- and carboxyl-terminal domains that can homotetramerize or heteromerize with PC1 in a 3:1 ratio through coiled-coil domains of both proteins (Grieben et al., 2017; Shen et al., 2016; Su et al., 2018; Wilkes et al., 2017; Yu et al., 2009). Additionally, PC2 shares structural features with transient receptor potential (TRP) channels as well as voltage-activated calcium and sodium channels, hence the alternate name TRPP2, suggesting PC2 may function as a calcium activated nonselective cation channel (Grieben et al., 2017; Koulen et al., 2002; Wilkes et al., 2017). Indeed, PC1 and PC2 can interact at the primary cilium where they are proposed to function as a calcium permeable receptor channel complex (Ha et al., 2020; Hanaoka et al., 2000; Lee & Somlo, 2014; Liu et al., 2018; Yoder et al., 2002).

1.2.1.2 Pathophysiology of ADPKD

1.2.1.2.1 Renal pathophysiology in ADPKD

ADPKD patients suffer from both renal and extrarenal complications (Cornec-Le Gall et al., 2019; Luciano & Dahl, 2014; Romao et al., 2006). Initiation of renal cysts was first described by P. P. Lambert in the 1940s as focal dilation of nephron tubules, and as cysts increase in number and size with disease progression, they pinch off from their parent tubule and become isolated structures (Calvet, 2015; Lambert, 1947; Paul & Vanden Heuvel, 2014). At this point, without parental contribution, cysts require trans-epithelial fluid secretion to enlarge (Choudhury et al., 2022; Grantham et al., 1987; Sullivan et al., 1998; Terryn et al., 2011). While renal cysts may originate from all segments of the nephron, the largest and most numerous cysts are consistently found within the collecting duct in patients and mouse models of ADPKD (Buchholz et al., 2011; Grantham et al., 1987; Happe et al., 2013; Muto et al., 2022; Paul & Vanden Heuvel, 2014; Raphael et al., 2009; Verani & Silva, 1988). Although all cells of the

nephron carry the same germline mutation, microdissection of young adult ADPKD kidneys or ultrasonography of children who inherited mutated *PKD1* gene demonstrated that only a few cysts arise per nephron, in fact, most nephrons appear completely normal (Baert, 1978; Fick et al., 1994; Gabow et al., 1997). To explain the focal nature of cyst formation, a "two-hit" model of cystogenesis has been proposed where a mutated *PKD1* or *PKD2* gene is inherited from one parent with ADPKD, and a normal gene is inherited from the unaffected parent. During the lifetime of the individual, a small proportion of the inherited normal allele undergoes somatic mutations in isolated renal epithelial cells, consequently leading to complete loss of *PKD1* or *PKD2* function in those cells, initiating cyst formation (Pei, 2001; Qian et al., 1996; Watnick et al., 1998). While disease inheritance is dominant, cysts occur by a recessive mechanism in this model. Indeed, somatic mutations haven been described in cells lining the cysts in both kidney and liver (Koptides et al., 1999; Pei et al., 1999; Watnick et al., 1998). Interestingly, the human kidney epithelial cells have inherent higher rate of somatic mutagenesis than other cells that increase exponentially with age (Colgin et al., 2002; Martin et al., 1996). This may in part explain how the discrete "second-hit" that initiates cystogenesis can lead to the numerous cysts observed in polycystic kidneys. Although the two-hit model is attractive, it requires both alleles to be inactivated to induce cyst formation. However, Pkd1 hypomorph murine models of ADPKD showed that cysts can develop even in presence of low PC1 levels which gave rise to an alternative hypothesis for cyst formation: haploinsufficiency may be sufficient to induce cystic phenotypes (Bastos et al., 2009; Hopp et al., 2012; Lantinga-van Leeuwen et al., 2007; Ong & Harris, 2015). It is suggested that a reduction in the levels of functional polycystins below a certain cystogenic threshold is sufficient to initiate both renal and extrarenal ADPKD phenotypes, and varies by mutation type, developmental stage and local stochastic factors

(Cornec-Le Gall, Torres, et al., 2018; Hopp et al., 2012; Lanktree et al., 2021; Lantinga-van Leeuwen et al., 2004; Qian et al., 1996; Takakura et al., 2009; Tan et al., 2018). Studies in transgenic animals suggest that the dosage model may be more precise in predicting cystogenesis as overexpression of *PKD1* or *Pkd1* induces renal and extrarenal ADPKD phenotypes, possibly in part due to the disruption of the stoichiometry of the polycystin complex that alters signaling function (Kurbegovic et al., 2010; Pritchard et al., 2000; Thivierge et al., 2006). Together these mechanisms may explain the observed persistent PC1 protein expression in a majority of cysts (Ong et al., 1999), as well as the detection of loss of heterozygosity in end-stage cystic tissues (Ong & Harris, 1997).

1.2.1.2.2 Extra-renal manifestations in ADPKD

Since the genes responsible for ADPKD are widely expressed in different tissues, extrarenal anomalies can be found in many tissues, such as the liver, ovaries, and choroid plexus, the most prevalent being polycystic liver (Cornec-Le Gall et al., 2019; Luciano & Dahl, 2014; Pirson, 2010; Romao et al., 2006; Watnick et al., 1998). Liver cysts originate from bile ducts and can contributes to hepatomegaly that is commonly observed among patients but generally do not disrupt normal liver function (Fedeles et al., 2014; Hogan et al., 2015; Judge et al., 2017). Other notable extrarenal manifestations include cerebral and coronary aneurysms, cardiac valvular abnormalities, and hypertension (Chapman et al., 2010; Ecder & Schrier, 2009; Flahault et al., 2018; Hadimeri et al., 1998).

1.2.2 Murine models of ADPKD

Initial murine studies were carried out in non-orthologous models of PKD and have contributed to the understanding of the fundamental driving forces behind cyst growth. Models based on the orthologous mouse genes *Pkd1* and *Pkd2* were later developed and further

contributed to our understanding of *in vivo* mechanisms of autosomal dominant and recessive forms of PKD. Those models are also frequently employed for the preclinical evaluation of new therapeutic strategies for ADPKD. From these diverse mouse models, we have notably learned that *Pkd1* dosage, as well as the timing of *Pkd1* inactivation, are important determinants of the severity and progression of cystic phenotypes.

1.2.2.1 Genetics and affected proteins learned from murine studies

1.2.2.1.1 *Pkd1* and polycystin-1

Unlike human ADPKD, heterozygous mutation of *Pkd1* or *Pkd2* is insufficient to trigger cyst formation in mouse models and requires a "second-hit" somatic mutation to initiate cystogenesis (Lantinga-van Leeuwen et al., 2004; Piontek et al., 2004; Wu et al., 1998; Wu et al., 2002). An elegant murine model that has allowed to validate this hypothesis is the $Pkd2^{WS25/-}$ mouse that carries an unstable *Pkd2* allele, in which somatic loss of *Pkd2* was required to trigger cystogenesis (Wu et al., 1998). Later studies revealed that the level of functional PC1 level can determine disease severity as defined by onset and degree of renal and extrarenal anomalies (Hopp et al., 2012; Kurbegovic et al., 2010; Lantinga-van Leeuwen et al., 2004; Lantinga-van Leeuwen et al., 2007; Thivierge et al., 2006; Wu et al., 2002; Yu et al., 2007). Homozygous or conditional *Pkd1* knockout mouse models generally present a rapidly progressive and severely cystic disease phenotype that range from embryonic lethality in homozygous *Pkd1* null mutants that also display pancreatic cysts which only appear at a relatively low frequency of 5% in human ADPKD, to lifespan of few weeks in conditional knockouts which is not reflective of the gradual kidney enlargement typical of ADPKD (Lanktree et al., 2021; Torres et al., 2007; Wu et al., 2002). In contrast, transgenic mice with overexpression of *Pkd1* experience a much milder disease and only develop cysts in adulthood (Kurbegovic et al., 2010; Thivierge et al., 2006).

More specifically, data suggest that cyst severity can be explained by a gene dosage effect where the cystic phenotype is more severe when the level of functional PC1 falls below the cystogenic threshold around 20-30%: a reduction to 40% of functional PC1 leads to a slow progressive disease, while a reduction to only 20% causes rapid disease progression (Hogan et al., 2009; Hopp et al., 2012; Lanktree et al., 2021; Ong & Harris, 2015). The more severe cystic phenotype in mice with trans-heterozygous *Pkd* gene mutations than additive effect of heterozygous *Pkd* mutations also support a gene dosage effect in determining disease severity (Wu et al., 2002).

Apart from germline and somatic mutations, additional factors can modulate cyst progression, namely developmental timing of *Pkd* gene inactivation (Lantinga-van Leeuwen et al., 2007; Piontek et al., 2007) and occurrence of acute kidney injury (Bastos et al., 2009; Takakura et al., 2009). Indeed, several studies suggested that kidney injury can serve as a "third hit" and as such exacerbate disease progression (Takakura et al., 2009; Torres et al., 2019). Importantly, mouse studies identified a critical developmental switch around Postnatal day 13 (P13) that determines disease onset and severity, around the time when major transcriptional changes in mouse kidneys occur (P12-P16), during which genes involved in mature renal function are induced and developmental genes are downregulated (Piontek et al., 2007; Sharma et al., 2013). Inactivation of *Pkd1* before P13 causes cysts to develop in just a few days and disease to rapidly progress to end stage, whereas later loss of *Pkd1* (after P13) results in later disease onset and a slow progressive disease (Piontek et al., 2007). The difference in disease progressivity is due in part by proliferative potential of the kidney at early versus later stages of development, but increased proliferation alone is insufficient to induce cysts in adult mouse models, adding complexity to the understanding of cystogenesis (Sharma et al., 2013).

1.2.2.1.2 Pkd2 and polycystin-2

Like *Pkd1* mouse models, *Pkd2* heterozygous mice present a very variable and mild disease phenotype, often developing cysts only near the end of life in contrast to the embryonic lethal *Pkd2* homozygous mice (Happe & Peters, 2014; Wu et al., 1998). Recently, reversal of ADPKD phenotypes was demonstrated in an inducible *Pkd2* knockout mouse model upon re-expression of *Pkd2* (Dong et al., 2021). Results from this study indicate that the kidney has an unexpected capacity for plasticity under the control of polycystins; indeed, renal cysts lined by flattened epithelial cells remarkably reverted to normal appearing nephrons with a columnar epithelium upon *Pkd2* re-expression, accompanied by complete or partial normalization of kidney size, proliferation, inflammation, and fibrosis (Dong et al., 2021). Interestingly, this reversal has a faster time course than cyst growth after loss of polycystin: cystic phenotypes usually take weeks or months to develop *in vivo* but cyst reversal only required days or weeks (Dong et al., 2021). In addition, in line with the developmental switch described in the previous section, the degree of resolution varies depending on the stage of underlying disease severity at which *Pkd2* is re-expressed: re-expression at early stage causes rapid phenotypic reversal within 1 week following re-expression, whereas at more advanced disease stages, fibrosis and inflammation are no longer fully reparable although kidney cysts are still completely reversed (Dong et al., 2021). These findings support polycystin's involvement in active maintenance and dynamic regulation of the 3D structural organization of the kidney, and the authors further suggest that therapies aimed at disease repair could be equally or even more efficient than therapies aiming to slow down disease progression if the *in vivo* observations can be fully translated to humans (Dong et al., 2021). The same experiment was conducted in a *Pkd1* mouse model, and the same outcome was documented (Dong et al., 2021).

1.2.2.2 Mouse models used to study PKD

Our understanding of the molecular mechanism underlying cystogenesis relies largely on rodent genetic models of PKD, with initial ones arising from spontaneous mutations and others by random mutagenesis, transgenic technologies, or gene-specific targeting (Gretz et al., 1996; Hopp et al., 2012; Kaspareit-Rittinghausen et al., 1990; Kurbegovic et al., 2010; Lager et al., 2001; Lantinga-van Leeuwen et al., 2007; Nauta et al., 1993; Piontek et al., 2004; Preminger et al., 1982; Schafer et al., 1994; Sommardahl et al., 1997; Takahashi et al., 1991; Thivierge et al., 2006; Thomson et al., 2003; Yamaguchi et al., 1997). These orthologous and non-orthologous models of autosomal dominant and recessive forms of PKD allow the elucidation of pathogenic mechanisms underlying cystogenesis and testing of potential therapies, and more importantly, they overcome the limited usage of heterozygous and homozygous mutants as neither are very suitable to study PKD due to extreme disease progressions (Ahrabi et al., 2007; Wu et al., 2002). In general, the rapidly progressive models are useful to observe an immediate effect of, for example, the administration of new therapeutic molecules due to the shorter time course, while slow progressive models may resemble more of the disease progression in human patients, thus allowing us to evaluate the long-term effect of treatments.

1.2.2.2.1 *Pkd* non-orthologous models

Initially characterized *Pkd* non-orthologous models arise from spontaneous mutations that predispose to PKD, some of which laid the foundation for transition of preclinical Tolvaptan application to clinical use. The *Pkd* non-orthologous models will be described below in chronological order.

The first *Pkd* mouse model *cpk/cpk* was described in 1982 and is a congenital mutant inherited in an autosomal recessive manner that closely resembles human infantile polycystic kidney disease (ARPKD) in inheritance, clinical course and kidney morphology (Preminger et

al., 1982). *Cpk* mice appear normal at birth, however, abdominal enlargement is apparent by P10-13 due to cystic kidneys that initiate in the proximal tubule followed by collecting duct, and die by 3 weeks of age due to renal failure as evidenced by significantly elevated blood urea nitrogen and serum creatinine levels (Gattone et al., 1999; Preminger et al., 1982).

The *jck* (juvenile cystic kidneys) mouse is another model for the recessive form of PKD that develops polycystic kidneys initiating from the proximal tubules with no extrarenal abnormalities (Atala et al., 1993). Renal cysts are evident as early as P3 but disease progression is intermediate with lifespan of approximately 4 months, onset of overt disease does not occur until 4-5 weeks of age and serum creatinine levels increase linearly with disease progression and age (Atala et al., 1993; Liu et al., 2002).

The *cpk* and *jck* mouse models show many renal clinical features of human ARPKD, but do not display the characteristic liver phenotypes, a more relevant model is the *bpk* (*BALB/c* polycystic kidneys) mouse that shows dual renal cyst growth and biliary epithelial hyperplasia (Nauta et al., 1993). *Bpk* mice appear clinically normal at birth with tubular dilations that initiate in proximal tubules and later shifts to collecting duct (Cogswell et al., 2003; Nauta et al., 1993). Progressive enlargement of renal cysts causes massive abdominal distension detectable by 2 weeks of age, and homozygous mutants die by 1 month of age due to renal failure (Cogswell et al., 2003; Nauta et al., 1993).

The *Han:SPRD-cy* rat is another model derived from a spontaneous mutation in the Sprague-Dawley strain inherited in an autosomal dominant pattern, where homozygous and heterozygous *Han:SPRD* mutants reveal striking differences in the severity of cystic disease (Kaspareit-Rittinghausen et al., 1990). Heterozygous mutants develop slow progressive uremia and survive for 1-2 years, while homozygous mutants display a rapidly progressive disease

(Gretz et al., 1996; Nagao et al., 2010). Kidney cysts in the heterozygous mutant predominantly involve proximal tubules and later shifts to all segments of the nephron, whereas extrarenal manifestations (liver and pancreatic cysts) only develop in very old females (Kranzlin et al., 1997; Schafer et al., 1994). In contrast, kidney cysts in homozygous mutants share the same pattern of kidney cyst origin as heterozygotes and are evident shortly after birth, rapidly enlarging kidneys, hindering survival to only three weeks due to severe uremia (Bihoreau et al., 1997; Brown et al., 2005; Cowley et al., 1993; Schafer et al., 1994). More importantly, this model supports the gene dosage effect in determining cystic phenotype.

Pcy (*DBA/2-pcy/pcy*) is a spontaneous occurrence of a recessively inherited PKD in the KK mouse strain (a model of diabetes mellitus) that progresses slowly and resembles human ADPKD (Takahashi et al., 1991). Like humans, cystic changes in kidneys begin *in utero* but are not evident until 8 weeks of age and progress over the lifetime of the animal (~30 weeks) with low incidence of intracranial aneurysms, uremia being the primary cause of death (Olbrich et al., 2003; Takahashi et al., 1991). Tubule dilations initiate from distal tubules and collecting ducts in newborns and later extend to all nephron segments with disease progression; by eight weeks of age cysts are found throughout the kidneys (Wallace et al., 2008).

The documentation of *c-Myc* overexpression in human ADPKD tissues led to the generation of the *SBM* mouse, a transgenic model with renal *c-Myc* overexpression that is sustained into adulthood when it normally should be undetectable (D'Agati & Trudel, 1992; Trudel et al., 1998; Trudel et al., 1991). Kidney cysts develop as early as E16.5 in the collecting duct and gradually progress over the lifetime (several months) into proximal tubules with no extrarenal abnormalities (Couillard et al., 2002; Couillard & Trudel, 2009; D'Agati & Trudel,

1992; Parrot et al., 2019; Trudel, 2015; Trudel et al., 1998; Trudel et al., 1994; Trudel et al., 1991; Trudel et al., 1997).

The *Orpk* mouse mutant is generated by an insertion mutation in a line of mouse at the Oak Ridge National Laboratory, formally known as *TgN737Rpw,* develops kidney cysts and biliary hyperplasia that are histologically identical to autosomal recessive form of human PKD (Moyer et al., 1994). Cysts initiate as mild dilations in the proximal tubules in newborns, which then extends to marked dilations and cyst formation in the collecting duct detectable by P7 (Guay-Woodford, 2003; Lehman et al., 2008; Sommardahl et al., 1997). These phenotypes are only observed among homozygotes, as heterozygotes are indistinguishable from wildtype (Sommardahl et al., 1997).

Finally, the *PCK* rat is a spontaneous occurring model in the rat strain *Crj:CD/SD* inherited in an autosomal recessive pattern and displays mild renal and hepatic histological abnormalities resembling human PKD that progresses slowly and only show slight elevations of blood urea nitrogen levels by 6 months of age (Lager et al., 2001). Like observed in many of the previously described models, kidneys appear normal at birth and cysts are detectable by P21, but unlike other models where cysts initiate from proximal tubules, cysts in *PCK* rats are mainly found in the distal tubules and collecting ducts (Lager et al., 2001; Masyuk et al., 2007; Wang et al., 2005). Interestingly, mild bile duct dilations precede kidney dilations, detectable as early as P1 and progressively become more prominent with age (Lager et al., 2001). The presence of both kidney and liver cysts makes the *PCK* rat a more pertinent model for studying ADPKD.

1.2.2.2.2 *Pkd1* orthologous models

The homozygous *Pkd1* mutant mouse model was generated by insertion of a neomycin cassette into exon 1 of *Pkd1*, producing no detectable transcript, and causes kidney cysts to

initiate early *in utero* at E15.5, preceded by pancreatic cysts that initiate at E14.5 (Wu et al., 2002). Kidney cysts are primarily found in proximal tubules and glomeruli which progress at an extremely rapid pace, causing embryonic lethality from mid-gestation at E12.5 (Wu et al., 2002). Viable *Pkd1*$^{-/-}$ embryos are rare after E16.5 but may survive until birth, only to die in the immediate perinatal period due to cardiovascular or placental failure but not as a direct consequence of the severely cystic kidneys (Magenheimer et al., 2006). Although this model does thus not permit *in vivo* studies, the embryonic kidneys are useful for *ex vivo* rapid testing of therapeutic targets. Since then, in the last two decades, numerous *Pkd1* orthologous mouse models have been generated and widely used to facilitate our understanding of *Pkd1*-induced cystogenesis. We describe below some of the most widely used models.

The *KspCre; Pkd1*$^{flox/flox}$ mouse is a conditional renal *Pkd1* knockout model whose *Pkd1* exons 2-4 are deleted exclusively in the kidneys mediated by *KspCre* recombinase (Piontek et al., 2004; Shao et al., 2002). At birth animals appear normal, cysts development becomes apparent after birth in the distal tubules and collecting ducts, in line with the expression pattern of *KspCre*, and can live for about 3 weeks (Piontek et al., 2004; Shibazaki et al., 2008).

As cysts mainly originate from the principal cells of the collecting duct, principal cell- and intercalated cell- specific *Pkd1* knockout mouse models were produced and compared to reveal cell type specific roles in the pathogenesis of renal cyst formation (Raphael et al., 2009; Torres et al., 2007). The principal cell specific *Pkd1* knockouts are generated by homologous recombination with principal cell specific *Cre* recombinase under the control of the *AQP2* promoter, deleting exons 2-4 selectively in principal cells (Raphael et al., 2009). Renal cysts are evident by one week of age in the collecting ducts, as principal cells are localized there, and can survive on average for 8 weeks (Raphael et al., 2009). In contrast, the intercalated cell specific

Pkd1 knockout model presents a much milder disease where only 1-2 cysts are found per kidney by 13 weeks of age and is generated using the *B1-Cre* mice expressing *Cre* selectively in intercalated cells (Raphael et al., 2009). With a lifespan of over 1.5 years, they are indistinguishable from wildtype mice; renal function remains unaffected throughout their life (Raphael et al., 2009). Together these two models show that principal cells are the major cell type leading to cyst formation in the collecting duct, while intercalated cells may not play a significant role in the pathogenesis of renal cyst formation.

The $Pkd1^{v/v}$ model presents a knock-in mutation in the murine endogenous *Pkd1* gene that prevents cleavage of PC1 at its GPS site, prohibiting correct intracellular trafficking of the protein (Kurbegovic et al., 2014; Woodward et al., 2010; Yu et al., 2007). Kidney cysts initiate after birth around P4 and animals are viable for about one month, presenting severe kidney as well as liver cysts at end stage (Yu et al., 2007). Kidney cysts primarily originate from distal tubules and collecting ducts, with the majority formed in the latter, whereas dilations in the liver are found in the common bile duct and intrahepatic biliary duct (Yu et al., 2007).

The $Pkd1^{RC/RC}$ knock-in mouse model matches the human disease variant *PKD1 p.R3277C*, which induces a temperature-sensitive folding/trafficking mutant (Arroyo et al., 2021; Hopp et al., 2012; Zhang et al., 2020). This model is functionally hypomorphic and contains about 40% of functional PC1, causing gradual cyst development in kidney and liver over the lifespan of one year (Hopp et al., 2012; Zhang et al., 2020). Like most models, kidney cysts initiate in the proximal tubules and are later predominantly found in the collecting ducts as the disease progresses (Hopp et al., 2012; Zhang et al., 2020).

The tamoxifen-inducible *tam-KspCad-*$CreR^{T2}$ *(Cre)* mouse is generated by tamoxifen administration induced renal deletion of exons 2-11 of *Pkd1* that causes cystic kidneys without

extrarenal manifestations and is particularly useful as the timing of *Pkd1* inactivation can be tightly controlled (Lantinga-van Leeuwen et al., 2006; Lantinga-van Leeuwen et al., 2007). Importantly, the time of tamoxifen induction determines disease phenotype: induction between 3-6 months causes mild cystic kidneys months later and cysts can be found in all nephron segments, whereas induction at P4 leads to more immediate effect (two weeks) and causes severe cysts that mainly arise from the distal tubules and collecting ducts (Lantinga-van Leeuwen et al., 2007). The differential response to tamoxifen induction suggests that the proliferative status of the renal epithelium at the time of *Pkd1* inactivation may influence PKD progression, in line with the developmental switch described by Piontek *et al.* in the same year, using a comparable inducible *Pkd1* knockout model (Piontek et al., 2007).

Finally, our lab has previously generated two *Pkd1* transgenic mouse models, one of which is the *SBPkd1*$_{TAG}$ (*^{SB}Pkd1)* model that expresses 2- to 15-fold *Pkd1* over endogenous levels in the kidney and is produced by homologous recombination using a modified *Pkd1* bacterial artificial chromosome (*Pkd1*-BAC) to target sustained overexpressed *Pkd1* transgene in the kidneys (Thivierge et al., 2006). Kidney specificity was achieved by insertion of the renal epithelial specific regulatory elements directly upstream of *Pkd1* start codon within the *Pkd1*-BAC, resulting in progressive cyst development in the kidneys over several months of lifespan in all nephron segments, and mice died of renal failure by mid-age (Thivierge et al., 2006). The second model *Pkd1*$_{TAG}$ *(Pkd1*^{wt}*)* was also produced using a *Pkd1*-BAC and overexpresses 2- to 15-fold *Pkd1* over endogenous *Pkd1* in renal and extrarenal tissues (Kurbegovic et al., 2010). In this model, the *Pkd1*-BAC was modified by insertion of a silent mutation to target sustained wildtype *Pkd1* expression within the native tissue, similarly causing kidney cyst development in all nephron segments, as well as extrarenal phenotypes such as liver cysts and cardiac anomalies

that resembled human ADPKD (Kurbegovic et al., 2010). These transgenic models demonstrate that overexpression of wildtype *Pkd1* is sufficient to trigger cystogenesis.

1.2.2.2.3 *Pkd2* orthologous models

The $Pkd2^{WS25/-}$ mouse model carries an unstable *Pkd2* allele that is prone to genomic rearrangement: the *WS* allele itself produces wildtype PC2 protein but during its somatic life spontaneously can rearrange to produce either a null or a wildtype allele (Wu et al., 1998). This model develops kidney cysts within three months of age.

1.2.3 Other model systems to study PKD cyst growth

Apart from murine models of PKD, other model systems are available and still widely used today, many of which provided our initial understanding of the secretive and proliferative nature of ADPKD cysts.

1.2.3.1 Madin-Darby canine kidney cells

The Madin-Darby canine kidney (MDCK) cell line is frequently used in ADPKD studies and is known for its fluid accumulation and cell proliferation properties (Cabrita, Buchholz, et al., 2020; Gattone & Grantham, 1991; Grantham et al., 1995; Ikeda et al., 2006; Mangoo-Karim et al., 1989; Tamma et al., 2017; Taub et al., 1979; Verghese et al., 2011; Yang et al., 2008; Yuajit et al., 2013; Yuajit et al., 2014). MDCK cells can be cultured as cell monolayers or dispersed within or on medium-hydrated collagen gel, where stimulation by cAMP allows individual cells to form spherical cysts with a simple epithelium surrounding a fluid-filled lumen, which then multiply by clonal growth (McAteer et al., 1987; Torres, 2004). These cells resemble tubule epithelial cells found in the distal nephron and possess characteristic structures of renal tubular cells, such as apical microvilli, solitary cilia, and apical tight junctions (Arthur, 2000; McAteer et al., 1987). The Diameter of MDCK cysts increases under the influence of cAMP due

to stimulation of cell proliferation and fluid secretion, hence allowing for assessment of inhibitors targeting these two processes (Grantham et al., 1987; McAteer et al., 1987). Due to their polarized nature and the ease to culture, MDCK is still widely used today in ADPKD research.

1.2.3.2 Primary cultures derived from isolated ADPKD cysts

Excised cysts from end stage ADPKD patients and cyst-derived cell monolayers are invaluable tools used initially in transepithelial fluid transport studies and are continually being used to understand the pathogenesis of ADPKD (Desrochers et al., 2014; Dixon & Woodward, 2018; Grantham et al., 1995; Lebeau et al., 2002; Sullivan et al., 1998; Weydert et al., 2019; Yamaguchi et al., 2003; Ye & Grantham, 1993). Individual cysts can range from 5g to 58g. By aspirating cyst fluid from the cyst lumen and replacing with a smaller amount of medium, Grantham *et al.* found that cysts are capable of secreting and accumulating fluid within the cyst lumen at a very low rate, which could be stimulated by over 4-fold by forskolin, a cAMP activator (Grantham et al., 1995). Cell monolayers derived from excised ADPKD cysts are frequently analyzed alongside human kidney cortex (HKC) cells for their ability to form microcysts (Belibi et al., 2002; Sullivan et al., 1998; Wang et al., 2006; Yamaguchi et al., 2003; Ye et al., 1992). Like MDCK cells, HKC cells primarily derive from the distal nephron and microcysts retain the same polarity as that of MDCK cysts, but forskolin does not induce microcysts in HKC cells in the absence of epidermal growth factor (EGF) or transforming growth factor α (TGFα). Either EGF or TGFα is sufficient to induce microcyst formation and growth in HKC cells (Du & Wilson, 1995; Yamaguchi et al., 2003; Zheleznova et al., 2011). In contrast, primary cultures of ADPKD cysts do not develop cyst with growth factor alone and require forskolin stimulation (Sullivan et al., 1998; Yamaguchi et al., 2003; Ye et al., 1992). The

response of above-mentioned cell lines to cAMP clearly supports cAMP's involvement in cell proliferation and cystic fluid.

1.2.3.3 Mouse embryonic kidney

Metanephroi give rise to the permanent kidney that can be isolated from their host and have become widely used in research in the last two decades as they provide a unique environment for investigation of trans-epithelial fluid transport and allow for rapid assessment of therapeutic target (Giuliani et al., 2008; Koslowski et al., 2020; Magenheimer et al., 2006; Sun et al., 2011). Due to their avascular nature and absence of glomerular filtration, any tubular dilation in the metanephroi is attributed to their intrinsic capacity for trans-epithelial fluid transport (Giuliani et al., 2008; Magenheimer et al., 2006). While tubules of *Pkd1*$^{-/-}$ metanephroi are predisposed to dilations, cyst formation requires cAMP induction like in the above-mentioned cell lines, and dilations rapidly occur as early as 1 hour after stimulation with cAMP in some tubules (Magenheimer et al., 2006), like in human ADPKD kidneys and murine models where cysts initiate in only a small proportion of tubules (Harris, 1999; Koptides et al., 1999; Pei, 2001; Pei et al., 1999; Qian et al., 1996; Shibazaki et al., 2008). Furthermore, cysts in metanephroi initiate from proximal tubules and later extend to collecting ducts, in the same pattern as documented in mouse models (Arroyo et al., 2021; Happe et al., 2013; Nauta et al., 1993; Schafer et al., 1994; Takahashi et al., 1991). As renal cysts initiate at E15.5 in *Pkd1*$^{-/-}$ or *Pkd2*$^{-/-}$ mice, metanephroi are often isolated and cultured around E13.5-14.5, at a time when isolation is possible, and no disease phenotype has yet developed (Magenheimer et al., 2006). The metanephroi study conducted by Magenheimer *et al.* elegantly demonstrated the dependency of cAMP-induced cyst fluid secretion on other factors, such as ion channels, transporters, as well as enzymes regulating cAMP, and opened new possibilities to take advantage of this model

(Magenheimer et al., 2006). Since then, the metanephroi model has been more widely used in PKD research as a tool to screen and identify therapeutic targets (Lakhia et al., 2022; Snyder et al., 2011; Sundar et al., 2022; Wang et al., 2015; Yang et al., 2008; Zhu et al., 2018).

1.2.3.4 Human kidney organoids

Human kidney organoids are a more recent tool for PKD disease modeling (Desrochers et al., 2014; Koslowski et al., 2020). Initially kidney organoids were derived from human pluripotent stem cells (hPSC), but hPSC-derived renal cells resemble in their characteristics those of early human kidney development and may not be ideal to model adult ADPKD (Freedman et al., 2015; Takasato et al., 2015; Wu et al., 2018). In the search for a more suitable organoid to model adult epithelial kidney disease, cells outgrowing from tubular fragments or from the urine excreted by adult human kidneys were employed and organoids were derived thereof, but whether ADPKD phenotypes could be induced in this model remain to be uncovered (Shimizu et al., 2020). More recently, a more ideal organoid termed tubuloid, derived from a distinct $CD24^+$ epithelial subpopulation, has been described and could serve as an advanced model for adult PKD (Xu et al., 2022). While all other renal cells are unable to generate tubuloids, $CD24^+$ cells in the nephron, especially those in proximal tubules and the Loop of Henle, have the strongest capacity to generate organoids and outcompete those from other nephron segments in long term cultures (Shimizu et al., 2020; Xu et al., 2022). *PKD1* or *PKD2* can be deleted using multiplex CRISPR-Cas9 gene editing to model ADPKD cysts in tubuloids, and the morphology of these cysts highly resembles those found in human ADPKD tissues and share great similarities in hyperactivation of disease-driven pathways such as MAPK (Xu et al., 2022). More importantly, while hPSC are unresponsive to tolvaptan, cyst size in tubuloids is

significantly reduced by tolvaptan, making tubuloids the most ideal organoid to study ADPKD to date (Xu et al., 2022).

1.3 Cellular and molecular processes mediating ADPKD

Studies completed in the above-mentioned model systems allowed us to identify important contributors of cyst growth, including active cyst fluid secretion, hyper proliferation in renal epithelial cells and development of kidney fibrosis. The role of primary cilia is less certain and is still being actively investigated.

1.3.1 Stimulation of fluid secretion in cystogenesis

Cysts begin by focal dilation of a small proportion of nephrons and as they increase in size and number, they separate from their parent tubule and progression is largely dependent on fluid secretion (Fig. 4) (Magenheimer et al., 2006; Mangoo-Karim et al., 1989; Reif & Wallace, 2019; Sullivan et al., 1998; Terryn et al., 2011). Stimulation of trans-epithelial fluid secretion in cystic epithelia has been demonstrated by a shift in the localization of ion transport proteins as well as a change in the direction of fluid transport (Brill et al., 1996; Carone et al., 1994; Du & Wilson, 1995; Grantham et al., 1995; Klein et al., 2016; Wilson et al., 1991). In absence of forskolin, fluid flow can be bidirectional: basolateral-apical flux or apical-basolateral absorption, while forskolin only permits basolateral-apical fluid transport (Brill et al., 1996). Analyses conducted in human ADPKD kidneys, cell lines, metanephroi and animal models revealed important members of the fluid secretory pathway, many of which are normally found in both apical and basolateral membranes but localize exclusively to one side in ADPKD kidneys (Brill et al., 1996; Cabrita, Kraus, et al., 2020; Gattone et al., 2003; Magenheimer et al., 2006; Tamma et al., 2017; Torres, 2005; Yang et al., 2008). Immunostaining of various ion transport proteins show non-uniform expression, suggesting that the involvement of different players taking part in

cyst fluid accumulation varies between different cell subpopulations (Brill et al., 1996; Klein et al., 2016; Lebeau et al., 2002; Magenheimer et al., 2006; Sullivan et al., 1998). Given that fluid secretion in normal secretory epithelia probably reflects a well-balanced ion transport, one would expect aberrant ion transport to drive cyst fluid accumulation in ADPKD. Consequently, pharmacologically inhibition of one or a combination of these players may be possible to reduce the size of polycystic kidneys.

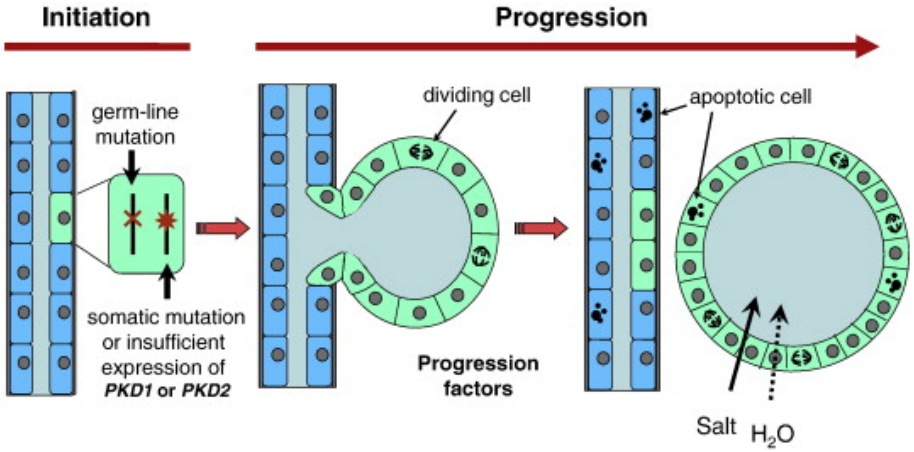

Fig. 4 Schematic representation of cyst initiation and progression in PKD. Following initiation of cysts by genetic mutation and secondary loss of non-mutated allele, progression factors such as cAMP agonists stimulate renal epithelial cell proliferation and fluid secretion into cyst lumen, resulting in cyst expansion. From *"Cyclic AMP-mediated cyst expansion," Biochimica et Biophysica Acta,* permission obtained (Wallace, 2011).

1.3.1.1 Identification of members of the cyst fluid secretory pathway

1.3.1.1.1 Vasopressin 2 Receptor (V2R)

Elevation in vasopressin and its receptor V2R are well documented in ADPKD patients and in *Pkd* murine models including *cpk, pcy, Pkd2*$^{WS25/-}$ mouse and *PCK* rat (Gattone et al., 1999; Torres, 2005; Zittema et al., 2012). The importance of V2R in stimulating cyst growth has been demonstrated by Tolvaptan, a V2R antagonist and the only drug approved for ADPKD, which markedly lowers renal cAMP levels and delays or reverses cyst growth *in vivo* (Aihara et al., 2014; Gattone et al., 2003; Kanhai et al., 2020; Miyazaki et al., 2007; Tamma et al., 2017;

Torres et al., 2016; Torres et al., 2004; Wang et al., 2005; Wulfmeyer et al., 2019). Binding of vasopressin to V2R is necessary for adenylyl cyclase 6 (AC6) to produce cAMP, a major driver of cyst growth that stimulates both fluid secretion and cell proliferation (Tamma et al., 2017; Wang et al., 2010). More specifically, vasopressin binds to two G protein coupled receptors (GPCRs), V2 and V1α, in the collecting duct, which leads to activation of AC6 and increases cAMP production which then activates protein kinase A (PKA) (Agarwal et al., 2019; Calvet, 2015; Tamma et al., 2017; Wang et al., 2010). One of the downstream targets that PKA phosphorylates is aquaporin 2 (AQP2), which upon PKA activation, traffics to and inserts itself in the apical membrane to increase water permeability (Wilson et al., 2013). Interestingly, this activation cascade contains an internal brake to keep V2R activity balanced: vasopressin binding to V1α receptors releases calcium from the ER and limits V2R activity through inhibition of AC6 (Tamma et al., 2017; Wang et al., 2010).

1.3.1.1.2 Cystic Fibrosis Transmembrane Conductance Regulator (CFTR)

The analogy between the net chloride secretion in ADPKD cells and secretory epithelia in general suggests that that CFTR may be responsible for the cAMP-stimulated chloride secretion (Devuyst et al., 1996; Hanaoka et al., 1996; Jouret & Devuyst, 2020; Magenheimer et al., 2006; Sullivan et al., 1998; Terryn et al., 2011). CFTR immunoreactivity can be detected on the apical membrane as early as 12 weeks of gestation in the human fetal kidney, first detected in proximal tubules and collecting ducts at 13 weeks of gestation and maintains expression until after birth, then becomes downregulated in adult kidneys (Devuyst et al., 1996). In contrary to lowered *CFTR* mRNA expression in adult kidneys, ADPKD kidney cysts and cystic epithelia derived from ADPKD patients show sustained *CFTR* expression associated with the apical cell membrane in all segments of the kidney except glomeruli (Brill et al., 1996). Indeed, more than

half of all human ADPKD kidney cysts express *CFTR* and show channel activity, which is thought to be sufficient to stimulate cyst growth (Devuyst et al., 1996; Lebeau et al., 2002). Alternatively, there may be other redundant mechanisms such as the mislocalization of Na^+-K^+-ATPase to the apical membrane, that facilitate cyst growth (Hanaoka et al., 1996; Thomson et al., 2003; Zheleznova et al., 2011). Apart from human ADPKD kidneys, a cAMP-activated chloride current is also observed *in vitro* in primary cultures of ADPKD cysts (Albaqumi et al., 2008). CFTR is normally present on the apical membrane, basolateral membrane, and intracellularly, but is exclusively found on the apical membrane in presence of forskolin, consistent with what is observed in human ADPKD kidneys (Klein et al., 2016). In addition, *Cftr* expression can be found on the apical membrane of cyst-lining epithelial cells *in vivo* (Hanaoka et al., 1996; Lebeau et al., 2002; Sullivan et al., 1998; Terryn et al., 2011). These findings support forskolin facilitates a change in CFTR localization to favour basolateral-apical fluid flow. Ikeda *et al.* utilized MDCK cells to understand how abnormal PC1 function may increase *CFTR* expression on the apical membrane to favour cAMP-stimulated chloride and fluid secretion in PKD (Ikeda et al., 2006). Transfection of MDCK cells with wildtype PC1 maintains low apical *CFTR* expression and channel activity, but transfection of a PC1 mutant disrupts this balance and enhances *CFTR* expression and chloride secretion into cyst lumen, suggesting wildtype PC1 modulates cellular ion transport by regulating the subcellular localization of CFTR, likely mediated by the carboxyl terminal of PC1 activating heterotrimeric G proteins, consequently leading to the inhibition of AC, and thereby reducing cAMP, which in consequence limits *CFTR* expression and activity (Ikeda et al., 2006).

Using *Pkd1*$^{-/-}$ metanephroi, Magenheimer *et al.* demonstrated that the capacity for *Pkd1*$^{-/-}$ to induce cystogenesis depends on the dosage of *Cftr*, where cysts are completely abolished upon

genetic inactivation of *Cftr* and partially rescued by Cftr inhibitor $CFTR_{inh}172$ (Magenheimer et al., 2006). The authors showed that, like in human kidneys, *Cftr* is expressed early and non-uniformly in the murine embryonic kidney in proximal tubules and can later be found in all nephron segments, suggesting different cell subpopulations in cyst epithelia are equipped differently to mediate ion transport (Magenheimer et al., 2006). No observed developmental abnormalities in $Cftr^{-/-}$ metanephroi suggest it may be inessential for renal development and may help explain the lack of renal problems in cystic fibrosis patients. The important implication of Cftr in cyst growth was later demonstrated *in vivo* where inhibition of Cftr with $CFTR_{inh}172$ or BPO-27 significantly delayed cyst growth (Snyder et al., 2011; Yang et al., 2008).

1.3.1.1.3 Tmem16A (Anoctamin 1)

Cftr has always been considered the apical chloride channel responsible to drive chloride secretion mediating cyst growth, but recently, increasing evidence suggest Tmem16a, another apical chloride channel, is also critically implicated in ADPKD cyst growth (Cabrita, Buchholz, et al., 2020; Cabrita, Kraus, et al., 2020; Talbi et al., 2021). Studies show that Tmem16a is pro-proliferative and closely associates with Cftr as it mediates Cftr-dependent chloride secretion, and that, like Cftr and other key members of the fluid secretory pathway, *Tmem16a* expression is highly elevated in ADPKD (Cabrita, Kraus, et al., 2020; Talbi et al., 2021). Genetic inactivation or pharmacologic inhibition of Tmem16a significantly improves cystic phenotypes in an adult *Pkd1* mouse model (Cabrita, Kraus, et al., 2020). *In vitro* study reveals that knocking down either polycystins in M1 cells causes elevation in *Tmem16ai* expression, proliferation, and chloride secretion (Cabrita, Buchholz, et al., 2020). Tmem16a is thought to drive renal cyst growth by enhancing ER calcium store release, thus stimulating proliferation of the cystic

epithelium, and increasing calcium-activated chloride secretion, all of which favour cyst growth (Cabrita, Buchholz, et al., 2020).

1.3.1.1.4 Na^+-K^+-Cl^- Cotransporter (NKCC1)

Nkcc1 is expressed early in the mouse embryo like Cftr and can be found first in the collecting ducts, then later in all nephron segments (Magenheimer et al., 2006). Nkcc1 is thought to replenish the chloride ions actively secreted through Cftr into the cyst lumen while co-transporting sodium and potassium ions (Flores et al., 2007; Lebeau et al., 2002). The implication of Nkcc1 in cyst growth has been demonstrated in *Pkd1*$^{-/-}$ metanephroi where bumetanide, a Nkcc1 inhibitor, severely impairs cAMP-induced cyst progression (Magenheimer et al., 2006). Although limited immunoreactivity is found in normal kidneys, *NKCC1* expression is significantly elevated in human ADPKD kidneys and can be found in about one third of all cysts, mainly concentrated along the basolateral membrane (Lebeau et al., 2002). Interestingly, all cysts that are NKCC1 positive (~1/3 of all cysts) also express CFTR, supporting the cooperation between the two transporters in mediating cyst growth, while additional basolateral pathways may be present in cysts not stained by NKCC1, namely anion exchanger type I (AE1) which is found in about 1/10 of cysts and also localized to the basolateral membrane (Lebeau et al., 2002).

1.3.1.1.5 Na^+-K^+-ATPase

Initially, Na^+-K^+-ATPase was found predominantly in the basolateral membrane and was thought to be mis-localized to the apical side to mediate fluid secretion by actively transporting sodium into the cyst lumen (Wilson et al., 1991). Indeed, application of Na^+-K^+-ATPase inhibitor, ouabain, on the apical membrane but not basolateral membrane, blocked secretory flux of sodium in ADPKD epithelia (Wilson et al., 1991). However, the predominant apical

localization reported by Wilson *et al.* has been strongly debated since animal models failed to show a mis-polarized Na^+-K^+-ATPase on the apical membrane of cystic epithelia, and subsequent studies consistently found Na^+-K^+-ATPase on basolateral membranes (Brill et al., 1996; Carone et al., 1994; Thomson et al., 2003). Those findings are coherent with other observed locations of Na^+-K^+-ATPase in secretory epithelia in general, as Na^+-K^+-ATPase likely recycles the intracellularly accumulated sodium ions brought in by Nkcc1 (Larsen et al., 2014; Lebeau et al., 2002; Thomson et al., 2003). Na^+-K^+-ATPase are primarily detected in the basolateral membrane of intact cysts from ADPKD kidneys and in cyst epithelia derived from ADPKD patients, and only infrequently found on the apical membrane (Brill et al., 1996; Carone et al., 1994). In another study, ouabain applied to excised ADPKD kidney cysts in the basolateral but not apical medium inhibited fluid secretion and reduced short circuit currents, supporting localization of Na^+-K^+-ATPase on the basolateral membrane (Grantham et al., 1995).

1.3.1.1.6 Aquaporin 2 (AQP2)

AQP2 is a water permeable channel expressed in principal cells of the renal collecting duct (Kwon et al., 2013; Tamma et al., 2017; Wilson et al., 2013). Vasopressin binding to V2R induces insertion of AQP2 in the apical membrane, increasing membrane permeability to water and stimulates water transport under a favourable osmotic driving force (Tamma et al., 2017; Wilson et al., 2013). Most AQP2 are recycled with only a small portion (~3%) excreted into the urine, hence, urinary-AQP2 (U-AQP2) serves as an indicator of vasopressin action. As Tolvaptan targets V2R, it reduces the membrane insertion of AQP2 and subsequently reduces release of U-AQP2, therefore patients who receive Tolvaptan generally show reduced U-AQP2 (Tamma et al., 2017). In fact, the initial reduction in U-AQP2 per milligram of urinary creatinine (U-AQP2/Cr) in the first month of treatment could be an indicator of renal prognosis in patients

receiving the treatment (Makabe et al., 2021). Patients who experience a greater reduction in U-AQP2/Cr tend to present a better renal prognosis as indicated by a lower annual decline in glomerular filtration rate (eGFR) (Makabe et al., 2021).

1.3.1.2 Overview of the cyst fluid secretory pathway

1.3.1.2.1 Forskolin induces transition from absorptive to secretive fluid transport in ADPKD cysts

Early observation of polarized secretion in ADPKD cyst-derived primary cell culture in response to the cAMP activator, forskolin, led scientists to speculate there may be a transition from absorptive to secretive fluid transport in ADPKD cysts (Mangoo-Karim et al., 1989; Ye & Grantham, 1993). Likewise, intact cysts excised from human ADPKD kidneys, when maintained in culture, secreted more fluid under forskolin stimulation, whereas normal renal tubules usually absorb a large quantity of electrolytes and water to conserve the glomerular filtrate (Grantham et al., 1995). Excised ADPKD cysts and cyst-derived primary cultures retain this absorptive capacity under basal conditions, but when stimulated by forskolin, transition to a secretive state in just 24 hours, giving rise to 3- to 10-fold increase in the rate of secretion over the rate of absorption (Grantham et al., 1995).

1.3.1.2.2 Apical chloride secretion drives cyst growth

Sodium and chloride are the major electrolytes secreted by excised ADPKD cysts upon stimulation with forskolin (Grantham et al., 1995). Since then, multiple *in vitro* and *in vivo* studies have demonstrated that the fluid secretion across cyst-lining epithelial cells is driven by chloride secretion through the apical membrane into cyst lumen, predominantly by Cftr, and stimulated by the elevation in cAMP that is typical of ADPKD tissues (Brill et al., 1996; Calvet, 2015; Hanaoka et al., 1996; Jouret & Devuyst, 2020; Snyder et al., 2011; Sullivan et al., 1998;

Terryn et al., 2011; Wallace, 2011; Yang et al., 2008). The heterogeneity in *CFTR* expression in cyst-lining epithelial cells suggest that other chloride channels may be involved (Brill et al., 1996; Hanaoka et al., 1996), namely TMEM16A (Cabrita, Buchholz, et al., 2020). This chloride transport is considered the driving force for cyst fluid secretion, indeed, the chloride gradient established by Cftr drives the activity of other channels and transporters of the pathway, namely NKCC1, a cation chloride co-transporter localized to the basolateral membrane (Lebeau et al., 2002).

1.3.1.2.3 Accumulation of salt and water in cyst lumen causes cyst enlargement

The sodium that is accumulating in the cell, brought in by NKCC1, can be recycled through sodium transporters, one of them being Na^+-K^+-ATPase (Brill et al., 1996; Larsen et al., 2014; Terryn et al., 2011). The transepithelial chloride secretion through CFTR also generates a gradient that favours transport of sodium into the cyst lumen, yet the nature of this transepithelial sodium pathway remains elusive, with epithelial sodium channel (ENaC) on the apical membrane (Fig. 5) suggested to be one of the potential contributors, although contribution of ENaC to cyst formation is still debated (Graffe et al., 2012; Zheleznova et al., 2011). For instance, reduced ENaC activity has been reported in cystic in comparison to normal tubules in animal models of PKD, suggesting sodium reabsorption is reduced and contributes to accumulation of sodium in luminal fluid (Pavlov et al., 2015; Veizis et al., 2004; Yanda et al., 2019). Progressive salt transport across the apical membrane gives rise to an osmotic gradient that favours water flow through APQ2 into the cyst lumen, therefore causing cyst enlargement (Graffe et al., 2012; Kwon et al., 2013; Wilson et al., 2013).

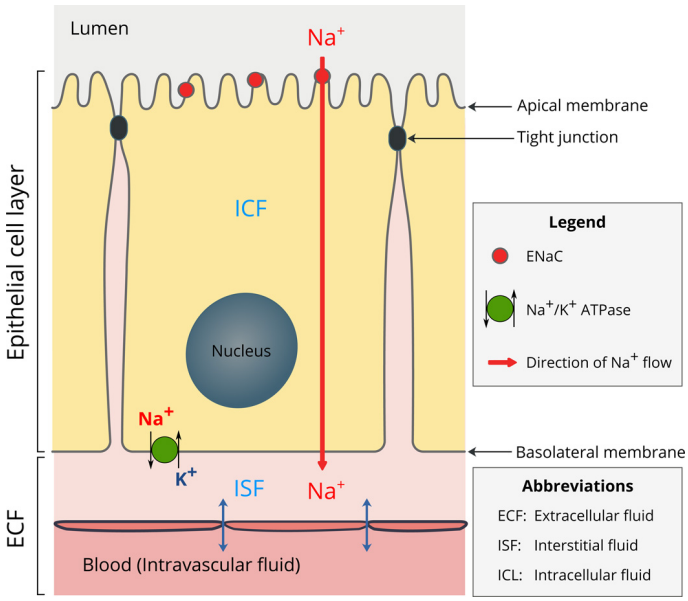

Fig. 5 Schematic representation of ENaC localization and function in epithelial cells. ENaC is predominantly found in the apical membrane and allows sodium to enter the cell from the lumen, before being transported into the interstitial fluid through the basolateral Na^+/K^+-ATPase. Reduced ENaC activity in PKD could suggest reduced sodium transport through ENaC and hence accumulation in the cyst lumen. From *"Epithelial sodium channel (ENaC) family: Phylogeny, structure-function, tissue distribution, and associated inherited diseases," Gene,* permission obtained (Hanukoglu & Hanukoglu, 2016).

1.3.2 Hyper activation of renal epithelial cell proliferation

1.3.2.1 cAMP is mitogenic in cystic epithelia

cAMP can either stimulate or inhibit cell proliferation through MAPK signaling, depending on cell type and context. B-Raf may also be implicated (Dugan et al., 1999; Pearson & Cobb, 2002; Qiu et al., 2000). For instance, neurons express B-Raf and allows MAPK activation via cAMP, while in astrocytes, where B-Raf is absent, cAMP reduces MAPK/ERK activity (Dugan et al., 1999). When analyzed by western blotting, the B-Raf protein can be detected as 95kDa or 68kDa isoforms. In general, cells with higher level of 95kDa isoform relative to 68kDa isoform proliferate, while cAMP inhibits proliferation in cells not expressing B-Raf or expressing only the 68kDa isoform (Fujita et al., 2002; Kip et al., 2005; Takahashi et al., 2004). The relative expression of the two B-Raf isoforms also depends on cellular density,

with the 95kDa isoform predominantly found in subconfluent cells and the 68kDa isoform more prevalent in confluent cells (Takahashi et al., 2004). cAMP is mitogenic in ADPKD cells where it stimulates proliferation through activation of B-Raf and ERK, while neither proliferation nor B-Raf and ERK are activated in HKC cells in response to cAMP stimulation (Yamaguchi et al., 2003). The same group of scientists later identified calcium to play an important role in determining the switch from cAMP growth-inhibiting to growth-stimulating phenotype in murine wildtype principal (M-1) cells, by demonstrating that M-1 incubation in a low calcium medium or in the presence of calcium channel blockers increases the level of the 95kDa B-Raf isoform, allowing cAMP activation of B-Raf/ERK (Yamaguchi et al., 2004). These observations are in line with dysregulation in calcium signaling in ADPKD due to mutations in polycystins (Mangolini et al., 2016).

1.3.2.2 ADPKD kidneys show high proliferative index

Non-cystic tubules in end stage human ADPKD kidneys are 40 times more proliferative than normal tubules in healthy human kidneys, suggesting that proliferation precedes cyst formation and likely represents one of the earliest events in cyst growth (Chang et al., 2006). Further of interest is that non-cystic tubules in ADPKD kidneys are also more proliferative than cystic tubules, suggesting proliferation may be an early event in cyst formation but does not persist as cysts enlarge, therefore, increases in proliferative activity alone may not be sufficient for cyst progression (Chang et al., 2006).

1.3.2.3 Signaling pathways associated with proliferation

1.3.2.3.1 Proliferation predisposes and drives cyst growth

Hyperproliferation has been recognized as one of the hallmark features of cystic epithelia, but it was uncertain whether proliferation is an early event predisposing to cyst growth

or a later event driving cyst progression (Dong et al., 2021; Lakhia et al., 2022; Ramasubbu et al., 1998; Reif & Wallace, 2019; Takahashi et al., 2004; Wang et al., 2006; Zheleznova et al., 2011). Increased proliferation was suggested to predispose the tubular cells to somatic mutations which are necessary for cyst formation (Chang et al., 2006). In line with greater proliferation in non-cystic tubules in human ADPKD kidneys, studies in *Pkd2*$^{+/-}$ mice also demonstrated that proliferation may be an early event, as the proliferative index of non-cystic tubules in this model was observed to be 5- to 10-fold higher than that of wildtype (Chang et al., 2006). Proliferation as an early event in cyst growth has also been demonstrated in the *Han:SPRD* rat and in *Pkd2*$^{WS25/-}$ mice, where proliferative activity is present not only in cystic epithelia but also in non-cystic tubules and interstitial cells (Kuehn et al., 2002; Ramasubbu et al., 1998; Thomson et al., 2003). Interestingly, heterozygous germline *Pkd1* mutation alone seems to increase proliferation by 5- to 20-fold when compared to wildtype mouse kidneys, but *Pkd1* deficiency does not appear to initiate autonomous cell proliferation beyond control as the number of renal epithelial cells in which both alleles of *Pkd1* are disrupted does not rapidly expand to form cysts in adult mice, suggesting additional stimuli are required (Lantinga-van Leeuwen et al., 2007).

1.3.2.3.2 Calcium and cAMP signaling

Elevation in cAMP has been well documented in ADPKD across a wide range of tissues, including the kidney, liver, vascular smooth muscle, and choroid plexus (Banizs et al., 2007; Hopp et al., 2012; Kip et al., 2005; Masyuk et al., 2007). Elevation in renal cAMP has been consistently reported in both non-orthologous and orthologous models of PKD, including *PCK*, *pcy*, *Pkd2*$^{ws25/-}$ and *Pkd1*$^{RC/RC}$ murine models (Gattone et al., 2003; Hopp et al., 2012; Torres et al., 2004; Yamaguchi et al., 1997). It is well accepted that cAMP drives cyst growth by hyperactivating both fluid secretion and cell proliferation, and targeting cAMP with V2R

antagonists lowers cAMP levels which subsequently delays PKD development and progression (Aihara et al., 2014; Miyazaki et al., 2007; Tamma et al., 2017; Torres et al., 2016; Wang et al., 2005). cAMP levels are regulated by the activities of adenylyl cyclase (AC) and phosphodiesterase (PDE): AC synthesizes while PDE hydrolyzes cAMP (Wang et al., 2010). AC6, PDE1 and 4 are the main isoforms of those enzymes in collecting duct principal cells, where larger and most cysts are found in human and mouse cystic kidneys (Wallace, 2011). All isoforms of *PDE1, 3,* and *4,* are elevated in cystic mouse kidneys, but much lower protein levels are found compared to wildtype, with PDE4 being the lowest expressed PDE in the collecting duct (Wang et al., 2010), suggesting the alterations in PDE activities may in part account for cAMP elevation in PKD.

It is generally accepted that the functional loss of polycystins disrupts intracellular calcium homeostasis and stimulates the elevation of cAMP, which through activation of proliferative and fluid secretory pathways, causes cystogenesis (Fig. 6) (Calvet, 2015; Mangolini et al., 2016; Yamaguchi et al., 2004). As calcium is an important regulator of ACs and PDEs, any disruption in calcium homeostasis can greatly influence their activities and contribute to the overall elevation in cAMP, indeed, the reduced intracellular calcium level commonly reported in PKD can stimulate cAMP production through calcium inhibitable AC6 and/or calcium dependent PDE1 (Calvet, 2015; Halls & Cooper, 2011; Mangolini et al., 2016; Wallace, 2011; Wang et al., 2010; Yamaguchi et al., 2004).

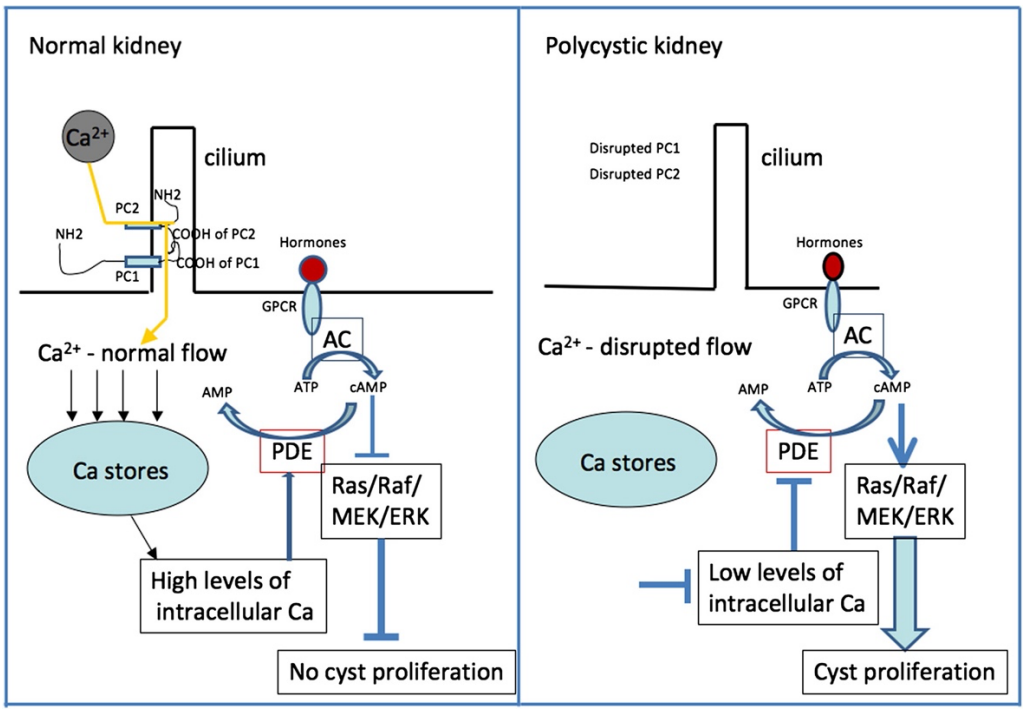

Fig. 6 Schematic representation of disrupted calcium and cAMP signaling in PKD. Under normal conditions, functional polycystins interact and enable calcium entry which stimulates calcium release from intracellular stores. The high level of intracellular calcium keeps cAMP levels in a steady state through ACs and PDEs. Cells remain in a non-proliferative state since low levels of cAMP are unable to stimulate proliferative pathways such as MAPK/ERK signaling. However, this steady state is disrupted by mutated polycystins in PKD and triggers a series of events that stimulates production of cAMP and proliferation of cystic epithelial cells through activation of MAPK/ERK. From *"Calcium-mediated mechanisms of cystic expansion," Biochimica et Biophysica Acta (BBA) – Molecular Basis of Disease,* permission obtained (Abdul-Majeed & Nauli, 2011).

1.3.2.3.3 Canonical Wnt signaling

Among the signaling pathways that favour cyst growth, canonical Wnt/β-catenin signaling is a strong driving force for the hyperproliferative phenotypes in PKD. The canonical Wnt/β-catenin signaling is important for kidney development and disruption can lead to cystic kidney phenotypes (Benzing et al., 2007; Lancaster & Gleeson, 2010; Shao et al., 2020). Signaling initiates when ligand binding activates Dishevelled (Dvl) which in turn inhibits a complex of proteins which degrades the major downstream mediator of Wnt signaling, β-catenin, when Wnt signaling is inactive (Lancaster & Gleeson, 2010). Activation of this pathway allows

β-catenin accumulation in the cytosol and facilitates β-catenin entry into the nucleus where it drives transcription of Wnt target genes along with T-cell factor/lymphoid enhancer factor (TCF/LEF) transcription factors (Lancaster & Gleeson, 2010). The carboxyl-terminal of PC1 can positively modulate the Wnt/β-catenin pathway by stabilizing nuclear accumulation of β-catenin, and overexpression of the PC1 carboxyl-terminal can even induce dorsal curvature in zebrafish embryos, which is consistent with an increase in canonical Wnt signaling (Kim, Arnould, Sellin, Benzing, Fan, et al., 1999). Additional evidence for this has been found in cancer cells and osteoblasts (Xiao et al., 2010; Zheng et al., 2008). This modulation requires a fine balance between PC1 expression and post-translational cleavage of its carboxyl-terminal, as the overexpression of PC1 carboxyl-terminal can also inhibit downstream transcription of Wnt/β-catenin, while disruption of this balance is suggested to lead to cyst development (Lal et al., 2008). The importance of a balanced Wnt/β-catenin signaling has been demonstrated in both β-catenin overexpressing and loss-of-function mutants that display renal cysts (Marose et al., 2008; Saadi-Kheddouci et al., 2001).

1.3.2.3.4 Mitogen-activated protein kinase/extracellular-regulated kinase (MAPK/ERK) signaling

There is strong evidence for MAPK/ERK activation in mediating proliferation in human ADPKD cyst-derived primary cultures as well as non-orthologous and orthologous Pkd1 mouse kidneys, where MAPK/ERK signals are predominantly localized in the epithelial cells lining the cysts (Nagao et al., 2003; Omori et al., 2006; Shibazaki et al., 2008; Yamaguchi et al., 2003; Yamaguchi et al., 2004). The opposite response of cAMP in cystic versus normal kidney epithelia in stimulating proliferation through MAPK/ERK (Fig. 7) demonstrate that MAPK/ERK can be activated through two complementary signaling cascades depending on whether the

stimulus is cAMP or epidermal growth factor (Yamaguchi et al., 2003). The traditional receptor tyrosine kinase signaling pathway activates Ras which recruits Raf-1, and phosphorylates MAPK kinase (MEK), activating MAPK. Alternatively, in the presence of cAMP, MEK activation proceeds through Rap1 and B-Raf instead of Ras/Raf-1. Rap1 activates B-Raf, which phosphorylates MAPK. The regulation of MAPK/ERK signaling is well coordinated such that in cells that lack B-Raf, Rap1 directly inhibits Ras-dependent stimulation of MAPK (Vossler et al., 1997). Targeting the MAPK/ERK pathway *in vivo* showed heterogenous results. MEK inhibitors did not have any effect on cyst progression in an early-onset Pkd1 mouse model (Shibazaki et al., 2008), but delayed cyst progression in a non-orthologous mouse model (Omori et al., 2006). It appears that the outcome could be dependent on the age at treatment onset, genotype, and which step of the pathway is being targeted.

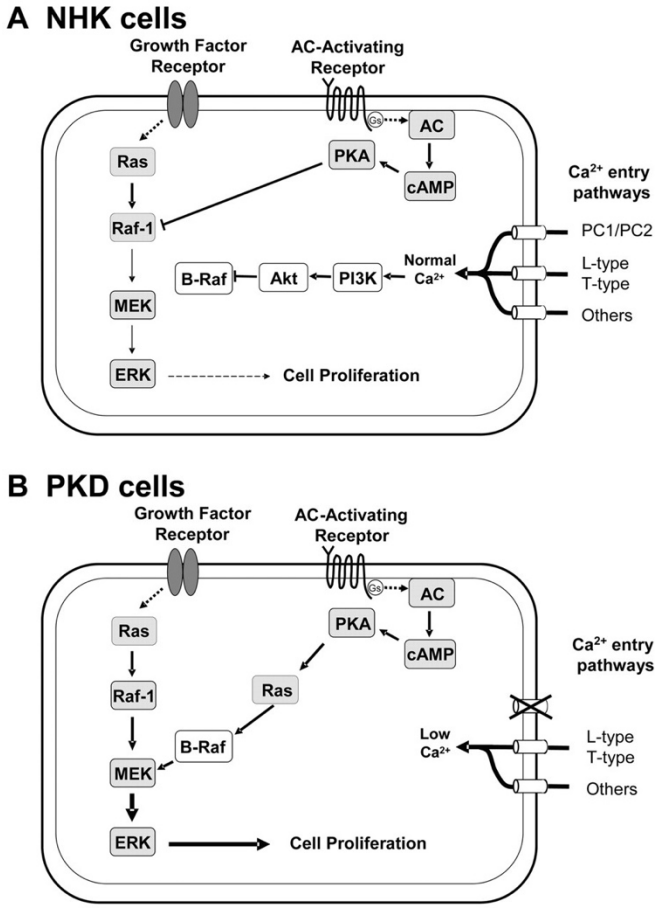

Fig. 7 Schematic representation of MAPK/ERK signaling-mediated proliferation in NHK versus PKD cells. Cell proliferation in a normal state is stimulated by growth factors binding to receptor tyrosine kinase, causing sequential activation of Ras, Raf-1, MEK, and ERK. The differences in cAMP levels determine the opposite responses found in NHK versus PKD cells. (A) In NHK cells, basal intracellular calcium level prevents activation of B-Raf by cAMP that is needed to stimulate cell proliferation. (B) In PKD cells, reduced intracellular calcium level relieves inhibition of B-Raf, allowing cAMP to signal through B-Raf to activate MEK and ERK, stimulating cell proliferation. From *"Calcium restores a normal proliferation phenotype in human polycystic kidney disease epithelial cells," Journal of the American Society of Nephrology,* permission obtained (Yamaguchi et al., 2006).

1.3.2.3.5 Mammalian target of rapamycin (mTOR) signaling

Mammalian target of rapamycin (mTOR) pathway is activated in PKD and contributes to the elevation in epithelial cell proliferation (Shillingford et al., 2006). Targeting mTOR with metformin or rapamycin effectively delays cyst growth in *Pkd* mouse models (Cox et al., 2023; Leonhard et al., 2019; Pastor-Soler et al., 2022; Pema et al., 2016; Shillingford et al., 2006; Su et al., 2022). Metformin is originally a widely used drug for type 2 diabetes mellitus. It was shown to effectively delay cyst growth in both rapid and slow progressive Pkd1 mouse models, and appeared to target Cftr-mediated fluid secretion, proliferation, cAMP, MAPK/ERK signaling, inflammation, and even improved kidney function in the adult mouse model (Pastor-Soler et al., 2022). However, these results did not translate well for human use in ADPKD patients. A recent metformin phase II clinical trial reported no improvement in glomerular filtration rate or total kidney volume, and resulted in adverse symptoms mainly in the gastrointestinal tract (Brosnahan et al., 2022).

More recently, another drug, PF-0649577, approved for diabetic nephropathy, osteosarcoma, non-alcoholic fatty liver disease, and non-alcoholic steatohepatitis, was repurposed for ADPKD (Su et al., 2022). PF-0649577 was effective in delaying renal cyst progression by targeting the mTOR pathway, as has been demonstrated *in vitro* in MDCK cells, *ex vivo* in wildtype metanephroi, and *in vivo* in an early-onset *Pkd1* mouse model (Su et al.,

2022). By directly measuring Cftr-dependent short circuit currents in MDCK cells and combining these results with the other measurements and observations of their study, the authors concluded that PF-0649577 stimulates AMPK phosphorylation and causes concurrent inhibition of mTOR and Cftr, together delaying cyst progression by inhibition of proliferation and cyst fluid secretion (Su et al., 2022). This elegant study incorporates different models to illustrate that there could be a tight association between signaling pathways and function of chloride transporters, thus suggesting that the use of drugs with dual action to target multiple pathways could be advantageous for ADPKD treatment. The authors have conveniently used a drug that targets proliferation, as well as fluid secretion, which are both essential to cyst growth in ADPKD (Su et al., 2022).

1.3.3 Kidney fibrosis develops with PKD progression

Kidney fibrosis, defined by excessive accumulation of extracellular matrix proteins (ECM) consisting of mainly type I collagen, is considered one of the major features of ADPKD. Fibrosis in tissues causes inflammation and leaves scarring, thus interfering with normal tissue architecture (Fragiadaki et al., 2020; Fragiadaki et al., 2011; Norman, 2011). The ECM undergoes dynamic rearrangements when the kidney is injured and responds with tissue scarring, which, when excessive, can impact the organ's function (Fragiadaki et al., 2020; Norman, 2011). How fibrosis is involved in ADPKD progression is still being debated. In humans, it is only during the embryonic stages of development that kidney tissues can be repaired without causing inflammation, scarring or fibrosis, although the exact mechanism underlying this process remains elusive (Ferguson & O'Kane, 2004; Whitby & Ferguson, 1991). Fibrosis appears to have different roles as ADPKD progresses with the three phases of fibrosis progression in ADPKD described below.

1.3.3.1 Cellular phases of fibrosis progression

1.3.3.1.1 Fibrosis in the initial phase is a protective mechanism that limits disease progression

Fibrosis can be triggered by kidney injury such as ischemia or can be predisposed by genetic mutation in the case of ADPKD (Bastos et al., 2009; Chang et al., 2006; Happe et al., 2013; Hassane et al., 2010; Ikeda et al., 2006; Kuehn et al., 2002; Kurbegovic et al., 2010; Lager et al., 2001; Zhang et al., 2020). Fibrosis appears to be a consequence of cyst onset and not a triggering factor in murine models (Okada et al., 2000). In the initial phase, 4 weeks following cyst onset, fibrosis even promotes regression of cyst growth in a *Pkd1* mouse model, although not improved, kidney function did not decline further for the remainder of life (Happe et al., 2013). Massive fibrosis was in fact documented in collapsed cysts from human ADPKD patients (Fragiadaki et al., 2020). In line with these findings, Caroli *et al.* suggest that the volume of interstitial fibrosis may be a more accurate predictor of kidney functional loss in ADPKD patients than the absolute cyst volume (Caroli et al., 2011). The regression in cysts with the onset of fibrosis seems to trigger a protective mechanism that limits the disease in the initial phase of ADPKD.

1.3.3.1.2 Persistent inflammation leads to enhanced extracellular matrix production

Persistent inflammation is a direct response to kidney injury and causes enhanced ECM production, triggered by the infiltration of immune cells producing cytokines. Macrophages are one of the key inflammatory cells involved in fibrosis and promote cyst growth as it has been demonstrated by studies in human patients and experimental models of ADPKD (Fragiadaki et al., 2020; Swenson-Fields et al., 2013; Wen et al., 2021). While macrophages can be protective or disease-causing in other pathologies, they are primarily associated with disease progression in

ADPKD. Scientists attempted to explain how macrophages are recruited to the kidneys in presence of *Pkd1* mutations. One hypothesis is that monocyte chemoattractant protein 1 (MCP1) expression is normally suppressed at homeostasis by a complex within the primary cilia that contains *PKD1*, hence, when *PKD1* is mutated, restriction of macrophage recruitment is lifted, promoting a ciliopathy phenotype (Viau et al., 2018). During this stage of fibrosis progression, resident fibroblasts who reside in the kidney interstitium also play a major role; they are activated and transformed into myofibroblasts, which then rapidly produce excess ECM components, particularly collagen (type I, III, and IV) and fibronectin (Fragiadaki et al., 2020). Depletion of macrophages significantly improves disease outcome as demonstrated by improved cystic indices, reduced proliferation, and preserved function *in vivo* (Cassini et al., 2018; Karihaloo et al., 2011; Zimmerman et al., 2019).

1.3.3.1.3 Excess fibrous tissue is established and interferes with kidney function in the late phase of ADPKD

Tissue homeostasis requires balanced matrix production and breakdown. Imbalanced ECM deposition leads to fibrosis and ultimately organ failure, and can be attributed to increased synthesis or reduced degradation of matrix proteins by matrix metalloproteinases (MMPs) (Fragiadaki et al., 2020; Nakamura et al., 2000; Norman, 2011; Schaefer et al., 1996). Interestingly, there are no reports of elevated MMP1 activity in ADPKD kidneys, although MMP1 is associated with common ADPKD cardiovascular events and a high serum MMP1 level is considered a risk factor (Ameku et al., 2016). As MMPs are inhibited by tissue inhibitor of metalloproteinases (TIMPs), another group analyzed MMP2 and TIMPs activities *in vivo* and found reduction in MMP2 paralleled with increases in TIMP-1 and TIMP-2 activities (Schaefer et al., 1996). The enhanced TIMP activity would limit ECM breakdown, thereby contributing to

fibrosis. Elevation in TIMP-1 but not TIMP-2 was later confirmed in ADPKD patients when compared to healthy individuals (Dekker et al., 2019; Nakamura et al., 2000).

1.3.3.2 Signaling pathways associated with fibrosis

1.3.3.2.1 Janus Kinase and Signal Transducers of Transcription (JAK/STAT) signaling

The Janus Kinase and Signal Transducers of Transcription (JAK/STAT) pathway is involved in epithelial-mesenchymal transition (EMT), fibrogenesis and cell proliferation (Jin, 2020). The activity of JAK/STAT is altered in ADPKD and is proposed to be a defining feature of disease progression, but its role in regulation of fibrosis is still not fully understood (Strubl et al., 2020). Of this family of tyrosine kinases and transcription factors, STAT3, STAT5 and JAK2 appear to be relevant for ADPKD. STAT5 has been shown to drive proliferation in ADPKD as inhibition blocks cyst growth (Fragiadaki et al., 2017). Although unclear how it is involved in fibrosis in ADPKD, STAT5 has also be shown to interact with and upregulate the expression of different components driving EMT to promote EMT in contexts such as hepatocellular carcinoma (Wendt et al., 2014; Zhao et al., 2017). In contrast, although STAT3 expression is elevated in models of ADPKD, it seems to act by limiting renal inflammation, hence not promoting disease progression like STAT5 (Formica et al., 2019; Viau, Baaziz, et al., 2020). JAK2 can activate both STAT3 and STAT5, which seem to be acting in opposite ways in cyst progression. Like STAT3 and STAT5, JAK2 is highly elevated in murine models of ADPKD, and when JAK2 is inhibited, reduced cyst growth is observed (Patera et al., 2019). The contributions of JAK2, STAT3, and STAT5 in EMT and fibrosis are still being explored.

1.3.3.2.2 Transforming growth factor beta (TGFβ) signaling

Transforming growth factor beta (TGFβ) signaling regulates cell proliferation, differentiation, apoptosis, adhesion and migration, and is highly expressed in cystic epithelia of

human patients and murine models of ADPKD (Hassane et al., 2010; Liu et al., 2011; Zhang et al., 2020). TGFβ is a key factor for ECM production; *in vivo* studies suggest that the elevation of *TGFβ* expression and activation of TGFβ-Smad signaling correlate with the progression of fibrosis and cyst growth rather than the initiation of cysts, as activation was not observed in the initiation phase but at mild and advanced stages of the disease, where many interstitial fibroblasts are found surrounding cysts (Hassane et al., 2010). Overexpression of *TGF-β1* in collecting ducts of a *Pkd1* mouse model led to increased cyst epithelial cell proliferation, EMT markers, extensive interstitial fibrosis that accelerated renal functional decline and a shortened lifespan (Zhang et al., 2020).

1.3.4 Role of primary cilia and ciliary signaling in cystogenesis

ADPKD is also considered a "ciliopathy" as mutation of ciliary genes, including the polycystins, causes cystic kidneys. The function of primary cilia in ADPKD is still debated and being actively studied. Some of our current understanding that are relevant to the topic of this thesis are described below.

1.3.4.1 Primary cilia in human ADPKD kidneys

1.3.4.1.1 Structure and function of primary cilia

Primary cilia are long, thin tubular structures that originate from the basal body and are found on the surface of most cells, consisting of a ciliary membrane continuous with the cell membrane and a central axoneme composed of microtubules (Bai et al., 2022; Deane et al., 2013; Lee & Somlo, 2014; Ma et al., 2017; Wang et al., 2021; Yoder, 2007). Renal tubular epithelial cells of all nephron segments have 1 to 2 primary cilia, with the single exception of intercalated cells (Deane et al., 2013). Renal primary cilia are immotile and protrude from the apical cell membrane into the tubular lumen and may possess chemosensory or mechanosensory

functions, thought to respond to luminal fluid flow by deflection, signals are transduced into intracellular cues to influence gene expression mediated by calcium signaling (Bai et al., 2022). There is increasing evidence for the implication of primary cilia in PKD pathogenesis. Their involvement in PKD was first suggested by studies in the *orpk* mouse. The gene mutated in this model encodes the Ift88 or polaris protein, which is expressed in ciliated cells and implicated in cilium assembly and maintenance (Moyer et al., 1994). Indeed, the primary cilia on the surface of collecting ducts in the *orpk* mouse are severely stunted (Pazour et al., 2000).

1.3.4.1.2 Polycystins in primary cilia

It was suggested that aberrant primary cilia function could be important for cystogenesis since most, if not all proteins encoded by genes associated with cyst formation, including the polycystins, can be localized along the primary cilium or at the basal body (Lee & Somlo, 2014; Ma et al., 2017). There are many reports of alterations in primary cilia length in PKD models and more recently, Shao *et al.* found longer primary cilia in human ADPKD kidneys (Shao et al., 2020). However, the molecular functions of primary cilia in the pathogenesis of ADPKD remain incompletely defined. The polycystin complex situated in the primary cilia membrane is thought to act as a fluid flow receptor inducing calcium influx in response to cilia bending, as it has been observed that polycystin mutant cells lose calcium influx in response to fluid flow (Ong & Harris, 2015). However, changes in ciliary calcium were insufficient to trigger a global cytoplasmic calcium response, hence, scientists speculate that a stimulus other than mechanical flow, such as a ligand, may serve to perpetuate ciliary cues into the cell (Delling et al., 2016). Consequently, mutations in polycystins could disrupt these pathways that regulate important cellular processes such as proliferation and differentiation of renal tubular cells, and lead to cystogenesis.

1.3.4.2 Primary cilia length modulation and function

1.3.4.2.1 Regulation of cilia length

Length regulation in primary cilia is a dynamic process and is controlled by the intraflagellar transport (IFT) machinery (Wang et al., 2021). Transport of IFT particles toward the cilium tip increases its length (anterograde) while transport toward the basal body reduces cilia length (retrograde). Shortening, absence and elongation in primary cilia have all been reported in PKD (Hopp et al., 2012; Ma et al., 2013; Shao et al., 2020). One of the factors that can signal primary cilia elongation is cAMP which was demonstrated *in vitro* to act through PKA activation (Besschetnova et al., 2010; Wann & Knight, 2012). In just three hours after cAMP stimulation or calcium induction, primary cilia length is increased by 2-fold, mediated by elevation in anterograde transport of IFT88 particles, and can be shortened accordingly by reducing intracellular cAMP or calcium levels (Besschetnova et al., 2010; Wann & Knight, 2012). Interestingly, primary cilia length can also reduce in response to shear stress, and this sensitivity is dependent on the initial length (Besschetnova et al., 2010). The response of primary cilia to cAMP, calcium, and shear stress is mediated by the polycystins, and when polycystins are disrupted, cilia length adaptation is impaired, suggesting polycystins could act as brakes on this signaling, and with a lack of functional polycystin proteins in PKD, can continue unabated (Besschetnova et al., 2010).

Primary cilia elongation is also a common feature of renal injury in both humans and mice, achieved through the hypoxia-inducible mechanism by elevating HIF-1α following renal injury (Verghese et al., 2011). As inflammation is often associated with renal injury, primary cilia length can also increase in response to inflammatory cytokines such as interleukin-1 and consequently drives the inflammatory response by positively regulating the release of

chemokines (Tran et al., 2008). In contrast, in absence of primary cilia, interleukin-1 induced chemokine response is reduced (Wann & Knight, 2012).

1.3.4.2.2 Functional significance of primary cilia length

The functional significance of primary cilia and their lengths remains elusive. The primary cilium is thought to be a sensory organelle that receives and integrates extracellular stimuli into intracellular signaling to mediate cellular processes such as proliferation (Badano et al., 2006; Besschetnova et al., 2010; Mangolini et al., 2016). How its length influences this signaling transduction and how the polycystins are involved in this process is not completely understood. A heteromeric transient receptor potential (TRP) channel formed by PKD1L1 and PKD2L1, in humans and mice, was thought to act as a ciliary calcium channel allowing calcium flow into the cells (Delling et al., 2013). However, the same group later disputed this hypothesis and reported that the intracellular influx in calcium they had detected previously could not have originated from primary cilia, but rather more likely to come from the cell body, and concluded that primary cilia are not calcium-responsive (Delling et al., 2016). On the other hand, the link between primary cilia length and polycystins appears more consolidated; primary cilia length has been associated with the level of functional PC1 (Hopp et al., 2012; Ong & Harris, 2015). There may be an inherent anti-cystogenic repair program regulated through primary cilia, which, when dysregulated, contributes to cystic phenotypes (Hopp et al., 2012). As many signaling molecules that stimulate cyst growth reside within the primary cilium, changes in primary cilia length may potentially modulate epithelial cell proliferation and differentiation, and ultimately PKD progression (Anvarian et al., 2019; Lee & Somlo, 2014; Pala et al., 2017; Yoder, 2007; Yoder et al., 2002). Indeed, a recent study proposed that primary cilia length can regulate cystogenesis in ADPKD based on the ability of reduced primary cilia length to limit cyst formation in the kidney

and liver of both *Pkd1* and *Pkd2* knockout mice (Shao et al., 2020). Their data suggest a novel link between primary cilia length and disease severity. Firstly, the authors noticed that the primary cilia length gradually increased with disease progression in the polycystin knockout mice. Additionally, they found a positive correlation between cyst size and primary cilia length in small cysts below 2000mm^2 in human ADPKD kidneys (Shao et al., 2020). By genetically inactivating *Ift88* which encodes a core component of IFT, the lengthened primary cilia in *Pkd1* or *Pkd2* mutants were shortened to the level of wildtype, cyst growth was delayed, and proliferation was reduced through downregulation of Wnt/β-catenin, AMPK and mTOR pathways, showing that primary cilia length reduction, and not complete loss, is sufficient to suppress cystogenesis (Shao et al., 2020). Notably, the length of primary cilia inversely correlated with the degree of rescue in the double knockout mice, and there appears to be a dose-dependent rescue of cystic phenotypes depending on whether 1 or both alleles of *Ift88* are inactivated in a polycystin knockout background (Shao et al., 2020). Most recently, a novel role for primary cilia to function as a sensor for nutrient availability was demonstrated *in vitro* and *in vivo* (Steidl et al., 2023). Steidl *et al.* showed that primary cilia adjust their length as a response to nutrient availability, such that length increases in response to nutrient stress in cells deprived of glutamine and in mice fasted for 24 or 48 hours, while glutamine supplementation reverses this process *in vitro* and *in vivo* (Steidl et al., 2023). This finding is highly relevant as metabolic dysregulation, notably increase uptake of glutamine for growth, is well documented in both mouse models and human ADPKD tissue (Pagliarini & Podrini, 2021).

1.3.4.3 Cilia signaling in murine models of PKD

1.3.4.3.1 Disruption of ciliary genes causes cyst formation

Disruption of components of the IFT machinery (*Kif3a, Ift20* or *Ift88*) causes cilia loss and embryonic lethality, while conditional disruption in the kidneys induces renal cystogenesis (Davenport et al., 2007; Jonassen et al., 2008; Lin et al., 2003; Tian et al., 2017). Like the developmental switch observed between P13 and P14 in murine kidneys, when genes that are involved in mature renal function are induced while developmental genes are downregulated and significantly influence disease progression in conditional polycystin mutants, there appears to be a similar switch around the same time in ciliary mutants that equally determines the progressivity of cystogenesis (Ong & Harris, 2015; Patel et al., 2008; Sharma et al., 2013). For instance, the "switch" has been determined to be between P11 and P12 for *Ift88* mutants, such that *Ift88* mutants induced on and before, but not after, P11, develop cysts rapidly, while induction in adults leads to late onset and slow progressive disease (Sharma et al., 2013).

1.3.4.3.2 Cilia dependent cyst activation

Mutation of the polycystins alone is sufficient to induce renal cyst formation, and so is mutation of ciliary components (Davenport et al., 2007; Hopp et al., 2012; Jonassen et al., 2008; Lin et al., 2003; Shibazaki et al., 2008; Tian et al., 2017). However, when primary cilia are disrupted following inactivation of the polycystins, the developed cystic disease is severely restricted (Fedeles et al., 2014). This phenomenon is termed cilia dependent cyst activation (CDCA) and polycystins are thought to be negative regulators of CDCA; only in the presence of intact cilia does polycystin disruption drive destructive remodeling of kidney tubules and advancement to ADPKD (Ma et al., 2017; Ma et al., 2013). The severity of the cystic disease depends on the time interval between initial loss of polycystins and subsequent loss of primary cilia: longer time interval between those two events leads to more severe cystic phenotypes (Ma et al., 2017; Ma et al., 2013). Importantly, CDCA applies equally to PC1 and PC2, to early- and

late-onset disease models, and to both cystic kidneys and cystic livers; this degree of universality in the rescue of cystic phenotypes by inactivation of primary cilia genes following polycystin inactivation is remarkable (Ma et al., 2017; Ma et al., 2013). Ideally, a therapeutic strategy for ADPKD should be equally effective regardless of the timing or tissue of cyst formation.

1.3.4.3.3 Primary cilia-associated signaling

Primary cilia-associated receptors can integrate extracellular signals to coordinate cellular processes such as cell proliferation, differentiation and growth through pathways including Wnt, mTOR, and Hedgehog (Pala et al., 2017). Disruptions in signaling are associated with ciliopathies, and due to prevalence of ciliated cells such as those located on renal epithelial cells, can cause a wide spectrum of anomalies in multiple organs including polycystic kidneys (Anvarian et al., 2019; Badano et al., 2006; Bai et al., 2022). The exact roles of the primary cilia in different signaling pathways involved in PKD is still being debated and largely explored *in vitro* (Corbit et al., 2005; Corbit et al., 2008; Delling et al., 2013; Lancaster et al., 2011; Steidl et al., 2023; Tran et al., 2008; Viau, Kotsis, et al., 2020; Wann & Knight, 2012). There are several overlapping pathways that are involved in both PKD and regulated by primary cilia, yet only two studies have analyzed some of these pathways in polycystin cilia double knockout animals, namely ERK and mTOR (Ma et al., 2013; Shao et al., 2020). Some of the studies that have investigated primary cilia-associated signaling in PKD are highlighted below.

1.3.4.3.3.1 Wnt signaling

Primary cilia are proposed to regulate both canonical and non-canonical Wnt signaling, inducing downstream cellular processes that mediate diverse developmental and pathological events including cell proliferation and differentiation (Anvarian et al., 2019; Lal et al., 2008; Lancaster et al., 2011; Vlad et al., 2008). Wnts are lipoproteins that bind to Frizzled receptors to

activate Wnt signaling, which, within the primary cilia is complex and could be inhibiting or activating depending on the ciliary protein and inherent differences between model systems (Corbit et al., 2008; Kim, Arnould, Sellin, Benzing, Fan, et al., 1999; Lal et al., 2008; Lancaster et al., 2011; Nakaya et al., 2005; Pala et al., 2017; Wann & Knight, 2012). For instance, primary cilia restrain canonical Wnt signaling in mouse embryonic fibroblasts through Kif3a, as unciliated cells depleted of Kif3a respond to Wnt stimulation robustly more than ciliated cells as indicated by greater accumulation of β-catenin (Corbit et al., 2008). Another mechanism in which ciliary proteins regulate canonical Wnt signaling is demonstrated *in vitro* by the ciliary protein Jouberin (Jbn) through spatial compartmentalization during embryonic development, where Jbn dampens canonical Wnt signals by sequestering β-catenin from the nucleus to limit its nuclear entry (Lancaster et al., 2011). In contrast, HEK293 cells depleted of Kif3a activate β-catenin in the absence of Wnt stimulation (Corbit et al., 2008; Lancaster et al., 2011). The length of primary cilia is thought to determine the magnitude of canonical Wnt signaling, making it a key inducer of cystogenesis downstream of primary cilia (Wann & Knight, 2012). A multistage analysis of signaling pathways indicated that among Wnt, mTOR, Hedgehog and ERK, Wnt/β-catenin activation appears to be the earliest and most prominent event, the only one steadily activated from very early cystic stages when only slight dilations occur, to later cystic stages, in both *Pkd1* and *Pkd2* knockout mice (Shao et al., 2020). Interestingly, β-catenin is also the only one of the studied proteins completely restored following shortening of primary cilia length by genetically targeting *Ift88* in these mice (Shao et al., 2020).

1.3.4.3.3.2 mTOR signaling

Altered mTOR signaling has been documented in ADPKD and has been linked to cilia function in the regulation of cell size (Viau, Kotsis, et al., 2020). One of the downstream effects

of elevated mTOR signaling is a reduction in the amount of functional PC1 that traffics to the primary cilia (Pema et al., 2016). As described in section 1.1.2.1.1, the level of functional PC1 is determinant of the severity of the cystic phenotypes, hence, the amelioration in disease observed with rapamycin treatment, an mTOR inhibitor, may in part be due to an elevation/restauration of the level of functional PC1. One study measured mTOR activation in wildtype, *Pkd1* knockout and cilia *Pkd1* double knockout kidneys at multiple stages but found no difference, mTOR activation does not appear to be a major contributor to ADPKD in this model (Ma et al., 2013). A more recent study monitored the activation of mTOR signaling in adult-onset *Pkd1* and *Pkd2* knockout mouse models following primary cilia length reduction (Shao et al., 2020). The response of mTOR and AMPK to PC2 is quite controversial, but in this study the authors showed that in both *Pkd1* and *Pkd2* knockout mice, reduced AMPK activation is coupled with increased mTOR activation, and is partially normalized by inactivation of *Ift88* which caused shortened primary cilia length, supporting activating AMPK as a therapeutic approach for PKD caused by mutations in *Pkd2* (Shao et al., 2020). This is also coherent with the observation that metformin, which can also inhibit mTOR signaling, improves ADPKD in a *Pkd1* murine model of the disease (Pastor-Soler et al., 2022).

1.3.4.3.3.3 Hedgehog signaling

Abnormal Hedgehog (Hh) signaling has been reported to be one of the causes for the cystic phenotype in ADPKD (Corbit et al., 2005; Ma et al., 2017; Ong & Harris, 2015; Pala et al., 2017; Rohatgi et al., 2007; Tran et al., 2008; Wann & Knight, 2012). Hh signaling is critical during embryonic development and in adult stem cell function, requiring primary cilia for signal transduction (Corbit et al., 2008; Pala et al., 2017). Activation of Hh signaling pathway requires reciprocal translocation of Patched1 (Ptc1) away from the primary cilia coupled to Smoothened

(Smo) into the primary cilia; this activation requires Sonic Hedgehog (Shh) protein, which binds to Ptc1 receptors and prevents them from inhibiting Smo accumulation in the primary cilium (Rohatgi et al., 2007). Several components of the pathway such as Smo are constitutively found in primary cilia and their expression is markedly upregulated following stimulation by Shh (Rohatgi et al., 2007). Smo transition to the primary cilium appears to be a key regulated step in transducing Hh activation (Corbit et al., 2005). *Pkd2* knockout mice show increased Hedgehog signaling at cystic stages only, while Hh elevation seems to be less relevant in earlier disease stages, which leads to suggest that Hh signaling is unlikely a driver of cystogenesis (Shao et al., 2020). Interestingly, however, the investigators also observed that the shortening of primary cilia, greatly reduced Hedgehog signaling at all stages (Shao et al., 2020).

1.3.4.3.3.4 MAPK/ERK signaling

It is generally accepted that MAPK/ERK signaling is highly activated in PKD, however, studies in *Pkd1* mouse models show that it is unlikely to be responsible for primary cilia dependent cyst growth inducing signaling (Ma et al., 2013; Shao et al., 2020). Two independent studies, both using adult-onset *Pkd1* or *Pkd2* mouse models of ADPKD, showed that the elevation in MAPK/ERK signaling following inactivation of either polycystins remains stable upon removal or shortening of primary cilia (Ma et al., 2013; Shao et al., 2020). Additionally, multistage analysis also indicates that ERK is not activated until after cysts have developed, occurring much later than the above-mentioned pathways, suggesting ERK is not implicated in primary cilia mediated cyst growth (Ma et al., 2013; Shao et al., 2020). Whether cilia dependent MAPK/ERK signaling could be more relevant in early-onset mouse models remains to be studied (Ma et al., 2013; Shao et al., 2020). Whether cilia dependent MAPK/ERK signaling could be more relevant in early-onset mouse models remains to be studied.

1.4 Potassium channels are involved in fluid secretion and proliferation

As we proposed that the potassium channel Kcnn4 could be a potential member of the fluid secretory pathway in ADPKD, the characteristics of the potassium channel family as well as the secretive, proliferative, and pro-fibrotic properties of Kcnn4 that are relevant to ADPKD are described in the following sections.

1.4.1 Overview of the potassium channel family

1.4.1.1 Structure and expression

Potassium channels were initially described in nerve membranes where they mediate the potassium flow necessary for generating action potentials (Hille, 1992). Since then, potassium channels have been described in all cell types and in all organisms and implicated in a multitude of physiological functions (Checchetto et al., 2016; Gonzalez et al., 2012; Hibino et al., 2010; Miller, 2000; Nelson & Quayle, 1995; Shieh et al., 2000; Urrego et al., 2014). Potassium channels are tetrameric transmembrane aqueous pores that allow potassium flux and resemble PC2 in their structure; both carboxyl- and amino-termini localize in the cytoplasmic side of the membrane (Choe, 2002; Doyle et al., 1998; Gonzalez et al., 2012; Kuang et al., 2015). Their ubiquitous expressions and multifaceted functions are unlike any other ion channels, accentuating the importance of potassium channels in biological processes (Kuang et al., 2015; Villa & Combi, 2016). Potassium channels generally participate in physiological events by inducing membrane hyperpolarization following potassium secretion, a critical event that occurs in physiological contexts for various purposes, from action potential termination in excitable nerve cells to balancing electrolytes in non-excitable renal epithelial cells (Albaqumi et al., 2008; Bi et al., 2013; Devor et al., 1999; Kshatri et al., 2018; Larsen et al., 2014; Nelson & Quayle, 1995; Penna & Stutzin, 2015; Shumilina et al., 2008). Cells generally maintain a higher

cytoplasmic potassium concentration in comparison to extracellular space, hence, favouring opening of potassium channels which causes potassium outflow from the cytoplasm into the extracellular space and automatically prompts hyperpolarization (Kuang et al., 2015; Miller, 2000). There are four major subfamilies of potassium channels: six-transmembrane voltage-gated K_v, six-transmembrane K_{Ca}, two-transmembrane inward-rectifier K_{ir}, and four-transmembrane tandem pore domain channels (Kuang et al., 2015; Shieh et al., 2000).

1.4.1.2 Calcium-activated potassium channel family

The calcium-activated potassium channels (K_{Ca}) open in response to increases in cytosolic calcium and modulate calcium signaling and membrane potential in both excitable and non-excitable cells (Fioretti et al., 2006; Huang et al., 2014; Jin et al., 2019; Klein et al., 2009; Lozano-Gerona et al., 2020; Penna & Stutzin, 2015; Vandorpe et al., 1998; Wong & Schlichter, 2014; Yu et al., 2013). Human genome sequencing identified eight K_{Ca} channels that were initially categorized into two groups based on their genetics, single channel conductance and calcium sensing: the first group includes $K_{Ca}1.1$, $K_{Ca}4.1$, $K_{Ca}4.2$ and $K_{Ca}5.1$, whereas the second group consists of $K_{Ca}2.1$, $K_{Ca}2.2$, $K_{Ca}2.3$, and $K_{Ca}3.1$, which is described in detail in the following sections (Wei et al., 2005). Since then, K_{Ca} channels are more frequently defined by their single-channel conductance (small-, intermediate-, and large-conductance) and distinct pharmacological profiles: while large conductance calcium-activated potassium (BK) channels are gated by calcium and voltage, small (SK) and intermediate (IK) conductance calcium-activated potassium channels are gated exclusively by intracellular calcium and present a higher sensitivity to calcium than BK channels (Begenisich et al., 2004; Gueguinou et al., 2014; Ishii et al., 1997).

1.4.1.3 Implication of potassium channels in diseases

Potassium channels are implicated in vital cellular signaling processes that in pathophysiological conditions drive disease progression (Checchetto et al., 2016; Gonzalez et al., 2012; Miller, 2000; Shieh et al., 2000; Urrego et al., 2014). Members of the potassium channel family are critical for membrane excitability that regulate processes such as epithelial electrolyte transport, smooth muscle contraction, cell volume regulation and neuronal excitability, to ensure proper functioning of vital organs such as the heart, where functioning channels are critical to sustain a normal heartbeat (Bardou et al., 2009; Cruse et al., 2006; Duffy et al., 2015; Gonzalez et al., 2012; Hibino et al., 2010; Kshatri et al., 2018; Nelson & Quayle, 1995; Schilling et al., 2004; Schwab et al., 2012; Sforna et al., 2018; Shieh et al., 2000; Tharp et al., 2006; Villa & Combi, 2016). This critical process requires coordination between various classes of potassium channels to allow the tight regulation and right execution of each phase (Grandi et al., 2017; Schmitt et al., 2014; Tamargo et al., 2004). Additionally, mutations in potassium channels and/or altered channel function have been described in various pathophysiological conditions and genetic diseases of the heart, kidney, pancreas, and central nervous system, all of which provide a basis to develop appropriate therapies targeting potassium channels (Albaqumi et al., 2008; Bardou et al., 2009; Bi et al., 2013; Ghanshani et al., 2000; Huang et al., 2014; Pellegrino & Pellegrini, 1998; Rapetti-Mauss et al., 2015; Schwab et al., 2012).

1.4.2 Intermediate conductance calcium activated potassium channel KCNN4

1.4.2.1 Structural features, tissue localization, and calcium dependency

The intermediate conductance channel $K_{Ca}3.1$ (also known as KCNN4, SK4, IK1, will be called KCNN4 or Kcnn4 in the following sections) is encoded by the *KCNN4* gene on human chromosome 19 and is prominently expressed in hematopoetic cells and in organs involved in salt and fluid transport in several tissues, including the colon, lung, kidney, and salivary glands

(Albaqumi et al., 2008; Anumanthan et al., 2018; Begenisich et al., 2004; Chiang et al., 2017; Cruse et al., 2006; Doyle et al., 1998; Gueguinou et al., 2014; Ishii et al., 1997; Jensen et al., 1998; Lozano-Gerona et al., 2020; Nelson & Quayle, 1995; Pellegrino & Pellegrini, 1998; Penna & Stutzin, 2015; Philp et al., 2018; Vandorpe et al., 1998; von Hahn et al., 2001). It was first described by Gardos in 1958 when he noticed that calcium is required for potassium efflux to occur in erythrocytes (Gardos, 1958). Four decades later, the human intermediate-conductance potassium channel (hIK1) was cloned from the pancreas in 1997 by scientists at Oregon Health Sciences University and Icagen (Ishii et al., 1997). Structural analysis revealed hIK1 as a homotetrameric membrane protein; each subunit is organized into six transmembrane segments (S1 to S6) with a pore motif between S5 and S6 (Sforna et al., 2018). Expressing hIK1 in *Xenopus* oocytes bathed in potassium led to inwardly rectifying potassium current (potassium flow into cells) as measured by inside-out patch-clamp recording. This potassium current can be activated by sub-micromolar concentrations of intracellular calcium ($K_{0.5}$=0.3μM), which binds to the EF-hand motif in calmodulin, a calcium sensor constitutively associated with the carboxyl-terminal of hIK1 (Gerlach et al., 2000; Ishii et al., 1997; Vandorpe et al., 1998). Within the potassium channel family, hIK1 is highly conserved among species and is most structurally similar to the SK channel subfamily, sharing 87% sequence similarity with murine Kcnn4; both are equally sensitive to calcium activation, but hIK1 has higher calcium affinity (for activation) than SK, which means at levels near resting internal calcium level (~0.1μM): hIK1 would be activated but SK channels would be silent (Gerlach et al., 2000; Ishii et al., 1997; Vandorpe et al., 1998). In fact, SK channels expressed in *Xenopus* oocytes are inactive without elevating internal calcium, while IK channels already show some basal activity (Gerlach et al., 2000; Ishii et al., 1997; Vandorpe et al., 1998). Originally identified and thought to be exclusively expressed

in non-excitable tissues, Kcnn4 was later also found in excitable tissues (Gueguinou et al., 2014; Sforna et al., 2018; Shieh et al., 2000). Since then, Kcnn4 has been identified in a wide range of tissues, most notably and perhaps the most extensively studied being erythrocytes, vascular smooth muscle cells and neurons (Bi et al., 2013; Gilli et al., 1998; Grgic, Kaistha, et al., 2009; Gueguinou et al., 2014; Kshatri et al., 2018). Structural studies indicate that the activation gate of Kcnn4 lies within the channel pore; therefore, modulators are vastly designed to bind there (Doyle et al., 1998; Gonzalez et al., 2012; Kuang et al., 2015).

1.4.2.2 Physiological roles of Kcnn4 learned from pathophysiological disorders

Until now, only one human disease caused by mutations in *KCNN4* has been described, hereditary xerocytosis, a rare autosomal dominant congenital hemolytic anemia characterized by abnormal erythrocyte hydration, but otherwise non-life threatening (Rapetti-Mauss et al., 2015). Elevation in Kcnn4 expression is well documented in many pathophysiological conditions including cancer, immune disorders, and vascular inflammation, while modulation of Kcnn4 expression and activity has been reported to influence therapeutic outcomes (Anumanthan et al., 2018; Di et al., 2010; Flores et al., 2007; Grgic, Kiss, et al., 2009; Huang et al., 2014; Jin et al., 2019; Klein et al., 2009; Paka et al., 2017; Philp et al., 2018; Yu et al., 2013), including one study in which they found exacerbation of skin diseases in epidermal *Kcnn4* transgenic mice (Lozano-Gerona et al., 2020). Because of its ubiquitous expression, lack of phenotypes in *Kcnn4* knockout mice and a good tolerance to Kcnn4 inhibitors in clinical trials (Ataga et al., 2008; Begenisich et al., 2004; Sforna et al., 2018; Wulff & Castle, 2010), Kcnn4 constitutes an attractive target to improve conditions ranging from atherosclerosis and tumor progression to asthma and brain injury (Ataga et al., 2011; Ataga et al., 2021; Granfeldt et al., 2022; Icagen, 2009b; Jin et al., 2019; Paka et al., 2017; Tubman et al., 2016). Perhaps the most relevant and

widespread role of Kcnn4 is attributed to the regulation of cellular calcium signaling; by inducing hyperpolarization through potassium secretion, Kcnn4 promotes calcium entry through calcium release-activated calcium (CRAC) channels (Bi et al., 2013; Cahalan & Chandy, 1997; Duffy et al., 2015; Joiner et al., 2001; Kshatri et al., 2018; Pellegrino & Pellegrini, 1998; Penna & Stutzin, 2015; Sforna et al., 2018; Tharp et al., 2006). Other processes regulated by Kcnn4 include T lymphocyte activation, volume regulation in erythrocytes, proliferation of vascular smooth muscle cells (VSMC), fibrosis, and inflammation (Bi et al., 2013; Di et al., 2010; Grgic, Kiss, et al., 2009; Stocker et al., 2003; Yu et al., 2013).

1.4.2.2.1 Volume regulation and fluid secretion

Our initial understanding of the physiological role of Kcnn4 came from Gardos when he demonstrated in erythrocytes that calcium entry activated potassium efflux (Gardos, 1958). The channel responsible for this potassium conductance was later identified as Kcnn4, which not only allowed potassium efflux but also promoted water loss in erythrocytes, inducing dehydration and shrinkage, the cause of sickle cell anemia (Ataga et al., 2011; Ataga et al., 2008; Brugnara et al., 1996; De Franceschi et al., 1994; Stocker et al., 2003). Epithelial cells were later found to be the major conduit for Kcnn4 to actively drive electrolyte and fluid transport, hence the channel's widespread expression in epithelia lining the gastrointestinal tract and lung, in ducts of fluid secreting glands such as the salivary gland and pancreas, and in stratified epithelia including cornea and skin (Anumanthan et al., 2018; Bernard et al., 2003; Devor et al., 1999; Duffy et al., 2015; Flores et al., 2007; Hoffmann & Simonsen, 1989; Klein et al., 2009; Lozano-Gerona et al., 2020; Rufo et al., 1996; Vandorpe et al., 1998; Yu et al., 2013). Subcellularly, Kcnn4 is generally localized to the basolateral membrane, where it maintains a polarized potassium flow to facilitate apical chloride secretion and water transport (Fig. 1) (Devor et al., 1999; Rufo et al.,

1996). Aside from the tissues mentioned above, volume regulation by Kcnn4 has been demonstrated in other cell types such as T lymphocytes and mast cells, indeed, *Kcnn4* knockout mice have been shown to be less responsive to environmental osmotic changes (Begenisich et al., 2004; Vandorpe et al., 1998). Perhaps the most relevant example of volume regulation through Kcnn4 demonstrated in both clinical and pre-clinical settings is in sickle cell anemia, where the augmented Kcnn4 activity accelerates water loss and causes shrinkage of erythrocytes, giving rise to the sickled erythrocyte shape frequently found in patients and *in vivo* (Ataga et al., 2006; Ataga et al., 2011; Ataga et al., 2008; Ataga et al., 2021; Brugnara et al., 1996; De Franceschi et al., 1994; Icagen, 2003; Stocker et al., 2003). Volume regulation by Kcnn4 is likely mediated by other channels, one of which being chloride channels; indeed, the involvement of Kcnn4 in anion secretion was demonstrated in mouse intestines where abolition of anion secretion and increased stool dehydration were found in mice lacking *Kcnn4* (Flores et al., 2007). In addition, dehydration of sickled erythrocytes appears to result from hyperactivated Kcnn4 channel as well as the potassium-chloride cotransport pathway (Ataga et al., 2008). More relevant to ADPKD, Kcnn4 is essential for Cftr-mediated chloride secretion, cyst formation and enlargement in MDCK cells and ADPKD cyst derived primary cultures; modulation of Kcnn4 with an inhibitor or an activator greatly affected Cftr activity and cyst size, clearly demonstrating Kcnn4's close association with Cftr and critical role in ADPKD cyst progression (Albaqumi et al., 2008).

Proper cell volume regulation also concerns fundamental biological processes such as cell proliferation, migration, and apoptosis (Hoffmann & Simonsen, 1989). Cell membranes are highly permeable to water, and the regulatory volume decrease (RVD) mechanism is activated in swelling cells to restore cell volume, where an increase in cytosolic calcium induces or facilitates the combined electroneutral efflux of potassium, chloride, organic osmolytes and the extrusion of

osmotic water (Hoffmann & Simonsen, 1989). The calcium dependence of RVD correlates with the calcium dependency of potassium efflux, in most cases mediated by Kcnn4, the first evidence came from cloned mIK1 Kcnn4 channel expressed in *Xenopus* oocytes (Vandorpe et al., 1998). While control oocytes subjected to hypotonic solution swelled without inducing RVD, mIK1-expressing oocytes showed a marked RVD response that was sensitive to Kcnn4 blocker and to calcium chelating agents (Vandorpe et al., 1998). Since then, the critical role of Kcnn4 in the RVD response has been identified in different cell types including glioma C6 cells, where a gradual but not a sudden decrease in osmolarity can activate Kcnn4 channels (Ordaz et al., 2004).

1.4.2.2.2 Calcium signaling and proliferation

Perhaps the most well-defined role of Kcnn4 is to regulate calcium entry into cells, which is necessary for the modulation of calcium signaling to ensure proper functioning of physiological processes (Cahalan & Chandy, 2009; Doyle et al., 1998; Gueguinou et al., 2014). Calcium influx through store operated Orai calcium channels following depletion of calcium from the ER causes membrane depolarization, which limits additional calcium entry through CRAC or TRP channels due to reduced electrochemical driving force for calcium, but calcium dependent ion channels such as Kcnn4 can be activated by the elevation in intracellular calcium (Duffy et al., 2015; Gueguinou et al., 2014). In fact, Kcnn4 has also been shown to interact physically with Orai1 in human lung mast cells, suggesting that calcium influx through Orai1 in particular facilitates Kcnn4 activation through the proximity of Kcnn4's calcium-binding microdomain to the store-operated calcium channel (Duffy et al., 2015). Potassium efflux through Kcnn4 could subsequently oppose the membrane depolarization, hence increasing the electrochemical force to facilitate calcium entry, establishing a positive feedback loop where

calcium influx stimulates potassium efflux and causes hyperpolarization which then further promotes calcium entry, ultimately amplifying signal transduction. This paradigm is well demonstrated in macrophages, mast cells, and T cells (Cahalan et al., 2001; Penna & Stutzin, 2015; Shumilina et al., 2008). Indeed, activated T cells isolated from *Kcnn4* knockout mice show reduced calcium response to T cell receptor activation (Di et al., 2010). The prerequisite role of Kcnn4 in calcium signaling has been demonstrated for the production of inflammatory chemokines and cytokines and in macrophages and mast cells (Cruse et al., 2006; Ghanshani et al., 2000), as well as for the migration of macrophages, microglia, VSMC, and mast cells (Chung et al., 2002; Cruse et al., 2006; Schilling et al., 2004; Tharp et al., 2006). The need for Kcnn4 mediated calcium signaling in proliferation has been shown in several cell types including VSMC, endothelial cells, T and B cells, fibroblasts, stem cells and cancer cells, as proliferation in these contexts is associated with elevation in Kcnn4. In contrast, proliferation is inhibited when Kcnn4 is blocked (Anumanthan et al., 2018; Bi et al., 2013; Cruse et al., 2006; Ghanshani et al., 2000; Huang et al., 2014; Millership et al., 2011; Shumilina et al., 2008; Tharp et al., 2006; Urrego et al., 2014). For instance, Kcnn4 regulates proliferation in VSMC by modulating the expression of transcription factors and cyclins through intracellular calcium levels, hence, overexpression (inducing proliferation) or blockade (inhibiting proliferation) of Kcnn4 can modulate the development of vascular disease (Bi et al., 2013). Interestingly, the proliferative potential of Kcnn4 is independent of potassium conductance (Millership et al., 2011). It is known that ion channels can have non-conducting functions such as participation in intracellular signaling pathways by activating enzymes linked to these pathways, and this function does not depend on their activity as ion channels (Forzisi & Sesti, 2022). Potassium channel expression is in fact linked to cell proliferation; normally not found in proliferating cells, their expression is

highly upregulated in certain cancers (Kaczmarek, 2006). Transfection of mutant Kcnn4 (trafficking mutant, functional mutant without K^+ conductance or Ca^{2+} entry stimulation) into HEK293 cells does not inhibit Kcnn4's ability to increase proliferation, indicating Kcnn4 induces proliferation is independent of its function as a conducting ion channel but rather dependent on ERK1/2 and JNK MAPK signaling pathways (Millership et al., 2011).

1.4.2.2.3 Fibrosis

Implication of Kcnn4 in the development of fibrotic disorders has been demonstrated in the kidney, cornea, liver, and lung, and is largely mediated through TGF-β1 signaling via the MAPK/ERK pathway (Anumanthan et al., 2018; Cruse et al., 2006; Grgic, Kiss, et al., 2009; Huang et al., 2014; Paka et al., 2017; Roach et al., 2015). Renal fibrosis can be induced in mice by unilateral ureteral obstruction (UUO) where Kcnn4 is selectively upregulated in affected kidneys and in murine renal fibroblasts, but not the related channel subtypes $K_{Ca}1.1$ and $K_{Ca}2.3$, accompanied by increased expression of fibrotic markers including *collagen I, III* and *TGFβ* (Grgic, Kiss, et al., 2009). Targeting Kcnn4 genetically or with an inhibitor *in vivo* following UUO significantly suppressed development of renal fibrosis, reducing expression of fibrotic markers, lowering collagen deposition, and preserving renal parenchyma (Grgic, Kiss, et al., 2009). Kcnn4's pro-fibrotic role in the kidney is also demonstrated in diabetic nephropathy (DN), characterized by tubulointerstitial fibrosis involving myofibroblast activation and ECM accumulation, which ultimately leads to loss of renal function (Huang et al., 2014). Kcnn4 inactivation or inhibition in a mouse model of DN attenuated the disease as shown by the reduction in activation of fibroblasts and TGF-β1-induced signaling that facilitates ECM production, ultimately reducing interstitial fibrosis in the kidneys (Huang et al., 2014). To study Kcnn4's role in mediating fibrosis in the cornea, wildtype and *Kcnn4* knockout mice were

subjected to alkali injury (Anumanthan et al., 2018). The cornea haze caused by alkali injury was much less severe in the *Kcnn4* knockout mice in comparison to the wildtype, paralleled by lowered activation in the expression of pro-fibrotic markers such as *collagen type I* as well as reduced myofibroblast differentiation, contributing to a lower non-functional mass of fibrotic tissues in the absence of *Kcnn4* (Anumanthan et al., 2018). Likewise, pharmacologic inhibition of Kcnn4 significantly limited *TGF-β1*-activated pro-fibrotic gene expression and differentiation of fibroblasts into myofibroblasts, which is essential for progression of fibrosis (Anumanthan et al., 2018). The involvement of Kcnn4 in fibrosis progression in the liver has been studied in a model of non-alcoholic fatty liver disease (NAFLD), one of the features being excessive liver fibrosis that can ultimately contribute to organ failure (Paka et al., 2017). Targeting the highly elevated *Kcnn4* expression in NAFLD mice led to reduced TGF-β1 signaling, mitigating hepatic collagen accumulation, and thus helped preserve liver issue (Paka et al., 2017). Similarly, blocking Kcnn4 in primary human lung myofibroblasts derived from idiopathic pulmonary fibrosis (IPF) attenuated TGF-β1 dependent signaling and reduced type I collagen, limiting the pro-fibrotic activity of these cells (Roach et al., 2015).

1.4.2.2.4 T cell activation and immune response

While resting T cells show low baseline *Kcnn4* expression, *Kcnn4* is strongly upregulated during T cell activation by mitogens (Cahalan & Chandy, 2009; Chiang et al., 2017; Chimote et al., 2013; Di et al., 2010; Ghanshani et al., 2000). Stimulation of T cell receptors activates tyrosine kinases and calcium permeable ion channels found in the ER and on T cell membranes. Calcium does not appear to enter cells through inositol triphosphate (IP_3) but rather travel across the plasma membrane CRAC channels which are gated by calcium; once opened, an electrochemical gradient is required to drive calcium entry (Fracchia et al., 2013; Srivastava et

al., 2006; Srivastava et al., 2005; Trebak & Kinet, 2019). Both voltage-gated and calcium-activated potassium channels could participate in this process, allowing potassium efflux and facilitating hyperpolarization (Bardou et al., 2009; Chiang et al., 2017; Chimote et al., 2013; Fanger et al., 2001; Rader et al., 1996). More specifically, the resting membrane potential in T cells is uniquely set by the voltage-gated potassium channel, while calcium-activated channels are opened in response to a rise in calcium following T cell receptor engagement (Agarwal et al., 2019; Cahalan & Chandy, 1997; Chiang et al., 2017; Coleman et al., 2014; Thompson & Begenisich, 2009). While freshly isolated resting human T cells express 30-fold more voltage-gated potassium channels than Kcnn4, Kcnn4 is strongly enhanced as T cells become activated to proliferate, while voltage-gated potassium channels are sustained and only experience a modest enhancement (Chiang et al., 2017). Changes in expression have also been reported in murine T cells and in murine and human B cells (Ghanshani et al., 2000). Given Kcnn4's important role in T cell activation and expression in various immune cells, targeting Kcnn4 is attractive in modulating autoimmune responses by previously activated T cells.

1.4.2.3 *Kcnn4* knockout mice are indistinguishable from wildtype

It is important to check for health status of *Kcnn4* knockout mice before initiating mouse studies. Despite the ubiquitous expression of *Kcnn4*, no alterations in any major organs, health or fertility have been reported by Begenisich *et al.* (Begenisich et al., 2004) or our lab (unpublished observations) in the *Kcnn4* knockout mouse model. The lack of developmental abnormality might suggest that Kcnn4 could be compensated by other potassium channels. An example of a compensatory mechanism is demonstrated in T cells between Kcnn4 and voltage gated $K_v1.3$, the two dominant potassium channels expressed in human and rat T cells, where they complement and compensate each other to ensure proper regulation of redundant roles,

depending on stimulation (Cahalan & Chandy, 2009; Chiang et al., 2017). There are specific settings, such as responding to repeated tetanus toxoid stimulation where both are required, but for normal T cell activation, Kcnn4 can compensate for K_v1.3 as demonstrated in a *K_v1.3* knockout rat model that display a normal immune response following T cell activation (Chiang et al., 2017). However, for the development of the chronically activated effector memory T cell response, K_v1.3 is indispensable and cannot be replaced by Kcnn4 (Chiang et al., 2017). I contrast, Kcnn4 and K_{Ca}1.1 show an opposite interaction in the salivary glands where Kcnn4 inhibits K_{Ca}1.1 activity, likely achieved by their spatial proximity, such that Kcnn4 activation causes its amino-terminal to insert itself through the cytoplasmic side into the K_{Ca}1.1 channel, inhibiting ion flow (Thompson & Begenisich, 2009).

1.4.2.4 Modulators of Kcnn4 function and expression

1.4.2.4.1 Modulators of gating and function

1.4.2.4.1.1 cAMP

Kcnn4 modulation by cAMP through activation of PKA displays differences between species, cell types and the experimental approaches (Neylon et al., 2004; Pellegrino & Pellegrini, 1998; Sforna et al., 2018; von Hahn et al., 2001). Importantly, the modulation is positive in renal epithelia, where cAMP can elevate Kcnn4 channel activity (Albaqumi et al., 2008).

1.4.2.4.1.2 Calcium and calmodulin

The Kcnn4 channel opens following a small rise in calcium (from intracellular stores or through store operated calcium channels) that binds to calmodulin at Kcnn4's carboxyl-terminal, causing conformational change in calmodulin that opens Kcnn4 channel (Sforna et al., 2018). Calmodulin is highly conserved, presenting two globular lobes (N- and C-lobe) each containing two pairs of EF-hand motifs for a total of four calcium binding sites with vastly different

affinities to calcium (Gilli et al., 1998; Joiner et al., 2001; Sforna et al., 2018; Wong & Schlichter, 2014). Calcium-calmodulin binding and subsequent channel opening occur as a highly coordinated sequential event: as calcium binds to the motif with the highest affinity, it triggers conformational changes in calmodulin that increase the calcium binding affinity of the other sites (Gilli et al., 1998).

The association of calmodulin to its binding site at the Kcnn4 carboxyl-terminal is critical for the surface expression and tetramerization of Kcnn4 subunits (Joiner et al., 2001). The carboxyl-terminal leucine zipper domain is required for correct folding of its carboxyl-terminal domain and Kcnn4 trafficking to the plasma membrane (Syme et al., 2003). Kcnn4 has a short half-life (60-90 minutes) on the plasma membrane due to the very efficient internalization mediated by motifs in the carboxyl-terminal, and as a result, likely provides rapid changes in Kcnn4 plasma membrane expression (Schwab et al., 2012).

1.4.2.4.1.3 ATP

Kcnn4 is positively modulated by intracellular ATP through its interaction with a region in the protein's carboxyl-terminal tail, in proximity of the calmodulin domain, that can bind the activated nucleoside diphosphate kinase B (NDPK-B) which in turn phosphorylates the histidine within the motif, increasing Kcnn4 activity (Srivastava et al., 2006). Phosphorylation of the carboxyl-terminal region activates Kcnn4 while dephosphorylation inhibits Kcnn4 activity. NDPK-B as a Kcnn4 activator, is also a downstream effector of phosphoinositol-3-phosphate (PI3P), which is stably bound to the carboxyl-terminal of Kcnn4 and was shown to activate Kcnn4 channel (Srivastava et al., 2005). These findings suggest that PI3P levels are carefully controlled in the immediate vicinity of Kcnn4 to tune the needed channel activity of Kcnn4.

1.4.2.4.2 Modulators of *KCNN4* expression

1.4.2.4.2.1 c-Myc

Just over a decade ago while our collaborator was studying the regulation of transcription factors krüppel-like factor 1 (KLF1) and KLF2 on embryonic erythropoiesis, they noticed that the *KLF1*$^{-/-}$ *KLF2*$^{-/-}$ double knockout embryos were more anemic compared to single knockouts (Basu et al., 2007). To identify the genes causing this phenotypic difference, we conducted the ingenuity pathway analysis (IPA) and found that *Myc* is synergistically regulated by both *KLF1* and *KLF2* and more importantly, revealed that *KCNN4* is downstream of *MYC* (Pang et al., 2012).

1.4.2.4.2.2 MAPK/ERK

At the protein level, Kcnn4 function is increased by PKA and nucleoside diphosphate kinase B (NDPK-B) and inhibited by histidine phosphatase PHPT1 (Wulff & Castle, 2010). In T lymphocytes, the ERK1/2 pathway stimulates AP-1 and promotes the Kcnn4 current and cell proliferation (Ghanshani et al., 2000). In accordance, *Kcnn4* expression is positively modulated by ERK1/2 activity in GL-15 human glioblastoma cells and is particularly highly expressed in tumor cells (Fioretti et al., 2006).

1.4.2.4.2.3 AP-1 and REST

At the gene level, *KCNN4* transcription can be repressed by the Repressor Element 1-Silencing Transcription factor (*REST*) and activated through transcription factors Activation Protein-1 (*AP-1*) and Ikaros-2 (*Ik-2*) (Wulff & Castle, 2010). The *KCNN4* gene contains two Restrictive Element 1 (RE-1) sites where *REST* can bind to repress *KCNN4* gene transcription, reducing functional Kcnn4 level in accordance, such that when *REST* expression is reduced, *KCNN4* expression is upregulated, hence facilitating proliferation as demonstrated in VSMC (Cheong et al., 2005). Additionally, within the promoter region of *KCNN4*, there is a binding site

for *AP-1* to bind to augment *KCNN4* expression during specific cellular events such as T cell activation (Ghanshani et al., 2000). In T cells, *AP-1* dependent transcription of *KCNN4* occurs through stimulation of PKC and downstream Ras and JNK pathways, the resulting AP-1 (c-Fos/c-Jun heterodimer) complex binds to KCNN4 promoter and initiates transcription in conjunction with Ik-2, which sets a threshold for T cell mitogenesis (Ghanshani et al., 2000).

1.4.2.5 Pharmacological modulators of Kcnn4

1.4.2.5.1 Inhibitors of Kcnn4

The classic Kcnn4 inhibitors are peptide toxins and encompass charybdotoxin and maurotoxin, which bind Kcnn4 with high affinity (IC_{50} in the nM range), but they often block other potassium channels simultaneously (Bernard et al., 2003; Cruse et al., 2006; Ishii et al., 1997; Jensen et al., 1998; Ordaz et al., 2004; Rader et al., 1996; Schilling et al., 2004; Wulff et al., 2001). Since then, efforts to produce Kcnn4 inhibitors using the clotrimazole template have made several compounds available with greater affinity and selectivity, the most widely used being TRAM-34 (Agarwal et al., 2013; Albaqumi et al., 2008; Anumanthan et al., 2018; Grgic, Kiss, et al., 2009; Roach et al., 2015). Some of the most employed inhibitors of Kcnn4 are described below.

1.4.2.5.1.1 Clotrimazole

Clotrimazole blocks Kcnn4 by binding to its inner pore, and was one of the first compounds used to demonstrate that inhibition of Kcnn4 can reduce erythrocyte dehydration in mouse models and clinical trials of sickle cell disease (SAD) (Brugnara et al., 1996; De Franceschi et al., 1999; De Franceschi et al., 1994). Clotrimazole in clinical trials was generally well tolerated at doses up to 20mg/kg per day, but is unsuitable for long term use due to poor absorption, short half-life, and liver damage (Brugnara et al., 1996). Hence, the development of

clotrimazole as a treatment for sickle cell disease did not proceed. Instead, clotrimazole was modified to reduce adverse effects, one of the derivatives being TRAM-34.

1.4.2.5.1.2 TRAM-34

TRAM-34 binds to the inner pore of Kcnn4 like clotrimazole and blocks Kcnn4 with an IC_{50} of 20nM; it is 200- to 500-fold more selective for K_v channels and 1000-fold more selective for $K_{Ca}1.1$ and $K_{Ca}2$ channels than clotrimazole (Wulff et al., 2000). Contrary to clotrimazole, TRAM-34 was reported to not affect cytochrome P450 (CYP) activity thus reducing the risk of hepatotoxicity (Wulff et al., 2001). However, a more recent study later found that low micromolar concentration of TRAM-34 can in fact inhibit several CYP isoforms in rat and human and cautioned usage at high concentrations (Agarwal et al., 2013).

1.4.2.5.1.3 Senicapoc

Senicapoc (ICA-17043; bis(4-fluorophenyl)phenyl acetamide) is another derivative of clotrimazole and was initially developed for treatment of sickle cell anemia by scientists at Icagen Inc. Senicapoc shows a great potency with an IC_{50} of 11nM and an outstanding 900-fold selectivity for Kcnn4 over other potassium channels while displaying a promising pharmacokinetic and safety profile, selectively inhibiting potassium efflux from red blood cells of both human patients and sickle cell disease transgenic mouse models (Ataga et al., 2006; Ataga et al., 2011; Ataga et al., 2008; Brugnara et al., 1996; De Franceschi et al., 1994; Icagen, 2003; Stocker et al., 2003). Senicapoc is orally bioavailable in humans with superior metabolic stability (half-life of 12.8 days, 1 hour in mouse and 4 hours in rats) compared to previous Kcnn4 inhibitors, namely clotrimazole and TRAM-34, which have shorter half-life, are not orally available, and are sensitive to acid (Ataga et al., 2006). Sickle cell anemia is caused by a mutation in the hemoglobin gene and is characterized by erythrocyte dehydration due to loss of

potassium, chloride, and water (Stocker et al., 2003). Volume decrease causes erythrocytes to attain an abnormal rigid sickled shape which functionally causes increases in hemoglobin concentration and leads to an increased rate of hemoglobin polymerization under hypoxic conditions (Ballas & Smith, 1992; Brittenham et al., 1985; De Franceschi et al., 1999). As the hemoglobin S polymerization is highly dependent on its concentration, small increases dramatically enhance its rate of polymerization and the ensuing cell sickling, causing irreversibly sickled, dense and dehydrated erythrocytes that are more susceptible to becoming trapped in the capillaries and could lead to microvascular obstructions and chronic organ damage (Ballas & Smith, 1992; Brittenham et al., 1985). Senicapoc was designed to target Kcnn4 for treatment of sickle cell anemia as one of the main routes of potassium loss is through the Gardos channel, later known as Kcnn4 (De Franceschi et al., 1999; Gardos, 1958; Ishii et al., 1997; Stocker et al., 2003). Senicapoc was first tested in the SAD mouse and showed improved disease outcome; mice who received 10mg Senicapoc/kg of body weight orally twice a day for 21 days showed marked and constant inhibition of the Gardos channel activity, an increase in erythrocyte potassium content and decrease in hemoglobin concentration (De Franceschi et al., 1999; Stocker et al., 2003). More importantly, Senicapoc was well-tolerated with no sign of toxicity or body weight change. Recently, Sorensen *et al.* developed a high-throughput, sensitive and accurate method for determining Senicapoc concentration in plasma samples by using a ultra-high-performance liquid chromatography-tandem mass spectrometry method that could be useful for monitoring efficiency of Senicapoc intake for future studies (UHPLC-ESI-MS/MS) (Sorensen et al. 2021).

1.4.2.5.2 Activators of Kcnn4

Activators increase calcium affinity/potency for channel activation, therefore lower calcium concentration is needed to open the gate. Several compounds have been developed to increase the single channel open probability of Kcnn4 in a calcium-dependent manner, the classical one being the benzimidazolone 1-EBIO (von Hahn et al., 2001). The related dichloro-EBIO (DCEBIO) is 10-fold more potent (Strobaek et al., 2004). Neuroprotectant riluzole and its more selective derivative SKA-31 were developed later (Coleman et al., 2014). However, all of them are not very selective for Kcnn4 and only display 3- to 5-fold selectivity over $K_{Ca}2$ channels.

1.4.2.5.2.1 SKA-31 and SKA-111

As SK and IK channels are both activated by the calcium/calmodulin-mediated gating mechanism, there are positive gating modulators that activate both channels with similar potency (Albaqumi et al., 2008; Bernard et al., 2003; Coleman et al., 2014; Devor et al., 1999; Duffy et al., 2015; Strobaek et al., 2004; von Hahn et al., 2001; Yu et al., 2013). EBIO was initially developed and activates Kcnn4 with an EC_{50} of ~30μM, two structurally similar but more potent activators NS309 and SKA-31 were later developed (Coleman et al., 2014; Strobaek et al., 2004). NS309 has an EC_{50} of ~20nM but has an extremely short half-life *in vivo*. In contrast to the previous activators which show only 5- to 10-fold selectivity over IK, SKA-31 activates SK with an EC_{50} of 3mM and Kcnn4 with a much lower EC_{50} of 260nM, and while SKA-31 is 10 times less potent than NS309, it has become relatively widely used *in vivo* due to its long half-life of 12 hours in rats (Coleman et al., 2014). SKA-31was further modified to produce the more potent SKA-121 which activates Kcnn4 with an EC_{50} of 111nM (Coleman et al., 2014). An even more potent activator, SKA-111, that displays 123-fold selectivity for Kcnn4 over SK channels and over 200-fold selectivity over voltage-activated potassium, sodium, and calcium channels

was later generated (Coleman et al., 2014). Importantly, SKA-111 has a much longer half-life and is more brain penetrant than SKA-121.

1.4.2.6 Senicapoc in clinical trials

Senicapoc was originally designed for sickle cell anemia but is still actively being repurposed today for other conditions due to its safety profile. Some of the recently completed or currently ongoing clinical trials are described below.

1.4.2.6.1 Sickle cell anemia

The rate of vaso-occlusive painful crisis is the major clinical manifestation and is the primary clinical endpoint of sickle cell anemia, while the secondary end point is determined by hematological parameters including percentage of dense erythrocytes, reticulocytes, and various markers of hemolysis such as lactate dehydrogenase (Ataga et al., 2011; Ataga et al., 2008; Icagen, 2003; Icagen et al.). The Phase II trial was very promising and consisted of a 12-week treatment involving low-dose (6mg/day, 100mg loading dose), high-dose (10mg/day, 150mg loading dose) and placebo groups (Ataga et al., 2008; Icagen, 2003). In the high dose group, hemoglobin concentration increased with concomitant decrease in hemolysis, suggesting a possible increase in survival of sickled erythrocytes. The low dose group showed similar but smaller improvements in all parameters suggestive of a dose-dependent response. Together these changes in hematological parameters showed improvement in survival of sickled erythrocytes and amelioration of the anemic state (Ataga et al., 2008; Icagen, 2003). The safety and efficacy of Senicapoc were evaluated in parallel and indicated a good overall safety profile and good tolerance in both patients and healthy volunteers (Ataga et al., 2006; Ataga et al., 2011; Ataga et al., 2008). The most frequent adverse events reported were diarrhea and nausea which occurred sporadically and appeared dose-dependent, described as mild to moderate in intensity, but no

difference was detected in overall frequency of painful crises with Senicapoc treatment (Ataga et al., 2011). Furthermore, Senicapoc has shown favourable pharmacokinetics with a long half-life that permits once-daily dosing, therefore allowing easier repurposing for other disorders, including Alzheimer's and asthma, for which Senicapoc has progressed into clinical trials (Ataga et al., 2006; Jin et al., 2019; Shieh et al., 2000; Wulff & Castle, 2010). More recently, Senicapoc is evaluated in a clinical trial to treat COVID-19 patients in intensive care (Granfeldt et al., 2022). Despite the success of the Phase II trial for sickle cell anemia, Senicapoc failed to achieve its primary clinical endpoint in a 52-week Phase III trial and the trial had to terminate early, although hematological parameters appeared to reinforce the improved clinical outcomes observed in Phase II trial (Ataga et al., 2011). The Phase III trial consisted of a Senicapoc group and a placebo group. Patients received a loading dose of 20mg twice daily for 4 days following a maintenance dose of 10mg (Icagen et al.). The trial was terminated due to no significant improvement in the rate of sickle cell painful crises. A similar proportion of patients from both groups experienced at least one treatment-emergent adverse event. Both groups experienced similar adverse events, but the crises rate was significantly higher in the Senicapoc group than in the placebo group, with nausea and urinary tract infections being the most frequent. Regardless, the hematologic and pharmacodynamic data provide strong evidence that Senicapoc inhibits Kcnn4 channel and leads to positive outcome considering hematologic parameters in patients. Nevertheless, these results led to discontinuation of the clinical research for use Senicapoc in the treatment of sickle cell anemia (Icagen et al.). Recently, following the accelerated approval of another drug, voxelotor, for treating sickle cell anemia, the investigators of the Senicapoc trial revisited results of the Phase III trial and reanalyzed their data in the same way the analysis was done for the voxelotor trial (Ataga et al., 2021). Comparison between the Senicapoc and the

voxelotor trials revealed that a lower dose of Senicapoc achieved a more pronounced improvement in hemolysis compared to voxelotor (used at 900mg/day), with no differences in the crises rate. Hence, if the Senicapoc trial were to be analyzed with the current criteria which emphasize hemoglobin increase, the authors believe that Senicapoc could have been approved (Ataga et al., 2021).

1.4.2.6.2 Alzheimer's disease

Aberrant microglial activation is a feature of Alzheimer's Disease (AD). Markedly enhanced microglial *Kcnn4* expression and activity was detected in brains of an AD mouse model and post-mortem brain tissues from AD patients, making Kcnn4 highly biologically relevant and a microglial target for treatment of AD (Jin et al., 2019; Maezawa et al., 2012). Preclinical studies provide strong evidence to repurpose Senicapoc for treatment of AD and/or mild cognitive impairment. Senicapoc has shown excellent brain penetrance (C_{brain}/C_{plasma}~5, which is 5 to 7 times greater than plasma concentration) and oral availability (~60%) in AD mouse model, where Senicapoc also reduced neuroinflammation, cerebral amyloid load and enhanced hippocampal neuronal plasticity (Jin et al., 2019). In 2022, a 52-week long 10mg/day clinical phase II trial for AD was initiated in patients with early AD by University of California Davis (Principal Investigator John Olichney, MD), with a visit at 78 weeks to determine any disease-modifying effect (University of California, 2024). Outcomes will be measured by cognitive and blood test as well as CSF markers of neuroinflammation.

1.4.2.6.3 Asthma

Icagen Inc. completed Phase II trials for use of Senicapoc in allergic asthma (Icagen, 2009a) and later for exercise-induced asthma (Icagen, 2009b). Both trials consisted of 80mg loading dose twice daily for 3 days, followed by 11 days or 25 days of daily 40mg intake for

allergic or exercise-induced asthma, respectively. The outcome of the allergic asthma trial was encouraging, patients who received Senicapoc demonstrated an improvement in the late asthmatic response following a challenge of inhaled allergen (Icagen, 2009a). In addition, Senicapoc was well-tolerated and with no serious adverse events. However, the trial for exercise-induced asthma was not successful as it failed to improve pulmonary function (Icagen, 2009b). No detailed reports are publicly available, but the company stopped clinical development of Senicapoc for asthma since then. Despite the marked improvement of airway inflammation and airway hyperresponsiveness in animal models of asthma by Senicapoc (Van Der Velden et al., 2013; Yu et al., 2013), these benefits were not reflected in clinical trials.

1.4.2.6.4 COVID-19

A Senicapoc phase II clinical trial for COVID-19 patients who developed severe respiratory insufficiency and required supplemental oxygen sponsored by University of Aarhus (Principal Investigator Steffen Christensen, MD) was completed recently (University et al., 2021). As Kcnn4 is a key regulator of fluid transport and the inflammatory response, the objective of this trial was to improve gas exchange 72 hours after the start of treatment, measured as arterial-to-inspired oxygen (PaO_2/FiO_2) ratio (Granfeldt et al., 2022). Although PaO_2/FiO_2 ratio at primary endpoint (72 hours) favoured standard care, later secondary endpoints pointed toward a protective effect of Senicapoc, suggesting the effect of Senicapoc may be gradual and may help to reduce mortality and even the need for renal replacement when compared to standard care in a 28-day period (Granfeldt et al., 2022).

1.4.2.7 Advances and limitations in targeting members of the fluid secretory pathway

Attempts to delay cyst growth by targeting the fluid secretory pathway has been successful *in vitro* or *ex vivo* but are mainly limited to these contexts, considering their essential

roles in biological processes. Of all the members, only V2R antagonist (Tolvaptan) has successfully progressed into human use, while effects of Cftr antagonists remain elusive due to their inconsistency *in vivo.*

1.4.2.7.1 V2R antagonists

The necessity of vasopressin binding V2R to stimulate production of cAMP through AC in the collecting duct principal cells provides a strong rationale for preclinical studies of V2R antagonists for ADPKD treatment (Calvet, 2015; Terryn et al., 2011; Wallace, 2011). Encouraging results with OPC31260 were initially reported in the *cpk* mouse (Gattone et al., 1999), followed by the *PCK rat, pcy* and *Pkd2*$^{WS25/-}$ murine models (Aihara et al., 2014; Torres et al., 2004; Wang et al., 2005) where OPC31260 lowered renal cAMP and markedly inhibited disease development and progression. These encouraging results led to investigation of a more potent and selective human V2R antagonist, namely OPC-41061 (Tolvaptan) *in vivo*. This antagonist was found to significantly lower renal cAMP levels, reduce kidney weights, cyst indices, fibrosis, and inhibit Ras and ERK activation, but ineffective in limiting the development of polycystic liver disease, consistent with the absence of V2R in the liver (Kanhai et al., 2020; Miyazaki et al., 2007; Tamma et al., 2017). Tolvaptan was shown to be highly specific and bind V2R with 1.8-fold higher affinity than vasopressin, while being 29-fold more selective for V2R with respect to the V1A receptor (Miyazaki et al., 2007). Tolvaptan was then introduced into clinical trials, which were successfully completed with positive outcomes, making it the only FDA approved drug for use in ADPKD (Cornec-Le Gall, Blais, et al., 2018; Nobakht et al., 2020; Torres et al., 2016; Wulfmeyer et al., 2019). One limitation was the use of renal function assessment as the primary outcome measure, since in ADPKD, renal function is normal for decades and only declines in later stages of the disease, despite progressive kidney cyst

formation and enlargement. To address this issue, the NIH funded a Consortium for Radiologic Imaging Studies of PKD to validate surrogate markers of disease progression (Grantham et al., 2006). By following patients and measure total kidney and cyst volume and glomerular filtration rate, they found that the rate of renal growth is a good predictor of functional decline and justifies the kidney volume as a good indicator of disease progression, therefore used by subsequent clinical trials as the primary outcome measure (Grantham et al., 2006).

One interesting recent study explored drug-target interaction of Tolvaptan and found that the residence time is more indicative of the inhibitory effect of Tolvaptan in wildtype metanephroi and in both early- and adult-onset mouse models (Zhang et al., 2022). Conventional drug evaluation relies heavily on affinity, which is often measured *in vitro* under equilibrium, and hence not capitulating the dynamic drug-target interaction *in vivo* that rarely reaches equilibrium (Annis et al., 2007; Sun et al., 2022). The authors developed multiple Tolvaptan derivatives with divergent affinities and binding kinetics and found that the residence time (reciprocal of the dissociation rate constant) of V2R antagonists binding with its target V2R, but not affinity (probability of V2R antagonists to bind V2R), that correlates with inhibitory efficacy (Zhang et al., 2022). Indeed, prolonged residence time translates into superior inhibitory efficacy on cyst development *ex vivo* and *in vivo*, therefore, considering not only equilibrium binding parameters but also the residence time of ligand-receptor interaction (kinetics-directed drug candidate selection) may improve drug development for ADPKD (Zhang et al., 2022).

1.4.2.7.2 Chloride channel inhibitors

CFTR inhibitors have consistently shown remarkable results *in vitro* and *ex vivo,* reducing or nearly abolishing cyst growth in MDCK cells, ADPKD cyst-derived monolayers, as well as mouse metanephroi (Magenheimer et al., 2006; Snyder et al., 2011; Yang et al., 2008).

However, the effect of Cftr inhibitors is less consistent when given *in vivo*. The same inhibitor, $CFTR_{inh}$-172, when given to rapid or slow progressive *Pkd1* mouse models, produced opposite outcomes and the degree of rescue is incomparable to *in vitro* and *ex vivo* findings (Cabrita, Kraus, et al., 2020; Snyder et al., 2011; Talbi et al., 2021; Yang et al., 2008). Another Cftr inhibitor, steviol, effectively inhibits MDCK cyst growth and markedly reduced cyst indices and kidney function in an early-onset *Pkd1* mouse model (Yuajit et al., 2013; Yuajit et al., 2014). Recent studies showed great rescue of cystic kidneys in an adult-onset *Pkd1* mouse model by targeting an alternative chloride channel, Tmem16a (Talbi et al., 2021). Comparison of *Cftr* versus *Tmem16a* knockout mice on a polycystin knockout background demonstrate that inactivation of *Tmem16a* has a greater impact on cyst growth than *Cftr*, and that the whole cell chloride conductance in $Pkd1^{-/-}$ cells were predominantly contributed by *Tmem16a* (Cabrita, Buchholz, et al., 2020; Cabrita, Kraus, et al., 2020; Talbi et al., 2021).

1.4.3 Direct link between Kcnn4 and Cftr

A literatures survey of Kcnn4 and Cftr reveal several links that support interaction in promoting cyst growth in ADPKD and are described below.

1.4.3.1 Kcnn4 is essential for Cftr activity *in vitro*

Using MDCK cells, ADPKD cyst and ADPKD cyst-derived cell monolayers, Albaqumi *et al.* demonstrated that Kcnn4 is critical and is likely the predominant potassium channel regulating cAMP-dependent chloride secretion through Cftr, thus mediating cyst growth (Albaqumi et al., 2008). The authors applied Kcnn4 inhibitor or activator to the cell culture and found significant modulation of Cftr activity (by measuring chloride current) as well as cyst growth: TRAM-34 treatment inhibited this current and severely limited cyst enlargement and

cyst formation *in vitro*, as indicated by reductions in both cyst size and number, while DCEBIO enhanced both parameters (Albaqumi et al., 2008).

1.4.3.2 *Kcnn4* is a modifier gene of cystic fibrosis

Cystic fibrosis (CF) patients have impairments in epithelial chloride and bicarbonate transport, and hence accumulate viscous mucus in the epithelial surface, causing severe obstruction in organs such as the intestine, airways, and pancreas (Bergeron & Cantin, 2019). Genes other than *CFTR* might be modifying the severity of CF, one of them being *KCNN4*, located within the modifier locus of *CFTR* (Jensen et al., 1998; Vandorpe et al., 1998). Silencing *Kcnn4* in CF mice significantly reduced lethality, through downregulation of the immune response rather than directly affecting intestinal epithelial secretion, supporting Kcnn4 being a modifier gene of intestinal CF (Philp et al., 2018).

1.4.3.3 Kcnn4 and Cftr co-localize on the plasma membrane

Most transepithelial chloride transport needs to be coupled to a potassium channel to maintain an electrochemical driving force for apical anion secretion. Two potassium channels, KcLQT1 and Kcnn4, have been associated with chloride secretion in the airways, and were thought to be exclusively localized in the basolateral membrane (Bardou et al., 2009; Hollenhorst et al., 2011). Evidence suggests they may be found in the apical membrane in the human bronchial cell lines, as activators and inhibitors of Kcnn4 can modulate short-circuit current at both basolateral and apical membranes (Bernard et al., 2003). An advantage of having Kcnn4 in the apical membrane is facilitating functional and physical interactions with Cftr. Interactions between Cftr and other ion transport proteins to modulate fluid transport have been previously described, but very few have been reported to directly interact with Kcnn4 (Brill et al., 1996; Lebeau et al., 2002; Magenheimer et al., 2006; Yuajit et al., 2013). Klein *et al.* found that Kcnn4

and Cftr proteins physically interact *in vitro* and occurs through calmodulin domains in amino- and carboxyl-termini in Kcnn4 with corresponding regions in Cftr (Klein et al., 2016). Co-expression of Kcnn4 with Cftr did not affect surface expression of Cftr, and Cftr did not influence trafficking of Kcnn4 under basal calcium concentration, but interaction between Kcnn4 and Cftr demonstrated by aggregation is promoted by elevation of intracellular calcium (Klein et al., 2016).

1.5 Hypothesis and objectives

As we have described in previous sections, large efforts have been dedicated to identification and targeting members of the secretory pathway to restrict ADPKD cyst growth. Aside from V2R antagonist Tolvaptan that successfully transitioned from preclinical to human use, targeting other members of the pathway is limited due to their essential roles in biological processes. The localization and cyst-mediating properties of Kcnn4 learned from various pathophysiological conditions strongly suggest it could be a member of the pathway and more importantly can be targeted safety as shown by the many clinical trials Senicapoc is actively part of, yet no preclinical study to date has investigated Kcnn4 in mediating ADPKD cyst growth. We are the first group to investigate the role of Kcnn4 in ADPKD and we hypothesize that targeting Kcnn4 using genetic or pharmacologic approaches would result in significant rescue of ADPKD phenotypes by strongly limiting Kcnn4-implicated cyst-driven processes.

To test this hypothesis, we will determine if renal cyst growth can be delayed by targeting Kcnn4 using genetic and pharmacologic approaches. We utilized the *Pkd1* metanephroi model as well as two mechanistically different *Pkd1* orthologous mouse models (early-onset rapid progressive $Pkd1^{cko}$ versus adult-onset slow progressive $^{SB}Pkd1$) to evaluate cyst-driven events including proliferation, fibrosis, and cyst indices, following disruption of *Kcnn4*, to determine if

Kcnn4 could be a potential therapeutic target. More importantly, we will determine whether Senicapoc could be repurposed for treating ADPKD. Our study consists of the following sub objectives:

1. To investigate the upregulation of *Kcnn4* expression and establish the level of fluid secretion- and proliferation- associated cAMP and MAPK/ERK activation *in vivo.*
2. To study Kcnn4 modulation of cystogenesis in *Pkd1*$^{-/-}$ metanephroi using Kcnn4 pharmacologic activator, inhibitor, and genetic Kcnn4 inactivation.
3. To identify the cyst-mediating processes that are modulated by Kcnn4 by analyzing *Pkd1* mouse models following *Kcnn4* genetic inactivation using histomorphometrics, immunohistochemistry, protein, and RNA expression analysis.
4. To administer Kcnn4 pharmacologic inhibitor Senicapoc to *Pkd1* mouse models and evaluate cyst indices and kidney function.
5. To determine potential synergistic drug partners of Senicapoc *ex vivo* for future work.

CHAPTER 2: MATERIALS AND METHODS

2.1 Mouse models

2.1.1 Mouse lines and genotyping

Mouse lines used in this study were generated previously by our lab and by others. All animal manipulations were performed in line with all ethical regulations and conducted with the approval by the Institut de Recherches Cliniques Animal Care Committee, in compliance with the Canadian Council of Animal Care ethical guidelines for animal experiments.

Endogenous *Pkd1* mutant models

The homozygous *Pkd1* knockout mutant mouse model $Pkd1^{tm1Som}$ ($Pkd1^{-/-}$) contains a selectable neo cassette inserted into exon 1 of the *Pkd1* gene, producing no detectable transcript or partial protein products (Wu et al., 2002). The renal *Pkd1* conditional knockout mouse model *C57BL/6-Tg(Cdh16-cre)91Igr;* $Pkd1^{tm2Ggg}$ ($Pkd1^{cko}$) was produced by homologous recombination of a neomycin cassette flanked by FRT sites where two loxP sites were inserted at intron 1 and at intron 4 of the *Pkd1* gene, causing the deletion of exon 2-4 upon expression of *Cre* recombinase (Piontek et al., 2004). The non-cleavable knockin *Pkd1* mutant $Pkd1^{tm1.1Fq1}$ ($Pkd1^{v/v}$) model contains a T3041V mutation that prevents cleavage of the PC1 protein at its GPS domain (Yu et al., 2007).

Pkd1 transgenic models

In the renal *Pkd1* dosage increase murine model *C57BL/6J-Tg(Pkd1*)39Mtru* ($^{SB}Pkd1$), the endogenous *Pkd1* promoter was replaced with the "SB" renal specific promoter, inserted upstream of the *Pkd1* initiation codon. This randomly inserted transgene gives rise to a 2- to 15-fold increase in renal *Pkd1* RNA expression levels (Thivierge et al., 2006). The global *Pkd1*

dosage increase model *C57BL/6J-Tg(Pkd1)26Mtru (Pkd1^{wt})* was generated similarly, from a modified *Pkd1*-BAC, in this case containing all the *Pkd1* endogenous proximal regulatory elements, to promote sustained increased wildtype *Pkd1* expression within the native tissue following its endogenous temporal regulation. In this model, *Pkd1* RNA expression is also increased by 2- to 15-fold in the kidneys and the animals show both renal and extrarenal anomalies (Kurbegovic et al., 2010). Both the renal targeted and the systemic *Pkd1* dosage increase models carry a silent tag (G2355A) introduced via homologous recombination into exon 10 of the *Pkd1* transgene, giving rise to a new EcoRI restriction site. In addition, Pc1 protein expression in both models is elevated when compared to wildtype.

To generate double *Pkd1^{cko}; Kcnn4$^{-/-}$* and *^{SB}Pkd1; Kcnn4$^{-/-}$* mutant mouse models, *Pkd1^{cko}* and *^{SB}Pkd1* were first outcrossed with *Kcnn4$^{-/-}$*. *Kcnn4$^{-/-}$* mice (*Kcnn4^{tm1Jemn}*) were generated by deletion of exon 1 upon insertion of a neo cassette replacing 1.7kb surrounding and including exon 1. Mice show normal appearance and fertility (Begenisich et al., 2004). F_1 animals were then intercrossed, and the offspring were analyzed by PCR to select the genotype of interest.

For all employed models, to prepare samples for PCR genotyping, a piece of tail from each mouse was digested overnight with pronase (20mg/mL; Roche, Ref.: 11459643001) at 55^{o}C and DNA extraction was carried out the next day. Briefly, the digested tails were centrifuged for 5 minutes at 13,000 rpm and the supernatant was transferred to a fresh tube. 35µL of sodium acetate (3M, pH 6.9) and 450µL of 100% ethanol were added and the tubes were vigorously agitated. The precipitated DNA was then pelleted 5 minutes at 13,000 rpm and the pellet was washed with 200µL of 70% ethanol. The DNA pellet was then left to air dry and subsequently resuspended in 50µL of TE buffer (10mM Tris-Cl pH 8.0, 1mM EDTA pH 8.0). Primers used

for PCR genotyping are provided in Table 1. To determine tagged transgene presence when relevant, an EcoRI digestion was carried out following the PCR reaction.

Table 1. List of primers used for PCR genotyping.

KspCre	Forward	5' AGG TTC GTG CAC TCA TGG A 3'
	Reverse	5' TCG ACC AGT TTA GTT ACC C 3'
Pkd1flox	Forward	5' CCT GCC TTG CTC TAC TTT CC 3'
	Reverse	5' AGG GCT TTT CTT GCT GGT CT 3'
Kcnn4	Forward	5' TTG GTG TGC TCA GAC CTG CTG 3'
	Reverse	5' GAG CTC ACG CAG TCA CAC AT 3'
V allele	Forward	5' CCA AAC AAC TCA GAC CAG G 3'
	Reverse	5' ACC AGG ACA GCA AGA AAA C 3'
Exon 7-15	Forward	5' TGG TAC CTG ATT GGG CAT GAT 3'
	Reverse	5' GTT TTG CCT GGA TCC GCT GTT G 3'

2.1.2 Sample collection and analysis

Mouse kidney and blood samples were collected at two ages that serve to represent early and later stages of the disease: P5 or P10 for *Pkd1*^{cko} and 1-2 months or 6-8 months for ^{SB}*Pkd1*. Samples from *Pkd1*^{cko}*; Kcnn4*$^{-/-}$*,* ^{SB}*Pkd1; Kcnn4*$^{-/-}$*,* and age-matched wildtype controls were collected in parallel. Kidney and body mass were measured for the calculation of the kidney weight to body weight ratio (KBW). Each isolated kidney was sectioned in half. Two halves were snap-frozen in liquid nitrogen and stored at -80^{o}C for western blot analysis, cyclic Adenosine Monophosphate (cAMP) quantification, and RNA analysis. The remaining two halves were fixed in 4% formalin overnight and then processed in the Citadel Tissue Processor for embedding in paraffin blocks. Kidney paraffin blocks were sectioned at 4mm thickness using the microtome (Leica RM2145) for subsequent hematoxylin and eosin (H&E) staining, *Kcnn4 in situ* hybridization, and immunohistochemistry. Blood samples were collected at experimental endpoints, centrifuged for isolation of plasma, and stored at -80^{o}C for blood urea nitrogen (BUN) assessment. A separate group of P10 *Pkd1*^{cko} and *Pkd1*^{cko}*; Kcnn4*$^{-/-}$*,* together with 2-month-old ^{SB}*Pkd1* and ^{SB}*Pkd1; Kcnn4*$^{-/-}$ were anesthetized for kidney perfusion, after which kidneys were

cut in half and stored in Tissue-Tek optimal cutting temperature (OCT) compound (Sakura Finetek, Ref.: 2580274) at -80ºC for primary cilia staining and analysis. For quantification of renal *Kcnn4* expression and protein levels of key components of the mitogen-activated protein kinases/extracellular signal-regulated kinases (MAPK/ERK) pathway, a group of P10 $Pkd1^{v/v}$ and 6–8-month-old $Pkd1^{wt}$ kidneys were also processed as described above. All image analyses were performed blinded with respect to the genotypes.

2.1.3 Metanephroi culture and treatment plan

To generate $Pkd1^{-/-}$ metanephroi, $Pkd1^{+/-}$ breeders were set up and checked daily for the presence of a vaginal plug. Any presence of a vaginal plug was noted as E0.5. Two weeks later, E14.5 embryos were isolated from pregnant $Pkd1^{+/-}$ females. A piece of tail was removed from each embryo for DNA extraction as described above. During PCR genotyping, embryos were stored individually in cold phosphate buffered saline (PBS) on ice. $Pkd1^{+/+}$ and $Pkd1^{-/-}$ embryos were selected and metanephroi were isolated under the dissection microscope and then placed on 0.4mm Falcon cell culture inserts (Fisher, Ref.: 08-770). Inserts carrying metanephroi were then put into 12 well tissue culture plates. Media (400mL) consisting of DMEM:F12 (Wisent, Ref.: 319-075-CL) supplemented with sodium bicarbonate (Sigma, Ref.: S5761-500G), HEPES (Fisher, Ref.: 15630106), ITS universal culture supplement (Wisent, 315-080-XL), prostaglandin E2 (Sigma-Aldrich, P5640), penicillin and streptomycin (ThermoFisher, Ref.: 15070063) were added below all inserts into the wells. E14.5 was denoted as day 0 of metanephroi culture. On day 1, the media was replaced with fresh media containing 8-Br-cAMP (Sigma, Ref.: B7880-25MG) and supplemented with or without the following reagents: Kcnn4 activator SKA-111 (Aobious, Ref.: AOB6599), Kcnn4 inhibitors Senicapoc (BOC Sciences, Ref.: B2693-089474) and TRAM-34 (Tocris, Ref.: 2946), Cftr inhibitor PPQ-102 (Tocris, Ref.: 4303) and Tmem16a

inhibitor CaCCinh-A01 (Sigma, Ref.: 208293). The media was replaced again on day 3 with the supplemented reagents. Metanephroi culture was maintained in a 37°C humidified CO_2 incubator at 5% CO_2 until day 4. Pictures were taken daily with 4X objective in brightfield using Zeiss Axiovert S100TV microscope. Cyst number per metanephros and percent cyst area were quantified after completion of the experiment using the Volocity software version 6.0 (Quorum Technologies Inc., Ontario, Canada).

To determine if *Kcnn4* genetic inactivation alters *Pkd1*$^{-/-}$ cyst growth, *Pkd1*$^{-/-}$*; Kcnn4*$^{-/-}$ metanephroi were generated from *Pkd1*$^{+/-}$*; Kcnn4*$^{-/-}$ breeders. Metanephroi were cultured and treated with 8-Br-cAMP as described above. To determine the response of established *Pkd1*$^{-/-}$ cysts to Senicapoc, Senicapoc was added on day 3 instead of day 1 and cultured until day 5.

2.2 Expression analysis

2.2.1 RNA isolation and RT-qPCR

Human ADPKD kidneys were surgically removed from patients and stored at -80°C. Total RNA from human and mouse kidneys were extracted using the TRIzol (Fisher, Ref.: 15596026) - chloroform method (Rio et al., 2010). Extracted RNA were checked for quality on agarose gel, then reverse transcribed using Moloney murine leukemia virus (MMLV) reverse transcriptase (Promega, Ref.: M1701) to cDNA for real-time quantitative PCR. Reactions were carried out in triplicate using the Applied Biosystems PowerUp SYBR Green master mix (Fisher, Ref.: A25741) to determine the expression of *KCNN4, Kcnn4, Aqp1, Aqp2, Nkcc1, Nkcc2*, and *Cftr*. Analysis was completed using the QuantStudio Real-Time PCR Software. Results were expressed as fold increase from healthy human kidneys or age-matched wildtype mouse kidneys. RNA analysis was normalized to mouse ribosomal protein subunit 16 (*S16*) for quantification of

mouse genes. *KCNN4* expression in human ADPKD kidneys was normalized to *HPRT*. The primers used for determining RNA expression are listed in Table 2.

Table 2. List of primers used for qPCR.

KCNN4	Forward	5’ CGT GCA CAA CTT CAT GAT GGA 3’
	Reverse	5’ CGC CGC TGA CTC CTT CA 3’
AQP1	Forward	5’ CAT TTG GCT CTG CTG TGC TC 3’
	Reverse	5’ TGA TGT CGT CAG CAT CCA GG 3’
AQP2	Forward	5’ CCA TTG GTT TCT CTG TTA CCC TG 3’
	Reverse	5’ CGG TGA AAT AGA TCC CAA GGA G 3’
NKCC1	Forward	5’ GGA TGG CTT TGC GAA TGG AG 3’
	Reverse	5’ TGC AGC GGA CTA ATA CAC CC 3’
NKCC2	Forward	5’ CTG GCC TCA TAT GCG CTT ATT 3’
	Reverse	5’ AGA TTT GGC ATA CGA GGC ATG 3’
CFTR	Forward	5’ CGG CGA TGC TTT TTC TGG AG 3’
	Reverse	5’ TGG GTG AAG AAG CAG TGT CC 3’
S16	Forward	5’ GCT ACC AGG GCC TTT GAG ATG 3’
	Reverse	5’ AGG AGC GAT TTG CTG GTG TGG 3’
HPRT	Forward	5’ GGC CAG ACT TTG TTG GAT TTG 3’
	Reverse	5’ TGC GCT CAT CTT AGG CTT TGT 3’

2.2.2 RNA *In situ* hybridization

P5 *Pkd1*^{cko} and 4–6-month-old ^{SB}*Pkd1* kidneys with age-matched wildtype kidneys were isolated and fixed overnight in formalin, embedded in paraffin, sectioned in 4mm thickness, and placed onto positively charged glass slides. RNA *In situ* hybridization was conducted using the Multiplex Fluorescent Reagent Kit v2 (Advanced Cell Diagnostics, Ref.: 323100) following manufacturer’s instructions. Briefly, kidney sections were deparaffinized in xylene, re-hydrated in graded alcohols, and permeabilized with H_2O_2 to block endogenous peroxidase activity to allow the probe to access its target RNA. Samples were then hybridized with murine *Kcnn4* probe (Advanced Cell Diagnostics, Ref.: 569381) to bind its target RNA. Hybridization signals were amplified with amplifier reagents followed by dye-labeled probes to facilitate the visualization of fluorescent signals. Images were acquired with Leica DM6 fluorescent microscope at 20X. Each punctate fluorescent white dot represents a single mRNA transcript.

2.3 Kidney cyst characterization

2.3.1 Cyst quantification

Formalin-fixed paraffin-embedded (FFPE) kidneys were sectioned at 4mm thickness and coloured with H&E for cyst quantification. Briefly, kidney slides were baked at 55^{o}C for 30 minutes prior to deparaffinization in xylene. Slides were processed in serial graded alcohols to rehydrate samples, followed by incubation in hematoxylin solution (Fisher, Ref.: SH26-500D). To remove excess hematoxylin, slides were placed under running tap water, followed by incubation with eosin (Sigma, Ref.: E511-25). Excess eosin was removed by 95% ethanol followed by a quick dip in water. Slides were dehydrated under serial graded alcohols and then xylene before placing coverslips using Permount mounting medium (Fisher, Ref.: SP15-500). Images were taken with a Leica MZ12 microscope in brightfield mode. Quantifications of percent cyst surface area and cyst number per μm^2 of kidney surface were carried out with the Northern Eclipse software (Empix Imaging Inc., Ontario, Canada).

2.3.2 Cyst tubular origin

FFPE kidneys were sectioned in 4mm thickness, deparaffinized in xylene, re-hydrated in graded alcohols, and washed in PBS. A heat-induced epitope retrieval step was carried out to break methylene bridges that formed during the fixation step, allowing exposure of antigenic sites for antibody binding. The slides were submerged in a preheated solution containing citric acid (Sigma, Ref.: C0759) and sodium citrate (EMD, Ref.: SX0445-3) and heated in a pressure cooker for a total of 15 minutes. Heated slides were cooled down under running tap water for 30 minutes, then incubated for 30 minutes in fresh 0.1%$NaBH_4$ (Fisher, Ref.: 5678-10) solution to remove autofluorescence. The slides were washed with PBS between each step. Before proceeding to incubation with primary antibodies, samples were incubated for 20 minutes in blocking solution containing 1% bovine serum albumin (BSA) (Sigma-Aldrich, Ref.: A3059-

100G), 10% normal goat serum (Vector Labs, Ref.: S-1000), and 0.1 mM $CaCl_2$ (Sigma-Aldrich, Ref.: C4901-100G) in PBS. The following antibodies were diluted in blocking solution and incubated overnight with samples at 4°C in the dark: Lotus tetragonolobus lectin (LTL, 1:200; Vector Laboratories, Ref.: L-1320-5), Lycopersicon esculentum lectin (LEL, 1:100; Vector Laboratories, Ref.: L-1170-2) and Dolichos biflorus agglutinin (DBA, 1:50; Vector Laboratories, Ref.: RL-1032-2), which are specific markers for proximal tubule (green), distal tubule (blue) and collecting duct (red), respectively. On the following day, antibody solutions were removed, and the slides were washed with PBS. Lycopersicon esculentum lectin required an additional 2-hour incubation at room temperature in the dark with the secondary antibody AMCA Streptavidin diluted in blocking solution (1:100; Vector Laboratories, Ref.: SA-5008-1). The slides were washed before adding ProLong Gold Antifade Mountant (ThermoFisher, Ref.: P36930) to seal the samples with coverslips. Images were acquired using Leica DM5 fluorescent microscope. To quantify the percentage of cystic tubules within each nephron segment, wildtype kidneys were examined to determine the diameter threshold of non-cystic tubules within each segment using Volocity software by manual tracing. Any tubular diameter surpassing the threshold of wildtype tubules (40mm) was considered cystic. Results were expressed as the percentage of cystic tubules within each nephron segment.

2.4 Protein analysis

2.4.1 cAMP measurement

cAMP levels in kidney lysates were detected using the Direct cAMP ELISA Kit from Enzo life sciences (Ref.: ADI-901-066A) following the manufacturer's instructions. Frozen mouse kidneys stored at -80°C were ground into fine powder under liquid nitrogen, weighed, and homogenized in 10 volumes of 0.1M HCl to release cAMP, then centrifuged at 600 x g for 10

minutes to pellet the debris. The supernatant was used for the assay. To prepare the cAMP standards, the stock solution (at 2000 pmol/mL) was used for serial dilutions to obtain standards at 20, 5, 1.25, 0.312, and 0.078 pmol/mL concentrations. Apart from the 5 wells reserved for the standards, additional wells were dedicated for total activity (TA), blank, non-specific binding (NSB), and 0 pmol/mL standard (Bo). To prepare the assay plate, 50uL of Neutralizing Reagent was first added to all wells except Blank and TA. 100mL of 0.1M HCl was then added into NSB and Bo wells. 100mL of standards or samples were loaded to corresponding wells, followed by 50mL blue conjugate to all wells except Blank and TA. 50mL yellow antibody was added next to all wells except Blank, TA, and NSB. The plate was sealed upon completion of sample loading and incubated for 2 hours at room temperature at low speed (~500rpm). After incubation, all contents were emptied, and wells were washed. For conjugate-substrate reaction, 5mL of blue conjugate was added to the TA well, 200mL substrate solution was added to all wells and the plate was incubated again for 1.5 hours at room temperature with shaking. To stop the reaction, 50mL stop solution was added to all wells. The plate was read at 405nm. The average net OD of each well was calculated using the equation: "Average Net OD = Average OD - Average NSB OD". The standard curve was plotted using the calculated average net OD. The concentration of cAMP in each sample was then extrapolated using the equation of the standard curve. To normalize for protein content, protein concentrations of all samples were measured using bicinchoninic acid (BCA) protein assay (ThermoFisher, Ref.: 23228). The final values were expressed as pmol cAMP per mg of total protein, calculated by dividing cAMP concertation by the total protein concentration.

2.4.2 Protein extraction and western blot

Frozen kidney tissues were homogenized in 500µL ice-cold RIPA buffer (20mM Tris pH 7.5, 2mM EDTA pH 8, 150mM NaCl, and 0.5% Triton) supplemented with Phenylmethanesulfonyl fluoride (Sigma-Aldrich, Ref.: P7626) and protease inhibitor cocktail (Sigma-Aldrich, Ref.: P8340) using an electric Polytron homogenizer. The homogenates were centrifuged at 16,000 x g for 15 minutes at 4^{o}C to pellet the debris. Supernatants were collected and stored at -80^{o}C in aliquots. Protein concentration was quantified using BCA protein assay (ThermoFisher, Ref.: 23228) according to the manufacturer's instructions. To initiate electrophoresis, equal amounts of protein extracts (40-45mg) were mixed with Laemmli sample buffer containing β-mercaptoethanol and denatured for 10 minutes at 95^{o}C. Denatured samples were loaded onto hand-casted 8, 10, or 12% SDS-polyacrylamide gels along with a molecular weight marker and separated at ~80V until the 37kDa marker reaches about 1cm before the bottom of the gel. Proteins in the gel were transferred onto PVDF or nitrocellulose membranes overnight at 4^{o}C using ~20V and blocked for a minimum of 6 hours at 4^{o}C in PBS containing 0.1% Tween-20 (Sigma-Aldrich, Ref.: P1379) and 5% milk. Immunoblots were hybridized overnight with primary antibodies: rabbit anti-cellular myelocytomatosis oncogene (c-Myc) antibody(1:1000; Abcam, Ref.: ab32072), mouse anti-phospho-p44/42 MAPK (Erk1/2) antibody (1:1000; Cell signaling, Ref.: 9106), rabbit anti-p44/42 MAPK (Erk1/2) antibody (1:1000; Cell signaling, Ref.: 4695), mouse anti-active β-catenin antibody (1:2000; Millipore, Ref.: 05-665), anti-β-catenin antibody (1:2000; Millipore, Ref.: 06-734), or mouse anti-GAPDH antibody (1:10000; Abcam, Ref.: ab8245), followed by 3 washes with PBS containing 0.1% Tween-20. Next, immunoblots were incubated with corresponding secondary antibodies: rabbit anti-mouse IgG (1:5000; Sigma-Aldrich, Ref.: A9044) or goat anti-rabbit IgG (1:2000; Sigma-Aldrich, Ref.: A0545) for 4 hours at 4^{o}C and washed again. For signal development, immunoblots were

incubated with Amersham ECL Prime western blotting detection reagent (Fisher, Ref.: 12316992) for 5 minutes and covered in transparent plastic wrap. Images were acquired in the darkroom using Kodak films. Quantification and analysis of protein levels were executed with the ImageJ software (Schneider et al., 2012).

2.5 Immunohistochemistry

2.5.1 Proliferation assay

4mm thick FFPE kidney sections were deparaffinized with xylene, re-hydrated with a series of graded alcohols, and washed with water. The samples were permeabilized with 10-minute incubation of 2% H_2O_2 and then washed in PBS. Heat-induced epitope retrieval was necessary to facilitate antibody binding, where slides immersed in pre-heated retrieval solution containing citric acid (Sigma, Ref.: C0759) and sodium citrate (EMD, Ref.: SX0445-3) were heated in a pressure cooker for 15 minutes, then cooled under running tap water for 30 minutes. Slides were washed in PBS containing 0.02% Tween-20 (Sigma-Aldrich, Ref.: P1379) and then samples were blocked in PBS solution containing 0.02% Tween-20, 10% normal goat serum (Vector Labs, Ref.: S-1000), and 1% BSA (Sigma-Aldrich, Ref.: A3059-100G) for 45 minutes in preparation for overnight 4^{o}C incubation with the primary antibody, prepared by diluting anti-Ki67 antibody in blocking solution (1:100; Leica, Ref.: NCL-Ki67p). On the following day, the primary antibody was washed, and samples were incubated with biotinylated anti-rabbit antibody in blocking solution (1:300; Vector Laboratories, Ref.: BA-1000-1.5) for 90 minutes at room temperature. Following this incubation, samples were incubated with Vectastain ABC-HRP reagent (Vector Laboratories, Ref.: PK-7100) for 30 minutes at room temperature. The slides were washed with PBS, then colored with DAB substrate kit (Vector Laboratories, Ref.: SK-4100) for detection of Ki67 signals. To complete the experiment, slides were dehydrated in a

series of graded alcohols followed by xylene and finally covered with coverslips using Permount mounting medium (Fisher, Ref.: SP15-500). Images were acquired with Leica MZ12 microscope in brightfield. Proliferation was quantified by manually counting the number of tubules with two or more Ki67-positive epithelial cells. The final values were expressed as the number of Ki67-positive nuclei per mm^2 of kidney surface, the latter was determined using the Northern Eclipse software.

2.5.2 Kidney fibrosis

4µm thick FFPE kidney sections were de-paraffinized in xylene, then re-hydrated in a series of graded alcohols. Sections were washed in distilled water for 5 minutes before 30 minutes of incubation with Sirius Red (Sigma-Aldrich, Ref.: 365548) dissolved in picric acid (0.1%; Sigma, Ref.: P-6744-1GA) prepared 24 hours in advance. After incubation with Sirius Red for 45 minutes, slides were rinsed with tap water for 3 minutes followed by graded alcohols for dehydration. Finally, slides were immersed in xylene and covered with coverslips using Permount mounting medium (Fisher, Ref.: SP15-500). Images were taken with a Leica MZ12 microscope in brightfield mode. Sirius red binds to collagen I and IV and appears dark red compared to pink non-fibrotic surfaces. Kidney fibrosis was quantified using the Northern Eclipse software and expressed as the percent of collagen area within the entire kidney surface.

2.5.3 Kidney perfusion and primary cilia immunostaining

To perfuse the kidneys, the mouse needed to be anesthetized with Avertin (2.5%) given by intraperitoneal injection at 0.0165µL per g of mouse weight. Once anesthetized, the mouse was stabilized onto a platform to open the abdomen cavity and cut the diaphragm and rib cage to fully expose the heart. A 26G1/2 needle was inserted into the left ventricle of the heart and the following fluids (made in PBS) were perfused: 20mL PBS (1X), 50mL Paraformaldehyde (4%),

and 20mL sucrose (10%). The heart should continue to pump throughout the perfusion procedure, while the color of the kidneys should gradually turn pale, being an indicator of perfusion efficiency and blood wash-out. After completion, kidneys were cut in half to check for proper perfusion, if successful the interior should be white-colored. Kidneys were then placed in 10% sucrose for 1 hour at 4^{o}C, then immersed in 30% sucrose for 3 hours at 4^{o}C. Finally, the perfused kidneys were stored in OCT compound at -80^{o}C.

Perfused kidneys stored in OCT compound were sectioned at low temperature using a cryostat-microtome (Leica CM3050S) and stored at -80^{o}C. Tris buffered saline (TBS) wash solution (0.1M Tris pH 7.5, 150mM NaCl) was prepared one day before the experiment using fresh 1M Tris-HCl pH 7.5. Slides were allowed to thaw to room temperature prior to immunostaining (~30 minutes) and then washed in TBS followed by 30 minutes incubation in 0.1% $NaBH_4$ (Fisher, Ref.: 5678-10) solution. Slides were washed again to remove residual $NaBH_4$ and incubated in 1% SDS for 5 minutes before another wash. Blocking solution incubation followed and lasted for 45 minutes at 4^{o}C in a sealed box. The blocking solution was prepared by diluting unconjugated goat anti-mouse IgG (1:5; Jackson Immunoresearch, Ref.: 115-005-166) in a TBS solution consisting of 10% normal goat serum (Vector Labs, Ref.: S-1000) and 1% BSA (Sigma-Aldrich, Ref.: A3059-100G). The slides were washed and incubated overnight (ideally for 14 hours) at 4^{o}C with the primary antibody in a sealed box. The primary antibody was prepared by diluting mouse monoclonal anti-acetylated tubulin antibody (1:1000; Sigma-Aldrich, Ref.: T7451) in the blocking solution. On the following day, slides were washed with TBS incubated with secondary antibody for 1 hour at 4^{o}C in a sealed dark box. The secondary antibody was prepared by diluting goat anti-mouse IgG conjugated to Alexa Fluor 555 (1:500; Invitrogen, Ref.: A28180) in the blocking solution. From this step onwards, slides must

be protected from light. The slides were washed with TBS containing 0.02% Tween-20 (Sigma-Aldrich, Ref.: P1379) followed by TBS wash. Nuclei were colored with DAPI for 3 minutes at room temperature, washed with TBS and a rapid dip in water, and finally ProLong Gold Antifade Mountant (ThermoFisher, Ref.: P36930) was added to seal samples with coverslips. Images were acquired with Leica DM5 fluorescent microscope. To analyze primary cilia length, each primary cilia was manually traced using the Volocity software and sorted by length into corresponding intervals. The distribution of primary cilia length was plotted based on the percentage of primary cilia within each interval. The average primary cilia length was also displayed as a bar graph.

2.6 Blood urea nitrogen measurement

Blood urea nitrogen (BUN) in mouse serum was measured using the QuantiChrom™ Urea Assay Kit from BioAssay Systems (Ref.: DIUR-100) following manufacturer's instructions. Before assaying samples, a quick test was done to determine the dilution factor that should be used so that all values fall within the detection range. A dilution factor of 10 was sufficient, therefore, all serum samples were diluted 1/10 in distilled water prior to the assay. 5µL of samples, water blank and standard were loaded in duplicates in a 96 well clear bottom plate. The working reagent was prepared just prior to use by mixing equal volumes of reagent A and B so that 200µL can be loaded to each well. The plate was incubated for 20 minutes at room temperature with low speed shaking and was read at 520nm. Urea concentration was calculated with the equation below:

$$[\text{Urea}] = \frac{OD_{SAMPLE} - OD_{BLANK}}{OD_{STANDARD} - OD_{BLANK}} \times n \times 50\ (mg/dL)$$

BUN was converted from urea: BUN (mg/dL) = [Urea] / 2.14

2.7 *In vivo* drug administration

2.7.1 Treatment plan and sample collection

For treatment of the adult-onset *Pkd1* mouse models, histological kidney sections at different ages were examined to determine the age of treatment onset. Treatment initiated at 3 weeks in $^{SB}Pkd1$ and at 6 weeks in $Pkd1^{wt}$ and C57. These times were chosen so that treatment began around the time of cyst initiation. Animals were separated into 3 treatment groups: vehicle (PEG/Cremophor), 30mg Senicapoc/kg of body weight in vehicle solution (low dose), and 120mg Senicapoc/kg of body weight in vehicle solution (high dose). Senicapoc was freshly prepared each week in the vehicle solution at 80:10:10 (Senicapoc:PEG:Cremophor) and administered daily to all animals by oral gavage for 3 months. Mice were monitored daily for health status and weighed weekly to monitor body weight change.

The early-onset *Pkd1* mouse models $Pkd1^{cko}$ and $Pkd1^{v/v}$ were divided into 2 treatment groups: vehicle and 120mg Senicapoc/kg of body weight in vehicle solution. Animals received Senicapoc directly into the corner of the mouth using a pipette soon after birth (P2) and through milk from P0 until P5 for $Pkd1^{cko}$ or until P10 for $Pkd1^{v/v}$. For direct oral administration, 1-2µL was given twice daily equivalent to 120mg Senicapoc/kg of body weight/day. For Senicapoc administration through milk, mothers were given 120mg Senicapoc/kg of body weight once daily by oral gavage from the day $Pkd1^{cko}$ and $Pkd1^{v/v}$ were born (P0).

All animals were sacrificed at the experimental endpoint.

2.7.2 Sample analysis

Upon completion of treatment at the experimental endpoints, all organs were examined macroscopically for adverse phenotypes. Blood samples were collected and processed for isolation of serum which was stored at -80°C. Due to reagent availability, only the high dose

group in the two adult-onset models were assessed for BUN. The body and kidney mass were measured. Kidneys were half formalin-fixed and half snap-frozen and stored as described above.

2.8 Statistical analysis

All values and graphs are expressed as mean ± standard error of the mean (SEM). Comparison of data sets were conducted with the unpaired Student's T Test except for the Kaplan-Meier curve which was analyzed by the log-rank test. All statistical analysis was carried out using GraphPad Prism version 8 (GraphPad Software, San Diego, California USA). P value of <0.05 is considered significant. *$p<0.05$, **$p<0.01$, ***$p<0.001$, ****$p<0.0001$.

CHAPTER 3: RESULTS

3.1 Characterization of *Kcnn4*-related pathways in 2 orthologous *Pkd1* mouse models

3.1.1 *Kcnn4* RNA expression is selectively upregulated in ADPKD kidneys

RNA analysis of kidneys surgically removed from human ADPKD patients revealed a marked 23-fold elevation in *KCNN4* RNA expression compared to healthy human kidneys (Fig. 8A). *KCNN4* RNA expression in healthy human kidneys showed small deviation between individuals. In contrast, the range was much wider in ADPKD patients and varied from 2- to 51-fold increase as compared to the mean of healthy kidneys. Despite the wide range, all ADPKD individuals consistently expressed greater renal *KCNN4* RNA expression than healthy individuals.

Like our observations in human ADPKD kidneys, we found consistent upregulation of renal *Kcnn4* RNA expression by 2- to 6-fold across all analyzed *Pkd1* orthologous mouse models of different disease onset and progressivity: early-onset rapidly progressive $Pkd1^{cko}$ and $Pkd1^{v/v}$, and adult-onset slowly progressive $^{SB}Pkd1$ and $Pkd1^{wt}$, in comparison to age-matched wildtype animals (Fig. 8B). Renal *Kcnn4* RNA expression was elevated by 1.9±0.3-fold in P10 $Pkd1^{cko}$ and by 1.7±0.2-fold in P10 $Pkd1^{v/v}$ compared to wildtype. Comparison between the two early-onset models indicated that the more rapidly progressive $Pkd1^{cko}$ experienced a greater increase in renal *Kcnn4* RNA expression. Likewise, the two adult-onset models expressed a similar fold increase in renal *Kcnn4* RNA expression, but the relatively more rapidly progressive $^{SB}Pkd1$ experienced a greater increase than the $Pkd1^{wt}$. $^{SB}Pkd1$ kidneys at 2 months showed 6.2±1.3-fold increase while $Pkd1^{wt}$ at 7 months showed a 5.5±1.3-fold increase in *Kcnn4* RNA expression. We also analyzed $^{SB}Pkd1$ kidneys at a later stage of disease (8 months) and found a small decrease in *Kcnn4* RNA expression in comparison to 2 months but was nevertheless still highly elevated by 4.5±1.1-fold compared to wildtype. We used another method, *in situ* hybridization

assay, to detect and confirm upregulation of *Kcnn4* RNA expression in FFPE *Pkd1*^{cko} and ^{SB}*Pkd1* kidneys, two models we extensively analyzed in this study (Fig. 8C). Each white dot indicated binding of the *Kcnn4* probe to a corresponding mRNA transcript. To properly visualize the RNA signals, we first set the threshold using the negative control probe so that no signal is detected. With this threshold, we did not detect any signal in the wildtype samples, consistent with low *Kcnn4* RNA expression after development in healthy tissues. In contrast, distinct signals representing binding of *Kcnn4* mRNA transcript were easily detectable in *Pkd1*^{cko} and ^{SB}*Pkd1* kidneys. Kcnn4 protein levels were not measured due to unavailability of validated antibody.

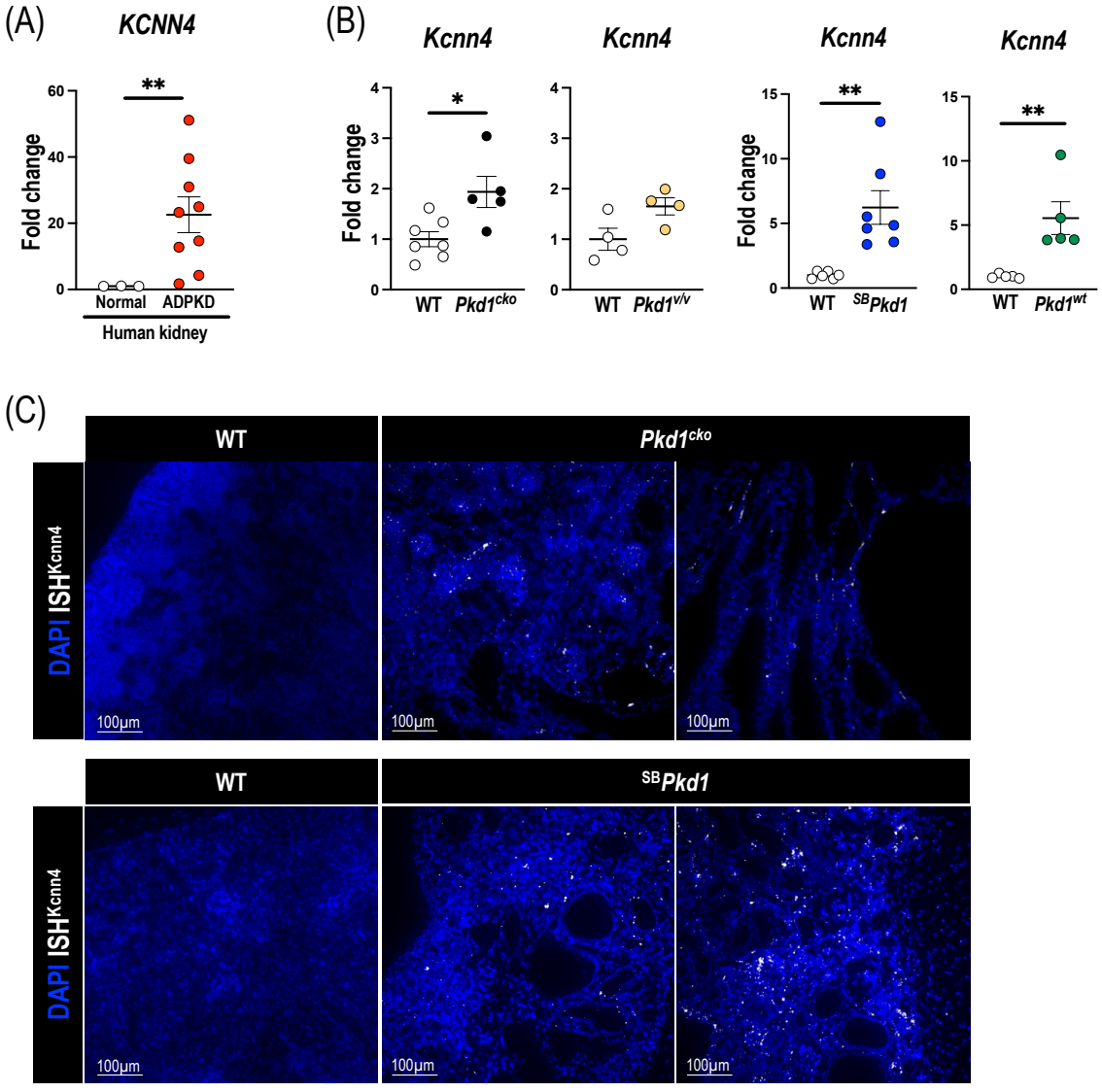

Fig. 8 Analysis of *Kcnn4* RNA expression in the kidneys of human ADPKD and *Pkd1* mouse models. (A) Analysis of human *KCNN4* RNA expression in healthy/normal and ADPKD kidney tissues by quantitative PCR. (B) Analysis of mouse *Kcnn4* expression in *Pkd1*^{cko} (P10; black dot), *Pkd1*$^{v/v}$ (P10; yellow dot), ^{SB}*Pkd1* (2 months; blue dot) and *Pkd1*^{wt} (7 months; green dot) kidneys relative to age-matched wildtype (WT; white dot) by quantitative PCR. (C) RNA *in situ* hybridization overview of *Kcnn4* expression by RNAscope in kidneys of *Pkd1*^{cko} (P5) and ^{SB}*Pkd1* (4 months) with age-matched WT. *p<0.05, **p<0.01

We analyzed the RNA expression of other known channels and transporters of the fluid transport pathway driving cyst fluid secretion which promotes cyst growth: *Nkcc1, Nkcc2, Cftr, Aqp1* and *Aqp2* in P10 *Pkd1*^{cko} (Fig. 9A) and 4–6-month-old ^{SB}*Pkd1* kidneys (Fig. 9B). The RNA expression of these members did not increase and even reduced compared to wildtype controls.

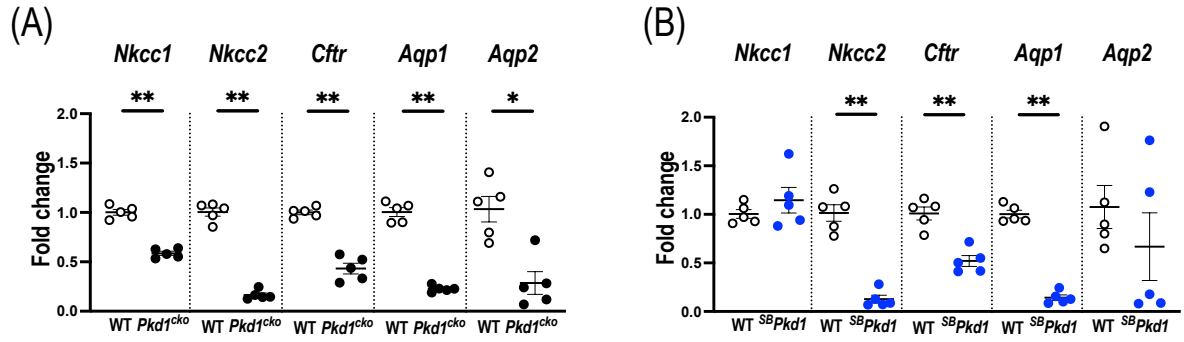

Fig. 9 RNA expression analysis of key channels and transporters in the epithelial secretory pathway in *Pkd1* mouse kidneys. Analysis of *Nkcc1, Nkcc2, Cftr, Aqp1* and *Aqp2* in P10 *Pkd1*^{cko} (A) and 6–8-month-old ^{SB}*Pkd1* (B) mouse kidneys by quantitative PCR. *p<0.05, **p<0.01

3.1.2 *Kcnn4* is expressed early in embryonic kidneys

Kcnn4 expression during early kidney development had not previously been determined. Thus, to investigate modulation of *Pkd1*$^{-/-}$ cysts by *Kcnn4*, we first needed to confirm that *Kcnn4* is expressed at the age we begin metanephroi studies, E14.5. RNA was extracted from embryonic kidneys at E14.5 and E16.5, reverse transcribed to cDNA and then performed PCR reactions using specific primers for Kcnn4 and S16. We successfully amplified Kcnn4 in all

samples and found that Kcnn4 is expressed as early as E14.5 (Fig. 10). A validated Kcnn4 antibody is needed to determine if Kcnn4 protein is also expressed at these time points.

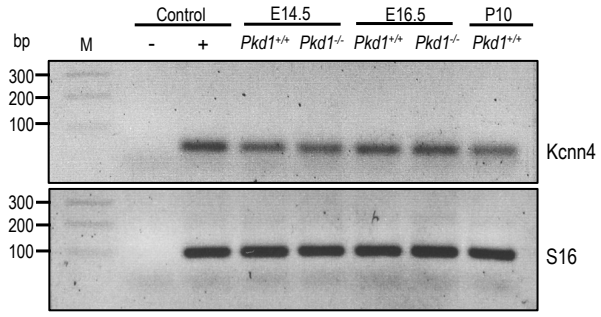

Fig. 10 Analysis of *Kcnn4* expression in mouse embryonic kidneys. Amplification of *Kcnn4* (58bp) and S16 (103bp) cDNA via quantitative PCR using RNA extracted from E14.5 and E16.5 metanephroi showing Kcnn4 is expressed early in embryo.

3.1.3 Highly elevated renal cAMP correlates with increased proliferation through activation of MAPK/ERK signaling pathway *in vivo*

We measured cAMP levels in kidneys of *Pkd1* orthologous mouse models $Pkd1^{cko}$, $^{SB}Pkd1$ and $Pkd1^{wt}$ and found a significant increase in comparison to age-matched wildtype controls (Fig. 11). At baseline, in wildtype kidneys, renal cAMP level varied from ~5 to ~14 pmol/mg protein between different ages, however, individual values within each age group were highly consistent. We found 225±23, 19±3 and 27±4 pmol cAMP/mg protein in P10 $Pkd1^{cko}$, 5–6-week-old $^{SB}Pkd1$ and 6–8-month-old $Pkd1^{wt}$, respectively. Although variations exist between individual values in these *Pkd1* mouse models, all values were highly elevated in comparison to wildtype kidneys. The fold increase in renal cAMP when compared to age-matched wildtype controls was greater in the early-onset $Pkd1^{cko}$ kidneys (16-fold) than in the adult-onset $^{SB}Pkd1$ (3.8-fold) and $Pkd1^{wt}$ (2.7-fold).

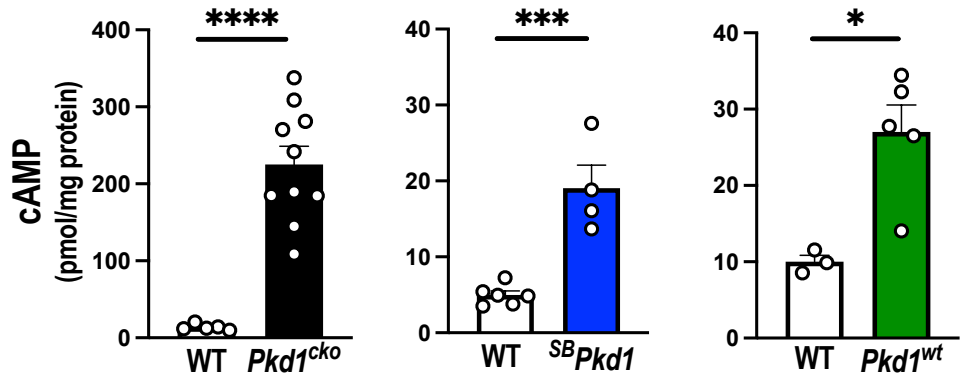

Fig. 11 Analysis of renal cAMP level in orthologous *Pkd1* mouse models. Quantification of cAMP levels (pmol cAMP per mg of protein) in P10 *Pkd1*^{cko} (black bar), 5–6-week-old ^{SB}*Pkd1* (blue bar) and 6-8month-old *Pkd1*^{wt} (green bar) kidneys in comparison to age-matched WT kidneys (open bar). *p<0.05, ***p<0.001, ****p<0.0001

As cAMP is known to stimulate proliferation through MAPK/ERK signaling, we measured protein levels of phospho-ERK, total ERK and downstream effector c-Myc in mouse kidneys. Both early- and adult-onset *Pkd1* mouse kidneys showed significant hyperactivation of MAPK/ERK (Fig. 12A-D). In P10 *Pkd1*^{cko}, the protein levels of phospho-ERK, phospho-ERK/total ERK and c-Myc increased by 4.7±0.8, 5.4±0.6 and 10.9±0.8 fold compared to controls, respectively (Fig. 12A). While the total amount of ERK protein was unchanged, the proportion of the activated form of ERK was highly increased, likely contributing to increases in c-Myc level. Likewise, in P10 *Pkd1*$^{v/v}$, phospho-ERK, phospho-ERK/total ERK and c-Myc protein levels were increased by 3.5±0.4, 4.6±0.6 and 2.6±0.4 fold, respectively (Fig. 12B). We observed similar activation in the adult-onset models ^{SB}*Pkd1* and *Pkd1*^{wt}, where we found greater activation in the relatively more rapidly progressive model ^{SB}*Pkd1;* phospho-ERK, phospho-ERK/total ERK and c-Myc protein levels increased by 6.5±1.3, 9.6±1.1 and 6.0±0.9 fold compared to wildtype measured at 5-6 weeks of age (Fig. 12C). In 6–8-month-old *Pkd1*^{wt}, we found 2.5±0.4, 6.3±0.7 and 6.5±0.8-fold increase in phospho-ERK, phospho-ERK/total ERK and c-Myc protein levels, respectively (Fig. 12D). This is the only model where we found a change

in total ERK levels compared to controls. Indeed, total ERK was reduced by over 50% and may in part contribute to the elevation in phospho-ERK.

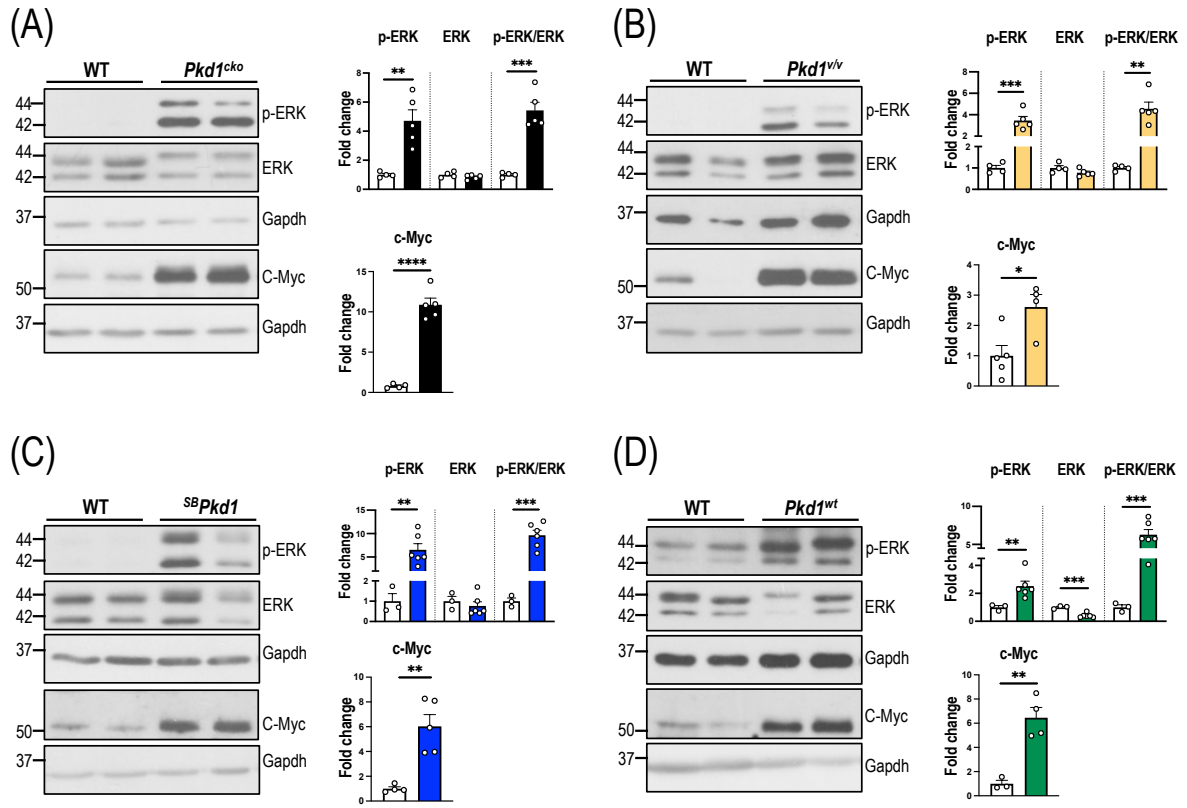

Fig. 12 Analysis of cAMP signaling cascade MAPK/ERK/Myc in distinct orthologous *Pkd1* mouse models. Representative western blot analysis (left) and quantification (right) of cAMP downstream effectors phospho-ERK, total ERK and c-Myc in P10 *Pkd1*^{cko} (A), P10 *Pkd1*$^{v/v}$ (B), 5–6-week-old ^{SB}*Pkd1* kidneys (C), 6–8-month-old *Pkd1*^{wt} (D), in comparison to age-matched wildtype (white bar). *p<0.05, **p<0.01, ***p<0.001, ****p<0.0001

3.1.4 *Kcnn4* knockout mice are healthy

The consistent elevation in *Kcnn4* expression across all analyzed mouse models provides a strong basis for targeting Kcnn4 for treatment of ADPKD. Before proceeding with genetic inactivation or pharmacologic inhibition of Kcnn4, we analyzed *Kcnn4* knockout mice to confirm Kcnn4 is safe to target. The *Kcnn4* knockout mice were indistinguishable from the wildtype, with no discernible phenotypes in the kidneys (Fig. 13) or any other organs. In addition, they had normal lifespan and fertility. As the major phenotype of ADPKD is found in

the kidneys, we also evaluated kidney function by measuring blood urea nitrogen (not shown) level and found no alterations.

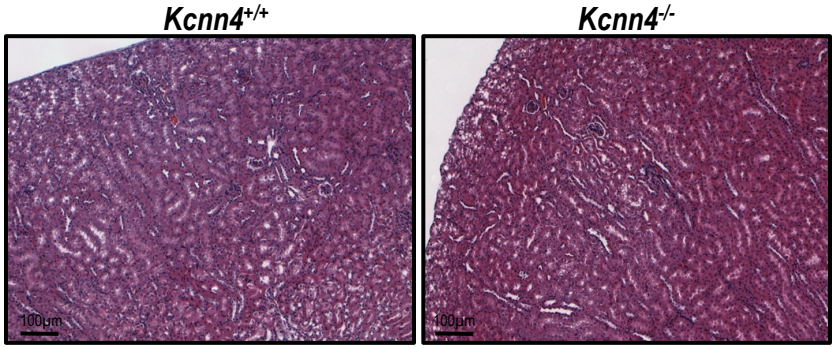

Fig. 13 Histological analysis of adult *Kcnn4* knockout mouse kidneys. Representative H&E histological sections of 7-month-old adult mouse kidneys comparing *Kcnn4* knockout (*Kcnn4*$^{-/-}$) to age-matched wildtype (Kcnn4$^{+/+}$).

3.2 Modulation of Kcnn4 in the embryonic kidney model

3.2.1 A Kcnn4 agonist exacerbates cysts in *Pkd1*$^{-/-}$ metanephroi and induces cysts in Pkd1$^{+/+}$

As renal cysts in *Pkd1*$^{-/-}$ mice usually initiate around E15.5, to study metanephroi cysts in culture, metanephroi needed to be isolated from E14.5 embryos and cultured for 4 days in humidified 37^{o}C incubator with CO_2 (Fig. 14A). We attempted culturing metanephroi beyond 4 or 5 days, but the conditions were no longer optimal for metanephroi development as they began to lose their well-defined outline and growth appeared restricted perhaps due to limited space in the cell insert. Once in culture, *Pkd1*$^{-/-}$ metanephroi required 8-Br-cAMP to be added on day 1 for cyst induction and had to be replaced in fresh media every two days. Any regimens to be tested were simultaneously added with 8-Br-cAMP. In contrary to the inherent ability of *Pkd1*$^{-/-}$ metanephroi to form cysts, Pkd1$^{+/+}$ metanephroi were generally non-cystic with rare sporadic tubular dilations and unresponsive to 8-Br-cAMP (Fig. 14B). We introduced Kcnn4 agonist SKA-111 to Pkd1$^{+/+}$ at 3 concentrations (10, 20 or 30μM) to test if cysts can be induced. Indeed, cysts were detectable within 1-2 days post treatment. Quantification of percent cyst area revealed

dose-dependent increase (Fig. 14C). Concentrations up to 30µM were tolerable as demonstrated by unchanging kidney volume and normal metanephroi development.

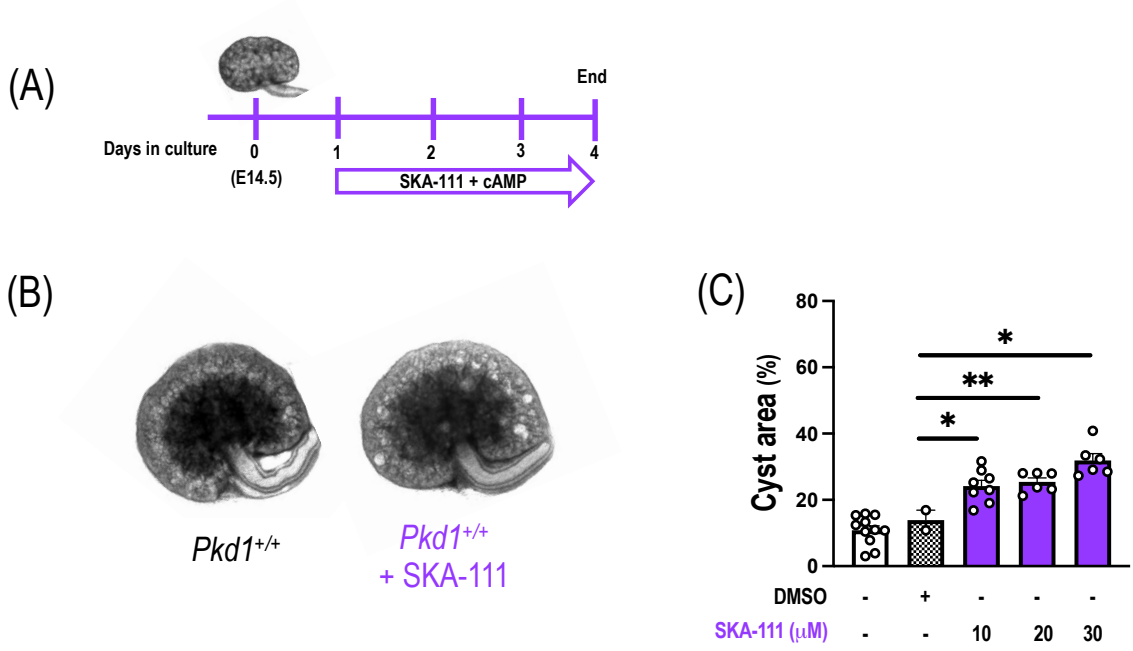

Fig. 14 Treatment of mouse metanephroi with Kcnn4 activator SKA-111. (A) Schematic representation of the experimental design: isolated E14.5 Pkd1$^{+/+}$ and *Pkd1*$^{-/-}$ metanephroi are stimulated with 100µM cAMP from day 1 until day 4 with or without simultaneous addition of Kcnn4 activator SKA-111. (B) Representative images of Pkd1$^{+/+}$ metanephroi with (right) or without (left) 30µM SKA-111 upon completion of treatment on day 4. (C) Quantification of percentage cyst area (%) in Pkd1$^{+/+}$ metanephroi treated with 10µM, 20µM or 30µM SKA-111 in comparison to vehicle (DMSO) is carried out upon completion of experiment. *p<0.05, **p<0.01

E14.5 *Pkd1*$^{-/-}$ metanephroi were highly responsive to 8-Br-cAMP; cysts were detectable as early as 1 day post treatment, the earliest timepoint we imaged metanephroi. Different concentrations of DMSO (0.1-1%) were tested in *Pkd1*$^{-/-}$ metanephroi to determine the optimal concentration for use without inducing a non-specific effect on cyst formation. Our results (not shown) indicated that up to 0.25% was acceptable, but we still selected the lowest concentration tested (0.1% DMSO) for all *ex vivo* experiments to minimize any unwanted non-specific effects on cyst formation. *Pkd1*$^{-/-}$ metanephroi subjected to 10µM of Kcnn4 agonist SKA-111 appeared

progressively more cystic with time than those treated with vehicle (DMSO) while there was no apparent toxicity on metanephroi development (Fig. 15A). Quantification upon completion of treatment on day 4 showed that SKA-111 led to a marked increase in percent cyst surface area and cyst number by 34 % and 44% in comparison to vehicle, respectively (Fig. 15B-C).

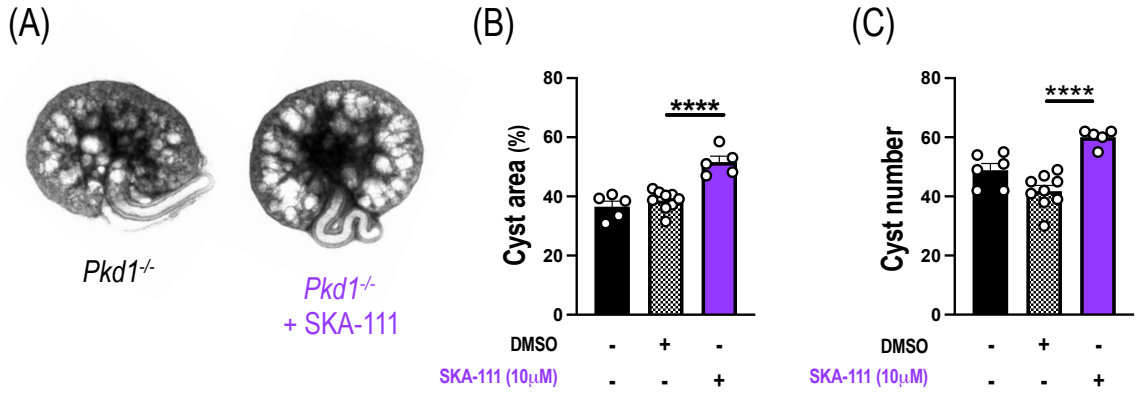

Fig. 15 Treatment of *Pkd1*$^{-/-}$ metanephroi with SKA-111. (A) Representative images of *Pkd1*$^{-/-}$ metanephroi with (right) or without (left) 10μM SKA-111 upon completion of treatment on day 4. Quantification of percentage cyst area (B) and cyst number (C) in *Pkd1*$^{-/-}$ metanephroi treated with 10μM SKA-111 in comparison to vehicle is carried out upon completion of experiment. ****p<0.0001

3.2.2 *Pkd1*$^{-/-}$*; Kcnn4*$^{-/-}$ metanephroi are less responsive to cAMP

To investigate whether *Kcnn4* genetic inactivation can influence *Pkd1*$^{-/-}$ cystogenesis, *Pkd1*$^{+/-}$*; Kcnn4*$^{-/-}$ breeders were setup to generate *Pkd1*$^{-/-}$*; Kcnn4*$^{-/-}$ embryos for metanephroi isolation, which were compared to *Pkd1*$^{-/-}$ metanephroi cyst growth. 8-Br-cAMP was added to the media on day 1 and replaced on day 3 (Fig. 16A). Differences in severity of cysts between *Pkd1*$^{-/-}$ and *Pkd1*$^{-/-}$*; Kcnn4*$^{-/-}$ metanephroi were evident from day 1 and became progressively more prominent. A macroscopic comparison on day 4 revealed obvious differences in the severity of cysts (Fig. 16B). Cysts in *Pkd1*$^{-/-}$*; Kcnn4*$^{-/-}$ metanephroi were smaller in size and fewer in number than *Pkd1*$^{-/-}$ metanephroi. Indeed, the relative cyst surface area, as well as cyst number were reduced by 38% and 31%, respectively, upon *Kcnn4* genetic inactivation when

compared to *Pkd1*$^{-/-}$ metanephroi (Fig. 16C-D). Importantly, *Kcnn4* inactivation did not alter metanephroi development; *Pkd1*$^{-/-}$*; Kcnn4*$^{-/-}$ metanephroi were healthy with no reduction in kidney volume.

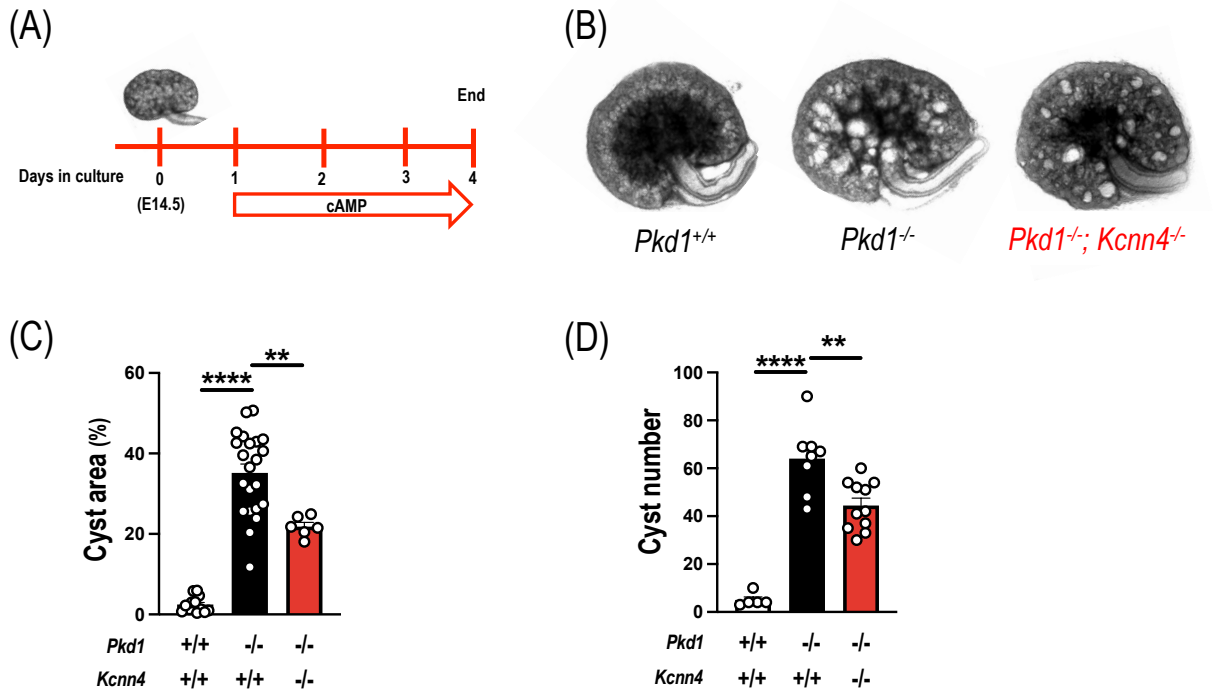

Fig. 16 Analysis of cyst indices in *Pkd1*$^{-/-}$ metanephroi upon *Kcnn4* genetic inactivation. (A) Schematic representation of the experimental design: isolated E14.5 Pkd1$^{+/+}$, *Pkd1*$^{-/-}$ and *Pkd1*$^{-/-}$*; Kcnn4*$^{-/-}$ metanephroi are stimulated with 100µM cAMP from day1 until day 4. (B) Representative images of Pkd1$^{+/+}$, *Pkd1*$^{-/-}$ and *Pkd1*$^{-/-}$*; Kcnn4*$^{-/-}$ metanephroi stimulated with 100µM cAMP upon completion of treatment on day 4. Quantification of percentage cyst area (C) and cyst number (D) in Pkd1$^{+/+}$, *Pkd1*$^{-/-}$ and *Pkd1*$^{-/-}$*; Kcnn4*$^{-/-}$ metanephroi stimulated with 100µM cAMP is carried out upon completion of experiment. **p<0.01, ****p<0.0001

3.2.3 Kcnn4 pharmacologic inhibition prevents cyst growth and regresses pre-formed cysts

To understand if Kcnn4 pharmacologic inhibition can prevent or delay *Pkd1*$^{-/-}$ cyst growth, we introduced two Kcnn4 inhibitors of different potency into the metanephroi culture media on day 1 simultaneously with 8-Br-cAMP (Fig. 17A). As Pkd1$^{+/+}$ metanephroi tolerated well 30µM of SKA-111, we applied 20µM or 40µM of TRAM-34 to *Pkd1*$^{-/-}$ metanephroi (Fig.

17B-C). Both concentrations were tolerable; metanephroi showed normal growth. The difference in percent cyst area between *Pkd1*$^{-/-}$ metanephroi and those treated with 20µM or 40µM TRAM-34 led to similar reduction (26% versus 28%).

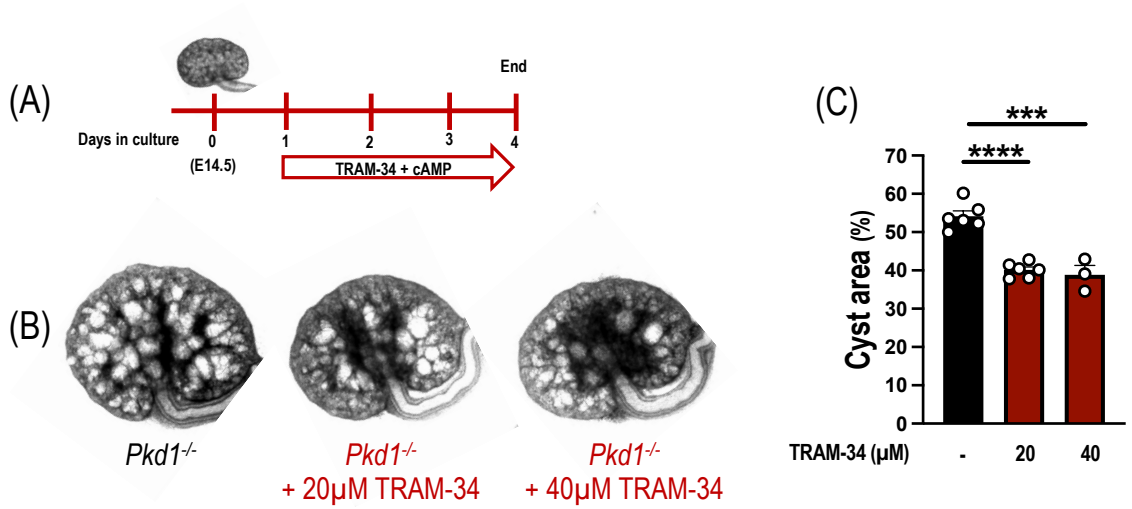

Fig. 17 Treatment of *Pkd1*$^{-/-}$ metanephroi with Kcnn4 inhibitor TRAM-34. (A) Schematic representation of the experimental design: *Pkd1*$^{-/-}$ metanephroi isolated at E14.5 were stimulated with 100µM cAMP from day 1 until day 4 with or without simultaneous addition of Kcnn4 inhibitor TRAM-34 used at 20µM or 40µM. (B) Representative images of *Pkd1*$^{-/-}$ metanephroi treated with (center and right) or without (left) TRAM-34 upon completion of treatment on day 4. (C) Quantification of percentage cyst area in *Pkd1*$^{-/-}$ metanephroi in comparison to those treated with 20µM or 40µM of TRAM-34 is carried out upon completion of experiment. ***p<0.001, ****p<0.0001

Pkd1$^{-/-}$ metanephroi subjected to 20µM of a more potent Kcnn4 inhibitor, Senicapoc, were substantially less cystic compared to vehicle treated metanephroi (Fig. 18B). When Senicapoc was given simultaneously with 8-Br-cAMP, both percent cyst area and cyst number greatly reduced by 91% and 87% upon completion of experiment on day 4, respectively (Fig. 18C-D). This striking reduction resulted in nearly indistinguishable tissue morphology from wildtype.

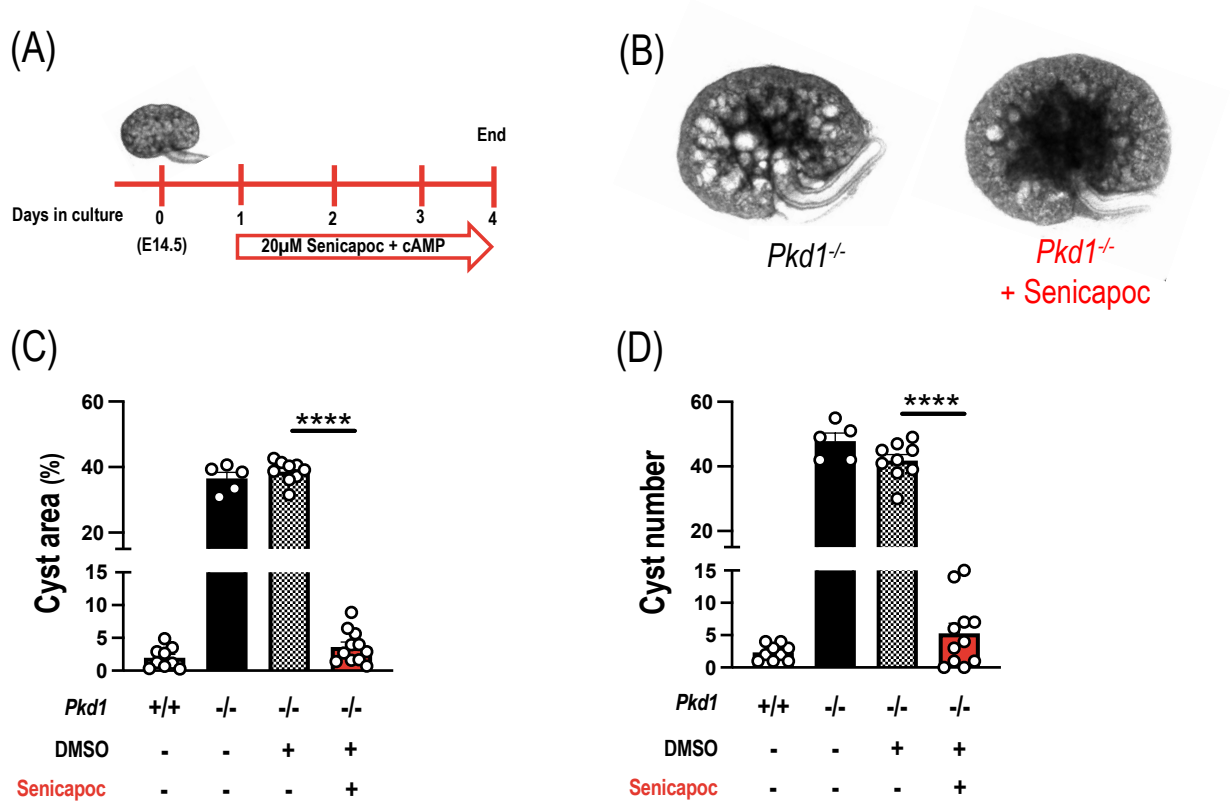

Fig. 18 Treatment of *Pkd1*$^{-/-}$ metanephroi with Kcnn4 inhibitor Senicapoc at time of cyst induction. (A) Schematic representation of the experimental design: *Pkd1*$^{-/-}$ metanephroi isolated at E14.5 were stimulated with 100μM cAMP on day 1 until day 4 with or without simultaneous addition of Kcnn4 inhibitor Senicapoc used at 20μM. (B) Representative images of *Pkd1*$^{-/-}$ metanephroi with (right) or without (left) 20μM Senicapoc upon completion of treatment on day 4. Quantification of percentage cyst area (C) and cyst number (D) in *Pkd1*$^{-/-}$ metanephroi in comparison to vehicle upon completion of treatment on day 4. ****p<0.0001

We then tested if Senicapoc can be effective towards established *Pkd1*$^{-/-}$ cysts by adding Senicapoc on day 3, which was 2 days after cyst induction (Fig. 19A). On the following day (day 4), a clear difference was readily detected; those treated with Senicapoc were much less cystic. Cysts diminished in size and number progressively (Fig. 19B). We plotted percent cyst area in form of a bar graph (Fig. 19C) and a line graph (Fig. 19D) to show that when compared to *Pkd1*$^{-/-}$ metanephroi where cyst area progressively increased from Day 3 to Day 5, cyst growth in those treated with Senicapoc were markedly restricted, and even progressively reduced established cysts. On day 4, percent cyst area was reduced by 50% and by 61% on day 5. To test if cyst

modulation was reversible, we removed Senicapoc and found that cysts indeed re-developed (not shown).

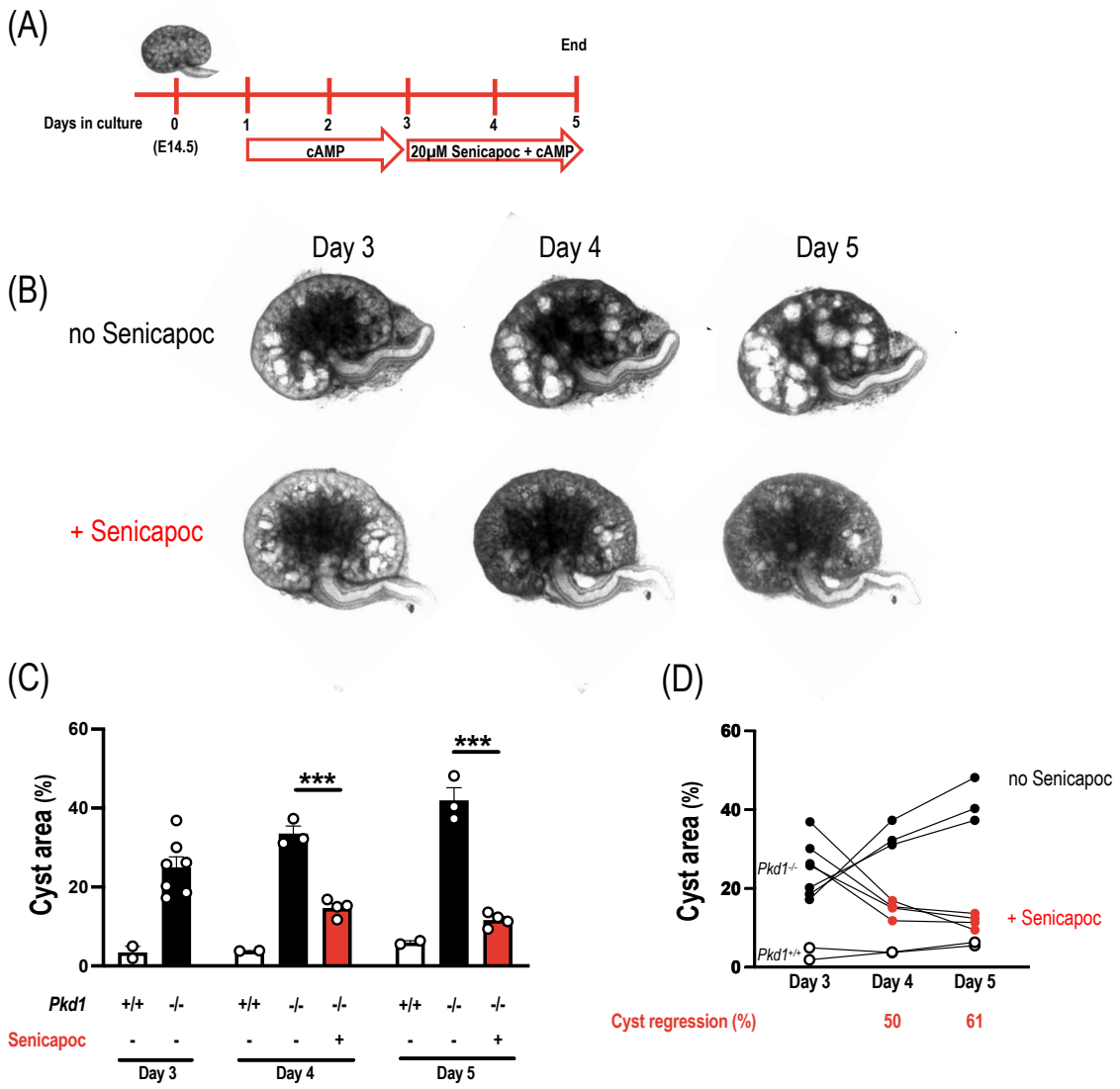

Fig. 19 Treatment of *Pkd1*$^{-/-}$ metanephroi with Senicapoc 2 days after cyst induction. (A) Schematic representation of the 5-day experimental design: *Pkd1*$^{-/-}$ metanephroi isolated at E14.5 were stimulated with 100μM cAMP on day 1. On day 3, metanephroi were treated with or without 20μM Senicapoc until day 5. (B) Representative images of *Pkd1*$^{-/-}$ metanephroi with (bottom) or without (top) Senicapoc on day 3, 4, and 5 of the experiment. (C) Quantification of percentage cyst area in *Pkd1*$^{-/-}$ metanephroi with (red bar) or without (black bar) Senicapoc relative to Pkd1$^{+/+}$ (open bar) from day 3 to day 5. (D) Quantification of percentage cyst area in *Pkd1*$^{-/-}$ metanephroi with (red circle) or without (black circle) Senicapoc relative to Pkd1$^{+/+}$ (open circle) from day 3 to day 5. Each curve follows longitudinal progression of cyst area in individual metanephros over 3-day period. ***p<0.001

3.3 *Kcnn4* genetic inactivation causes delay in disease progression in 2 *Pkd1* mouse models of different disease onset and severity

3.3.1 *Kcnn4* genetic inactivation improves cyst indices and ultimately reduces kidney size in early-onset rapid progressive model *Pkd1^{cko}*

Renal cysts in the early-onset rapid progressive model *Pkd1^{cko}* were detectable as early as P2 and progressively increased in number and size until end of life around 3 weeks of age. We analyzed *Pkd1^{cko}* at P5 and P10, representing early and mid-stage of disease progression, respectively. The abdomen of *Pkd1^{cko}* were extended due to enlarged cystic kidneys and became more prominent with disease progression. At P10, isolated kidneys were macroscopically larger in size and paler in colour than wildtype kidneys (Fig. 20A). KBW of cystic P5 *Pkd1^{cko}* kidneys increased by 3.8-fold over wildtype and progressively enlarged with age, reaching 11.4-fold by P10. In comparison, *Pkd1^{cko}; Kcnn4$^{-/-}$* had smaller abdomens and isolated kidneys were smaller than *Pkd1^{cko}* kidneys. Accordingly, KBW reduced by 29% at P5 and by 20% at P10. We stained kidney sections with H&E to quantify cysts. P10 *Pkd1^{cko}* kidney was highly cystic with little intact tissue remaining compared to the wildtype, while genetic *Kcnn4* inactivation helped to preserve more healthy tissue (Fig. 20B). Percent cyst area increased by 16.5-fold in P5 *Pkd1^{cko}* and by 24.2-fold in P10 *Pkd1^{cko}* compared to wildtype (Fig. 20C). In just 5 days, we found a 40% increase in percent cyst area in P10 *Pkd1^{cko}* compared to P5 *Pkd1^{cko}*. *Kcnn4* inactivation reduced percent cyst area equally at both ages, by 20% in P5 *Pkd1^{cko}* and by 18% in P10 *Pkd1^{cko}*. Contrary to the significant 40% increase in percent cyst area between P5 and P10 *Pkd1^{cko}*, overall cyst number did not increase at the same rate and only increased by 14% (Fig. 20D). Genetic *Kcnn4* inactivation effectively reduced cyst number at both ages and was significantly greater at P5 (28%) than at P10 (16%).

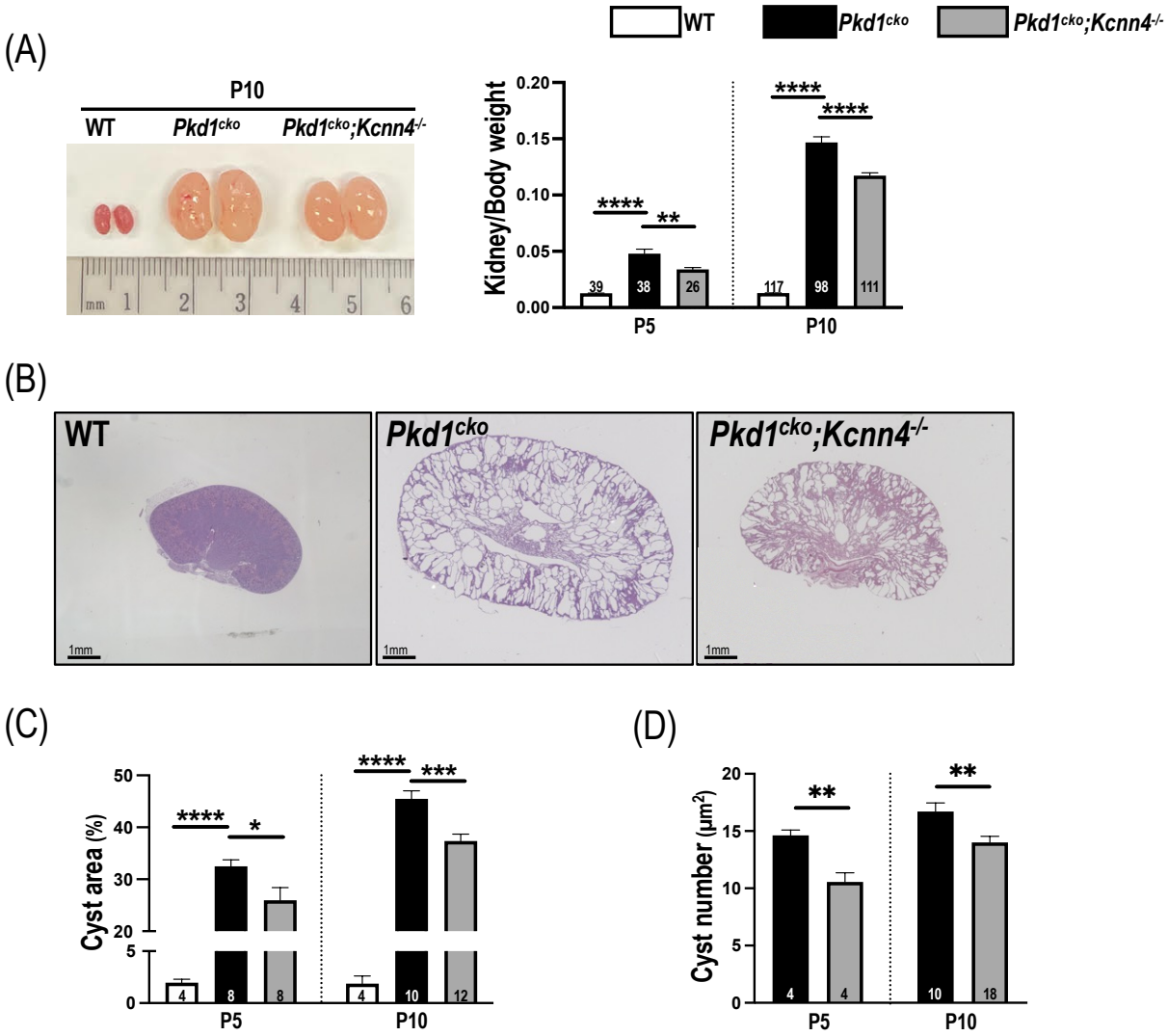

Fig. 20 Histomorphometric analysis of *Pkd1^{cko}* and *Pkd1^{cko}; Kcnn4$^{-/-}$* kidneys. (A) Macroscopic kidney images of P10 WT, *Pkd1^{cko}* and *Pkd1^{cko}; Kcnn4$^{-/-}$* and quantification (right) of kidney weight to body weight ratio (KBW) of WT (open bar), *Pkd1^{cko}* (black bar), *Pkd1^{cko}; Kcnn4$^{-/-}$* (grey bar) at P5 and P10 (the number of animals analyzed are written within the bars). (B) Representative H&E histologic kidney sections of P10 WT, *Pkd1^{cko}*, and *Pkd1^{cko}; Kcnn4$^{-/-}$*. Quantification of percentage cyst area (C) and cyst number per mm^2 of kidney area (D) in *Pkd1^{cko}* and *Pkd1^{cko}; Kcnn4$^{-/-}$* at P5 and P10 in comparison to WT. *p<0.05, **p<0.01, ***p<0.001, ****p<0.0001

To determine which factor contributed more to the reduced cyst indices, we sorted individual cysts by size and plotted the distribution of *Pkd1^{cko}* and *Pkd1^{cko}; Kcnn4$^{-/-}$* at P5 and at P10 (Fig. 21). Overall, P10 animals had bigger cysts and greater proportion of larger cysts

compared to P5. Comparison between *Pkd1*^{cko} and *Pkd1*^{cko}*; Kcnn4*$^{-/-}$ at P5 or at P10 showed that cyst distribution was unchanged upon genetic inactivation of *Kcnn4*.

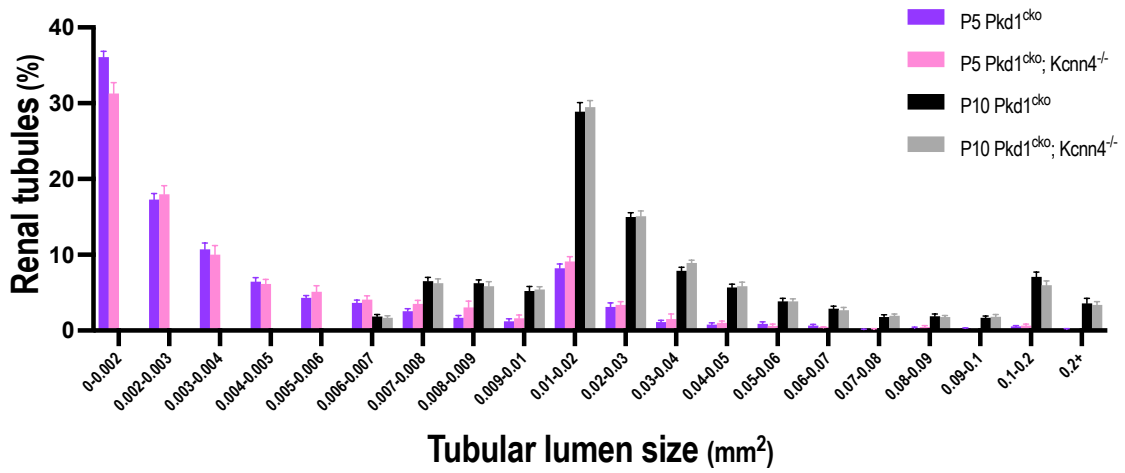

Fig. 21 Analysis of individual cysts based on tubular lumen size. Cysts in kidney sections of P5 and P10 *Pkd1*^{cko} and *Pkd1*^{cko}*; Kcnn4*$^{-/-}$ are listed by size and sorted into corresponding size intervals.

3.3.2 Genetic *kcnn4* inactivation reduces cysts from distal tubules and collecting ducts but is insufficient to improve kidney function or extend lifespan in *Pkd1*^{cko}

We analyzed cyst tubular origins of *Pkd1*^{cko} to determine which nephron segments were affected by *Kcnn4* inactivation by labeling P5 FFPE kidney sections with tubular segment specific lectin markers (Fig. 22). The proximal, distal, and collecting tubules were coloured in green, blue, and red, respectively. Based on the tubular diameter threshold we determined using the wildtype control (cf. section 2.3.2), we did not detect any cysts of proximal tubular origin. All cysts were found exclusively in distal tubules and collecting ducts, consistent with localized expression of *Ksp-cadherin*. There were fewer large cysts in *Pkd1*^{cko}*; Kcnn4*$^{-/-}$ based on our images. We quantified the proportion of cystic tubules within distal and collecting segments and found 1.9-fold greater proportion of cysts in the collecting duct. *Kcnn4* inactivation effectively reduced the proportion of cysts in both tubular segments at P5 in the *Pkd1*^{cko}. Cysts in the distal tubules were reduced by 31%, while those in the collecting ducts were reduced by 30%.

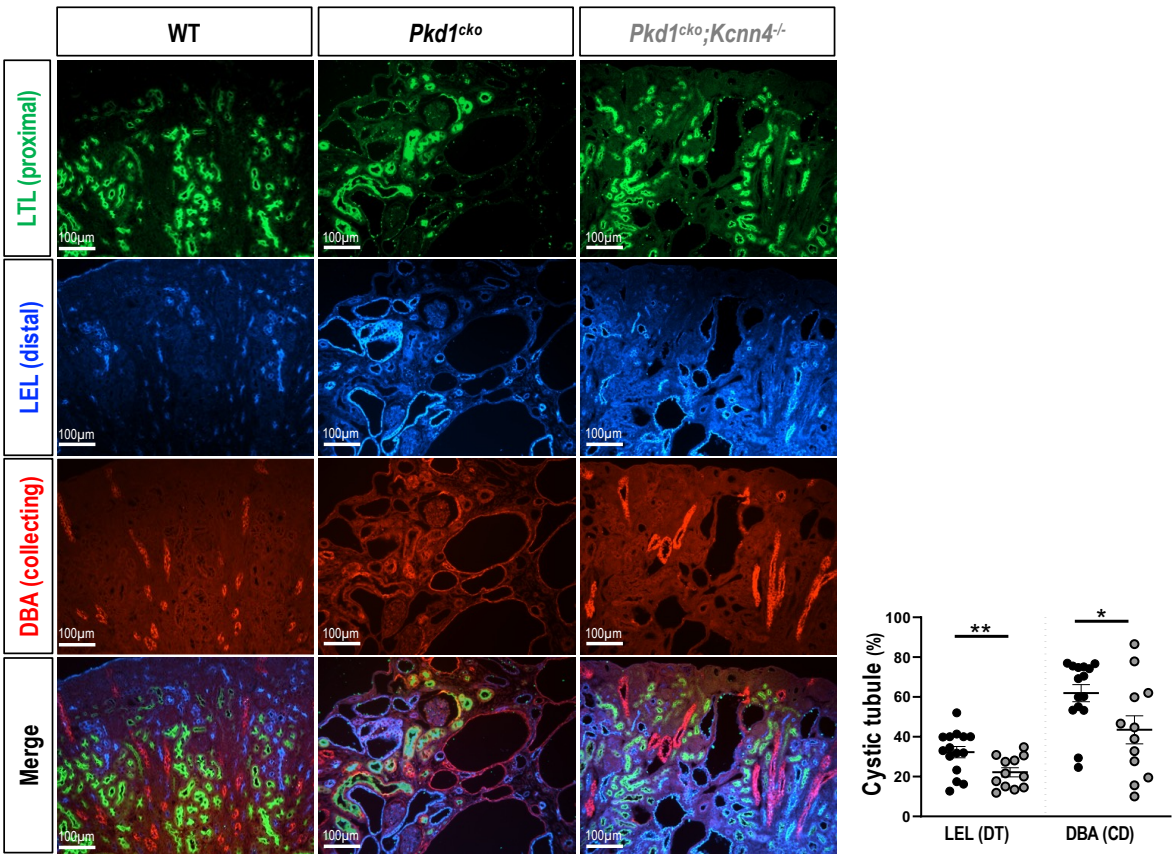

Fig. 22 Analysis of cyst tubular origin in *Pkd1^{cko}* and *Pkd1^{cko}; Kcnn4$^{-/-}$* kidneys. Cyst tubular origin in P5 WT, *Pkd1^{cko}* and *Pkd1^{cko}; Kcnn4$^{-/-}$* kidneys was analyzed by immunofluorescence using markers specific for proximal tubule (LTL; green), distal tubule (LEL; blue) and collecting duct (DBA; red). No proximal tubular cysts are observed in WT, *Pkd1^{cko}* or *Pkd1^{cko}, Kcnn4$^{-/-}$* kidneys. Quantification of percentage cystic tubules (%) in distal tubule (DT) and collecting duct (CD) of *Pkd1^{cko}* (black dot) and *Pkd1^{cko}, Kcnn4$^{-/-}$* (grey dot) kidneys is shown on the right. *p<0.05, **p<0.01

We determined serum BUN levels and plotted a Kaplan-Meier curve to determine if the improvement in tissue morphology and cyst indices we observed were reflected by an improvement in kidney function and survival. The BUN level increased by 2.7-fold in P5 *Pkd1^{cko}* and by 4.4-fold in P10 *Pkd1^{cko}* compared to wildtype (Fig. 23A). However, *Kcnn4* inactivation did not reduce the BUN levels at any measured timepoint. In both cases, there were large variations between individual samples, but we did not find a correlation between BUN levels and the size of cystic kidneys. We also monitored for survival in *Pkd1^{cko}* and *Pkd1^{cko}; Kcnn4$^{-/-}$* and

found no apparent extension of lifespan upon genetic *Kcnn4* inactivation. Median survival was 18 days in *Pkd1*^{cko} and 16 days in *Pkd1*^{cko}*; Kcnn4*$^{-/-}$ (Fig. 23B).

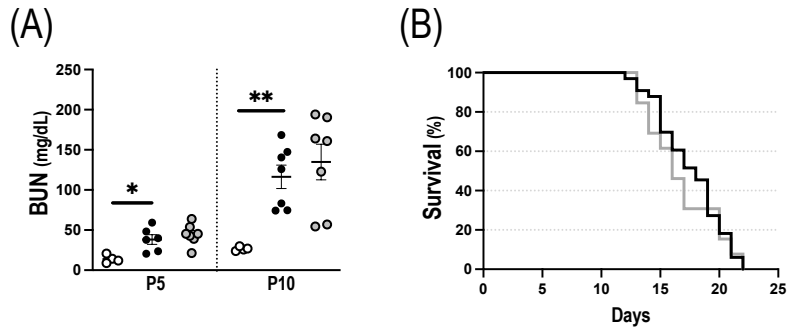

Fig. 23 Assessment of kidney function and survival in *Pkd1*^{cko} and *Pkd1*^{cko}*; Kcnn4*$^{-/-}$. (A) Blood Urea Nitrogen (BUN) analysis of P10 WT (open circle), *Pkd1*^{cko} (black circle) and *Pkd1*^{cko}*; Kcnn4*$^{-/-}$ (grey circle) kidneys. (B) Kaplan-Meier survival curve of *Pkd1*^{cko} versus *Pkd1*^{cko}*; Kcnn4*$^{-/-}$. *p<0.05, **p<0.01

3.3.3 Reduction in renal cAMP levels dampens proliferation, improves kidney fibrosis and lowers primary cilia length in *Pkd1*^{cko}

As cAMP was consistently upregulated in our mouse models and is known to associate closely with major processes required for cyst progression in ADPKD, including proliferation, fibrosis, and primary cilia elongation, we measured cAMP levels in P10 *Pkd1*^{cko}*; Kcnn4*$^{-/-}$ and found a significant reduction by 37% compared to P10 *Pkd1*^{cko} upon loss of *Kcnn4* (Fig. 24A). As cAMP is known to stimulate proliferation through MAPK/ERK activation, we measured protein levels of phospho-ERK, total ERK and downstream effector c-Myc (Fig. 24B). While total ERK remained stable, we found striking reductions in the other components. Phospho-ERK and the phospho-ERK to total ERK ratio were almost restored to baseline, while c-Myc was reduced by more than half. We next measured proliferation in kidney epithelial cells in P10 *Pkd1*^{cko} using the proliferation marker ki67 (Fig. 24C). In comparison to wildtype controls, which rarely had more than one ki67-positive epithelial cell in a renal tubule, P10 *Pkd1*^{cko} tubular epithelia was highly proliferative with many ki67-positive epithelial cells frequently detected in

the same renal tubule. The number of ki67-positive nuclei correlated with cyst size: the larger the cyst, the more ki67-positive epithelial tubular cells. In line with these observations, the number of ki67-positive cells per μm^2 kidney was increased by 3.5-fold in P10 *Pkd1^{cko}* compared to wildtype. The number of highly proliferative cystic tubular cells in *Pkd1^{cko}* was greatly reduced by 43% upon genetic *Kcnn4* inactivation.

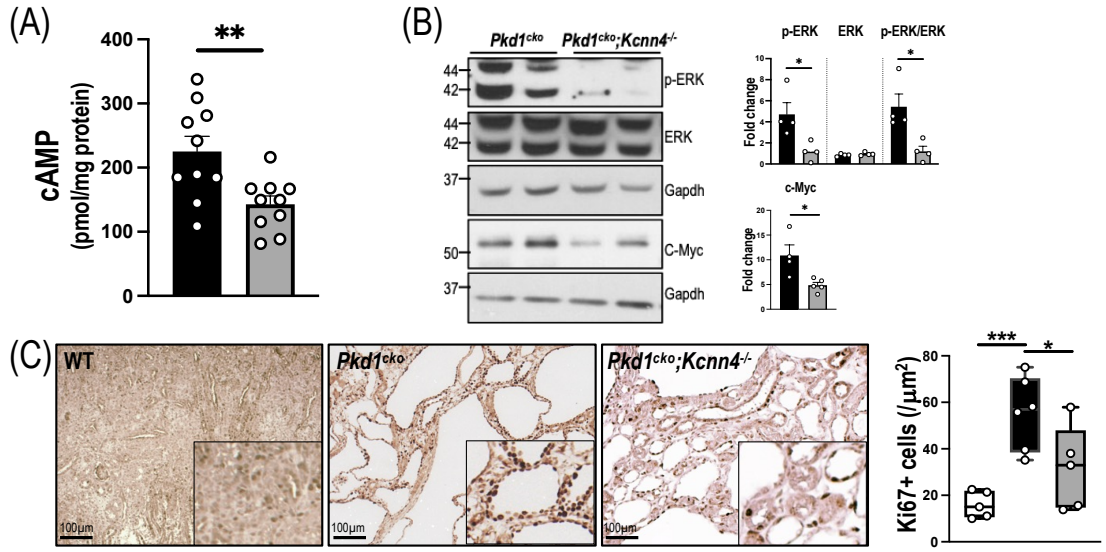

Fig. 24 Analysis of cAMP level and proliferation status of *Pkd1^{cko}* versus *Pkd1^{cko}; Kcnn4$^{-/-}$* kidneys. (A) cAMP level is measured by ELISA and is expressed as pmol cAMP per mg of protein. (B) Representative western blot analysis (left) and quantification (right) of cAMP downstream effectors phospho-ERK, total ERK and c-Myc in P10 *Pkd1^{cko}* versus *Pkd1^{cko}; Kcnn4$^{-/-}$* kidneys. (C) Quantification of renal epithelial cell proliferation by Ki67 immunohistochemistry in P10 WT, *Pkd1^{cko}* and *Pkd1^{cko}; Kcnn4$^{-/-}$* kidneys (right) with representative images shown on the left. Proliferation is expressed as the number of ki67 positive cells per μm^2 kidney surface. *p<0.05, **p<0.01, ***p<0.001

Since cAMP signaling also contributes to fibrosis, we stained kidney sections with Sirius Red, a marker for collagen I and IV, and found *Pkd1^{cko}* kidneys were highly fibrotic with many regions of intense red staining signifying collagen accumulation (Fig. 25). The relative fibrotic surface in P10 *Pkd1^{cko}* was increased by 4.8-fold compared to wildtype. *Kcnn4* inactivation reduced percent fibrosis by 39%.

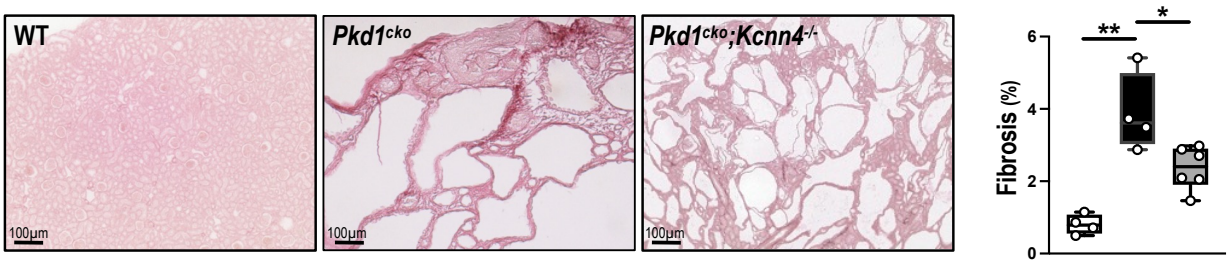

Fig. 25 Analysis of kidney fibrosis in *Pkd1^{cko}* versus *Pkd1^{cko}; Kcnn4$^{-/-}$*. Fibrosis is detected by Sirius Red and is expressed as the percentage of renal fibrotic surface (%) in P10 WT, *Pkd1^{cko}* and *Pkd1^{cko}; Kcnn4$^{-/-}$* kidneys. (right) Representative images are shown on the left. *p<0.05 **p<0.01

Additionally, as primary cilia length can also be modulated by cAMP levels, we stained primary cilia with anti-acetylated-tubulin and measured the length of each primary cilia in the kidney sections (Fig. 26A). The average primary cilia length was increased by 1.9-fold in P10 *Pkd1^{cko}*. We sorted primary cilia based on their length and plotted their overall distribution (Fig. 26B). About 70% of all the primary cilia found in P10 wildtype were below 3µm in length. In contrast, the ciliary distribution of P10 *Pkd1^{cko}* was reversed; nearly 80% of primary cilia were above 3µm in length. The distribution of *Pkd1^{cko}* cilia lengths was shifted to the right of the x-axis, with a strikingly greater proportion of longer primary cilia. We found a slight shift of ciliary distribution in *Pkd1^{cko}; Kcnn4$^{-/-}$* to the left of the x-axis. Accordingly, the increased average primary cilia length found in *Pkd1^{cko}* was reduced by 26%. As Wnt/β-catenin signaling is an important pathway in the primary cilia, we analyzed protein levels of active and total β-catenin using western blot (Fig. 26C). In comparison to wildtype, Wnt signaling was highly activated in P10 *Pkd1^{cko}* as shown by the significant elevation in active, total, and active/total β-catenin levels by 9.1-fold, 3.7-fold, and 2.4-fold, respectively, in line with results previous reported by the lab (Parrot et al., 2019). However, *Kcnn4* inactivation did not significantly contribute to Wnt signaling. Although there was a tendency for active and total β-catenin protein levels to reduce upon *Kcnn4* inactivation, the differences were not significant.

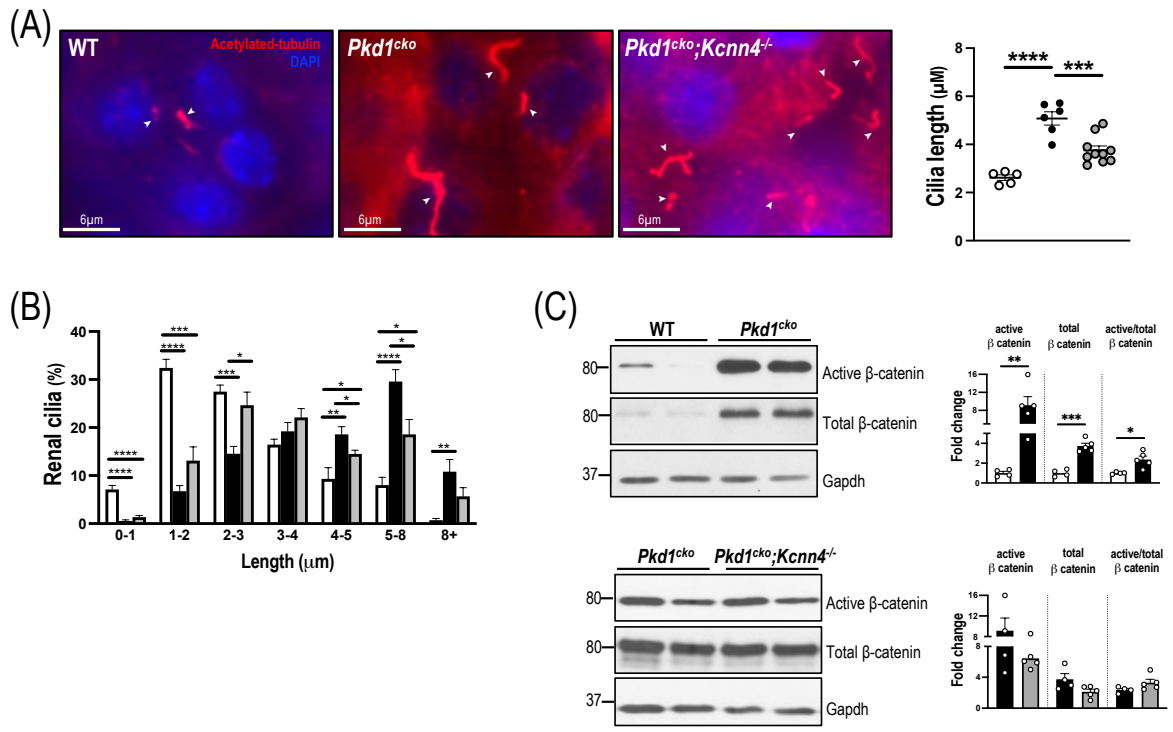

Fig. 26 Analysis of primary cilia length and canonical Wnt signaling in *Pkd1^{cko}* versus *Pkd1^{cko}; Kcnn4$^{-/-}$* kidneys. (A) Quantification of mean primary cilia length in P10 WT, *Pkd1^{cko}* and *Pkd1^{cko}; Kcnn4$^{-/-}$* kidneys using immunofluorescent anti-alpha acetylated tubulin marker (right). Representative images are shown on the left with white arrows pointing at individual cilium. (B) Length of all primary cilia found in the entire kidney section were measured and sorted into intervals based on their length. The primary cilia distribution of P10 *Pkd1^{cko}* showed a distinct shift towards the right of x-axis in comparison to WT that was shifted slightly towards the left upon genetic inactivation of Kcnn4. (C) Representative western blot analysis (left) and quantification (right) of active β-catenin and total β-catenin in P10 WT versus *Pkd1^{cko}* (top) and *Pkd1^{cko}* versus *Pkd1^{cko}; Kcnn4$^{-/-}$* (bottom) kidneys. *p<0.05, **p<0.01, ***p<0.001, ****p<0.0001

All western blot analyses were done in parallel at an earlier stage (P5) to monitor if the activation or rescue would be more prominent earlier in the disease. Representative images and quantifications analyzing MAPK/ERK, Wnt/β-catenin and c-Myc in P5 *Pkd1^{cko}* kidneys in comparison to wildtype are shown in Fig. 27A. Fig. 27B compares protein levels of the markers of those signaling pathways in P5 *Pkd1^{cko}; Kcnn4$^{-/-}$* kidneys in comparison to *Pkd1^{cko}*. Signaling analysis at P5 resembled that of P10.

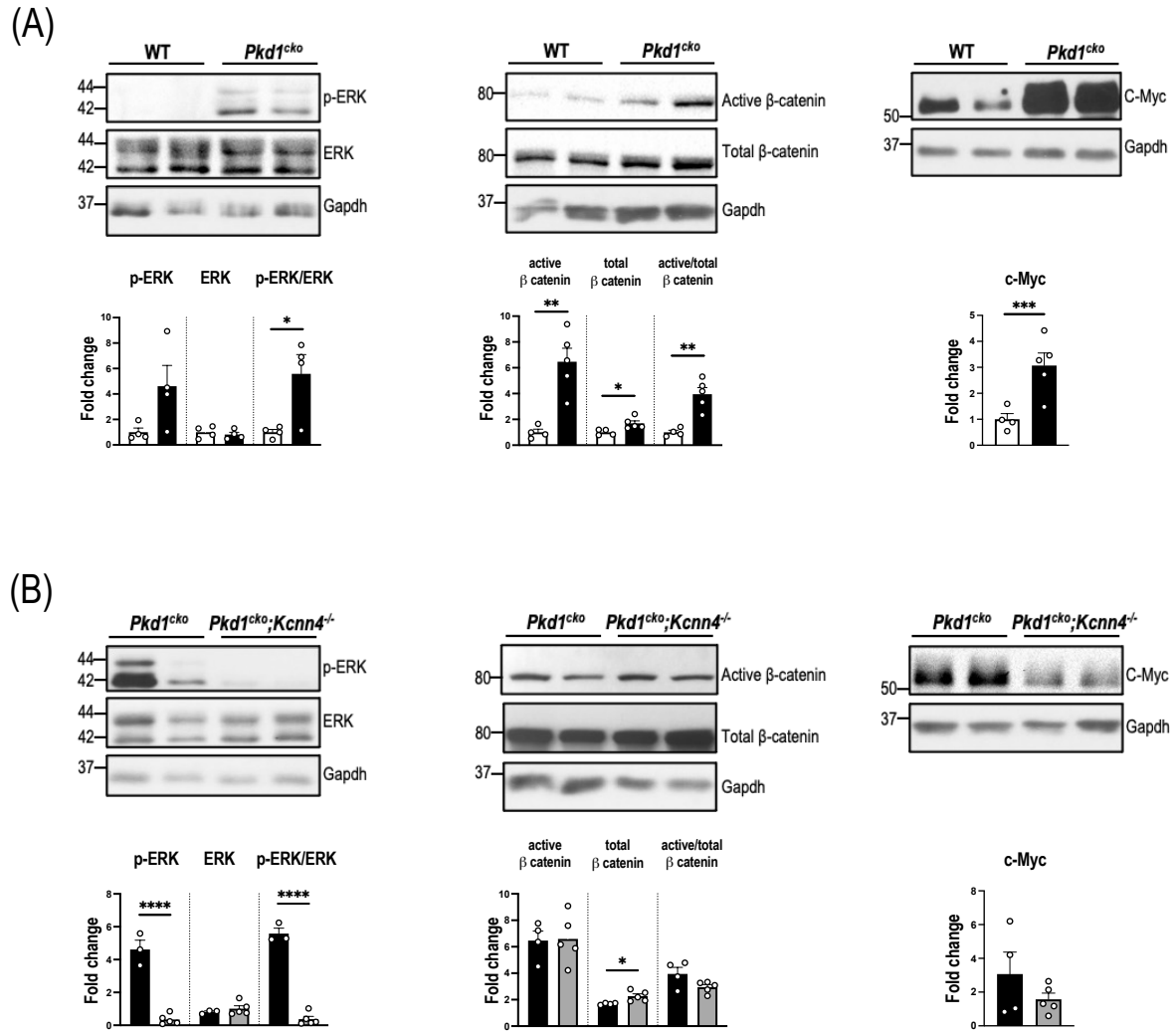

Fig. 27 Western blot analysis of MAPK/ERK/c-Myc and Wnt/β-catenin in *Pkd1*^{cko} versus *Pkd1*^{cko}*; Kcnn4*$^{-/-}$ at P5. (A) Representative western blot analysis (top) and quantification (bottom) of MAPK/ERK (left), Wnt/β-catenin (center) and c-Myc (right) in P5 WT versus *Pkd1*^{cko} kidneys. (B) Representative western blot analysis (top) and quantification (bottom) of MAPK/ERK (left), Wnt/β-catenin (center) and c-Myc (right) in P5 *Pkd1*^{cko} versus *Pkd1*^{cko}*; Kcnn4*$^{-/-}$ kidneys. *p<0.05, **p<0.01, ***p<0.001, ****p<0.0001

We listed the fold increase between *Pkd1*^{cko} and wildtype as well as percent change in *Pkd1*^{cko}*; Kcnn4*$^{-/-}$ compared to *Pkd1*^{cko} at P5 and P10 in Fig. 28 for direct numerical comparison between signaling pathway activation at P5 and P10. We found that the activation of MAPK/ERK in the *Pkd1*^{cko} model, as well as the rescue by genetic *Kcnn4* inactivation were highly consistent between P5 and P10. Although c-Myc hyperactivation was more prominent at P10 than at P5, *Kcnn4* inactivation reduced c-Myc by half at both ages (Fig. 28). The pattern of

Wnt/β-catenin activation and rescue by *Kcnn4* inactivation was less conclusive as the pattern was less consistent between P5 and P10 as shown in Fig. 27. For instance, there was greater increase of active β-catenin and total β-catenin, but less active/total β-catenin at P10 versus P5 *Pkd1*^{cko}. At P5, *Kcnn4* inactivation did not show tendency to influence active β-catenin levels, but since total β-catenin levels was elevated, the active/total β-catenin ratio was reduced. At P10, although both active and total β-catenin were reduced, total β-catenin was reduced to a greater extent, hence increased the active/total β-catenin ratio. The observed large variations between individual values may explain in part the inconsistency between P5 and P10 upon *Kcnn4* inactivation.

	P5 Pkd1^{cko} vs WT	**P10** Pkd1^{cko} vs WT		**P5** Pkd1^{cko}; Kcnn4$^{-/-}$ vs Pkd1^{cko}	**P10** Pkd1^{cko}; Kcnn4$^{-/-}$ vs Pkd1^{cko}
	Fold increase			Percent change	
Phospho-ERK	4.6	4.7		Normalized	Normalized
Total ERK	0.8	0.8		Normalized	Normalized
Phospho/total ERK	5.6	5.4		Normalized	Normalized
c-Myc	3.1	10.9		- 49%	- 55%
Active β-catenin	6.5	9.1		+ 2%	- 30%
Total β-catenin	1.7	3.7		+ 34%	- 43%
Active/total β-catenin	3.9	2.4		- 25%	+ 40%

Fig. 28 Multistage comparison of signaling activation between P5 and P10 *Pkd1*^{cko} and *Pkd1*^{cko}*; Kcnn4*$^{-/-}$ kidneys. Numerical comparison of MAPK/ERK, Wnt/β-catenin and c-Myc signaling between P5 and P10 kidneys. Values are displayed as fold increase from WT to *Pkd1*^{cko} (column 1 and 2) and percentage change (%) in *Pkd1*^{cko}*; Kcnn4*$^{-/-}$ from *Pkd1*^{cko} (column 3 and 4). Normalized: protein levels are returned to the level detected in WT.

3.3.4 Heterozygous *Kcnn4* knock-out is sufficient to improve cyst indices and kidney morphology in adult-onset slow-progressive model ^{SB}*Pkd1*

At 6 months, contrary to the enlarged abdomen observed in *Pkd1*^{cko}, both ^{SB}*Pkd1* and ^{SB}*Pkd1; Kcnn4*$^{-/-}$ had smaller body size when compared to age-matched wildtype, hence isolated kidneys were smaller as well. Macroscopic examinations showed that ^{SB}*Pkd1* kidneys were paler in colour compared to wildtype, whereas the colour of ^{SB}*Pkd1; Kcnn4*$^{-/-}$ kidneys were pinker,

suggestive of less cystic kidneys (Fig. 29A). We calculated KBW at 1 and 6 months of age in this model and found KBW was reduced following genetic *Kcnn4* inactivation at both ages, however, the reduction was only significant at 6 months. From 1 to 6 months, KBW of ^{SB}*Pkd1* increased by 1.4-fold, while the KBW of ^{SB}*Pkd1; Kcnn4*$^{-/-}$ was maintained stable with disease progression. When compared to ^{SB}*Pkd1*, genetic *Kcnn4* inactivation led to a 10% and 41% reduction in KBW ratio at 1 month and 6 months of age, respectively. Improvements in kidney morphology upon *Kcnn4* inactivation was evident in 7-month-old H&E stained histological kidney sections; ^{SB}*Pkd1; Kcnn4*$^{-/-}$ kidneys were significantly less cystic and had more intact tissues than ^{SB}*Pkd1* kidneys (Fig. 29B). This reduction was nicely reflected in the reduced relative cyst surface area (%) and cyst number (Fig. 29C-D). For this analysis, we also included heterozygous *Kcnn4* knockout (^{SB}*Pkd1; Kcnn4*$^{+/-}$) samples. Interestingly, heterozygous *Kcnn4* was sufficient to significantly lower the relative cyst surface area and cyst number to similar level as those quantified in ^{SB}*Pkd1; Kcnn4*$^{-/-}$ kidneys. Relative cyst surface area was reduced by 49% and 51%, while cyst number was reduced by 36% and 44% in ^{SB}*Pkd1; Kcnn4*$^{+/-}$ and ^{SB}*Pkd1; Kcnn4*$^{-/-}$ kidneys, respectively. *Kcnn4* inactivation had greater impact on the relative cyst surface area than on the cyst number, consistent with what we had observed in *Pkd1*^{cko} and *Pkd1*$^{-/-}$ metanephroi studies.

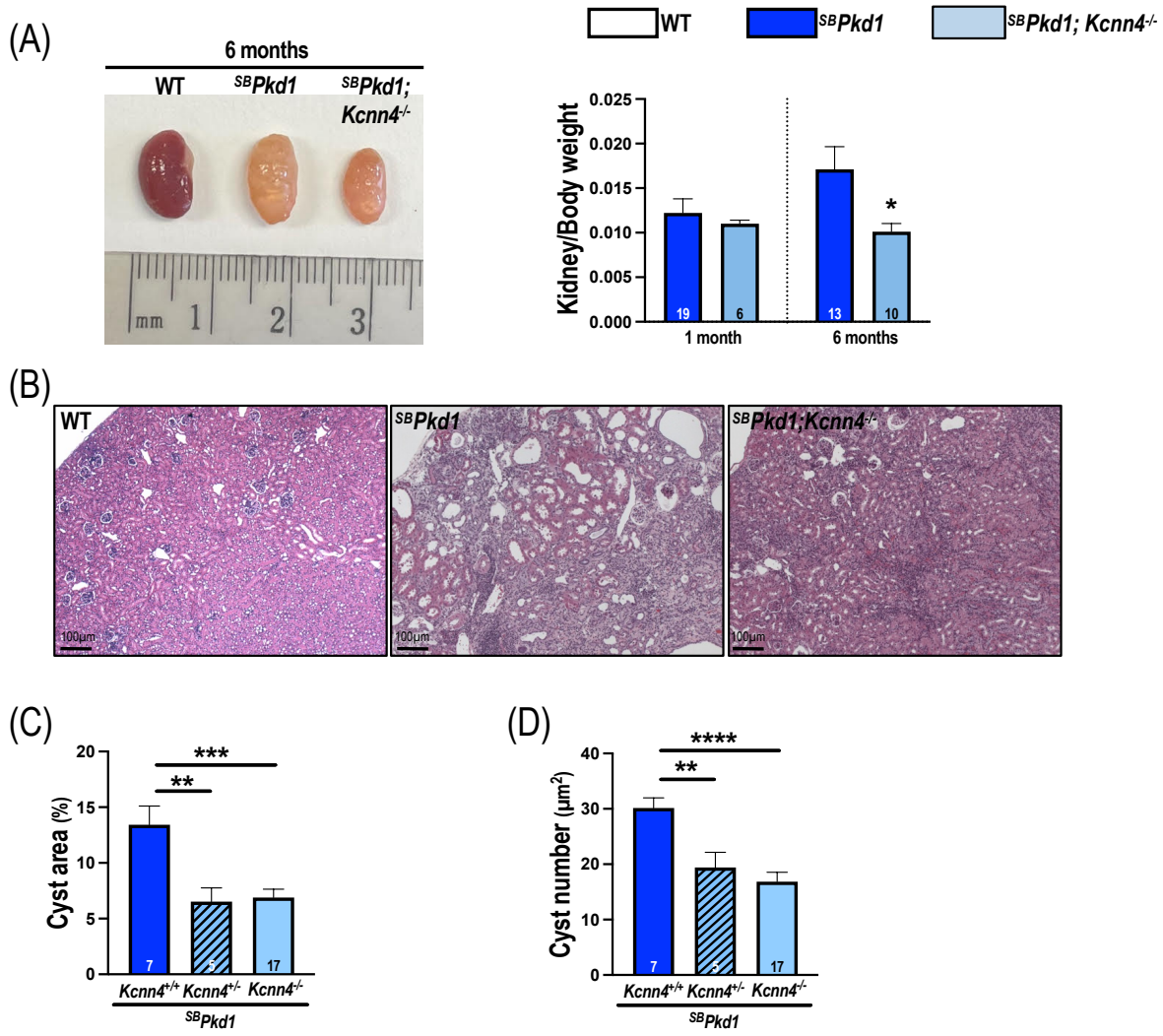

Fig. 29 Histomorphometric analysis of *SBPkd1* and *SBPkd1; Kcnn4*$^{-/-}$ kidneys. (A) Macroscopic kidney images of 6–8-month-old WT, *SBPkd1* and *SBPkd1; Kcnn4*$^{-/-}$. Quantification of KBW ratio of *SBPkd1* (blue bar) and *SBPkd1; Kcnn4*$^{-/-}$ (light blue bar) at 1 and 6 months are shown on the right (the number of animals analyzed are written within the bars). (B) Representative H&E histological kidney sections of 7-month-old WT, *SBPkd1* and *SBPkd1; Kcnn4*$^{-/-}$. (C) Quantification of percentage cyst area (%) in 6–8-month-old *SBPkd1* with none (Kcnn4$^{+/+}$), partial (heterozygous *Kcnn4*$^{+/-}$) or total (*Kcnn4*$^{-/-}$) Kcnn4 inactivation. Analysis of Kcnn4 contribution to kidney cyst area in *SBPkd1, SBPkd1; Kcnn4*$^{+/-}$ and *SBPkd1; Kcnn4*$^{-/-}$ suggest that total annihilation of Kcnn4 is not required for improvement of cystic phenotype. (D) Quantification of cyst number per mm^2 kidney in 6–8-month-old *SBPkd1, SBPkd1; Kcnn4*$^{+/-}$ and *SBPkd1; Kcnn4*$^{-/-}$. Contribution of Kcnn4 to the kidney cyst number parallels its involvement in cyst enlargement (cyst area). *p<0.05, **p<0.01, ***p<0.001, ****p<0.0001

Further analyses of the tubular origin of cysts revealed that cysts can be found in proximal tubules, distal tubules and collecting ducts (Fig. 30). Genetic *Kcnn4* inactivation in

^{SB}*Pkd1* reduced cysts by 61% in distal tubules and by 50% in collecting ducts, whereas cysts in proximal tubules were unaffected (quantification not shown).

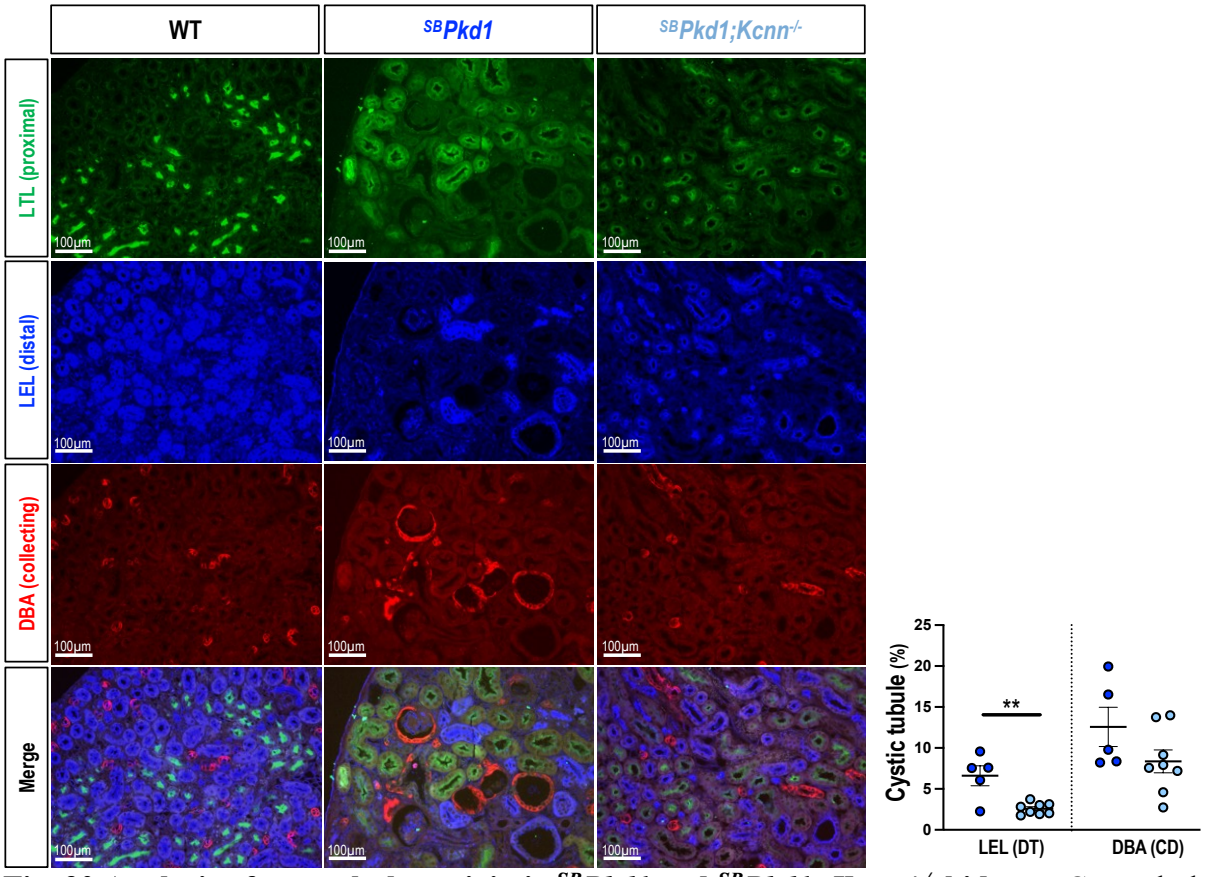

Fig. 30 Analysis of cyst tubular origin in ^{SB}*Pkd1* and ^{SB}*Pkd1; Kcnn4*$^{-/-}$ kidneys. Cyst tubular origin in 2-month-old WT, ^{SB}*Pkd1* and ^{SB}*Pkd1; Kcnn4*$^{-/-}$ kidneys was analyzed by immunofluorescence using proximal (LTL; green), distal (LEL; blue) and collecting (DBA; red) tubular markers. Quantification of percentage cystic tubules (%) in distal tubule (DT) and collecting duct (CD) of ^{SB}*Pkd1* and ^{SB}*Pkd1; Kcnn4*$^{-/-}$ kidneys are shown on the right. **p<0.01

3.3.5 Kidney function and lifespan are significantly improved in ^{SB}*Pkd1* upon genetic *Kcnn4* inactivation

Kidney function was evaluated by BUN (Fig. 31A). BUN in 6–8-month-old ^{SB}*Pkd1* increased by 10.1-fold in comparison to wildtype animals, and, strikingly, reduced by 60% upon *Kcnn4* inactivation. This likely contributed significantly to the observed extended lifespan of ^{SB}*Pkd1* upon genetic *Kcnn4* inactivation. Compared to the median survival of 182 days in ^{SB}*Pkd1*, the median survival of ^{SB}*Pkd1; Kcnn4*$^{-/-}$ animals was markedly extended to 250 days,

equivalent to a 37% increase in lifespan (Fig. 31B). We did not find any $^{SB}Pkd1$ animals surviving past one year of age, but about 20% of $^{SB}Pkd1; Kcnn4^{-/-}$ lived beyond one year. The Kaplan-Meier curve of $^{SB}Pkd1; Kcnn4^{-/-}$ was significantly shifted to the right of the x-axis, indicative of better survival.

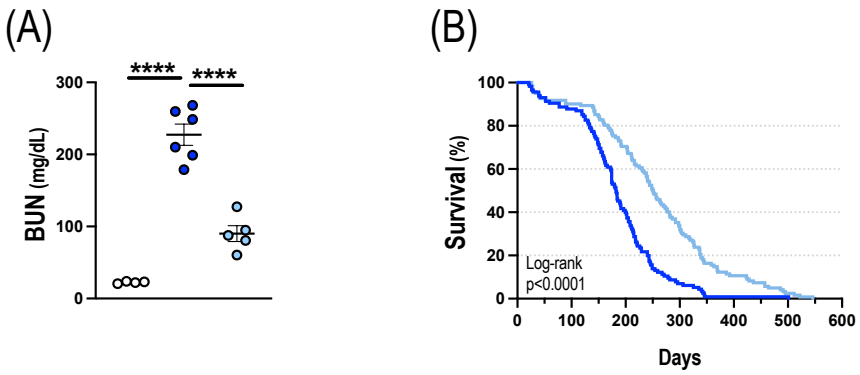

Fig. 31 Assessment of kidney function and survival in $^{SB}Pkd1$ and $^{SB}Pkd1; Kcnn4^{-/-}$. (A) BUN analysis of WT (open circle), $^{SB}Pkd1$ (blue circle) and $^{SB}Pkd1; Kcnn4^{-/-}$ (light blue circle) at 6-8 months. (B) Kaplan-Meier survival curve of $^{SB}Pkd1$ versus $^{SB}Pkd1; Kcnn4^{-/-}$. ****p<0.0001

3.3.6 Marked reduction in renal cAMP correlates with attenuation in cAMP-driven cystogenic cellular processes in $^{SB}Pkd1$

cAMP levels in $^{SB}Pkd1; Kcnn4^{-/-}$ kidneys were reduced by 45% when compared to $^{SB}Pkd1$, and led to reduced MAPK/ERK signaling, as indicated by reduced protein levels of phospho-ERK, phospho ERK/total ERK and c-Myc (Fig. 32A-B). For protein analysis of p-ERK and total ERK, more sample was loaded for $^{SB}Pkd1; Kcnn4^{-/-}$ in comparison to $^{SB}Pkd1$ as shown by thicker bands of Gapdh, but all quantifications were normalized to the level of Gapdh (Fig. 32B). Although the reduction in MAPK/ERK signaling was not significant, there was a tendency for MAPK/ERK downregulation that probably contributed in part to the significant reduction in c-Myc levels by 44% due to genetic *Kcnn4* inactivation. We used ki67 as a marker to evaluate the proliferative status of kidneys (Fig. 32C). 6–8-month-old wildtype controls showed only low proliferation levels as only a few tubules were ki67 positive, and in those tubules that expressed

ki67, only one cell per tubule was positively stained. In contrast, ki67 signals in ^{SB}*Pkd1* kidneys were more prevalent and often more than one ki67 positive cell was detected per tubule. Quantification of ki67 positive cells per μm^2 of kidney surface showed that proliferation increased by 4.3-fold in ^{SB}*Pkd1* tubular epithelia when compared to wildtype. Genetic *Kcnn4* inactivation significantly reduced proliferation and led to 60% reduction in ki67 signals, partially normalizing the proliferative status of ^{SB}*Pkd1* kidneys.

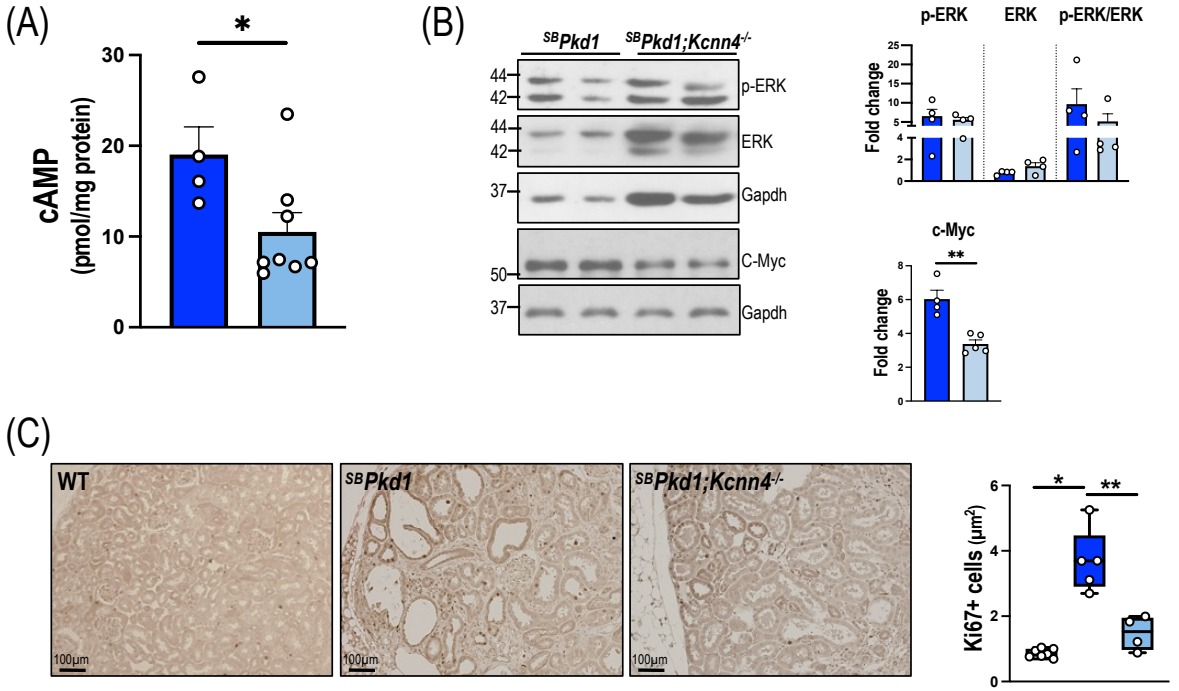

Fig. 32 Analysis of cAMP level and proliferation status of ^{SB}*Pkd1* versus ^{SB}*Pkd1; Kcnn4*$^{-/-}$ kidneys. (A) cAMP level is measured by ELISA and is expressed as pmol cAMP per mg of protein. (B) Representative western blot analysis (left) and quantification (right) of cAMP downstream effectors phospho-ERK, total ERK and c-Myc in 6-month-old ^{SB}*Pkd1* and ^{SB}*Pkd1; Kcnn4*$^{-/-}$ kidneys. (C) Quantification of renal epithelial cell proliferation by Ki67 immunohistochemistry in 6–8-month-old ^{SB}*Pkd1* and ^{SB}*Pkd1; Kcnn4*$^{-/-}$ kidneys (right) with representative images shown on the left. Proliferation is expressed as the number of ki67 positive cells per mm^2 kidney surface. *p<0.05 **p<0.01

At 6-8 months of age, ^{SB}*Pkd1* kidneys were highly fibrotic, many areas showed intense Sirius Red staining representing collagen deposition (Fig. 33). Relative renal fibrotic surface (%)

in *SBPkd1* increased by 13.7-fold compared to wildtype and reduced by 45% upon *Kcnn4* inactivation.

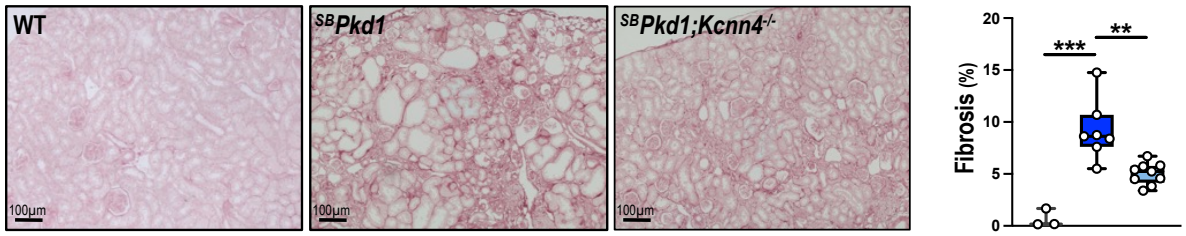

Fig. 33 Analysis of kidney fibrosis in *SBPkd1* versus *SBPkd1; Kcnn4-/-*. Fibrosis is detected by Sirius Red and is expressed as the percentage of renal fibrotic surface (%) in 6–8-month-old WT, *SBPkd1* and *SBPkd1; Kcnn4-/-* kidneys (right). Representative images are shown on the left. **p<0.01, ***p<0.001

Upon analysis of renal primary cilia length, we found a 1.3-fold increase in average primary cilia length in 2-month-old *SBPkd1* in comparison to wildtype, which was remarkably rescued and completely normalized upon *Kcnn4* inactivation (Fig. 34A). When we plotted the primary ciliary distribution, about 60% of all primary cilia in wildtype kidneys were shorter than 3µm, like P10 wildtype analyzed earlier (cf. section 3.3.3). In fact, the distribution of primary ciliary length in 2-month-old versus P10 wildtype were almost indistinguishable. The distribution of *SBPkd1* was less strikingly different from wildtype than the difference between *Pkd1cko* and age-matched wildtype, as 40% of all primary cilia were shorter than 3µm, while the remaining 60% evenly distributed within the longer cilia length categories (Fig. 34B). Remarkably, the plot of *SBPkd1; Kcnn4-/-* primary ciliary distribution completely overlapped with that of the wildtype, supporting primary cilia length was indeed normalized following *Kcnn4* inactivation.

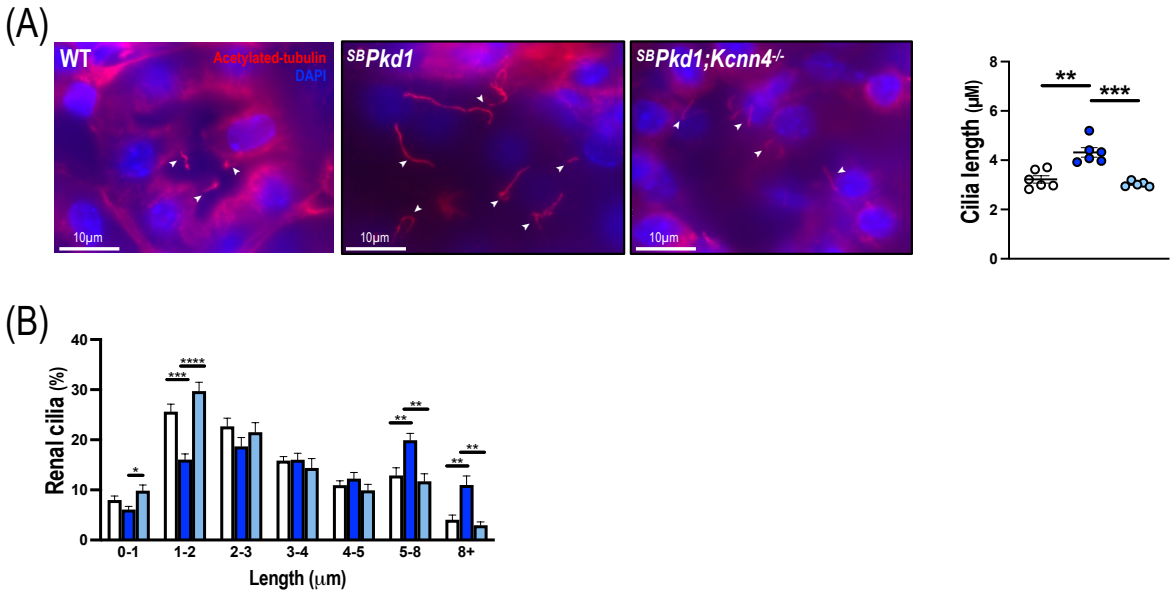

Fig. 34 Analysis of primary cilia length in *^{SB}Pkd1* versus *^{SB}Pkd1; Kcnn4$^{-/-}$* kidneys. (A) Quantification of mean primary cilia length in 2-month-old WT, *^{SB}Pkd1* and *^{SB}Pkd1; Kcnn4$^{-/-}$* kidneys using immunofluorescent anti-alpha acetylated tubulin marker (right). Representative images are shown on the left with white arrows pointing at individual cilium. Mean cilia length was virtually normalized upon loss of *Kcnn4*. (B) Length of all primary cilia found in the entire kidney section were measured and distributed into intervals based on their length. The primary cilia distribution of *^{SB}Pkd1* showed a distinct shift towards the right of x-axis in comparison to WT that was completely restored in *^{SB}Pkd1; Kcnn4$^{-/-}$*. *p<0.05, **p<0.01, ***p<0.001, ****p<0.0001

3.4 Administration of Kcnn4 pharmacologic inhibitor Senicapoc in 4 *Pkd1* Mouse models induces an improvement in disease status

3.4.1 Oral administration of Senicapoc is safe in wildtype mice

Initially we dissolved Senicapoc in DMSO solvent and administered to animals by daily intraperitoneal or subcutaneous injections. However, all animals including C57BL/6 wildtype mice lost ~20% in weight immediately after the first injection and did not regain weight or survive beyond 1 week of treatment. Since other groups who have administered Senicapoc *in vivo* mostly utilized oral gavage or through diet (Jin et al., 2019; Paka et al., 2017; Tubman et al., 2016), we then evaluated the effect of daily Senicapoc administration through oral gavage at low dose (30mg Senicapoc/kg of body weight) or high dose (120mg Senicapoc/kg of body weight) in

PEG/Cremophor/water solvent to 6-weekd-old wildtype mice for 3 months (Fig. 35A). We monitored their health daily and weighed all animals weekly and found that all wildtype mice completed the 3 months of treatment with no appreciable loss in body weight or deterioration in health status. Interestingly, Senicapoc even promoted weight gain throughout the course of treatment (Fig. 35B). By 6 weeks post treatment, mice in the high dose group doubled their weight when compared to before treatment and continued to gain weight. We are not aware of the cause of weight gain, another group also reported weight gain in mice treated with a TRAM-34 derived Kcnn4 inhibitor NS6180 (Strobaek et al., 2013). Perhaps mice who received Senicapoc increased food intake. Indeed, a recent *in vivo* study showed that invasive feeding methods such as injections or oral gavage pose stress on animals and significantly impacts metabolic parameters including food intake and body weight (Zapata et al., 2021). At the end of the treatment period, we isolated the kidneys and stained kidney sections with H&E (Fig. 35C). Kidneys from Senicapoc-treated animals were indistinguishable from vehicle-treated mice. Senicapoc did not alter the KBW or BUN in wildtype animals (Fig. 35C-D). This preliminary study led us to proceed with Senicapoc administration to early- and adult-onset *Pkd1* mouse models.

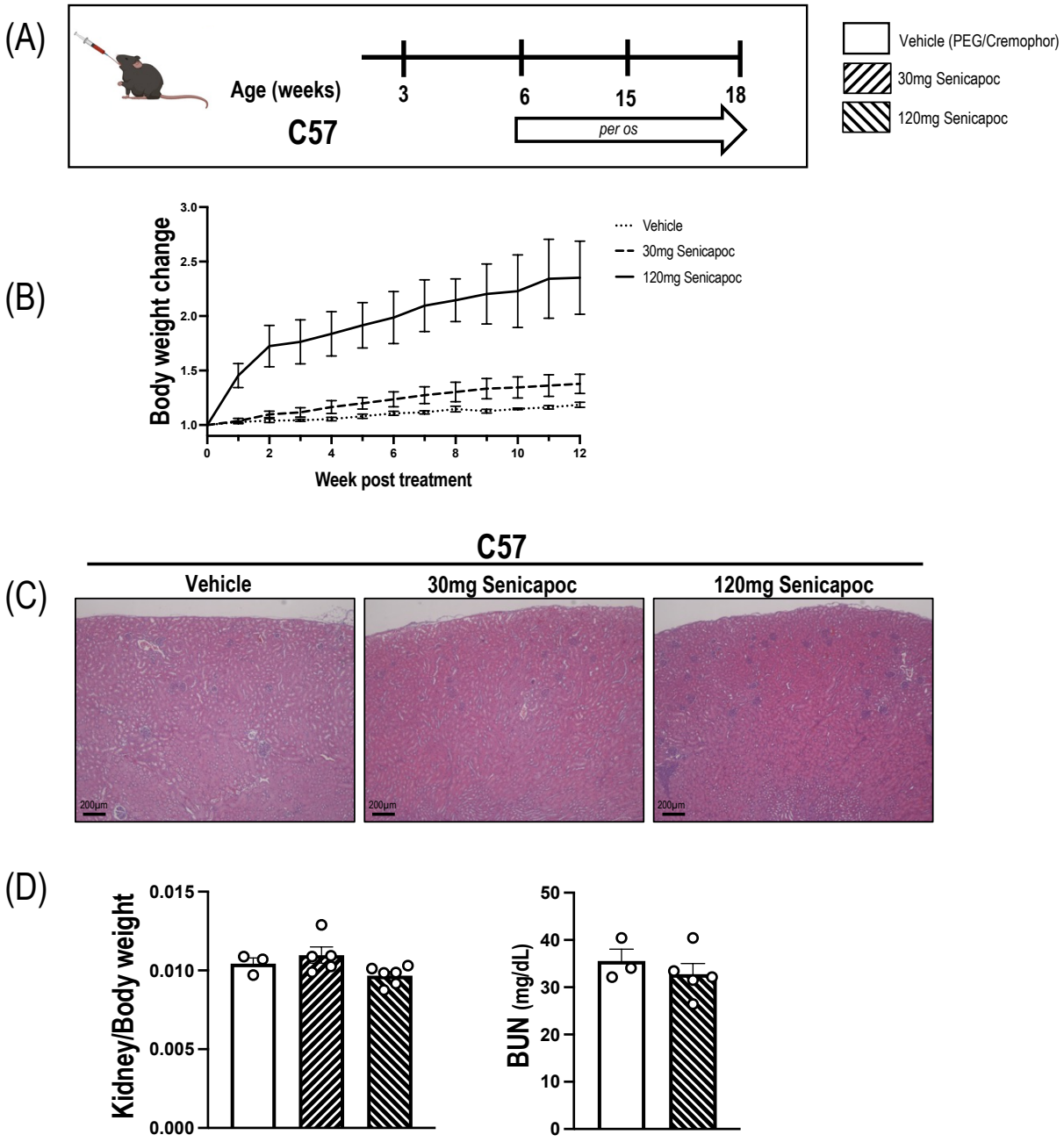

Fig. 35 Evaluation of Senicapoc use in adult wildtype mice. Animals are separated into 3 conditions: control vehicle (PEG/cremophor), 30mg Senicapoc/kg of body weight (low dose) or 120mg Senicapoc/kg of body weight (high dose). (A) Schematic representation of the experimental design for wildtype mice by daily oral gavage from 6 weeks to 18 weeks of age. (B) Body weight change show normal weekly weight gain following Senicapoc administration with greater gain in the high dose treatment group. (C) Representative H&E histological kidney sections of wildtype treated with vehicle, low dose, and high dose Senicapoc upon completion of treatment. (D) Quantification of KBW ratio and BUN show no impact upon Senicapoc administration.

3.4.2 Senicapoc treatment delays cyst growth in early-onset *Pkd1*$^{v/v}$

Senicapoc was given to 2 early-onset rapidly progressive *Pkd1* mouse models, *Pkd1*^{cko} and *Pkd1*$^{v/v}$, from P0 until P5 or P10 through two routes (Fig. 36). First, 120 mg Senicapoc/kg of body weight was given daily to mothers from the day of delivery (day 0) for 5 or 10 days. Senicapoc was also administrated daily to the newborn *Pkd1*^{cko} and *Pkd1*$^{v/v}$ pups directly in the corner of their mouth from P2 until the end of treatment at a concentration and volume that is equivalent to 120mg Senicapoc/kg of body weight. We initiated administration as early as possible given their rapid disease progression and short window for treatment.

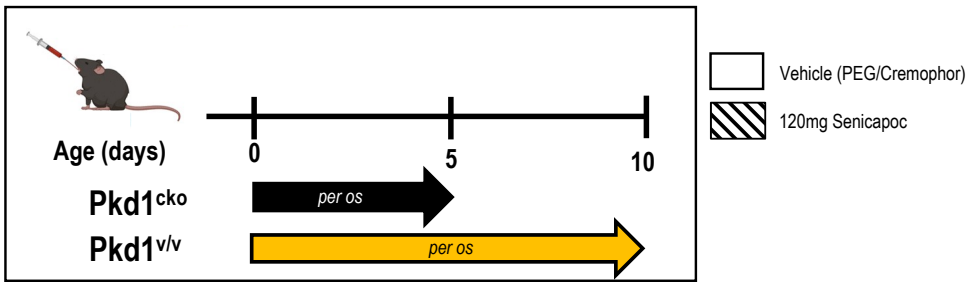

Fig. 36 Schematic representation of the experimental design for treatment of early-onset models *Pkd1*^{cko} and *Pkd1*$^{v/v}$. Animals are separated into 2 conditions: vehicle (PEG/cremophor) or 120mg Senicapoc/kg of body weight. Senicapoc is administered through daily oral gavage to mothers from P0 to P5 (*Pkd1*^{cko}) or to P10 (*Pkd1*$^{v/v}$) in addition to directly feeding into mouth of experimental models from P2 to P5 (*Pkd1*^{cko}) or P10 (*Pkd1*$^{v/v}$).

All animals tolerated Senicapoc well with no mortality by the end of treatment. Kidneys were isolated at P5 for *Pkd1*^{cko} and at P10 for *Pkd1*$^{v/v}$ and processed for H&E analysis. Kidneys from Senicapoc-treated *Pkd1*^{cko} appeared enlarged with bigger cysts compared to the vehicle group with no apparent improvement (Fig. 37A). Although fewer cysts were found in *Pkd1*^{cko} following Senicapoc treatment by 22%, cysts were larger and likely contributed to the 1.3-fold increase in percent cyst area, culminating in 1.6-fold increase in KBW (Fig. 37B). The reduction in cyst numbers was not sufficient to delay cyst enlargement or cause a global improvement in delaying cyst growth in *Pkd1*^{cko} kidneys.

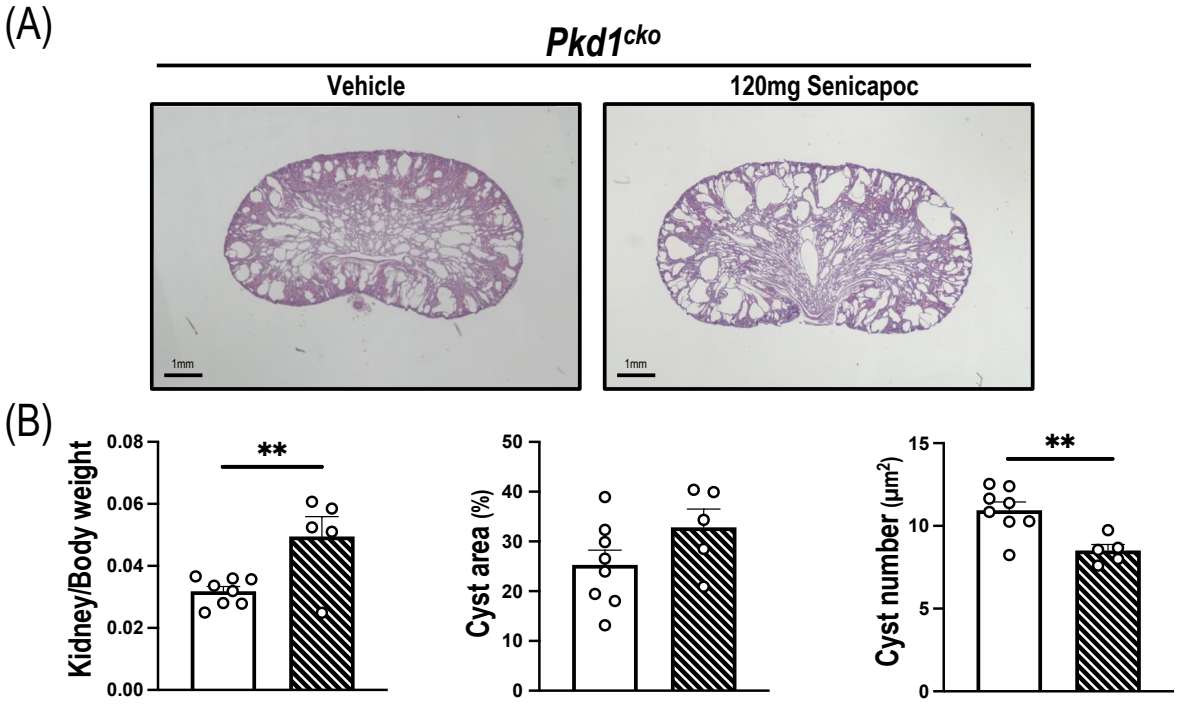

Fig. 37 Effect of 5 day Senicapoc treatment to *Pkd1*^{cko}. (A) Representative H&E histological kidney sections of *Pkd1*^{cko} treated with vehicle or 120mg Senicapoc/kg of body weight. (B) Quantification of KBW, percentage cyst area (%) and cyst number per mm^2 of kidney surface. **p<0.01

The less rapidly progressive early-onset *Pkd1*$^{v/v}$ were more responsive to Senicapoc treatment as illustrated by H&E-stained histological kidney sections (Fig. 38A). Kidneys from *Pkd1*$^{v/v}$ treated with Senicapoc were smaller in size, less cystic and retained more intact tissues when compared to kidneys from vehicle-treated animals. Quantifications of KBW, percent cyst surface area and cyst number indicated that although there is a non-significant 4% increase in cyst number, percent cyst area significantly reduced by 24%, culminating in 26% reduction in KBW (Fig. 38B).

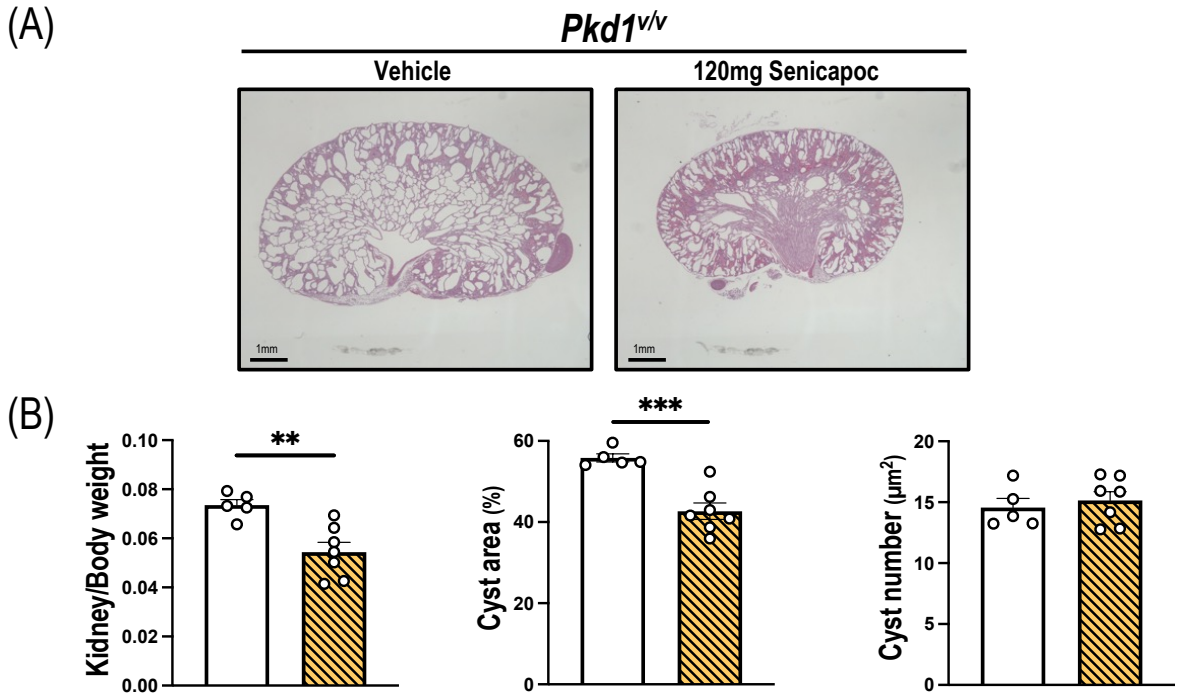

Fig. 38 Effect of 10 day Senicapoc treatment to *Pkd1*$^{v/v}$. (A) Representative H&E histological kidney sections of *Pkd1*$^{v/v}$ treated with vehicle or 120mg Senicapoc/kg of body weight. (B) Quantification of KBW, percentage cyst area (%) and cyst number per mm^2 of kidney surface show critical improvement of PKD phenotypes. **p<0.01 ***p<0.001

3.4.3 Senicapoc treatment delays kidney cyst growth and improves kidney function in the adult-onset models

The 3 months of Senicapoc daily oral administration for adult-onset models began at 3 weeks of age for ^{SB}*Pkd1* and at 6 weeks of age for *Pkd1*^{wt} (Fig. 39). These ages were chosen such that treatment began just before or around the time of kidney cysts initiation.

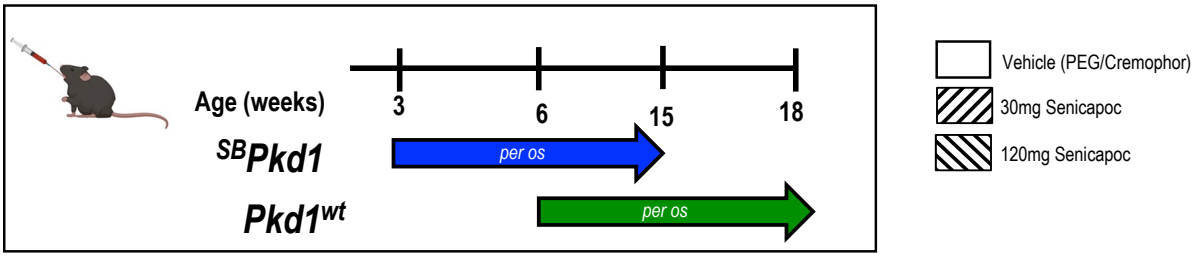

Fig. 39 Schematic representation of the experimental design for treatment of adult-onset models ^{SB}*Pkd1* and *Pkd1*^{wt}. Animals are separated into 3 conditions: vehicle (PEG/cremophor), 30mg Senicapoc/kg of body weight (low dose) or 120mg Senicapoc/kg of body weight (high dose). Senicapoc is administered through daily oral gavage of Senicapoc or vehicle (PEG/cremophor) from 3 weeks of age (^{SB}*Pkd1*) or 6 weeks of age (*Pkd1*^{wt}) for 3 months.

The weekly body weight change of low dose Senicapoc treated ^{SB}*Pkd1* animals was similar to vehicle treated animals of the same genotype (Fig. 40A). The high dose group experienced a small decrease of body weight in the middle of Senicapoc treatment during week 6 and 7, but quickly regained weight afterwards, surpassing that of low dose and vehicle groups. Examination of kidney cysts using H&E-stained kidney sections showed that the cystic kidneys in the low dose Senicapoc-treated group were less severe compared to vehicle-treated animals. However, in both groups, cysts can be found throughout the kidney, while the high dose Senicapoc-treated mice displayed a shift in cyst localization to the renal cortex, significantly reducing cyst presence in the medulla (Fig. 40B). To understand how Senicapoc treatment affect renal indices, we analyzed KBW, percent cyst surface area, cyst number and BUN (Fig. 40C). KBW lowered by 33% and 31% following low dose and high dose Senicapoc treatment, respectively. Although the reduction in relative renal cyst surface area was not significant, we observed a clear tendency for cyst surface area to reduce upon Senicapoc treatment, notably by 27% (low dose) and 36% (high dose). While cyst numbers did not reduce in the low dose group, and even increased by 11%, the high dose group displayed a reduction of cyst numbers by 43%. Although low dose Senicapoc improved some disease parameters, overall, the high dose had greater effect on cyst indices. Unfortunately, we did not detect improvement in kidney function, and even found a 30% increase in BUN levels in mice treated with high dose of Senicapoc.

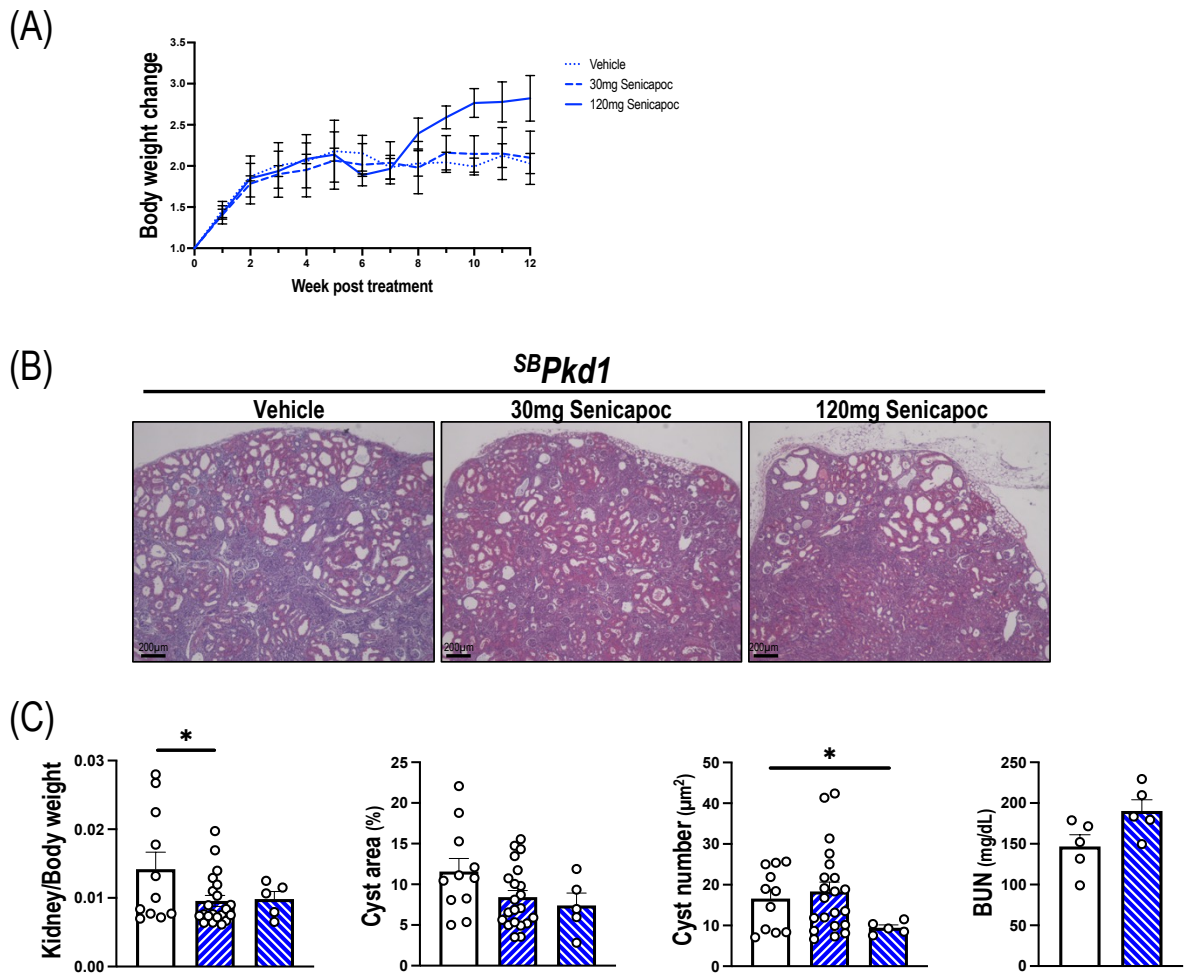

Fig. 40 Effect of 3 months Senicapoc treatment to ^{SB}*Pkd1*. (A) Body weight change show general weekly weight gain in ^{SB}*Pkd1* for the duration of Senicapoc treatment except for a short-term weight loss in the high dose group between week 6 to 7. (B) Representative H&E histological kidney sections of ^{SB}*Pkd1* kidneys treated with vehicle, low dose, and high dose Senicapoc upon completion of treatment. (C) Quantification of KBW, percentage cyst area (%), cyst number per mm^2 of kidney surface and BUN in ^{SB}*Pkd1* upon completion of treatment. *p<0.05

Next, we examined the effect of high and low dose Senicapoc administration in another moderately progressive adult-onset model, *Pkd1*^{wt}. The weekly body weight change of low and high dose Senicapoc treated *Pkd1*^{wt} was similar to vehicle-treated animals (Fig. 41A). Senicapoc did not induce excess body weight gain. Kidneys from Senicapoc treated animals removed after completion of treatment were pinker in colour macroscopically, indicative of more healthy renal tissue. We furthermore observed H&E-stained kidney sections and found that kidneys from

Pkd1^{wt} treated with Senicapoc were less cystic, with a greater effect in the high dose treatment group (Fig. 41B). We analyzed KBW ratio, relative cyst surface area (%), cyst number and BUN (Fig. 41C). Although we observed an increase in KBW by 2% and 14% in low and high dose Senicapoc treatment groups, respectively, all other parameters significantly improved after Senicapoc treatment. We found 50% and 61% reduction in percent cyst area, 38% and 51% reduction in cyst number, and 40% improvement in kidney function as indicated through serum BUN analysis.

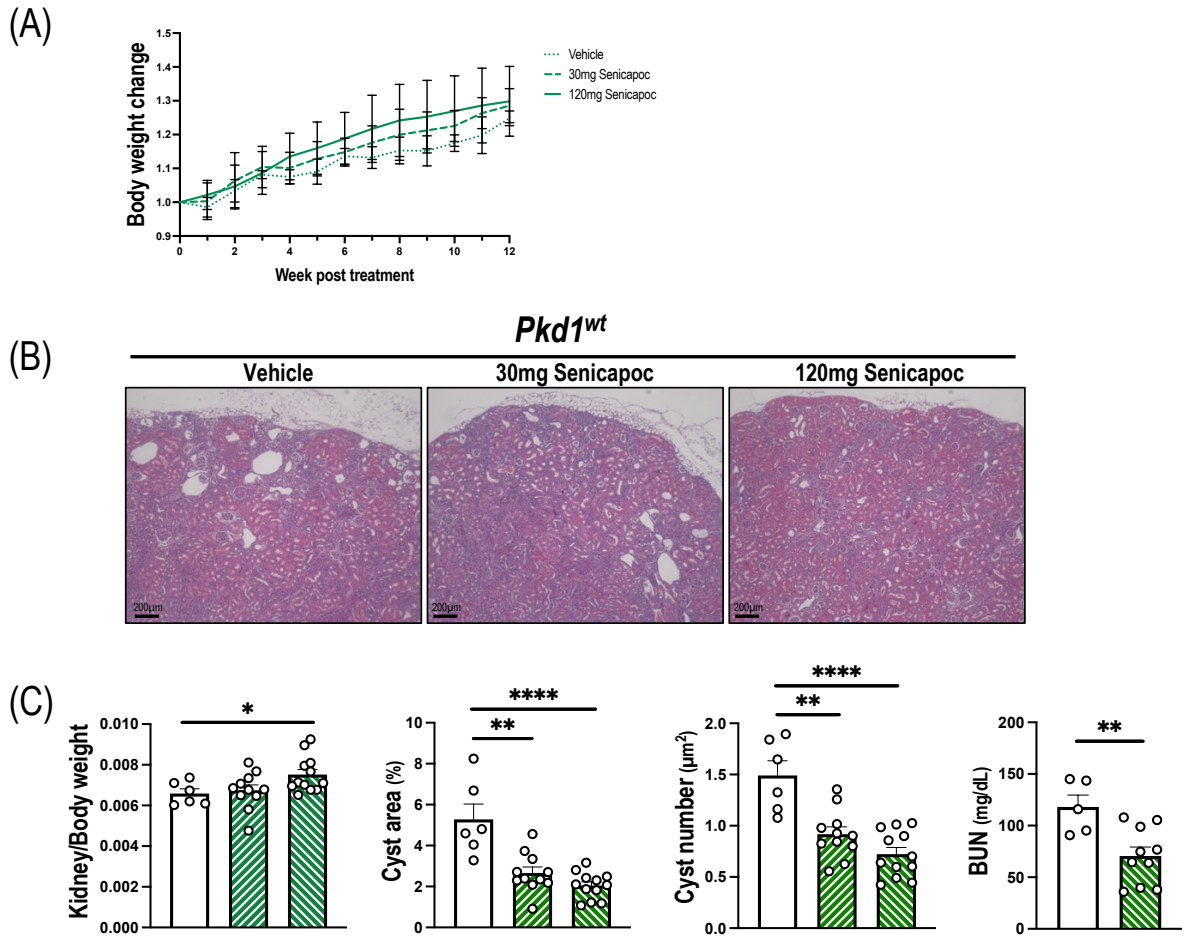

Fig. 41 Effect of 3 months Senicapoc treatment to *Pkd1*^{wt}. (A) Body weight change show general weekly weight gain in Pkd1^{wt} for the duration of treatment. (B) Representative H&E histological kidney sections of Pkd1^{wt} kidneys treated with vehicle, low dose, and high dose Senicapoc upon completion of treatment. (C) Quantification of KBW, percentage cyst area (%), cyst number per mm^2 of kidney surface and BUN in *Pkd1*^{wt} upon completion of treatment. Cyst indices are significantly reduced at low dose and at high dose in comparison to vehicle. Renal

function was significantly improved in *Pkd1*^{wt} kidneys treated with high dose Senicapoc. *p<0.05 **p<0.01 ****p<0.0001

3.5 Evaluation of combined channel inhibition versus single treatment on *ex vivo Pkd1*$^{-/-}$ cyst growth

3.5.1 Targeting *Pkd1*$^{-/-}$ cysts with single treatment

We first established the level of rescue of *Pkd1*$^{-/-}$ cysts by targeting each channel individually with different concentrations of specific inhibitors, then compared the results to those obtained through combined inhibition to find the optimal inhibitor combination for potential use in our animal models in the future.

3.5.1.1 Kcnn4 inhibitor Senicapoc

Pkd1$^{-/-}$ metanephroi were treated with 5, 10, and 20µM of Senicapoc added simultaneously with cAMP on day 1 and replaced on day 3 (Fig. 42A). Representative images of metanephroi after 4 days of culture showed increasing cystic phenotypic rescue as inhibitor dosage increased (Fig. 42B). There appeared to be a dose dependent reduction in cyst area from 5 to 10µM, causing 11% and 19% reduction in cyst area (Fig. 42C). However, at 20µM, cyst area drastically reduced by 91%.

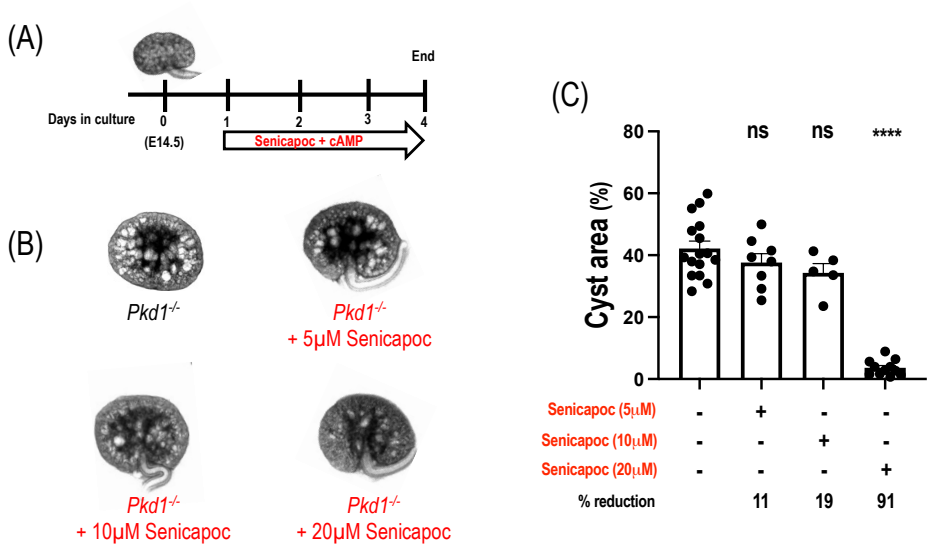

Fig. 42 Comparison of *Pkd1*$^{-/-}$ metanephroi cyst growth between different concentrations of Senicapoc. (A) Schematic representation of the experimental design: *Pkd1*$^{-/-}$ metanephroi isolated at E14.5 were stimulated with 100µM cAMP on day 1 until day 4 with or without simultaneous addition of Kcnn4 inhibitor Senicapoc. (B) Representative images of *Pkd1*$^{-/-}$ metanephroi with or without 5µM, 10µM and 20µM Senicapoc upon completion of treatment on day 4. (C) Quantification of percentage cyst area (%) in *Pkd1*$^{-/-}$ metanephroi treated with 5µM, 10µM and 20µM Senicapoc in comparison to the vehicle is carried out upon completion of experiment. ****p<0.0001

3.5.1.2 Cftr inhibitor PPQ-102

Pkd1$^{-/-}$ metanephroi were subjected to 1, 2, 5, 10, and 20µM of PPQ-102 on day 1 with cAMP in fresh media and replaced on day 3 (Fig. 43A). Representative images of metanephroi upon completion of the treatment showed a gradual reduction of the cystic phenotype with increasing dosage of PPQ-102 (Fig. 43B). This trend was also demonstrated by the reduction in cyst area with increasing PPQ-102 concentrations (Fig. 43C). While PPQ-102 has a higher IC_{50} compared to Senicapoc (90nM versus 11nM), we found that PPQ-102 treatment induced a more potent effect at low doses (below 20µM) in the metanephroi culture conditions. For instance, 2µM of PPQ-102 had the same rescue effect (determined as cyst area reduction) as 10µM of Senicapoc. At higher dose (20µM), the two inhibitors led to similar rescue effect.

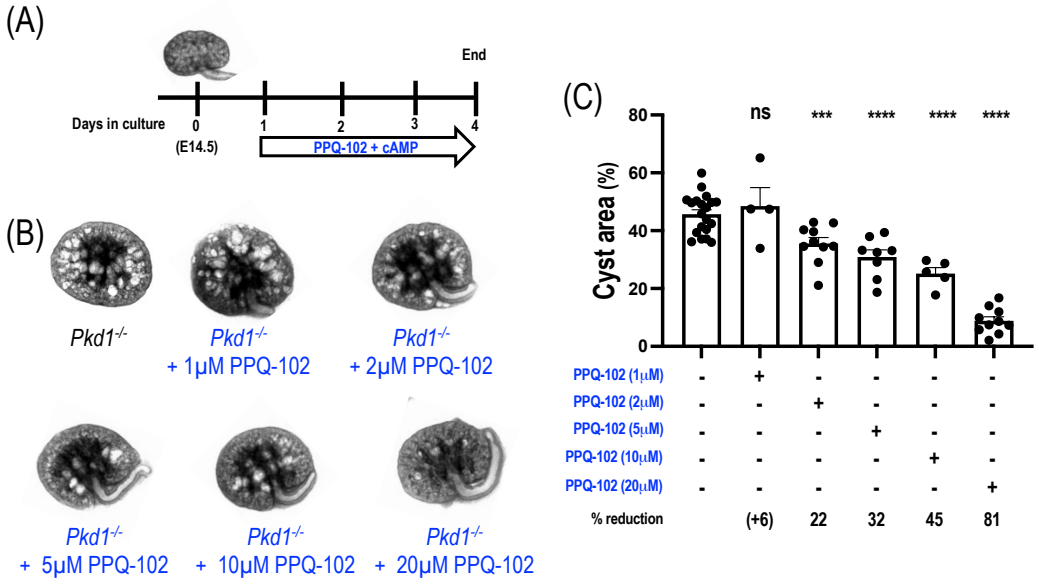

Fig. 43 Comparison of *Pkd1*$^{-/-}$ metanephroi cyst growth between different concentrations of PPQ-102. (A) Schematic representation of the experimental design: *Pkd1*$^{-/-}$ metanephroi isolated at E14.5 were stimulated with 100μM cAMP on day 1 until day 4 with or without simultaneous addition of Cftr inhibitor PPQ-102. (B) Representative images of *Pkd1*$^{-/-}$ metanephroi with or without 1μM, 2μM, 5μM, 10μM and 20μM PPQ-102 upon completion of treatment on day 4. (C) Quantification of percentage cyst area (%) in *Pkd1*$^{-/-}$ metanephroi treated with 1μM, 2μM, 5μM, 10μM and 20μM PPQ-102 in comparison to the vehicle is carried out upon completion of experiment. ***p<0.001, ****p<0.0001

3.5.1.3 Tmem16a inhibitor CaCCinh-A01

Pkd1$^{-/-}$ metanephroi were treated with 10, 20, 25, 30 and 35μM of CaCCinh-A01 on day 1 at the same time as cAMP in fresh media and replaced on day 3 (Fig. 44A). Treatment began with 10μM and 20μM but resulted in only small changes in cyst area. Concentrations of subsequent treatments were therefore increased in small increments rather than the 1/2/5 pattern used for Senicapoc and PPQ-102 to avoid toxic effects due to high concentration. Representative images of metanephroi upon completion of treatment showed very small differences between different doses, except for 35μM where the rescue was more prominent (Fig. 44B). There was an overall downward trend in percent cyst area with increasing doses of CaCCinh-A01 but was less consistent than the effect observed with the two previously described inhibitors (Fig. 44C). The only concentration that had a significant impact on cyst reduction was at 35μM, where cyst area lowered by 56%. The higher IC_{50} (2.1μM) explains why a much greater concentration is needed to induce an effect. Indeed, 25 or 30μM of CaCCinh-A01 was required to achieve the same reduction in cyst area as 2μM of PPQ-102 or 10μM of Senicapoc. Comparison between the three inhibitors showed that Senicapoc or PPQ-102 would potentially be better options when treatment efficiency is considered the only factor as they produced a larger rescue effect with smaller concentrations.

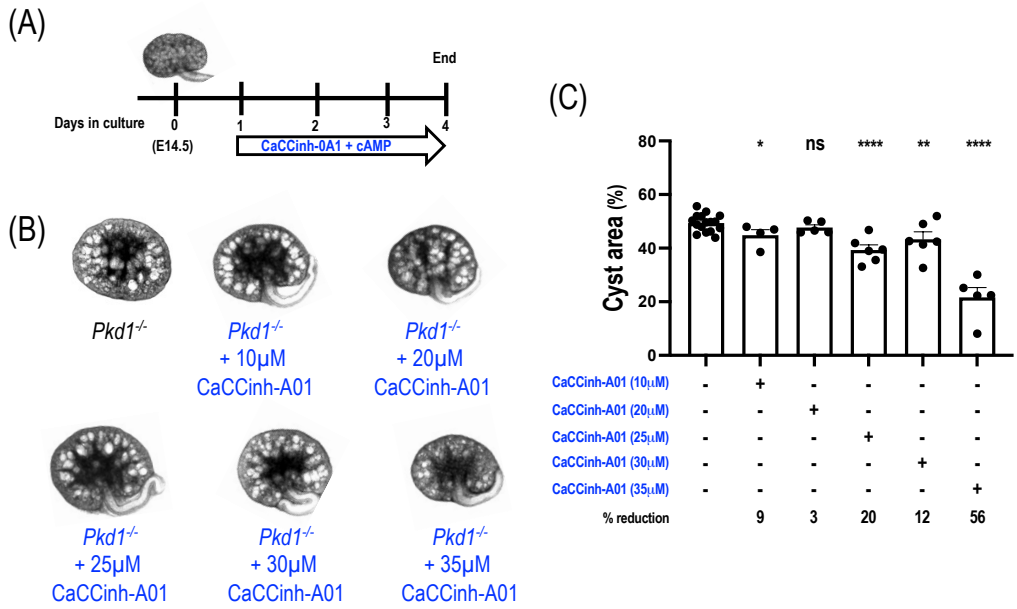

Fig. 44 Comparison of *Pkd1*$^{-/-}$ metanephroi cyst growth between different concentrations of CaCCinh-A01. (A) Schematic representation of the experimental design: *Pkd1*$^{-/-}$ metanephroi isolated at E14.5 were stimulated with 100μM cAMP on day 1 until day 4 with or without simultaneous addition of Tmem16a inhibitor CaCCinh-A01. (B) Representative images of *Pkd1*$^{-/-}$ metanephroi with or without 10μM, 20μM, 25μM, 30μM and 35μM CaCCinh-A01 upon completion of treatment on day 4. (C) Quantification of percentage cyst area (%) in *Pkd1*$^{-/-}$ metanephroi treated with 10μM, 20μM, 25μM, 30μM and 35μM CaCCinh-A01 in comparison to the vehicle is carried out upon completion of experiment. *p<0.05, **p<0.01, ****p<0.0001

3.5.2 Targeting *Pkd1*$^{-/-}$ cysts with combined treatment

There is an increasing interest in combination therapy, its main advantage being the potential to achieve a synergistic effect with overall lower dosages to reduce toxicity. Several *in vivo* studies have been done by others to test different treatment combinations in ADPKD models (Kanhai et al., 2020; Leonhard et al., 2019). Due to time limitations, we used the *ex vivo Pkd1*$^{-/-}$ metanephroi to screen two inhibitor combinations targeting channels or transporters that we believe could be interacting partners in driving ADPKD fluid secretion based on preliminary data and observations. Results from these studies should further be validated *in vivo* in the future.

3.5.2.1 Targeting Kcnn4 and Cftr results in synergistic effect

Pkd1$^{-/-}$ metanephroi were treated with 5 or 10μM of Senicapoc along with 2, 5 or 10μM of PPQ-102 on day 1 and replaced on day 3 (Fig. 45A). Representative images of Pkd1$^{-/-}$ metanephroi on day 4 comparing single and combination treatment clearly showed augmented rescue of cystic phenotypes through combination inhibition (Fig. 45B).

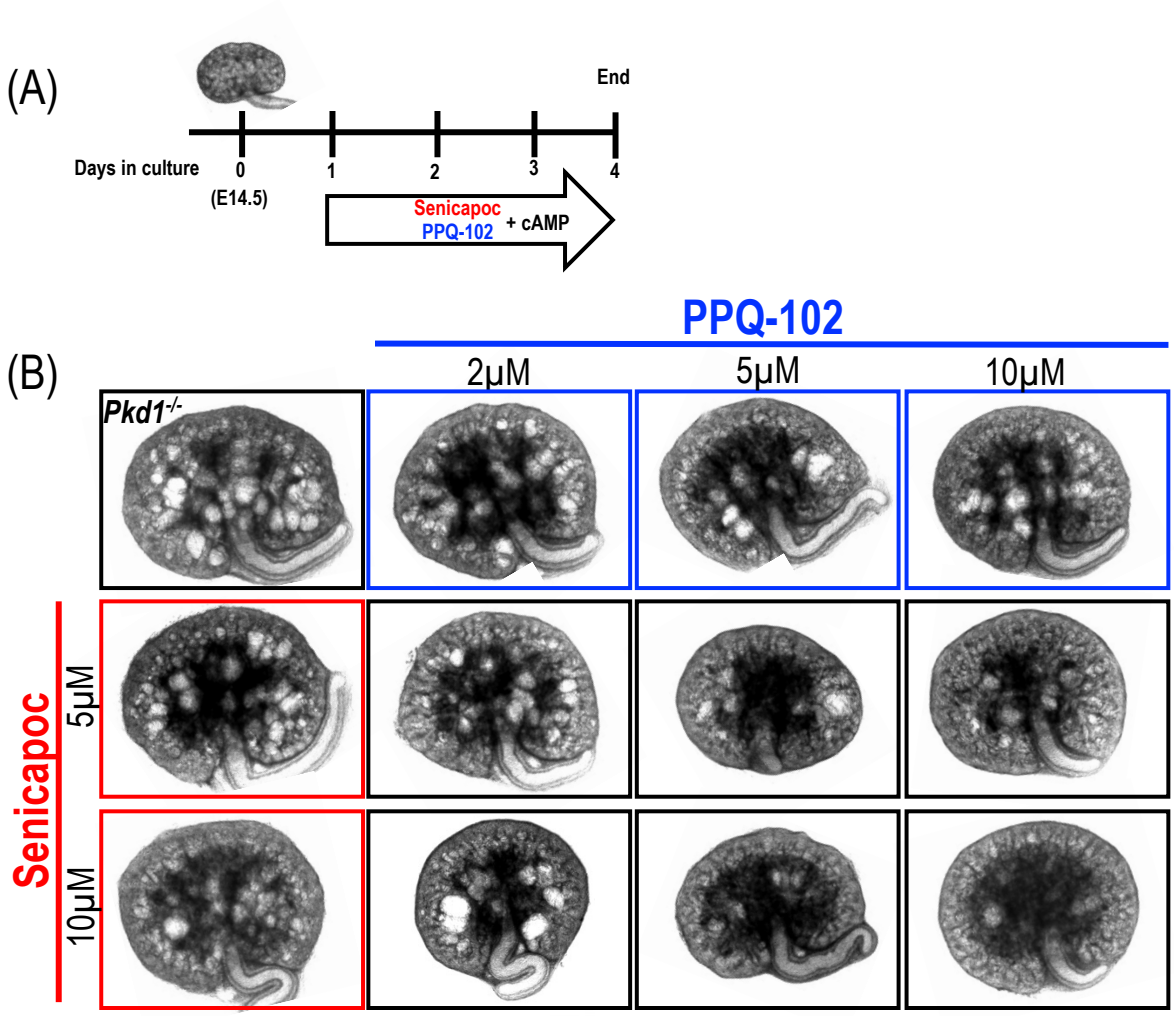

Fig. 45 Effect of combined Senicapoc and PPQ-102 inhibition versus Senicapoc only inhibition on cyst growth in *Pkd1*$^{-/-}$ metanephroi. (A) Schematic representation of the experimental design: *Pkd1*$^{-/-}$ metanephroi isolated at E14.5 were stimulated with 100μM cAMP on day 1 until day 4 with or without simultaneous addition of Senicapoc and PPQ-102. (B) Representative images of *Pkd1*$^{-/-}$ metanephroi with single or combined treatment upon completion of treatment on day 4.

The combinations of 5µM Senicapoc with different concentrations of PPQ-102 were quantified in Fig. 46A. Combinations with 10µM Senicapoc were quantified in Fig. 46B. Overall, both graphs showed a nice downward slope in percent cyst area by combining with increasing concentrations of PPQ-102. All combinations except the lowest one (5µM Senicapoc & 2µM PPQ-102 combination seems to be additive) suggest there is synergistic rescue of *Pkd1*$^{-/-}$ cysts, where lower total concentrations of Senicapoc and PPQ-102 achieved the same rescue effect as a higher dosage single inhibitor (Senicapoc or PPQ-102) treatment.

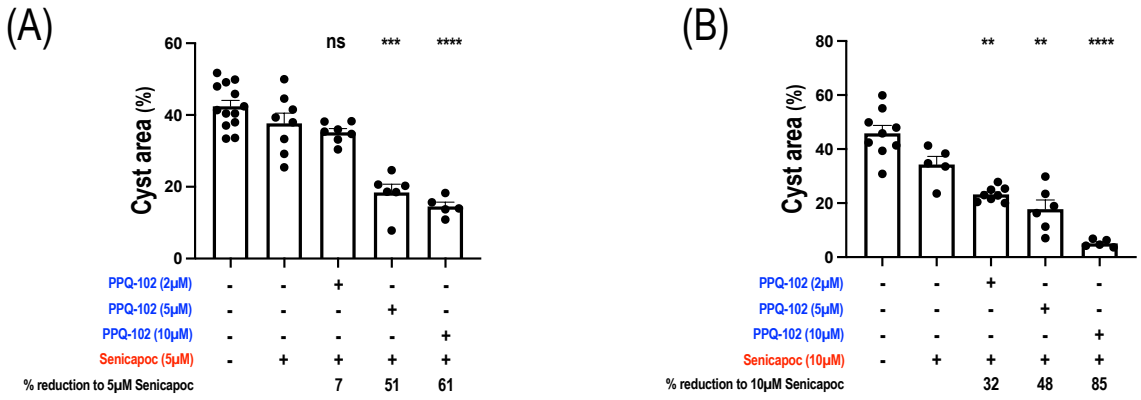

Fig. 46 Comparison of combined Senicapoc and PPQ-102 inhibition versus Senicapoc only inhibition on cyst growth in *Pkd1*$^{-/-}$ metanephroi. (A) Quantification of percentage cyst area (%) in *Pkd1*$^{-/-}$ metanephroi comparing Senicapoc/PPQ-102 combination inhibition to 5µM Senicapoc inhibition show synergistic effect. (B) Quantification of percentage cyst area (%) in *Pkd1*$^{-/-}$ metanephroi comparing Senicapoc/PPQ-102 combination inhibition to 10µM Senicapoc inhibition show synergistic effect. **p<0.01, ***p<0.001, ****p<0.0001

3.5.2.2 Targeting Kcnn4 and Tmem16a does not synergistically limit cyst growth

Pkd1$^{-/-}$ metanephroi were treated with 5µM of Senicapoc along with 10, 20, 25 or 30µM of CaCCinh-A01 on day 1 and replaced on day 3 (Fig. 47A). Representative images of *Pkd1*$^{-/-}$ metanephroi on day 4 submitted to the different treatment regimens are shown in Fig. 47B.

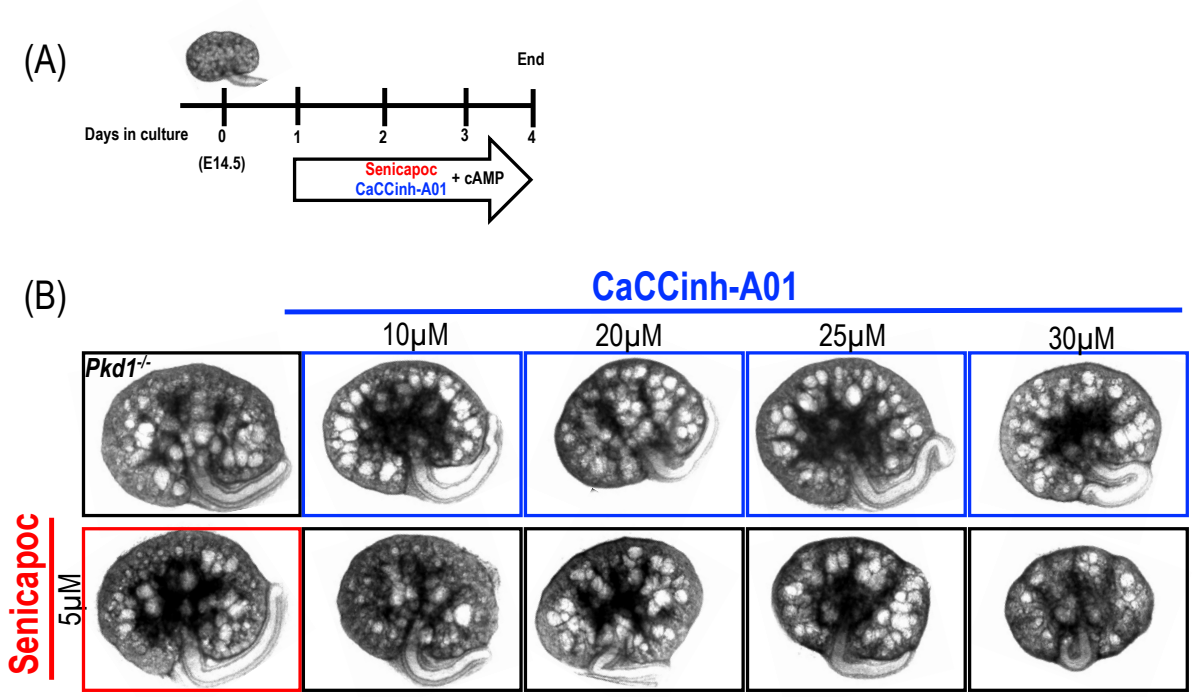

Fig. 47 Effect of combined Senicapoc and CaCCinh-A01 inhibition versus Senicapoc only inhibition on cyst growth in *Pkd1*$^{-/-}$ metanephroi. (A) Schematic representation of the experimental design: *Pkd1*$^{-/-}$ metanephroi isolated at E14.5 were stimulated with 100μM cAMP on day 1 until day 4 with or without simultaneous addition of Senicapoc and CaCCinh-A01. (B) Representative images of *Pkd1*$^{-/-}$ metanephroi with single or combined treatment upon completion of treatment on day 4.

The difference between single and combination treatment is less obvious here compared to the combination between Senicapoc and PPQ-102. In some cases, addition of CaCCinh-A01 did not cause greater reduction in cysts than using Senicapoc alone (Fig. 48). In fact, the combination of 5μM Senicapoc with 10 or 25μM CaCCinh-A01 even led to more cystic metanephroi. The only combination that showed synergy was 5μM Senicapoc with 30μM CaCCinh-A01. However, the degree of rescue gained from targeting these two channels can be achieved through the combination of PPQ-102 and Senicapoc at much lower concentrations, making the latter a more ideal combination to realize.

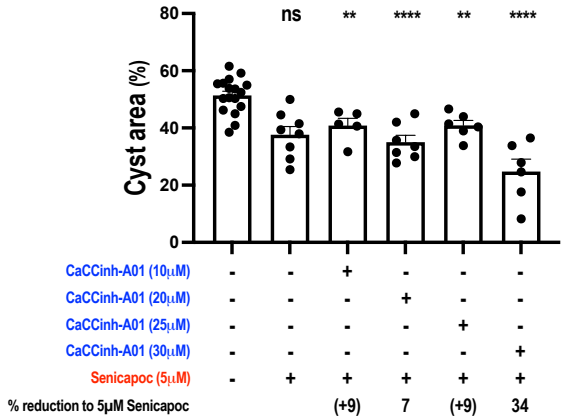

Fig.48 Comparison of combined Senicapoc and CaCCinh-A01 inhibition versus Senicapoc only inhibition on cyst growth in *Pkd1*$^{-/-}$ metanephroi. Quantification of percentage cyst area (%) in *Pkd1*$^{-/-}$ metanephroi comparing Senicapoc/CaCCinh-A01 combination inhibition to 5μM Senicapoc inhibition. **p<0.01, ****p<0.0001

CHAPTER 4: DISCUSSION

4.1 The significance of *Kcnn4* upregulation in ADPKD

Consistent *Kcnn4* RNA expression hyperactivation in various *Pkd1* mouse kidneys we have measured, and more importantly in human ADPKD kidneys, strongly suggests that Kcnn4 is implicated in the progression of ADPKD. Our results parallel with the *in vitro* work by Albaqumi *et al.,* where the investigators reported elevation in *Kcnn4* activity in cells derived from human ADPKD kidney cysts. Based on previous studies that document hyperactivation of *Kcnn4* RNA expression and activity in different pathophysiological contexts (Anumanthan et al., 2018; Chimote et al., 2013; Di et al., 2010; Grgic, Kiss, et al., 2009; Huang et al., 2014; Jin et al., 2019; Klein et al., 2009; Paka et al., 2017; Shumilina et al., 2008; Yu et al., 2013), we speculate many processes that associate with Kcnn4, such as fluid transport, proliferation and fibrosis may be hyper stimulated in ADPKD to drive cyst growth following *Kcnn4* overexpression in our mouse models. We designed our studies to elucidate the role of Kcnn4 in ADPKD progression using various mouse models, which also allowed us to analyze whether Kcnn4 may represent an attractive therapeutic target for ADPKD treatment. In the following discussion of our obtained results, we attempt to explain how Kcnn4 may be involved in ADPKD pathogenesis.

4.2 *Kcnn4* may be hyperactivated and sustained to maintain the cyst fluid secretory pathway

The current accepted model of cyst fluid secretion requires interaction between CFTR, NKCC1 and Na^+-K^+-ATPase to drive net fluid transport through apical AQP2 into the cyst lumen, hence progressively enlarging cysts (Jouret & Devuyst, 2020). One component that is not fully understood is how the excess potassium ions brought in by Nkcc1 and Na^+-K^+-ATPase are recycled. This step is critical as potassium efflux can cause hyperpolarization which is required

to drive continual chloride secretion through Cftr. The need for chloride secretion through Cftr to drive cyst growth is well documented by Magenheimer *et al. ex vivo* and by Yang *et al. in vivo*. We hypothesized that Kcnn4 could be a potential candidate to fulfill this role of potassium recycling due to its PKD-relevant properties demonstrated in other pathophysiological conditions, and based on our previous identification of *Kcnn4* as a downstream target of *c-Myc* (Pang et al., 2012), which is an inducer of PKD. Various components of the cyst fluid secretory pathway are generally studied independently and rarely altogether. Here we analyzed RNA expression of major components of the secretory pathway, *Nkcc1, Cftr* and *Aqp2* with isomers *Nkcc2* and *Aqp1*, in parallel with *Kcnn4*. We expected to find hyperactivated *Nkcc1, Cftr* and *Aqp2* but instead found selective upregulation of *Kcnn4.* RNA expression levels of *Nkcc1, Cftr* and *Aqp2* reduced, and were in fact indistinguishable from *Nkcc2* and *Aqp1* which are not directly implicated in ADPKD, suggesting *Cftr, Nkcc1* and *Aqp2* may be irresponsive or insensitive (to cystic conditions) at this time. This may be in part due to differences in gene regulation with disease progression. As we had conducted this analysis during mid-life in $Pkd1^{cko}$ (P10) and end stage in $^{SB}Pkd1$ (6–8-month-old), our results only illustrate the expression levels at these timepoints, which may not reflect the RNA expression levels at earlier stages. Based on our data, we propose that RNA expressions of *Cftr* and *Nkcc1* may be elevated during the early phase of the disease to activate the fluid secretory pathway, then *Kcnn4* RNA expression rises, stimulated by a small rise in intracellular calcium, to sustain this pathway. Once Kcnn4 begins to recycle the excess potassium ions and establish a hyperpolarized membrane, it provides a higher electrochemical driving force for chloride efflux through Cftr, consequently elevating Cftr and Nkcc1 activity without a requirement for increased expression of their mRNA. Instead, the upregulated *Kcnn4* RNA expression may be sustained throughout life in ADPKD (like we have

seen in 2 months versus 8 months $^{SB}Pkd1$ kidneys) and is sufficient to maintain and drive the fluid secretory pathway. To test this hypothesis and to better understand the interactions between various components of the pathway as disease progresses, an analysis of the RNA expression of those channels should be realized at different timepoints. This also highlights one of the limitations of this study, which is the lack of a comprehensive comparison between pre-cystic and established form of disease in both $Pkd1^{cko}$ and $^{SB}Pkd1$. As has been seen for fibrosis in ADPKD, its role in ADPKD progression transitions from initially protective to later disease driven (Fragiadaki et al., 2020). Likewise, components of the fluid secretory pathway could experience functional changes to fulfill the need in maintaining the pathway as disease progresses. Furthermore, as we did not measure channel activity or measure protein levels due to technical constraints, it is unknown if RNA expression is reflective of channel activity. Therefore, perhaps a thorough analysis of RNA expression, protein level and activity of major channels and transporters of the fluid secretory pathway at different phases of disease progression could help us understand better how the different components of the secretory pathway cooperatively mediate cyst fluid secretion with ADPKD progression. We attempted to address early versus later stages for analysis of $Pkd1^{cko}$ by comparing P5 versus P10, but perhaps a more meticulous approach would be to include pre-cystic age (~P1). We could not accomplish such extensive analysis for both early- and adult-onset models due to time constraints, but conducting a systematic analysis could help us identify and target key channels/transporters whose activity are selectively upregulated in the pre-cystic stage. As we had seen in Senicapoc-treated $Pkd1^{-/-}$ metanephroi, those who received Senicapoc at the time of cyst induction had greater impairment in cyst formation and growth than those who received Senicapoc two days

after cyst induction. Based on this observation, it could be more efficient to take preventative measures than to treat after disease is established.

4.3 Elevation in cAMP may reflect severity of cystic phenotypes

Elevated cAMP levels represent a central mechanism mediating cyst growth through stimulation of fluid secretion and proliferation (Calvet, 2015). Increased renal cAMP levels have been reported in several non-orthologous Pkd1 models (Wang et al., 2005; Yamaguchi et al., 1997), while reducing renal cAMP levels through vasopressin receptor V2 inhibition is the target of the only FDA approved drug for ADPKD, Tolvaptan. However, apart from $Pkd1^{RC/RC}$ where renal cAMP has also been found highly elevated (Hopp et al., 2012), cAMP has not been examined in other orthologous *Pkd1* models. We measured and confirmed that renal cAMP is consistently upregulated in all *Pkd1* orthologous mouse models we have analyzed. cAMP is thought to stimulate proliferation by MAPK/ERK activation, as demonstrated by *in vitro* studies conducted by Yamaguchi *et al.* We analyzed phospho-ERK and ERK levels and found consistent activation in both early- and adult-onset *Pkd1* mouse kidneys, consistent with proliferation being one of the major drivers of cyst growth, even in adult-onset models where proliferation is normally maintained at baseline in healthy animals. The greater fold increase in cAMP in $Pkd1^{cko}$ versus $^{SB}Pkd1$ did not stimulate higher proliferation measured by MAPK/ERK activation or ki67 positive cells per kidney surface area in this model, and indeed, both models encountered similar stimulation in proliferation. The greater proliferation in $Pkd1^{cko}$ at baseline compared to $^{SB}Pkd1$ is potentially due to differences in age, as seen in the wildtype where higher rate of proliferation is observed in P10 versus in adult. In fact, most of the analysis we conducted reveal a similar fold increase in $Pkd1^{cko}$ and $^{SB}Pkd1$ when compared to wildtype, which nicely illustrates that key features of ADPKD are reproducible, regardless of the underlying genetic cause. Upon

examination of the different parameters we have analyzed, fold increases in cAMP levels appear to associate more closely with disease progressivity as defined by severity of cysts (quantified by percent cyst surface area). Indeed, we observed greater cyst surface areas in *Pkd1*^{cko} versus ^{SB}*Pkd1*, which also reflects the proportional difference in cAMP levels. Aside from differences in cAMP levels, we also detected greater c-Myc activation in *Pkd1*^{cko} kidneys, while in ^{SB}*Pkd1* we observed more fibrotic kidneys with greater functional loss. Greater activation of c-Myc in *Pkd1*^{cko} kidneys can be explained in part by the higher renal cAMP level that stimulate greater activation of downstream effector c-Myc to sustain proliferation of renal epithelial cells. As cAMP is thought to differentially regulate proliferation (activation versus inhibition) depending on the pattern of B-Raf protein, analyzing B-Raf levels may help us understand the different elevation in cAMP we observed between rapid versus slow progressive mouse models. Fibrotic kidneys, on the other hand, require longer time to develop and exacerbate, therefore greater collagen accumulation in ^{SB}*Pkd1* may be expected given the longer lifespan. It is intriguing how greater decline in kidney function is found in ^{SB}*Pkd1* given the vastly different lifespan and cyst severity at the time of analysis. As ^{SB}*Pkd1* and *Pkd1*^{cko} are generated differently with opposing *Pkd1* levels and differ in cyst distribution (no proximal tubular cysts in *Pkd1*^{cko}), a direct comparison of kidney functional decline between the two models may be difficult as the differences in underlying mechanisms of cyst formation could play a role. More importantly, BUN in *Pkd1*^{cko} was analyzed around early- to mid-stages of disease progression, whereas ^{SB}*Pkd1* samples were collected near end stage. Understandably, greater kidney functional loss would be expected in ^{SB}*Pkd1*.

4.4 *Kcnn4* genetic inactivation causes greater rescue of MAPK/ERK signaling in the early-onset *Pkd1*^{cko} mouse model

Analyses of cyst-associated processes show a similar improvement in *Pkd1*^{cko} and ^{SB}*Pkd1* kidneys upon genetic *Kcnn4* inactivation, although the rescue in terms of kidney function parameters and lifespan was overall more effective in the ^{SB}*Pkd1* mouse model. The first phenomenon we had observed was the strikingly limited enlargement of ^{SB}*Pkd1; Kcnn4*$^{-/-}$ kidneys, which also remained stable with age while ^{SB}*Pkd1* kidneys continued to enlarge. This effect was not as pronounced in *Pkd1*^{cko}*; Kcnn4*$^{-/-}$ kidneys, which is likely due to their rapid progressivity. The only analysis where we observe a greater rescue upon genetic *Kcnn4* inactivation in the rapid progressive model (*Pkd1*^{cko}*; Kcnn4*$^{-/-}$) than in the slow progressive model (^{SB}*Pkd1; Kcnn4*$^{-/-}$) was in MAPK/ERK activation, where phospho-ERK, ERK, phospho-ERK/ERK are restored and downstream effector c-Myc is reduced by over half. This significant rescue led to ~43% reduction in proliferation measured by ki67 staining, suggesting c-Myc activation may be more indicative of downstream events such as proliferation. As there are numerous signaling pathways upstream of c-Myc, such as Wnt, the partial normalization of c-Myc despite complete restoration of MAPK/ERK signaling could be attributed to other signaling pathways unaffected by *Kcnn4* inactivation. As canonical Wnt signaling is hyperactivated in ADPKD, implicated in primary cilia assembly/disassembly, and more importantly, it is completely normalized in polycystin/*Ift88* double knockout mice (Lancaster et al., 2011; Parrot et al., 2019; Shao et al., 2020), we analyzed active and total β-catenin levels in *Pkd1*^{cko}*; Kcnn4*$^{-/-}$ compared to *Pkd1*^{cko} and found overall no significant rescue of the increased levels observed. In fact, Wnt/β-catenin activation even showed a tendency to increase upon *Kcnn4* inactivation (as indicated by greater total b-catenin levels), in part explaining why c-Myc is only partially

normalized. To address the signaling status in *Pkd1*^{cko} at an earlier age, we analyzed and compared the level of activation and rescue by *Kcnn4* inactivation of signaling pathways at P5. We expected to find greater activation and rescue at P5 compared to P10, since the proliferative status of renal epithelial cells reduces with age. However, we found identical hyperactivation of MAPK/ERK at both ages despite the marked greater increase in kidney size and cyst indices between P10 and wildtype, while greater fold increase of c-Myc reflects more severe P10 *Pkd1*^{cko} kidneys. This suggests that MAPK/ERK activation is sustained between P5 and P10 despite the supposed difference in proliferative status due to increasing age. It would be interesting to examine whether the activation of MAPK/ERK is maintained throughout the disease and if it translates into a sustained rate of increase in cyst indices. The remarkably normalized MAPK/ERK and reduced c-Myc by half at both ages upon *Kcnn4* inactivation indicate that targeting *Kcnn4* is equally effective in downregulating MAPK/ERK and effector c-Myc at early versus mid-stage in this model. This rescue is striking insofar that it not only shows that *Kcnn4* is tightly associated with MAPK/ERK signaling in *Pkd1*^{cko}, but it also indicates that the renal epithelial cells remain highly plastic in this rapid progressive model, such that targeting *Kcnn4* restores MAPK/ERK equally at P5 and P10. In contrast, the effect of *Kcnn4* inactivation on Wnt signaling is less conclusive in the *Pkd1*^{cko} model, as we found contrary results at the two ages. Upon genetic *Kcnn4* inactivation, Wnt/β-catenin activation in the kidneys appears to be reduced at P5, but tend to elevate at P10, although no significance is found at either age. This contrasting effect maybe in part due to large deviations between individual samples. These results suggest that Kcnn4 may not be a major regulator of canonical Wnt signaling in ADPKD. Therefore, we did not analyze this pathway further in ^{SB}*Pkd1*. In ^{SB}*Pkd1*, we found sustained hyperactivation of MAPK/ERK even at 6 months. It would be interesting to analyze and compare MAPK/ERK in

the ^{SB}Pkd1 at earlier ages, like we did for *Pkd1*^{cko} to better understand how MAPK/ERK signaling progresses with disease. Although we did not find significant downregulation of MAPK/ERK in ^{SB}*Pkd1; Kcnn4*$^{-/-}$, the 44% reduction in c-Myc levels upon genetic *Kcnn4* inactivation suggests that other pathways upstream of c-Myc may be more relevant for Kcnn4 mediated signal transduction stimulating proliferation in this moderately progressive mouse model. Analysis of signaling pathways reveal that the rescue of *Pkd1*^{cko} by genetic *Kcnn4* inactivation appears more efficient than in ^{SB}*Pkd1*, where phospho-ERK/ERK is not significantly reduced but is astonishingly more efficient at rescuing kidney function and extending lifespan. This contrasting behavior may suggest that cystogenesis is not necessarily regulated through identical upstream processes between (kidney specific) *Pkd1* over expressor and *Pkd1* knockout mouse models, although downstream events driving cyst growth appear to be similar.

4.5 Kcnn4 is implicated in cyst initiation and enlargement *ex vivo* and *in vivo*

To determine whether changes in Kcnn4 level may directly contribute to cystogenesis, we first studied the effects of a Kcnn4 activator on an *ex vivo* system of cystogenesis using *Pkd1*$^{-/-}$ metanephroi. Unlike previous metanephroi studies, where the gene of interest is frequently targeted by genetic inactivation and/or pharmacologic inhibition, we utilized both approaches, as well as a pharmacologic activator of Kcnn4 to validate the channel's implication in cyst growth. Results using all three approaches complement each other and converge to show that Kcnn4 modulates *Pkd1*$^{-/-}$ cyst growth. Indeed, our *ex vivo* observations led us to suggest that Kcnn4 is implicated in both cyst enlargement and cyst initiation, as shown by comparable changes in cyst area and cyst number using the different approaches.

We began our studies by first introducing Kcnn4 activator SKA-111 to *Pkd1*$^{-/-}$ metanephroi, which are inherently highly responsive to cyst induction by cAMP. *Pkd1*$^{-/-}$ metanephroi appeared more severely cystic upon treatment with SKA-111, accompanied by increased cyst number and cyst area, therefore suggesting that Kcnn4 promotes cyst growth by enhancing cyst initiation and enlargement. More importantly, when SKA-111 was added to the normally cAMP unresponsive Pkd1$^{+/+}$ metanephroi, cysts remarkably developed, implying that Kcnn4 can induce cysts upon cAMP stimulation *ex vivo.* Consequently, we would expect the hyperactivated *Kcnn4* RNA expression in *Pkd1* mouse models to favour cyst formation and growth. Following this hypothesis, the PKD phenotype of this model would thus be ameliorated by dampening Kcnn4 through genetic inactivation or pharmacologic inhibition, which could represent an attractive strategy for treatment of human ADPKD. We decided to investigate this first in our metanephroi model. When introducing pharmacologic inhibitors *ex vivo*, we selected two inhibitors of different potency and selectivity that are widely used *in vivo* and/or in clinical trials for targeting Kcnn4 in other pathological contexts. When *Pkd1*$^{-/-}$ metanephroi were subjected to TRAM-34 and cAMP, we only detected a mild reduction in cyst area, despite utilizing high concentrations of the inhibitor (20 and 40μM). In contrast, 20μM of the more potent and selective Senicapoc led to a major reduction in cystic parameters when added simultaneously with cAMP, virtually restoring *Pkd1*$^{-/-}$ metanephroi phenotype to normal. This finding is highly pertinent as it shows that Senicapoc may be preventative whereas currently there is no drug that can prevent ADPKD.

We closely monitored the rapid progressivity of *Pkd1*^{cko} when identifying the age of cyst onset. Tubule dilations and few cysts are detectable from P2. While P3 *Pkd1*^{cko} kidneys still retained the normal pink to red colour as seen in wildtype, P5 kidneys lost all colour and

completely turned pale. This drastic transition is remarkable and highly indicative of the rapid progressivity of *Pkd1*^{cko}. Although P5 kidneys still retained some intact renal tissue, it is insufficient to retain a normal appearance. P10 kidneys lost even more intact tissue and are filled with cysts. To compare the severity and degree of rescue by *Kcnn4* inactivation at early- versus mid-stage of the disease, we first quantified cysts in P5 and P10 *Pkd1*^{cko} kidneys. From P5 to P10, additional cysts formed (14%), fluid was actively secreted into the lumen of both new and existing cysts, greatly expanding cyst surface by 40%, culminating in larger kidneys shown by the 3.8-fold increase in KBW. Unlike the parallel increase in cyst number and cyst area observed *ex vivo* in *Pkd1*$^{-/-}$ metanephroi treated with SKA-111, we noticed a proportionally greater increase in cyst surface in our *Pkd1*^{cko} model, suggesting cyst enlargement has a greater contribution to cyst growth than initiation of new cysts *in vivo.* Another explanation could be that cyst initiation is a more gradual event and only a small subset is required to drive cyst growth. Doing a similar analysis examining cysts at two ages in the slowly progressive ^{SB}*Pkd1* would help clarify. We were able to compare KBW at two ages and found it remains stable and only increased by 1.4-fold from 1 month to 6 months of age in the slow progressive model. This shows that the robust machinery mediating cyst growth can adapt to both fast pace in *Pkd1*^{cko} or slow pace in ^{SB}*Pkd1* regardless of the underlying genetics.

Reduction in cyst indices in both rapidly and slowly progressive models due to *Kcnn4* inactivation correlates well with our *ex vivo* findings and supports implication of Kcnn4 in both cyst initiation and enlargement. As both indices tend to reduce in parallel upon loss of *Kcnn4*, it is difficult to decipher in which process Kcnn4 is more involved. To address this question, we sorted individual cysts in P5 and P10 *Pkd1*^{cko} and *Pkd1*^{cko}*; Kcnn4*$^{-/-}$ by size and found that at both ages, the distribution of cysts is unchanged between *Pkd1*^{cko} and *Pkd1*^{cko}*; Kcnn4*$^{-/-}$. *Kcnn4*

inactivation does not appear to influence the proportion of cysts within each size interval, suggesting the less severe cystic kidneys we observe in *Pkd1*^{cko}*; Kcnn4*$^{-/-}$ are likely due to Kcnn4 acting on cyst initiation. Therefore, our data suggest strongly that the improvement of the cystic phenotype in *Pkd1*^{cko}*; Kcnn4*$^{-/-}$ animals is a consequence of *Kcnn4* genetic inactivation limiting cyst initiation in the *Pkd1*^{cko} model and consequently restricted the amount of cyst fluid secretion that is normally found in *Pkd1*^{cko} kidneys. Furthermore, we found that genetic *Kcnn4* inactivation induces a more significant reduction in KBW and cyst indices at P5 versus P10, suggesting interventions during early phases of disease may be more effective. This is in line with the findings by Dong *et al.* where reversal of cysts in *Pkd1* or *Pkd2* knockout mice, upon re-expression of *Pkd1* or *Pkd2,* was more rapid in animals at earlier stages of disease (Dong et al., 2021). Additionally, when analyzing cysts in ^{SB}*Pkd1*, we discovered that the *Kcnn4* heterozygous knockout animals (^{SB}*Pkd1; Kcnn4*$^{+/-}$) have similar cyst area and cyst number as their homozygous ^{SB}*Pkd1; Kcnn4*$^{-/-}$ littermates. This leads to suggest that a complete knockout of *Kcnn4* is perhaps not essential to delay cyst growth, and that therefore a reduction of activity could be sufficient when disease progression is gradual, like in human ADPKD. This finding may have implications when planning the dosage to be given to patients as total blockage of Kcnn4 may not be necessary.

4.6 Renal plasticity is demonstrated in metanephroi

The striking rescue of the cystic phenotype by Senicapoc treatment made us speculate whether Senicapoc could rescue established cysts *ex vivo*. To evaluate this, we added the inhibitor to the metanephroi culture two days after cyst induction by cAMP, which allowed us to observe the evolution of individual cysts. When we followed the same cyst before and after

Senicapoc was introduced, we found the cyst size to reduce immediately on the following day and almost completely resorbed in just two days. Administration of Senicapoc thus not only prevented cyst growth, but even induced an important regression in cyst size. It has previously been reported by Dong *et al.* using a genetic approach of *Pkd* re-expression that a high degree of renal plasticity is retained by ADPKD kidneys *in vivo*. In line with these results, we report here renal plasticity in an *ex vivo* context using a pharmacologic Kcnn4 channel inhibitor. This is of significance insofar, as it implies that the treatment of ADPKD patients with Senicapoc after the disease is established could still be beneficial and may lead to regression of pre-existing cysts. Senicapoc may thus be effective not only as a preventative measure to delay cyst growth but also as a treatment for established cysts.

4.7 cAMP levels are modulated by Kcnn4

We continued our investigation *in vivo* to identify other cyst-mediating processes Kcnn4 may be implicated in. Given the critical requirement of cAMP for biological processes and the prevalence of Kcnn4 in many pathophysiological conditions, the reduction in renal cAMP in both $Pkd1^{cko}$ and $^{SB}Pkd1$ upon loss of *Kcnn4* is intriguing and worth investigating in the future as this could reveal a new mechanism by which cAMP levels may be modulated. cAMP levels are generally believed to be regulated by the balance between activities of two enzymes: adenylyl cyclase (AC) and cyclic nucleotide phosphodiesterase (PDE). Although there appears to be no direct link between the activity of an ion channel and the modulation of a second messenger, cAMP and Kcnn4 in fact share common features that may be facilitating this process. Firstly, both closely associate with MAPK/ERK signaling. AC and PDE activities are known to be regulated by numerous signaling pathways, including MAPK/ERK (Sassone-Corsi, 2012). Our

data also show that genetic *Kcnn4* inactivation can dampen MAPK/ERK signaling. Inactivation of *Kcnn4* can thus reduce AC and PDE levels in part through downregulation of MAPK/ERK signaling. AC and PDE levels would most likely be reduced in parallel since AC6 mediated-cAMP activation of PKA in turn can stimulate PDE4 (Agarwal et al., 2019), resulting in reduced cAMP level, which can in turn dampen MAPK/ERK signaling and reduce levels of AC and PDE. Secondly, both Kcnn4 and cAMP are tightly associated with calcium. Kcnn4 drives calcium entry, therefore facilitating calcium signaling by sustaining hyperpolarization, while AC6 and PDE4 levels are also regulated by calcium (Halls & Cooper, 2011; Wang et al., 2010). Lowered calcium signaling due to Kcnn4 inactivation could consequently modulate levels of AC6 and PDE4 such that cAMP production may be reduced. Finally, cAMP has been described by Sassone-Corsi to interact with ion channels. cAMP can bind to and modulate the function of a family of cyclic-nucleotide-gated ion channels permeable to calcium, potassium, and sodium. The calcium that is permitted to flow can in turn modulates cAMP production by regulating activity of ACs and PDEs. Since both V2R and Kcnn4 are localized on the basolateral membrane (Klein et al., 2009; Robben et al., 2004), it is also possible that they interact, and through this interaction Kcnn4 may modulate cAMP levels.

4.8 Kcnn4 is involved in renal proliferation, fibrosis, primary cilia elongation and influences kidney function and survival

As Kcnn4 has demonstrated to be pro-proliferative and profibrotic in other contexts (Anumanthan et al., 2018; Bi et al., 2013; Cruse et al., 2006; Huang et al., 2014; Paka et al., 2017; Yu et al., 2013), and as another potassium channel from the same family can cause elongation of primary cilia (Nam et al., 2022) *in vitro*, we decided to investigate those

parameters in our murine models of ADPKD. The elevation in proliferation, fibrosis, and primary cilia length we observed in *Pkd1*^{cko} and ^{SB}*Pkd1* were indeed partially, and sometimes even completely, normalized, upon genetically inactivating *Kcnn4*. Although ciliary length modulation is a dynamic process, the high overlap of renal primary ciliary distribution of P10 versus 2-month-old wildtype suggest that the primary cilia length is stably maintained in healthy conditions. While the functional role of primary cilia and its length is still being investigated, based on the findings of Shao *et al.* where reduction of primary cilia length impeded cyst formation and that the length in small cysts of human ADPKD kidneys correlated with cyst size (Shao et al., 2020), the observed shortened primary cilia following loss of *Kcnn4* in our mouse models very likely contributed to the amelioration of cystic phenotypes. More importantly, we reveal a new mechanism in which a non-IFT machinery component can modulate primary cilia length, supporting the recent report by Nam *et al.* where they showed K_{Ca}2.3 channel can increase primary cilia length (Nam et al., 2022). These results clearly demonstrate that Kcnn4 is strongly implicated in these cyst-mediating processes. Although *Kcnn4* inactivation was insufficient to limit kidney functional decline or improve survival in *Pkd1*^{cko} given the rapid progressivity of the disease, *Kcnn4* inactivation even partially rescued kidney function and extended lifespan by almost 40% in the much more gradual progressive ^{SB}*Pkd1* model.

4.9 Other potassium channels could be compensating for loss of Kcnn4

Treating *Pkd1*$^{-/-}$*; Kcnn4*$^{-/-}$ metanephroi with cAMP did not completely abolish cysts like it has been observed in *Pkd1*$^{-/-}$*; Cftr*$^{-/-}$ metanephroi in a study carried out by Magenheimer *et al.* This led us to speculate that other potassium channels may be compensating for the absence of Kcnn4. The less effective rescue in *Pkd1*$^{-/-}$*; Kcnn4*$^{-/-}$ metanephroi may indicate that Kcnn4 is

downstream of Cftr and provides the driving force for continuous chloride transport through Cftr but is unlikely to be the only source, since *Kcnn4* inactivation does not completely prevent cyst formation. Likewise, our *in vivo* work indicates *Kcnn4* inactivation led to partial rescue of various cyst-mediating events in *Pkd1*^{cko}*; Kcnn4*$^{-/-}$ and ^{SB}*Pkd1; Kcnn4*$^{-/-}$. Furthermore, the normal lifespan and lack of major functional defect in Kcnn4 knockout mice suggest that other transporting proteins or pathways could be compensating to partially offset the total loss of Kcnn4. In fact, there is evidence for a compensatory mechanism between Kcnn4 and K_v1.3 in T cells (Chiang et al., 2017). Potential compensatory mechanisms for Kcnn4 in PKD remains to be studied.

4.10 Delivering Senicapoc in DMSO solvent by intraperitoneal or subcutaneous injection is lethal for young and aged mice

The improvement in disease outcome from genetically targeting Kcnn4 led us to continue the investigation using a pharmacologic approach. We administered Senicapoc to both early-onset and adult-onset mouse models hoping that targeting Kcnn4 would be effective for both models. Other *in vivo* studies utilizing Senicapoc generally administer through diet and sometimes oral gavage. We began our study with intraperitoneal or subcutaneous injection, as this method would be most convenient, and the exact volume injected into the animals can easily be controlled. Unfortunately, neither the adult nor the young animals tolerated the injections well and most died within 1 week after treatment initiation. We then attempted administration through oral gavage. Animals tolerated oral gavage much better and were able to complete the treatment. In contrary to injections, where animals lost weight immediately after the first administration,

animals gained weight when treated orally, and in most cases were comparable to or exceeded those treated with the vehicle solution only.

Due to the smaller window for treatment we decided to introduce Senicapoc as early as possible for the early-onset rapid progressive models. We first attempted delivering Senicapoc by subcutaneous injection. However, like adults, young animals did not tolerate this route of administration, perhaps due to the solvent (DMSO) since DMSO alone was also not tolerable. Importantly, a previous *in vivo* study utilized DMSO solvent for short term subcutaneous injection of Cftr inhibitor into newborn mice but did not report any issues (Yang et al., 2008). Therefore, if the lethality in our models is not caused primarily by the combination of Senicapoc in DMSO solvent, then optimizing this administration technique or replacing DMSO may be needed if future students wish to pursue this method.

Since direct oral gavage is not possible in the newborns, we administered Senicapoc to the mothers as soon as pups are born. We also administered twice daily 1-2mL of very concentrated Senicapoc (15mg/mL) that is equivalent to 120mg Senicapoc/kg of bodyweight/day, directly in the corner of their mouth, which we observed they ingested from P2 onwards. Senicapoc ingestion was found tolerable for newborn animals with no body weight loss when compared to littermates, and all animals completed treatment.

4.11 Senicapoc is more effective in adult-onset models

Aside from the kidneys, no macroscopic anomalies were found in any organs after completion of treatment in both $^{SB}Pkd1$ and $Pkd1^{wt}$ animals. $^{SB}Pkd1$ kidneys were indistinguishable between the different treatment groups. In contrast, $Pkd1^{wt}$ kidneys treated with Senicapoc appeared pinker in colour which may suggest improved morphology and function, as

we have seen in the genetic $^{SB}Pkd1;\ Kcnn4^{-/-}$ model. Based on our experiences examining kidneys at different disease stages in various mouse models differing in rate of progressivity, more intense kidney color tends to associate with healthier blood supply and more intact tissues. The observation of an increased colour intensity of the kidney appears to be paralleled by the significant improvements in cyst indices leading to partial normalization of kidney function. Although, those improvements are less pronounced in the $^{SB}Pkd1$ model, KBW is reduced upon Senicapoc treatment and there is a tendency for cyst indices to be decreased. Comparison between treated $^{SB}Pkd1$ and $Pkd1^{wt}$ animals shows that Senicapoc is more effective towards in the more moderate progressive $Pkd1^{wt}$ model. The effect of Senicapoc appears to be gradual, as an effect is often only observed after daily long-term administration in other *in vivo* studies and in clinical trials (Ataga et al., 2011; Ataga et al., 2008; Jin et al., 2019; Paka et al., 2017). This frequent treatment regime is imposed by the molecule's short half-life. Therefore, it makes sense that we find a bigger effect in $Pkd1^{wt}$ where the phenotypes develop more slowly during its longer lifespan. Likewise, we expected therefore to observe a better improvement of kidney parameters in the relatively more moderate of our two early-onset group models, the $Pkd1^{v/v}$ model.

We postulated that in the very rapidly progressive $Pkd1^{cko}$, it may be too late to observe any beneficial effect from Senicapoc treatment if we analyze at P10, so we modified our treatment schedule to end at P5 for the $Pkd1^{cko}$ animals. We treated $Pkd1^{v/v}$ mice until P10 to allow cysts to develop, as in this model tubule dilations are observed to only occur from P4. In line with our hypothesis, we indeed observed a more pronounced improvement in the more moderate $Pkd1^{v/v}$ model. $Pkd1^{v/v}$ kidneys appeared smaller macroscopically and had smaller KBW after Senicapoc treatment. However, $Pkd1^{cko}$ kidneys treated with Senicapoc even

increased in size and slightly higher KBW ratios were observed than for the vehicle treated animals. Several groups had reported PEG and Cremophor could increase kidney weight in rats, but none had studied this effect in the mice before (Hermansky et al., 1995; Ikeda et al., 2006; Stokes et al., 2013). Here we report that mouse kidneys can also increase in weight after PEG and Cremophor administration, since we observed heavier kidneys in vehicle treated animals, when compared to untreated ones (data not shown). Those who received the vehicle solution had heavier kidneys compared to those without vehicle. Remarkedly, *Pkd1*$^{v/v}$-animals treated with Senicapoc overcame this increase in weight induced by the vehicle solution and even reduced KBW. Images of H&E stained kidney sections show that Senicapoc treatment not only reduced *Pkd1*$^{v/v}$ kidneys in size, but the kidneys also appeared notably less cystic than those of vehicle treated mice. The improvement in cyst indices is more prominent in the *Pkd1*$^{v/v}$ model than in the *Pkd1*^{cko} model. One limitation of the *in vivo* Senicapoc study is that the level of Senicapoc in the plasma and the kidneys of the Senicapoc treated animals were never determined because we sadly did not have the tools at our disposal. However, since younger mice generally have faster metabolic rates than adults, one could suggest that the smaller effect of Senicapoc treatment in the early-onset models may be due to insufficient Senicapoc uptake by the kidneys or faster excretion. Furthermore, as for newborns the treatment needs to be administered through the mother, and precise oral gavage is impossible in young pups, we expect an appreciable loss of Senicapoc along the digestive tract, while precise administration of the treatment is facilitated by their age in the adult-onset models. Using the currently available tools, we found better rescue by Senicapoc in the adult- than in the early-onset models. Measuring plasma Senicapoc levels using techniques such as UHPLC-ESI-MS/MS reported by Sørensen *et al.* (Sørensen et al. 2021) would help us understand if the route of administration or the short half-life of Senicapoc played

a role in our observation that Senicapoc treatment is more efficient in reducing cyst parameters in the adult- than in the early-onset models of ADPKD. Having such data would also facilitate optimization of our administration protocols. Another option to try to increase the efficient dose of Senicapoc delivered to the kidneys would be to administer higher doses. However, in our hands Senicapoc is insoluble in concentrations exceeding 15mg/mL in the vehicle solution. One way to overcome this barrier could be to administer Senicapoc using kidney-targeted nanoparticles, such as used by the Chung lab (Cox et al., 2023), that has become popular in recent years for more efficient drug delivery.

4.12 Genetic inactivation of *Kcnn4* is more efficient than Kcnn4 pharmacologic inhibition

We would generally expect to observe a greater rescue by genetically targeting *Kcnn4* than by use of the pharmacologic approach, as the former is considered to block the target gene more effectively and with fewer off-target effects. However, metanephroi culture, where the kidneys are taken out of the *in vivo* context, may not behave the same way as *in vivo* which may contribute to their contrasting behaviour. If we follow the conventional usage of 10μM of Senicapoc or below, we observe an approximately 2-fold greater rescue in cyst indices by genetic *Kcnn4* inactivation than by pharmacologic inhibition. However, when we introduced a greater dosage of Senicapoc (20μM), the opposite effect is observed, where Senicapoc treatment results in almost complete abolishment of cysts. As Senicapoc is highly specific to Kcnn4 over other potassium channels (Stocker et al., 2003), we can rule out the possibility that Senicapoc is non-specifically blocking other potassium channels simultaneously. Another explanation may be that Senicapoc has a cyst alleviating effect through a way other than blocking the Kcnn4 channel pore, such as reducing proliferation as observed in animal studies of Alzheimer's (Jin et al.,

2019). This is relevant especially in the isolated metanephroi culture where other requisite factors that are present *in vivo* are absent *ex vivo*. This could be tested by analyzing proliferation levels in *Pkd1*$^{-/-}$*; Kcnn4*$^{-/-}$ metanephroi compared to *Pkd1*$^{-/-}$ metanephroi treated with Senicapoc.

A more relevant *in vivo* comparison would be to examine kidneys of P5 *Pkd1*^{cko}*; Kcnn4*$^{-/-}$ animals with kidneys from P5 *Pkd1*^{cko} mice treated with Senicapoc. Compared to the small tendency for rescue from Senicapoc treatment this rapid progressive model *in vivo*, the improvements in kidney morphology and cyst indices in double transgenic *Pkd1*^{cko}*; Kcnn4*$^{-/-}$ animals are significantly more pronounced. This is consistent with the general consideration that genetic inactivation is more efficient than pharmacological inhibition. As we have explained earlier, the lack of improvement observed upon pharmacological Senicapoc treatment may be attributed to ineffective absorption of Senicapoc or an insufficient fraction of the molecule reaching the kidneys due to its short half-life and the high metabolic rate in newborn mice.
In the adult-onset murine models, we equally observed a higher improvement in disease parameters in double transgenic ^{SB}*Pkd1; Kcnn4*$^{-/-}$ mice, than in ^{SB}*Pkd1* animals treated with Senicapoc. Cyst analysis, KBW and kidney functional assay consistently improved to larger extent by genetically targeting *Kcnn4*. However, the difference in efficiency between the two approaches is less prominent in the late-onset models, than in the rapid progressive *Pkd1*^{cko} model. This leads us to suggest that Senicapoc may be more effective as a long-term treatment for a moderate progressive disease phenotype, as its effects appear gradual and therefore would be more appropriate for treatment of slowly progressing cases of the disease.

4.13 Dual inhibition of Kcnn4 and Cftr cause synergistic rescue of cysts *ex vivo*

Combination therapy may help to achieve higher beneficial effects with lower absolute treatment doses. There have been several attempts to find good partners to delay disease progression *in vivo* (Kanhai et al., 2020; Leonhard et al., 2019), given time constraints, we explored for potential partners for combination therapy *ex vivo* that could be tested *in vivo* in the future. We first treated *Pkd1*$^{-/-}$ metanephroi with Senicapoc, PPQ-102 (Cftr inhibitor), CaCCinh-A01 (Tmem16a inhibitor) separately and subsequently tested combinations of Senicapoc with the latter two compounds at different concentrations. While executing this experiment, we found that in contrary to previous metanephroi studies where generally no more than 10μM of regiments are used (Magenheimer et al., 2006; Snyder et al., 2011; Yang et al., 2008), higher concentrations can be well-tolerated without non-specific or toxic effect if prepared in higher stock concentration such as 20mM to achieve final concentration of 20μM when used at 0.1%. Synergy is demonstrated in *Pkd1*$^{-/-}$ metanephroi treated with Senicapoc and PPQ-102, where low dosages of both compounds, when given simultaneously, resulted in better rescue than the sum of individual contribution. This observation suggests that Kcnn4 and Cftr are part of the same pathway such that dual inhibition results in superior rescue of cysts. One advantage of synergistic inhibition is, that it allows lower total dosages to be given and thus reduces likelihood of adverse events. As ADPKD patients probably requires long term treatment, limiting toxicity and improving safety is highly important.

CHAPTER 5: CONCLUDING REMARKS

Our results are summarized in a schematic diagram shown in Fig. 49. The selective upregulation of *Kcnn4* in ADPKD correlates with elevations in cAMP and enhances cAMP-driven cystogenic processes. In addition to the conventional Kcnn4 being downstream of cAMP, we unraveled the regulation between cAMP and Kcnn4 is bidirectional, such that loss of inhibition of Kcnn4 greatly reduces cAMP as well as downstream pathways that are essential to cyst growth. By disrupting Kcnn4, we found that Kcnn4 is strongly implicated in many processes that drive cyst growth such as hyperproliferation and increased fluid secretion, as demonstrated by modulation of cyst initiation and cyst enlargement, elevation in kidney fibrosis and elongation of primary cilia. Additionally, in the adult-onset mouse model that may be more relevant for ADPKD for its moderate progression and longer lifespan, kidney function and survival are significantly improved.

We have learned over the past decades that the positive outcomes from preclinical studies do not always translate to clinical trials, often due to unexpected adverse effects. An ideal treatment might be a combination of therapies in low tolerable doses that address multiple cyst-driving targets at the same time, similar to a drug cocktail. Compared to limitations in targeting other members of the fluid secretory pathway such as chloride channel inhibitors, there are several advantages of targeting Kcnn4 for treatment of ADPKD. First, Kcnn4 is a multifunctional channel that is implicated in many cellular processes that mediate cyst growth, including fluid transport, proliferation, and fibrosis. By targeting Kcnn4, we are targeting several processes simultaneously and do not need to combine with other therapies to address multiple targets. Second, Senicapoc has been used for decades in clinical trials due to its good treatment tolerability and safety profile and is still actively being repurposed for other diseases due to its effectiveness in preclinical studies in various pathophysiological conditions. Third, the positive

outcome resulted from targeting Kcnn4 is consistent across all models utilized, regardless of age of onset or disease progressivity. Collectively, our results support Kcnn4 as a therapeutic target for treatment of ADPKD.

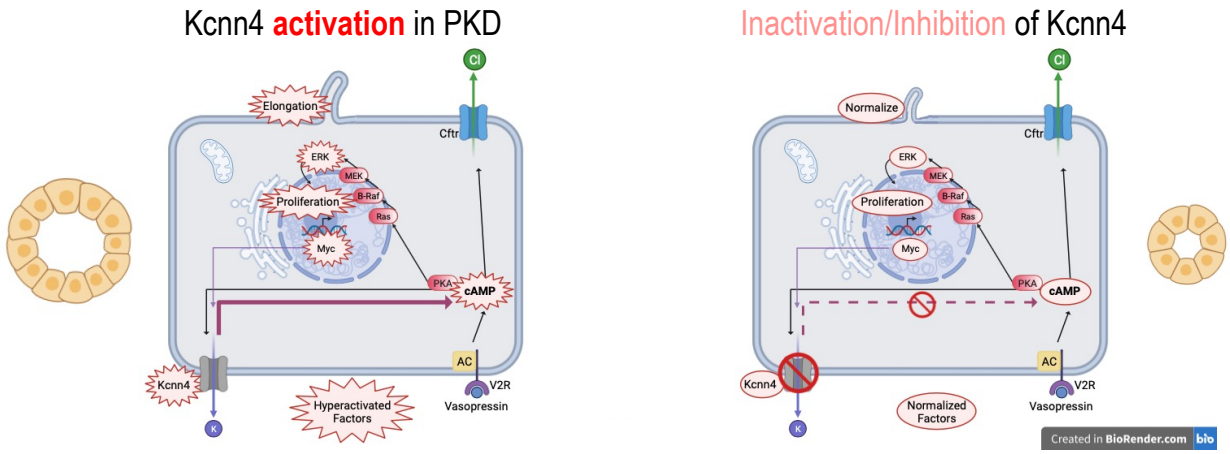

Fig. 49 Schematic representation of KCNN4 involvement in ADPKD cyst growth. Kcnn4 stimulates cyst growth by facilitating proliferation, fluid secretion, primary cilia elongation, and fibrosis. In ADPKD, elevation in Kcnn4 expression facilitates cAMP-mediated cyst driven processes, such that when Kcnn4 is disrupted, hyperactivated factors are partially or completely normalized, and collectively leads to delay in overall cyst growth. Created with Biorender.com

CHAPTER 6: REFERENCES

Abdul-Majeed, S., & Nauli, S. M. (2011). Calcium-mediated mechanisms of cystic expansion. *Biochim Biophys Acta*, *1812*(10), 1281-1290. https://doi.org/10.1016/j.bbadis.2010.09.016

Agarwal, J. J., Zhu, Y., Zhang, Q. Y., Mongin, A. A., & Hough, L. B. (2013). TRAM-34, a putatively selective blocker of intermediate-conductance, calcium-activated potassium channels, inhibits cytochrome P450 activity. *PLoS One*, *8*(5), e63028. https://doi.org/10.1371/journal.pone.0063028

Agarwal, S. R., Fiore, C., Miyashiro, K., Ostrom, R. S., & Harvey, R. D. (2019). Effect of Adenylyl Cyclase Type 6 on Localized Production of cAMP by beta-2 Adrenoceptors in Human Airway Smooth-Muscle Cells. *J Pharmacol Exp Ther*, *370*(1), 104-110. https://doi.org/10.1124/jpet.119.256594

Ahrabi, A. K., Terryn, S., Valenti, G., Caron, N., Serradeil-Le Gal, C., Raufaste, D., Nielsen, S., Horie, S., Verbavatz, J. M., & Devuyst, O. (2007). PKD1 haploinsufficiency causes a syndrome of inappropriate antidiuresis in mice. *J Am Soc Nephrol*, *18*(6), 1740-1753. https://doi.org/10.1681/ASN.2006010052

Aihara, M., Fujiki, H., Mizuguchi, H., Hattori, K., Ohmoto, K., Ishikawa, M., Nagano, K., & Yamamura, Y. (2014). Tolvaptan delays the onset of end-stage renal disease in a polycystic kidney disease model by suppressing increases in kidney volume and renal injury. *J Pharmacol Exp Ther*, *349*(2), 258-267. https://doi.org/10.1124/jpet.114.213256

Albaqumi, M., Srivastava, S., Li, Z., Zhdnova, O., Wulff, H., Itani, O., Wallace, D. P., & Skolnik, E. Y. (2008). KCa3.1 potassium channels are critical for cAMP-dependent chloride secretion and cyst growth in autosomal-dominant polycystic kidney disease. *Kidney Int*, *74*(6), 740-749. https://doi.org/10.1038/ki.2008.246

Ameku, T., Taura, D., Sone, M., Numata, T., Nakamura, M., Shiota, F., Toyoda, T., Matsui, S., Araoka, T., Yasuno, T., Mae, S., Kobayashi, H., Kondo, N., Kitaoka, F., Amano, N., Arai, S., Ichisaka, T., Matsuura, N., Inoue, S., . . . Osafune, K. (2016). Identification of MMP1 as a novel risk factor for intracranial aneurysms in ADPKD using iPSC models. *Sci Rep*, *6*, 30013. https://doi.org/10.1038/srep30013

Annis, D. A., Nickbarg, E., Yang, X., Ziebell, M. R., & Whitehurst, C. E. (2007). Affinity selection-mass spectrometry screening techniques for small molecule drug discovery. *Curr Opin Chem Biol*, *11*(5), 518-526. https://doi.org/10.1016/j.cbpa.2007.07.011

Anumanthan, G., Gupta, S., Fink, M. K., Hesemann, N. P., Bowles, D. K., McDaniel, L. M., Muhammad, M., & Mohan, R. R. (2018). KCa3.1 ion channel: A novel therapeutic target for corneal fibrosis. *PLoS One*, *13*(3), e0192145. https://doi.org/10.1371/journal.pone.0192145

Anvarian, Z., Mykytyn, K., Mukhopadhyay, S., Pedersen, L. B., & Christensen, S. T. (2019). Cellular signalling by primary cilia in development, organ function and disease. *Nat Rev Nephrol*, *15*(4), 199-219. https://doi.org/10.1038/s41581-019-0116-9

Arnould, T., Kim, E., Tsiokas, L., Jochimsen, F., Gruning, W., Chang, J. D., & Walz, G. (1998). The polycystic kidney disease 1 gene product mediates protein kinase C alpha-dependent and c-Jun N-terminal kinase-dependent activation of the transcription factor AP-1. *J Biol Chem*, *273*(11), 6013-6018. https://doi.org/10.1074/jbc.273.11.6013

Arroyo, J., Escobar-Zarate, D., Wells, H. H., Constans, M. M., Thao, K., Smith, J. M., Sieben, C. J., Martell, M. R., Kline, T. L., Irazabal, M. V., Torres, V. E., Hopp, K., & Harris, P. C. (2021).

The genetic background significantly impacts the severity of kidney cystic disease in the Pkd1(RC/RC) mouse model of autosomal dominant polycystic kidney disease. *Kidney Int*, *99*(6), 1392-1407. https://doi.org/10.1016/j.kint.2021.01.028

Arthur, J. M. (2000). The MDCK cell line is made up of populations of cells with diverse resistive and transport properties. *Tissue Cell*, *32*(5), 446-450. https://doi.org/10.1054/tice.2000.0135

Ataga, K. I., Orringer, E. P., Styles, L., Vichinsky, E. P., Swerdlow, P., Davis, G. A., Desimone, P. A., & Stocker, J. W. (2006). Dose-escalation study of ICA-17043 in patients with sickle cell disease. *Pharmacotherapy*, *26*(11), 1557-1564. https://doi.org/10.1592/phco.26.11.1557

Ataga, K. I., Reid, M., Ballas, S. K., Yasin, Z., Bigelow, C., James, L. S., Smith, W. R., Galacteros, F., Kutlar, A., Hull, J. H., Stocker, J. W., & Investigators, I. C. A. S. (2011). Improvements in haemolysis and indicators of erythrocyte survival do not correlate with acute vaso-occlusive crises in patients with sickle cell disease: a phase III randomized, placebo-controlled, double-blind study of the Gardos channel blocker senicapoc (ICA-17043). *Br J Haematol*, *153*(1), 92-104. https://doi.org/10.1111/j.1365-2141.2010.08520.x

Ataga, K. I., Smith, W. R., De Castro, L. M., Swerdlow, P., Saunthararajah, Y., Castro, O., Vichinsky, E., Kutlar, A., Orringer, E. P., Rigdon, G. C., Stocker, J. W., & Investigators, I. C. A. (2008). Efficacy and safety of the Gardos channel blocker, senicapoc (ICA-17043), in patients with sickle cell anemia. *Blood*, *111*(8), 3991-3997. https://doi.org/10.1182/blood-2007-08-110098

Ataga, K. I., Staffa, S. J., Brugnara, C., & Stocker, J. W. (2021). Haemoglobin response to senicapoc in patients with sickle cell disease: a re-analysis of the Phase III trial. *Br J Haematol*, *192*(5), e129-e132. https://doi.org/10.1111/bjh.17345

Atala, A., Freeman, M. R., Mandell, J., & Beier, D. R. (1993). Juvenile cystic kidneys (jck): a new mouse mutation which causes polycystic kidneys. *Kidney Int*, *43*(5), 1081-1085. https://doi.org/10.1038/ki.1993.151

Audrezet, M. P., Corbiere, C., Lebbah, S., Moriniere, V., Broux, F., Louillet, F., Fischbach, M., Zaloszyc, A., Cloarec, S., Merieau, E., Baudouin, V., Deschenes, G., Roussey, G., Maestri, S., Visconti, C., Boyer, O., Abel, C., Lahoche, A., Randrianaivo, H., . . . Heidet, L. (2016). Comprehensive PKD1 and PKD2 Mutation Analysis in Prenatal Autosomal Dominant Polycystic Kidney Disease. *J Am Soc Nephrol*, *27*(3), 722-729. https://doi.org/10.1681/ASN.2014101051

Audrezet, M. P., Cornec-Le Gall, E., Chen, J. M., Redon, S., Quere, I., Creff, J., Benech, C., Maestri, S., Le Meur, Y., & Ferec, C. (2012). Autosomal dominant polycystic kidney disease: comprehensive mutation analysis of PKD1 and PKD2 in 700 unrelated patients. *Hum Mutat*, *33*(8), 1239-1250. https://doi.org/10.1002/humu.22103

Babich, V., Zeng, W. Z., Yeh, B. I., Ibraghimov-Beskrovnaya, O., Cai, Y., Somlo, S., & Huang, C. L. (2004). The N-terminal extracellular domain is required for polycystin-1-dependent channel activity. *J Biol Chem*, *279*(24), 25582-25589. https://doi.org/10.1074/jbc.M402829200

Badano, J. L., Mitsuma, N., Beales, P. L., & Katsanis, N. (2006). The ciliopathies: an emerging class of human genetic disorders. *Annu Rev Genomics Hum Genet*, *7*, 125-148. https://doi.org/10.1146/annurev.genom.7.080505.115610

Baert, L. (1978). Hereditary polycystic kidney disease (adult form): a microdissection study of two cases at an early stage of the disease. *Kidney Int*, *13*(6), 519-525. https://doi.org/10.1038/ki.1978.75

Bai, Y., Wei, C., Li, P., Sun, X., Cai, G., Chen, X., & Hong, Q. (2022). Primary cilium in kidney development, function and disease. *Front Endocrinol (Lausanne)*, *13*, 952055. https://doi.org/10.3389/fendo.2022.952055

Ballas, S. K., & Smith, E. D. (1992). Red blood cell changes during the evolution of the sickle cell painful crisis. *Blood*, *79*(8), 2154-2163. https://www.ncbi.nlm.nih.gov/pubmed/1562742

Banizs, B., Komlosi, P., Bevensee, M. O., Schwiebert, E. M., Bell, P. D., & Yoder, B. K. (2007). Altered pH(i) regulation and Na(+)/HCO3(-) transporter activity in choroid plexus of cilia-defective Tg737(orpk) mutant mouse. *Am J Physiol Cell Physiol*, *292*(4), C1409-1416. https://doi.org/10.1152/ajpcell.00408.2006

Bardou, O., Trinh, N. T., & Brochiero, E. (2009). Molecular diversity and function of K+ channels in airway and alveolar epithelial cells. *Am J Physiol Lung Cell Mol Physiol*, *296*(2), L145-155. https://doi.org/10.1152/ajplung.90525.2008

Bastos, A. P., Piontek, K., Silva, A. M., Martini, D., Menezes, L. F., Fonseca, J. M., Fonseca, II, Germino, G. G., & Onuchic, L. F. (2009). Pkd1 haploinsufficiency increases renal damage and induces microcyst formation following ischemia/reperfusion. *J Am Soc Nephrol*, *20*(11), 2389-2402. https://doi.org/10.1681/ASN.2008040435

Basu, P., Lung, T. K., Lemsaddek, W., Sargent, T. G., Williams, D. C., Jr., Basu, M., Redmond, L. C., Lingrel, J. B., Haar, J. L., & Lloyd, J. A. (2007). EKLF and KLF2 have compensatory roles in embryonic beta-globin gene expression and primitive erythropoiesis. *Blood*, *110*(9), 3417-3425. https://doi.org/10.1182/blood-2006-11-057307

Begenisich, T., Nakamoto, T., Ovitt, C. E., Nehrke, K., Brugnara, C., Alper, S. L., & Melvin, J. E. (2004). Physiological roles of the intermediate conductance, Ca2+-activated potassium channel Kcnn4. *J Biol Chem*, *279*(46), 47681-47687. https://doi.org/10.1074/jbc.M409627200

Belibi, F. A., Wallace, D. P., Yamaguchi, T., Christensen, M., Reif, G., & Grantham, J. J. (2002). The effect of caffeine on renal epithelial cells from patients with autosomal dominant polycystic kidney disease. *J Am Soc Nephrol*, *13*(11), 2723-2729. https://doi.org/10.1097/01.asn.0000025282.48298.7b

Benzing, T., Simons, M., & Walz, G. (2007). Wnt signaling in polycystic kidney disease. *J Am Soc Nephrol*, *18*(5), 1389-1398. https://doi.org/10.1681/ASN.2006121355

Bergeron, C., & Cantin, A. M. (2019). Cystic Fibrosis: Pathophysiology of Lung Disease. *Semin Respir Crit Care Med*, *40*(6), 715-726. https://doi.org/10.1055/s-0039-1694021

Bernard, K., Bogliolo, S., Soriani, O., & Ehrenfeld, J. (2003). Modulation of calcium-dependent chloride secretion by basolateral SK4-like channels in a human bronchial cell line. *J Membr Biol*, *196*(1), 15-31. https://doi.org/10.1007/s00232-003-0621-3

Besschetnova, T. Y., Kolpakova-Hart, E., Guan, Y., Zhou, J., Olsen, B. R., & Shah, J. V. (2010). Identification of signaling pathways regulating primary cilium length and flow-mediated adaptation. *Curr Biol*, *20*(2), 182-187. https://doi.org/10.1016/j.cub.2009.11.072

Bi, D., Toyama, K., Lemaitre, V., Takai, J., Fan, F., Jenkins, D. P., Wulff, H., Gutterman, D. D., Park, F., & Miura, H. (2013). The intermediate conductance calcium-activated potassium channel KCa3.1 regulates vascular smooth muscle cell proliferation via controlling

calcium-dependent signaling. *J Biol Chem*, *288*(22), 15843-15853. https://doi.org/10.1074/jbc.M112.427187

Bihoreau, M. T., Ceccherini, I., Browne, J., Kranzlin, B., Romeo, G., Lathrop, G. M., James, M. R., & Gretz, N. (1997). Location of the first genetic locus, PKDr1, controlling autosomal dominant polycystic kidney disease in Han:SPRD cy/+ rat. *Hum Mol Genet*, *6*(4), 609-613. https://doi.org/10.1093/hmg/6.4.609

Brill, S. R., Ross, K. E., Davidow, C. J., Ye, M., Grantham, J. J., & Caplan, M. J. (1996). Immunolocalization of ion transport proteins in human autosomal dominant polycystic kidney epithelial cells. *Proc Natl Acad Sci U S A*, *93*(19), 10206-10211. https://doi.org/10.1073/pnas.93.19.10206

Brittenham, G. M., Schechter, A. N., & Noguchi, C. T. (1985). Hemoglobin S polymerization: primary determinant of the hemolytic and clinical severity of the sickling syndromes. *Blood*, *65*(1), 183-189. https://www.ncbi.nlm.nih.gov/pubmed/3965046

Brosnahan, G. M., Wang, W., Gitomer, B., Struemph, T., George, D., You, Z., Nowak, K. L., Klawitter, J., & Chonchol, M. B. (2022). Metformin Therapy in Autosomal Dominant Polycystic Kidney Disease: A Feasibility Study. *Am J Kidney Dis*, *79*(4), 518-526. https://doi.org/10.1053/j.ajkd.2021.06.026

Brown, J. H., Bihoreau, M. T., Hoffmann, S., Kranzlin, B., Tychinskaya, I., Obermuller, N., Podlich, D., Boehn, S. N., Kaisaki, P. J., Megel, N., Danoy, P., Copley, R. R., Broxholme, J., Witzgall, R., Lathrop, M., Gretz, N., & Gauguier, D. (2005). Missense mutation in sterile alpha motif of novel protein SamCystin is associated with polycystic kidney disease in (cy/+) rat. *J Am Soc Nephrol*, *16*(12), 3517-3526. https://doi.org/10.1681/ASN.2005060601

Brugnara, C., Gee, B., Armsby, C. C., Kurth, S., Sakamoto, M., Rifai, N., Alper, S. L., & Platt, O. S. (1996). Therapy with oral clotrimazole induces inhibition of the Gardos channel and reduction of erythrocyte dehydration in patients with sickle cell disease. *J Clin Invest*, *97*(5), 1227-1234. https://doi.org/10.1172/JCI118537

Buchholz, B., Teschemacher, B., Schley, G., Schillers, H., & Eckardt, K. U. (2011). Formation of cysts by principal-like MDCK cells depends on the synergy of cAMP- and ATP-mediated fluid secretion. *J Mol Med (Berl)*, *89*(3), 251-261. https://doi.org/10.1007/s00109-010-0715-1

Bycroft, M., Bateman, A., Clarke, J., Hamill, S. J., Sandford, R., Thomas, R. L., & Chothia, C. (1999). The structure of a PKD domain from polycystin-1: implications for polycystic kidney disease. *EMBO J*, *18*(2), 297-305. https://doi.org/10.1093/emboj/18.2.297

Cabrita, I., Buchholz, B., Schreiber, R., & Kunzelmann, K. (2020). TMEM16A drives renal cyst growth by augmenting Ca(2+) signaling in M1 cells. *J Mol Med (Berl)*, *98*(5), 659-671. https://doi.org/10.1007/s00109-020-01894-y

Cabrita, I., Kraus, A., Scholz, J. K., Skoczynski, K., Schreiber, R., Kunzelmann, K., & Buchholz, B. (2020). Cyst growth in ADPKD is prevented by pharmacological and genetic inhibition of TMEM16A in vivo. *Nat Commun*, *11*(1), 4320. https://doi.org/10.1038/s41467-020-18104-5

Cahalan, M. D., & Chandy, K. G. (1997). Ion channels in the immune system as targets for immunosuppression. *Curr Opin Biotechnol*, *8*(6), 749-756. https://doi.org/10.1016/s0958-1669(97)80130-9

Cahalan, M. D., & Chandy, K. G. (2009). The functional network of ion channels in T lymphocytes. *Immunol Rev*, *231*(1), 59-87. https://doi.org/10.1111/j.1600-065X.2009.00816.x

Cahalan, M. D., Wulff, H., & Chandy, K. G. (2001). Molecular properties and physiological roles of ion channels in the immune system. *J Clin Immunol*, *21*(4), 235-252. https://doi.org/10.1023/a:1010958907271

Cai, Y., Maeda, Y., Cedzich, A., Torres, V. E., Wu, G., Hayashi, T., Mochizuki, T., Park, J. H., Witzgall, R., & Somlo, S. (1999). Identification and characterization of polycystin-2, the PKD2 gene product. *J Biol Chem*, *274*(40), 28557-28565. https://doi.org/10.1074/jbc.274.40.28557

Calvet, J. P. (2003). Ciliary signaling goes down the tubes. *Nat Genet*, *33*(2), 113-114. https://doi.org/10.1038/ng1078

Calvet, J. P. (2015). The Role of Calcium and Cyclic AMP in PKD. In X. Li (Ed.), *Polycystic Kidney Disease*. https://doi.org/10.15586/codon.pkd.2015.ch8

Caroli, A., Antiga, L., Conti, S., Sonzogni, A., Fasolini, G., Ondei, P., Perico, N., Remuzzi, G., & Remuzzi, A. (2011). Intermediate volume on computed tomography imaging defines a fibrotic compartment that predicts glomerular filtration rate decline in autosomal dominant polycystic kidney disease patients. *Am J Pathol*, *179*(2), 619-627. https://doi.org/10.1016/j.ajpath.2011.04.036

Carone, F. A., Nakamura, S., Caputo, M., Bacallao, R., Nelson, W. J., & Kanwar, Y. S. (1994). Cell polarity in human renal cystic disease. *Lab Invest*, *70*(5), 648-655. https://www.ncbi.nlm.nih.gov/pubmed/8196361

Cassini, M. F., Kakade, V. R., Kurtz, E., Sulkowski, P., Glazer, P., Torres, R., Somlo, S., & Cantley, L. G. (2018). Mcp1 Promotes Macrophage-Dependent Cyst Expansion in Autosomal Dominant Polycystic Kidney Disease. *J Am Soc Nephrol*, *29*(10), 2471-2481. https://doi.org/10.1681/ASN.2018050518

Chang, M. Y., Parker, E., Ibrahim, S., Shortland, J. R., Nahas, M. E., Haylor, J. L., & Ong, A. C. (2006). Haploinsufficiency of Pkd2 is associated with increased tubular cell proliferation and interstitial fibrosis in two murine Pkd2 models. *Nephrol Dial Transplant*, *21*(8), 2078-2084. https://doi.org/10.1093/ndt/gfl150

Chapman, A. B., Stepniakowski, K., & Rahbari-Oskoui, F. (2010). Hypertension in autosomal dominant polycystic kidney disease. *Adv Chronic Kidney Dis*, *17*(2), 153-163. https://doi.org/10.1053/j.ackd.2010.01.001

Chauvet, V., Qian, F., Boute, N., Cai, Y., Phakdeekitacharoen, B., Onuchic, L. F., Attie-Bitach, T., Guicharnaud, L., Devuyst, O., Germino, G. G., & Gubler, M. C. (2002). Expression of PKD1 and PKD2 transcripts and proteins in human embryo and during normal kidney development. *Am J Pathol*, *160*(3), 973-983. https://doi.org/10.1016/S0002-9440(10)64919-X

Chebib, F. T., & Torres, V. E. (2016). Autosomal Dominant Polycystic Kidney Disease: Core Curriculum 2016. *Am J Kidney Dis*, *67*(5), 792-810. https://doi.org/10.1053/j.ajkd.2015.07.037

Checchetto, V., Teardo, E., Carraretto, L., Leanza, L., & Szabo, I. (2016). Physiology of intracellular potassium channels: A unifying role as mediators of counterion fluxes?

Biochim Biophys Acta, *1857*(8), 1258-1266. https://doi.org/10.1016/j.bbabio.2016.03.011

Cheong, A., Bingham, A. J., Li, J., Kumar, B., Sukumar, P., Munsch, C., Buckley, N. J., Neylon, C. B., Porter, K. E., Beech, D. J., & Wood, I. C. (2005). Downregulated REST transcription factor is a switch enabling critical potassium channel expression and cell proliferation. *Mol Cell*, *20*(1), 45-52. https://doi.org/10.1016/j.molcel.2005.08.030

Chiang, E. Y., Li, T., Jeet, S., Peng, I., Zhang, J., Lee, W. P., DeVoss, J., Caplazi, P., Chen, J., Warming, S., Hackos, D. H., Mukund, S., Koth, C. M., & Grogan, J. L. (2017). Potassium channels Kv1.3 and KCa3.1 cooperatively and compensatorily regulate antigen-specific memory T cell functions. *Nat Commun*, *8*, 14644. https://doi.org/10.1038/ncomms14644

Chimote, A. A., Hajdu, P., Kucher, V., Boiko, N., Kuras, Z., Szilagyi, O., Yun, Y. H., & Conforti, L. (2013). Selective inhibition of KCa3.1 channels mediates adenosine regulation of the motility of human T cells. *J Immunol*, *191*(12), 6273-6280. https://doi.org/10.4049/jimmunol.1300702

Choe, S. (2002). Potassium channel structures. *Nat Rev Neurosci*, *3*(2), 115-121. https://doi.org/10.1038/nrn727

Choudhury, M. I., Li, Y., Mistriotis, P., Vasconcelos, A. C. N., Dixon, E. E., Yang, J., Benson, M., Maity, D., Walker, R., Martin, L., Koroma, F., Qian, F., Konstantopoulos, K., Woodward, O. M., & Sun, S. X. (2022). Kidney epithelial cells are active mechano-biological fluid pumps. *Nat Commun*, *13*(1), 2317. https://doi.org/10.1038/s41467-022-29988-w

Chung, I., Zelivyanskaya, M., & Gendelman, H. E. (2002). Mononuclear phagocyte biophysiology influences brain transendothelial and tissue migration: implication for HIV-1-associated dementia. *J Neuroimmunol*, *122*(1-2), 40-54. https://doi.org/10.1016/s0165-5728(01)00462-3

Cogswell, C., Price, S. J., Hou, X., Guay-Woodford, L. M., Flaherty, L., & Bryda, E. C. (2003). Positional cloning of jcpk/bpk locus of the mouse. *Mamm Genome*, *14*(4), 242-249. https://doi.org/10.1007/s00335-002-2241-0

Coleman, N., Brown, B. M., Olivan-Viguera, A., Singh, V., Olmstead, M. M., Valero, M. S., Kohler, R., & Wulff, H. (2014). New positive Ca2+-activated K+ channel gating modulators with selectivity for KCa3.1. *Mol Pharmacol*, *86*(3), 342-357. https://doi.org/10.1124/mol.114.093286

Colgin, L. M., Hackmann, A. F., Emond, M. J., & Monnat, R. J., Jr. (2002). The unexpected landscape of in vivo somatic mutation in a human epithelial cell lineage. *Proc Natl Acad Sci U S A*, *99*(3), 1437-1442. https://doi.org/10.1073/pnas.032655699

Corbit, K. C., Aanstad, P., Singla, V., Norman, A. R., Stainier, D. Y., & Reiter, J. F. (2005). Vertebrate Smoothened functions at the primary cilium. *Nature*, *437*(7061), 1018-1021. https://doi.org/10.1038/nature04117

Corbit, K. C., Shyer, A. E., Dowdle, W. E., Gaulden, J., Singla, V., Chen, M. H., Chuang, P. T., & Reiter, J. F. (2008). Kif3a constrains beta-catenin-dependent Wnt signalling through dual ciliary and non-ciliary mechanisms. *Nat Cell Biol*, *10*(1), 70-76. https://doi.org/10.1038/ncb1670

Cornec-Le Gall, E., Alam, A., & Perrone, R. D. (2019). Autosomal dominant polycystic kidney disease. *Lancet*, *393*(10174), 919-935. https://doi.org/10.1016/S0140-6736(18)32782-X

Cornec-Le Gall, E., Audrezet, M. P., Chen, J. M., Hourmant, M., Morin, M. P., Perrichot, R., Charasse, C., Whebe, B., Renaudineau, E., Jousset, P., Guillodo, M. P., Grall-Jezequel, A., Saliou, P., Ferec, C., & Le Meur, Y. (2013). Type of PKD1 mutation influences renal outcome in ADPKD. *J Am Soc Nephrol*, *24*(6), 1006-1013. https://doi.org/10.1681/ASN.2012070650

Cornec-Le Gall, E., Audrezet, M. P., Rousseau, A., Hourmant, M., Renaudineau, E., Charasse, C., Morin, M. P., Moal, M. C., Dantal, J., Wehbe, B., Perrichot, R., Frouget, T., Vigneau, C., Potier, J., Jousset, P., Guillodo, M. P., Siohan, P., Terki, N., Sawadogo, T., . . . Le Meur, Y. (2016). The PROPKD Score: A New Algorithm to Predict Renal Survival in Autosomal Dominant Polycystic Kidney Disease. *J Am Soc Nephrol*, *27*(3), 942-951. https://doi.org/10.1681/ASN.2015010016

Cornec-Le Gall, E., Blais, J. D., Irazabal, M. V., Devuyst, O., Gansevoort, R. T., Perrone, R. D., Chapman, A. B., Czerwiec, F. S., Ouyang, J., Heyer, C. M., Senum, S. R., Le Meur, Y., Torres, V. E., & Harris, P. C. (2018). Can we further enrich autosomal dominant polycystic kidney disease clinical trials for rapidly progressive patients? Application of the PROPKD score in the TEMPO trial. *Nephrol Dial Transplant*, *33*(4), 645-652. https://doi.org/10.1093/ndt/gfx188

Cornec-Le Gall, E., Torres, V. E., & Harris, P. C. (2018). Genetic Complexity of Autosomal Dominant Polycystic Kidney and Liver Diseases. *J Am Soc Nephrol*, *29*(1), 13-23. https://doi.org/10.1681/ASN.2017050483

Couillard, M., Guillaume, R., Tanji, N., D'Agati, V., & Trudel, M. (2002). c-myc-induced apoptosis in polycystic kidney disease is independent of FasL/Fas interaction. *Cancer Res*, *62*(8), 2210-2214. https://www.ncbi.nlm.nih.gov/pubmed/11956070

Couillard, M., & Trudel, M. (2009). C-myc as a modulator of renal stem/progenitor cell population. *Dev Dyn*, *238*(2), 405-414. https://doi.org/10.1002/dvdy.21841

Cowley, B. D., Jr., Gudapaty, S., Kraybill, A. L., Barash, B. D., Harding, M. A., Calvet, J. P., & Gattone, V. H., 2nd. (1993). Autosomal-dominant polycystic kidney disease in the rat. *Kidney Int*, *43*(3), 522-534. https://doi.org/10.1038/ki.1993.79

Cox, A., Tung, M., Li, H., Hallows, K. R., & Chung, E. J. (2023). In vitro delivery of mTOR inhibitors by kidney-targeted micelles for autosomal dominant polycystic kidney disease. *SLAS Technol*. https://doi.org/10.1016/j.slast.2023.02.001

Cruse, G., Duffy, S. M., Brightling, C. E., & Bradding, P. (2006). Functional KCa3.1 K+ channels are required for human lung mast cell migration. *Thorax*, *61*(10), 880-885. https://doi.org/10.1136/thx.2006.060319

D'Agati, V., & Trudel, M. (1992). Lectin characterization of cystogenesis in the SBM transgenic model of polycystic kidney disease. *J Am Soc Nephrol*, *3*(4), 975-983. https://doi.org/10.1681/ASN.V34975

Darszon, A., Nishigaki, T., Lopez-Gonzalez, I., Visconti, P. E., & Trevino, C. L. (2020). Differences and Similarities: The Richness of Comparative Sperm Physiology. *Physiology (Bethesda)*, *35*(3), 196-208. https://doi.org/10.1152/physiol.00033.2019

Davenport, J. R., Watts, A. J., Roper, V. C., Croyle, M. J., van Groen, T., Wyss, J. M., Nagy, T. R., Kesterson, R. A., & Yoder, B. K. (2007). Disruption of intraflagellar transport in adult mice leads to obesity and slow-onset cystic kidney disease. *Curr Biol*, *17*(18), 1586-1594. https://doi.org/10.1016/j.cub.2007.08.034

De Franceschi, L., Brugnara, C., Rouyer-Fessard, P., Jouault, H., & Beuzard, Y. (1999). Formation of dense erythrocytes in SAD mice exposed to chronic hypoxia: evaluation of different therapeutic regimens and of a combination of oral clotrimazole and magnesium therapies. *Blood*, *94*(12), 4307-4313. https://www.ncbi.nlm.nih.gov/pubmed/10590075

De Franceschi, L., Saadane, N., Trudel, M., Alper, S. L., Brugnara, C., & Beuzard, Y. (1994). Treatment with oral clotrimazole blocks Ca(2+)-activated K+ transport and reverses erythrocyte dehydration in transgenic SAD mice. A model for therapy of sickle cell disease. *J Clin Invest*, *93*(4), 1670-1676. https://doi.org/10.1172/JCI117149

Deane, J. A., Verghese, E., Martelotto, L. G., Cain, J. E., Galtseva, A., Rosenblum, N. D., Watkins, D. N., & Ricardo, S. D. (2013). Visualizing renal primary cilia. *Nephrology (Carlton)*, *18*(3), 161-168. https://doi.org/10.1111/nep.12022

Dekker, S. E. I., Ruhaak, L. R., Romijn, F., Meijer, E., Cobbaert, C. M., de Fijter, J. W., Soonawala, D., & Consortium, D. (2019). Urinary Tissue Inhibitor of Metalloproteinases-2 and Insulin-Like Growth Factor-Binding Protein 7 Do Not Correlate With Disease Severity in ADPKD Patients. *Kidney Int Rep*, *4*(6), 833-841. https://doi.org/10.1016/j.ekir.2019.03.011

Delling, M., DeCaen, P. G., Doerner, J. F., Febvay, S., & Clapham, D. E. (2013). Primary cilia are specialized calcium signalling organelles. *Nature*, *504*(7479), 311-314. https://doi.org/10.1038/nature12833

Delling, M., Indzhykulian, A. A., Liu, X., Li, Y., Xie, T., Corey, D. P., & Clapham, D. E. (2016). Primary cilia are not calcium-responsive mechanosensors. *Nature*, *531*(7596), 656-660. https://doi.org/10.1038/nature17426

Desrochers, T. M., Palma, E., & Kaplan, D. L. (2014). Tissue-engineered kidney disease models. *Adv Drug Deliv Rev*, *69-70*, 67-80. https://doi.org/10.1016/j.addr.2013.12.002

Devor, D. C., Singh, A. K., Lambert, L. C., DeLuca, A., Frizzell, R. A., & Bridges, R. J. (1999). Bicarbonate and chloride secretion in Calu-3 human airway epithelial cells. *J Gen Physiol*, *113*(5), 743-760. https://doi.org/10.1085/jgp.113.5.743

Devuyst, O., Burrow, C. R., Schwiebert, E. M., Guggino, W. B., & Wilson, P. D. (1996). Developmental regulation of CFTR expression during human nephrogenesis. *Am J Physiol*, *271*(3 Pt 2), F723-735. https://doi.org/10.1152/ajprenal.1996.271.3.F723

Di, L., Srivastava, S., Zhdanova, O., Ding, Y., Li, Z., Wulff, H., Lafaille, M., & Skolnik, E. Y. (2010). Inhibition of the K+ channel KCa3.1 ameliorates T cell-mediated colitis. *Proc Natl Acad Sci U S A*, *107*(4), 1541-1546. https://doi.org/10.1073/pnas.0910133107

Dixon, E. E., & Woodward, O. M. (2018). Three-dimensional in vitro models answer the right questions in ADPKD cystogenesis. *Am J Physiol Renal Physiol*, *315*(2), F332-F335. https://doi.org/10.1152/ajprenal.00126.2018

Dong, K., Zhang, C., Tian, X., Coman, D., Hyder, F., Ma, M., & Somlo, S. (2021). Renal plasticity revealed through reversal of polycystic kidney disease in mice. *Nat Genet*, *53*(12), 1649-1663. https://doi.org/10.1038/s41588-021-00946-4

Doyle, D. A., Morais Cabral, J., Pfuetzner, R. A., Kuo, A., Gulbis, J. M., Cohen, S. L., Chait, B. T., & MacKinnon, R. (1998). The structure of the potassium channel: molecular basis of K+ conduction and selectivity. *Science*, *280*(5360), 69-77. https://doi.org/10.1126/science.280.5360.69

Du, J., & Wilson, P. D. (1995). Abnormal polarization of EGF receptors and autocrine stimulation of cyst epithelial growth in human ADPKD. *Am J Physiol*, *269*(2 Pt 1), C487-495. https://doi.org/10.1152/ajpcell.1995.269.2.C487

Duffy, S. M., Ashmole, I., Smallwood, D. T., Leyland, M. L., & Bradding, P. (2015). Orai/CRACM1 and KCa3.1 ion channels interact in the human lung mast cell plasma membrane. *Cell Commun Signal*, *13*, 32. https://doi.org/10.1186/s12964-015-0112-z

Dugan, L. L., Kim, J. S., Zhang, Y., Bart, R. D., Sun, Y., Holtzman, D. M., & Gutmann, D. H. (1999). Differential effects of cAMP in neurons and astrocytes. Role of B-raf. *J Biol Chem*, *274*(36), 25842-25848. https://doi.org/10.1074/jbc.274.36.25842

Ecder, T., & Schrier, R. W. (2009). Cardiovascular abnormalities in autosomal-dominant polycystic kidney disease. *Nat Rev Nephrol*, *5*(4), 221-228. https://doi.org/10.1038/nrneph.2009.13

Elisakova, V., Merta, M., Reiterova, J., Baxova, A., Kotlas, J., Hirschfeldova, K., Obeidova, L., Tesar, V., & Stekrova, J. (2018). Bilineal inheritance of pathogenic PKD1 and PKD2 variants in a Czech family with autosomal dominant polycystic kidney disease - a case report. *BMC Nephrol*, *19*(1), 163. https://doi.org/10.1186/s12882-018-0978-2

Fanger, C. M., Rauer, H., Neben, A. L., Miller, M. J., Rauer, H., Wulff, H., Rosa, J. C., Ganellin, C. R., Chandy, K. G., & Cahalan, M. D. (2001). Calcium-activated potassium channels sustain calcium signaling in T lymphocytes. Selective blockers and manipulated channel expression levels. *J Biol Chem*, *276*(15), 12249-12256. https://doi.org/10.1074/jbc.M011342200

Fedeles, S. V., Gallagher, A. R., & Somlo, S. (2014). Polycystin-1: a master regulator of intersecting cystic pathways. *Trends Mol Med*, *20*(5), 251-260. https://doi.org/10.1016/j.molmed.2014.01.004

Ferguson, M. W., & O'Kane, S. (2004). Scar-free healing: from embryonic mechanisms to adult therapeutic intervention. *Philos Trans R Soc Lond B Biol Sci*, *359*(1445), 839-850. https://doi.org/10.1098/rstb.2004.1475

Fick, G. M., Duley, I. T., Johnson, A. M., Strain, J. D., Manco-Johnson, M. L., & Gabow, P. A. (1994). The spectrum of autosomal dominant polycystic kidney disease in children. *J Am Soc Nephrol*, *4*(9), 1654-1660. https://doi.org/10.1681/ASN.V491654

Fioretti, B., Castigli, E., Micheli, M. R., Bova, R., Sciaccaluga, M., Harper, A., Franciolini, F., & Catacuzzeno, L. (2006). Expression and modulation of the intermediate- conductance Ca2+-activated K+ channel in glioblastoma GL-15 cells. *Cell Physiol Biochem*, *18*(1-3), 47-56. https://doi.org/10.1159/000095135

Flahault, A., Trystram, D., Nataf, F., Fouchard, M., Knebelmann, B., Grunfeld, J. P., & Joly, D. (2018). Screening for intracranial aneurysms in autosomal dominant polycystic kidney disease is cost-effective. *Kidney Int*, *93*(3), 716-726. https://doi.org/10.1016/j.kint.2017.08.016

Flores, C. A., Melvin, J. E., Figueroa, C. D., & Sepulveda, F. V. (2007). Abolition of Ca2+-mediated intestinal anion secretion and increased stool dehydration in mice lacking the intermediate conductance Ca2+-dependent K+ channel Kcnn4. *J Physiol*, *583*(Pt 2), 705-717. https://doi.org/10.1113/jphysiol.2007.134387

Formica, C., Malas, T., Balog, J., Verburg, L., t Hoen, P. A. C., & Peters, D. J. M. (2019). Characterisation of transcription factor profiles in polycystic kidney disease (PKD):

identification and validation of STAT3 and RUNX1 in the injury/repair response and PKD progression. *J Mol Med (Berl)*, *97*(12), 1643-1656. https://doi.org/10.1007/s00109-019-01852-3

Forzisi, E., & Sesti, F. (2022). Non-conducting functions of ion channels: The case of integrin-ion channel complexes. *Channels (Austin)*, *16*(1), 185-197. https://doi.org/10.1080/19336950.2022.2108565

Fracchia, K. M., Pai, C. Y., & Walsh, C. M. (2013). Modulation of T Cell Metabolism and Function through Calcium Signaling. *Front Immunol*, *4*, 324. https://doi.org/10.3389/fimmu.2013.00324

Fragiadaki, M., Lannoy, M., Themanns, M., Maurer, B., Leonhard, W. N., Peters, D. J., Moriggl, R., & Ong, A. C. (2017). STAT5 drives abnormal proliferation in autosomal dominant polycystic kidney disease. *Kidney Int*, *91*(3), 575-586. https://doi.org/10.1016/j.kint.2016.10.039

Fragiadaki, M., Macleod, F. M., & Ong, A. C. M. (2020). The Controversial Role of Fibrosis in Autosomal Dominant Polycystic Kidney Disease. *Int J Mol Sci*, *21*(23). https://doi.org/10.3390/ijms21238936

Fragiadaki, M., Witherden, A. S., Kaneko, T., Sonnylal, S., Pusey, C. D., Bou-Gharios, G., & Mason, R. M. (2011). Interstitial fibrosis is associated with increased COL1A2 transcription in AA-injured renal tubular epithelial cells in vivo. *Matrix Biol*, *30*(7-8), 396-403. https://doi.org/10.1016/j.matbio.2011.07.004

Freedman, B. S., Brooks, C. R., Lam, A. Q., Fu, H., Morizane, R., Agrawal, V., Saad, A. F., Li, M. K., Hughes, M. R., Werff, R. V., Peters, D. T., Lu, J., Baccei, A., Siedlecki, A. M., Valerius, M. T., Musunuru, K., McNagny, K. M., Steinman, T. I., Zhou, J., . . . Bonventre, J. V. (2015). Modelling kidney disease with CRISPR-mutant kidney organoids derived from human pluripotent epiblast spheroids. *Nat Commun*, *6*, 8715. https://doi.org/10.1038/ncomms9715

Fujita, T., Meguro, T., Fukuyama, R., Nakamuta, H., & Koida, M. (2002). New signaling pathway for parathyroid hormone and cyclic AMP action on extracellular-regulated kinase and cell proliferation in bone cells. Checkpoint of modulation by cyclic AMP. *J Biol Chem*, *277*(25), 22191-22200. https://doi.org/10.1074/jbc.M110364200

Gabow, P. A., Kimberling, W. J., Strain, J. D., Manco-Johnson, M. L., & Johnson, A. M. (1997). Utility of ultrasonography in the diagnosis of autosomal dominant polycystic kidney disease in children. *J Am Soc Nephrol*, *8*(1), 105-110. https://doi.org/10.1681/ASN.V81105

Gardos, G. (1958). The function of calcium in the potassium permeability of human erythrocytes. *Biochim Biophys Acta*, *30*(3), 653-654. https://doi.org/10.1016/0006-3002(58)90124-0

Gattone, V. H., 2nd, & Grantham, J. J. (1991). Understanding human cystic disease through experimental models. *Semin Nephrol*, *11*(6), 617-631. https://www.ncbi.nlm.nih.gov/pubmed/1767135

Gattone, V. H., 2nd, Maser, R. L., Tian, C., Rosenberg, J. M., & Branden, M. G. (1999). Developmental expression of urine concentration-associated genes and their altered expression in murine infantile-type polycystic kidney disease. *Dev Genet*, *24*(3-4), 309-318. https://doi.org/10.1002/(SICI)1520-6408(1999)24:3/4<309::AID-DVG14>3.0.CO;2-5

Gattone, V. H., 2nd, Wang, X., Harris, P. C., & Torres, V. E. (2003). Inhibition of renal cystic disease development and progression by a vasopressin V2 receptor antagonist. *Nat Med*, *9*(10), 1323-1326. https://doi.org/10.1038/nm935

Geng, L., Segal, Y., Peissel, B., Deng, N., Pei, Y., Carone, F., Rennke, H. G., Glucksmann-Kuis, A. M., Schneider, M. C., Ericsson, M., Reeders, S. T., & Zhou, J. (1996). Identification and localization of polycystin, the PKD1 gene product. *J Clin Invest*, *98*(12), 2674-2682. https://doi.org/10.1172/JCI119090

Gerlach, A. C., Gangopadhyay, N. N., & Devor, D. C. (2000). Kinase-dependent regulation of the intermediate conductance, calcium-dependent potassium channel, hIK1. *J Biol Chem*, *275*(1), 585-598. https://doi.org/10.1074/jbc.275.1.585

Ghanshani, S., Wulff, H., Miller, M. J., Rohm, H., Neben, A., Gutman, G. A., Cahalan, M. D., & Chandy, K. G. (2000). Up-regulation of the IKCa1 potassium channel during T-cell activation. Molecular mechanism and functional consequences. *J Biol Chem*, *275*(47), 37137-37149. https://doi.org/10.1074/jbc.M003941200

Gilder, A. L., Chapin, H. C., Padovano, V., Hueschen, C. L., Rajendran, V., & Caplan, M. J. (2018). Newly synthesized polycystin-1 takes different trafficking pathways to the apical and ciliary membranes. *Traffic*, *19*(12), 933-945. https://doi.org/10.1111/tra.12612

Gilli, R., Lafitte, D., Lopez, C., Kilhoffer, M., Makarov, A., Briand, C., & Haiech, J. (1998). Thermodynamic analysis of calcium and magnesium binding to calmodulin. *Biochemistry*, *37*(16), 5450-5456. https://doi.org/10.1021/bi972083a

Giuliani, S., Perin, L., Sedrakyan, S., Kokorowski, P., Jin, D., & De Filippo, R. (2008). Ex vivo whole embryonic kidney culture: a novel method for research in development, regeneration and transplantation. *J Urol*, *179*(1), 365-370. https://doi.org/10.1016/j.juro.2007.08.092

Gonzalez, C., Baez-Nieto, D., Valencia, I., Oyarzun, I., Rojas, P., Naranjo, D., & Latorre, R. (2012). K(+) channels: function-structural overview. *Compr Physiol*, *2*(3), 2087-2149. https://doi.org/10.1002/cphy.c110047

Graffe, C. C., Bech, J. N., Lauridsen, T. G., & Pedersen, E. B. (2012). Urinary excretion of AQP2 and ENaC in autosomal dominant polycystic kidney disease during basal conditions and after a hypertonic saline infusion. *Am J Physiol Renal Physiol*, *302*(8), F917-927. https://doi.org/10.1152/ajprenal.00616.2011

Grandi, E., Sanguinetti, M. C., Bartos, D. C., Bers, D. M., Chen-Izu, Y., Chiamvimonvat, N., Colecraft, H. M., Delisle, B. P., Heijman, J., Navedo, M. F., Noskov, S., Proenza, C., Vandenberg, J. I., & Yarov-Yarovoy, V. (2017). Potassium channels in the heart: structure, function and regulation. *J Physiol*, *595*(7), 2209-2228. https://doi.org/10.1113/JP272864

Granfeldt, A., Andersen, L. W., Vallentin, M. F., Hilberg, O., Hasselstrom, J. B., Sorensen, L. K., Mogensen, S., Christensen, S., Grejs, A. M., Rasmussen, B. S., Kristiansen, K. T., Strom, T., Johansen, I. S., Schjorring, O. L., & Simonsen, U. (2022). Senicapoc treatment in COVID-19 patients with severe respiratory insufficiency-A randomized, open-label, phase II trial. *Acta Anaesthesiol Scand*, *66*(7), 838-846. https://doi.org/10.1111/aas.14072

Grantham, J. J. (2001). Polycystic kidney disease: from the bedside to the gene and back. *Curr Opin Nephrol Hypertens*, *10*(4), 533-542. https://doi.org/10.1097/00041552-200107000-00008

Grantham, J. J., Geiser, J. L., & Evan, A. P. (1987). Cyst formation and growth in autosomal dominant polycystic kidney disease. *Kidney Int*, *31*(5), 1145-1152. https://doi.org/10.1038/ki.1987.121

Grantham, J. J., Torres, V. E., Chapman, A. B., Guay-Woodford, L. M., Bae, K. T., King, B. F., Jr., Wetzel, L. H., Baumgarten, D. A., Kenney, P. J., Harris, P. C., Klahr, S., Bennett, W. M., Hirschman, G. N., Meyers, C. M., Zhang, X., Zhu, F., Miller, J. P., & Investigators, C. (2006). Volume progression in polycystic kidney disease. *N Engl J Med*, *354*(20), 2122-2130. https://doi.org/10.1056/NEJMoa054341

Grantham, J. J., Ye, M., Gattone, V. H., 2nd, & Sullivan, L. P. (1995). In vitro fluid secretion by epithelium from polycystic kidneys. *J Clin Invest*, *95*(1), 195-202. https://doi.org/10.1172/JCI117638

Gretz, N., Kranzlin, B., Pey, R., Schieren, G., Bach, J., Obermuller, N., Ceccherini, I., Kloting, I., Rohmeiss, P., Bachmann, S., & Hafner, M. (1996). Rat models of autosomal dominant polycystic kidney disease. *Nephrol Dial Transplant*, *11 Suppl 6*, 46-51. https://doi.org/10.1093/ndt/11.supp6.46

Grgic, I., Kaistha, B. P., Paschen, S., Kaistha, A., Busch, C., Si, H., Kohler, K., Elsasser, H. P., Hoyer, J., & Kohler, R. (2009). Disruption of the Gardos channel (KCa3.1) in mice causes subtle erythrocyte macrocytosis and progressive splenomegaly. *Pflugers Arch*, *458*(2), 291-302. https://doi.org/10.1007/s00424-008-0619-x

Grgic, I., Kiss, E., Kaistha, B. P., Busch, C., Kloss, M., Sautter, J., Muller, A., Kaistha, A., Schmidt, C., Raman, G., Wulff, H., Strutz, F., Grone, H. J., Kohler, R., & Hoyer, J. (2009). Renal fibrosis is attenuated by targeted disruption of KCa3.1 potassium channels. *Proc Natl Acad Sci U S A*, *106*(34), 14518-14523. https://doi.org/10.1073/pnas.0903458106

Grieben, M., Pike, A. C., Shintre, C. A., Venturi, E., El-Ajouz, S., Tessitore, A., Shrestha, L., Mukhopadhyay, S., Mahajan, P., Chalk, R., Burgess-Brown, N. A., Sitsapesan, R., Huiskonen, J. T., & Carpenter, E. P. (2017). Structure of the polycystic kidney disease TRP channel Polycystin-2 (PC2). *Nat Struct Mol Biol*, *24*(2), 114-122. https://doi.org/10.1038/nsmb.3343

Guay-Woodford, L. M. (2003). Murine models of polycystic kidney disease: molecular and therapeutic insights. *Am J Physiol Renal Physiol*, *285*(6), F1034-1049. https://doi.org/10.1152/ajprenal.00195.2003

Gueguinou, M., Chantome, A., Fromont, G., Bougnoux, P., Vandier, C., & Potier-Cartereau, M. (2014). KCa and Ca(2+) channels: the complex thought. *Biochim Biophys Acta*, *1843*(10), 2322-2333. https://doi.org/10.1016/j.bbamcr.2014.02.019

Gunaratne, H. J., Moy, G. W., Kinukawa, M., Miyata, S., Mah, S. A., & Vacquier, V. D. (2007). The 10 sea urchin receptor for egg jelly proteins (SpREJ) are members of the polycystic kidney disease-1 (PKD1) family. *BMC Genomics*, *8*, 235. https://doi.org/10.1186/1471-2164-8-235

Ha, K., Nobuhara, M., Wang, Q., Walker, R. V., Qian, F., Schartner, C., Cao, E., & Delling, M. (2020). The heteromeric PC-1/PC-2 polycystin complex is activated by the PC-1 N-terminus. *Elife*, *9*. https://doi.org/10.7554/eLife.60684

Hadimeri, H., Lamm, C., & Nyberg, G. (1998). Coronary aneurysms in patients with autosomal dominant polycystic kidney disease. *J Am Soc Nephrol*, *9*(5), 837-841. https://doi.org/10.1681/ASN.V95837

Halls, M. L., & Cooper, D. M. (2011). Regulation by Ca2+-signaling pathways of adenylyl cyclases. *Cold Spring Harb Perspect Biol*, *3*(1), a004143. https://doi.org/10.1101/cshperspect.a004143

Hama, T., & Park, F. (2016). Heterotrimeric G protein signaling in polycystic kidney disease. *Physiol Genomics*, *48*(7), 429-445. https://doi.org/10.1152/physiolgenomics.00027.2016

Hanaoka, K., Devuyst, O., Schwiebert, E. M., Wilson, P. D., & Guggino, W. B. (1996). A role for CFTR in human autosomal dominant polycystic kidney disease. *Am J Physiol*, *270*(1 Pt 1), C389-399. https://doi.org/10.1152/ajpcell.1996.270.1.C389

Hanaoka, K., Qian, F., Boletta, A., Bhunia, A. K., Piontek, K., Tsiokas, L., Sukhatme, V. P., Guggino, W. B., & Germino, G. G. (2000). Co-assembly of polycystin-1 and -2 produces unique cation-permeable currents. *Nature*, *408*(6815), 990-994. https://doi.org/10.1038/35050128

Hanukoglu, I., & Hanukoglu, A. (2016). Epithelial sodium channel (ENaC) family: Phylogeny, structure-function, tissue distribution, and associated inherited diseases. *Gene*, *579*(2), 95-132. https://doi.org/10.1016/j.gene.2015.12.061

Happe, H., & Peters, D. J. (2014). Translational research in ADPKD: lessons from animal models. *Nat Rev Nephrol*, *10*(10), 587-601. https://doi.org/10.1038/nrneph.2014.137

Happe, H., van der Wal, A. M., Salvatori, D. C., Leonhard, W. N., Breuning, M. H., de Heer, E., & Peters, D. J. (2013). Cyst expansion and regression in a mouse model of polycystic kidney disease. *Kidney Int*, *83*(6), 1099-1108. https://doi.org/10.1038/ki.2013.13

Harris, P. C. (1999). Autosomal dominant polycystic kidney disease: clues to pathogenesis. *Hum Mol Genet*, *8*(10), 1861-1866. https://doi.org/10.1093/hmg/8.10.1861

Harris, P. C., & Hopp, K. (2013). The mutation, a key determinant of phenotype in ADPKD. *J Am Soc Nephrol*, *24*(6), 868-870. https://doi.org/10.1681/ASN.2013040417

Hassane, S., Leonhard, W. N., van der Wal, A., Hawinkels, L. J., Lantinga-van Leeuwen, I. S., ten Dijke, P., Breuning, M. H., de Heer, E., & Peters, D. J. (2010). Elevated TGFbeta-Smad signalling in experimental Pkd1 models and human patients with polycystic kidney disease. *J Pathol*, *222*(1), 21-31. https://doi.org/10.1002/path.2734

Hermansky, S. J., Neptun, D. A., Loughran, K. A., & Leung, H. W. (1995). Effects of polyethylene glycol 400 (PEG 400) following 13 weeks of gavage treatment in Fischer-344 rats. *Food Chem Toxicol*, *33*(2), 139-149. https://doi.org/10.1016/0278-6915(94)00119-9

Heyer, C. M., Sundsbak, J. L., Abebe, K. Z., Chapman, A. B., Torres, V. E., Grantham, J. J., Bae, K. T., Schrier, R. W., Perrone, R. D., Braun, W. E., Steinman, T. I., Mrug, M., Yu, A. S., Brosnahan, G., Hopp, K., Irazabal, M. V., Bennett, W. M., Flessner, M. F., Moore, C. G., . . . Investigators, C. (2016). Predicted Mutation Strength of Nontruncating PKD1 Mutations Aids Genotype-Phenotype Correlations in Autosomal Dominant Polycystic Kidney Disease. *J Am Soc Nephrol*, *27*(9), 2872-2884. https://doi.org/10.1681/ASN.2015050583

Hibino, H., Inanobe, A., Furutani, K., Murakami, S., Findlay, I., & Kurachi, Y. (2010). Inwardly rectifying potassium channels: their structure, function, and physiological roles. *Physiol Rev*, *90*(1), 291-366. https://doi.org/10.1152/physrev.00021.2009

Hille, B. (1992). *Ionic channels of excitable membranes* (2nd ed.). Sinauer Associates.

Hoffmann, E. K., & Simonsen, L. O. (1989). Membrane mechanisms in volume and pH regulation in vertebrate cells. *Physiol Rev*, *69*(2), 315-382. https://doi.org/10.1152/physrev.1989.69.2.315

Hogan, M. C., Abebe, K., Torres, V. E., Chapman, A. B., Bae, K. T., Tao, C., Sun, H., Perrone, R. D., Steinman, T. I., Braun, W., Winklhofer, F. T., Miskulin, D. C., Rahbari-Oskoui, F., Brosnahan, G., Masoumi, A., Karpov, I. O., Spillane, S., Flessner, M., Moore, C. G., & Schrier, R. W. (2015). Liver involvement in early autosomal-dominant polycystic kidney disease. *Clin Gastroenterol Hepatol*, *13*(1), 155-164 e156. https://doi.org/10.1016/j.cgh.2014.07.051

Hogan, M. C., Manganelli, L., Woollard, J. R., Masyuk, A. I., Masyuk, T. V., Tammachote, R., Huang, B. Q., Leontovich, A. A., Beito, T. G., Madden, B. J., Charlesworth, M. C., Torres, V. E., LaRusso, N. F., Harris, P. C., & Ward, C. J. (2009). Characterization of PKD protein-positive exosome-like vesicles. *J Am Soc Nephrol*, *20*(2), 278-288. https://doi.org/10.1681/ASN.2008060564

Hollenhorst, M. I., Richter, K., & Fronius, M. (2011). Ion transport by pulmonary epithelia. *J Biomed Biotechnol*, *2011*, 174306. https://doi.org/10.1155/2011/174306

Hopp, K., Ward, C. J., Hommerding, C. J., Nasr, S. H., Tuan, H. F., Gainullin, V. G., Rossetti, S., Torres, V. E., & Harris, P. C. (2012). Functional polycystin-1 dosage governs autosomal dominant polycystic kidney disease severity. *J Clin Invest*, *122*(11), 4257-4273. https://doi.org/10.1172/JCI64313

Huang, C., Shen, S., Ma, Q., Gill, A., Pollock, C. A., & Chen, X. M. (2014). KCa3.1 mediates activation of fibroblasts in diabetic renal interstitial fibrosis. *Nephrol Dial Transplant*, *29*(2), 313-324. https://doi.org/10.1093/ndt/gft431

Hughes, J., Ward, C. J., Aspinwall, R., Butler, R., & Harris, P. C. (1999). Identification of a human homologue of the sea urchin receptor for egg jelly: a polycystic kidney disease-like protein. *Hum Mol Genet*, *8*(3), 543-549. https://doi.org/10.1093/hmg/8.3.543

Hughes, J., Ward, C. J., Peral, B., Aspinwall, R., Clark, K., San Millan, J. L., Gamble, V., & Harris, P. C. (1995). The polycystic kidney disease 1 (PKD1) gene encodes a novel protein with multiple cell recognition domains. *Nat Genet*, *10*(2), 151-160. https://doi.org/10.1038/ng0695-151

Hwang, Y. H., Conklin, J., Chan, W., Roslin, N. M., Liu, J., He, N., Wang, K., Sundsbak, J. L., Heyer, C. M., Haider, M., Paterson, A. D., Harris, P. C., & Pei, Y. (2016). Refining Genotype-Phenotype Correlation in Autosomal Dominant Polycystic Kidney Disease. *J Am Soc Nephrol*, *27*(6), 1861-1868. https://doi.org/10.1681/ASN.2015060648

Icagen. (2003, November). *A Study of the Efficacy and Safety of ICA-17043 (With or Without Hydroxyurea) in Patients With Sickle Cell Anemia*. https://ClinicalTrials.gov/show/NCT00040677

Icagen. (2009a, March). *Safety and Efficacy Study of Oral Senicapoc on Allergen Challenge in Atopic Asthmatic Subjects*. https://ClinicalTrials.gov/show/NCT00861211

Icagen. (2009b, July). *Study to Assess Safety and Efficacy of Oral Senicapoc Administration on Exercise-induced Asthma*. https://ClinicalTrials.gov/show/NCT00861185

Icagen, Johnson, Johnson Pharmaceutical, R., & Development, L. L. C. *A Study Evaluating the Long-Term Safety of ICA-17043 in Sickle Cell Disease Patients With or Without Hydroxyurea Therapy*. https://ClinicalTrials.gov/show/NCT00294541

Igarashi, P., & Somlo, S. (2002). Genetics and pathogenesis of polycystic kidney disease. *J Am Soc Nephrol*, *13*(9), 2384-2398. https://doi.org/10.1097/01.asn.0000028643.17901.42

Ikeda, M., Fong, P., Cheng, J., Boletta, A., Qian, F., Zhang, X. M., Cai, H., Germino, G. G., & Guggino, W. B. (2006). A regulatory role of polycystin-1 on cystic fibrosis transmembrane conductance regulator plasma membrane expression. *Cell Physiol Biochem*, *18*(1-3), 9-20. https://doi.org/10.1159/000095133

Ishii, T. M., Silvia, C., Hirschberg, B., Bond, C. T., Adelman, J. P., & Maylie, J. (1997). A human intermediate conductance calcium-activated potassium channel. *Proc Natl Acad Sci U S A*, *94*(21), 11651-11656. https://doi.org/10.1073/pnas.94.21.11651

Jensen, B. S., Strobaek, D., Christophersen, P., Jorgensen, T. D., Hansen, C., Silahtaroglu, A., Olesen, S. P., & Ahring, P. K. (1998). Characterization of the cloned human intermediate-conductance Ca2+-activated K+ channel. *Am J Physiol*, *275*(3), C848-856. https://doi.org/10.1152/ajpcell.1998.275.3.C848

Jin, L. W., Lucente, J. D., Nguyen, H. M., Singh, V., Singh, L., Chavez, M., Bushong, T., Wulff, H., & Maezawa, I. (2019). Repurposing the KCa3.1 inhibitor senicapoc for Alzheimer's disease. *Ann Clin Transl Neurol*, *6*(4), 723-738. https://doi.org/10.1002/acn3.754

Jin, W. (2020). Role of JAK/STAT3 Signaling in the Regulation of Metastasis, the Transition of Cancer Stem Cells, and Chemoresistance of Cancer by Epithelial-Mesenchymal Transition. *Cells*, *9*(1). https://doi.org/10.3390/cells9010217

Joiner, W. J., Khanna, R., Schlichter, L. C., & Kaczmarek, L. K. (2001). Calmodulin regulates assembly and trafficking of SK4/IK1 Ca2+-activated K+ channels. *J Biol Chem*, *276*(41), 37980-37985. https://doi.org/10.1074/jbc.M104965200

Jonassen, J. A., San Agustin, J., Follit, J. A., & Pazour, G. J. (2008). Deletion of IFT20 in the mouse kidney causes misorientation of the mitotic spindle and cystic kidney disease. *J Cell Biol*, *183*(3), 377-384. https://doi.org/10.1083/jcb.200808137

Jouret, F., & Devuyst, O. (2020). Targeting chloride transport in autosomal dominant polycystic kidney disease. *Cell Signal*, *73*, 109703. https://doi.org/10.1016/j.cellsig.2020.109703

Judge, P. K., Harper, C. H. S., Storey, B. C., Haynes, R., Wilcock, M. J., Staplin, N., Goldacre, R., Baigent, C., Collier, J., Goldacre, M., Landray, M. J., Winearls, C. G., & Herrington, W. G. (2017). Biliary Tract and Liver Complications in Polycystic Kidney Disease. *J Am Soc Nephrol*, *28*(9), 2738-2748. https://doi.org/10.1681/ASN.2017010084

Kaczmarek, L. K. (2006). Non-conducting functions of voltage-gated ion channels. *Nat Rev Neurosci*, *7*(10), 761-771. https://doi.org/10.1038/nrn1988

Kanhai, A. A., Bange, H., Verburg, L., Dijkstra, K. L., Price, L. S., Peters, D. J. M., & Leonhard, W. N. (2020). Renal cyst growth is attenuated by a combination treatment of tolvaptan and pioglitazone, while pioglitazone treatment alone is not effective. *Sci Rep*, *10*(1), 1672. https://doi.org/10.1038/s41598-020-58382-z

Karihaloo, A., Koraishy, F., Huen, S. C., Lee, Y., Merrick, D., Caplan, M. J., Somlo, S., & Cantley, L. G. (2011). Macrophages promote cyst growth in polycystic kidney disease. *J Am Soc Nephrol*, *22*(10), 1809-1814. https://doi.org/10.1681/ASN.2011010084

Kaspareit-Rittinghausen, J., Deerberg, F., Rapp, K. G., & Wcislo, A. (1990). A new rat model for polycystic kidney disease of humans. *Transplant Proc*, *22*(6), 2582-2583. https://www.ncbi.nlm.nih.gov/pubmed/2264162

Kataoka, H., Fukuoka, H., Makabe, S., Yoshida, R., Teraoka, A., Ushio, Y., Akihisa, T., Manabe, S., Sato, M., Mitobe, M., Tsuchiya, K., Nitta, K., & Mochizuki, T. (2020). Prediction of Renal Prognosis in Patients with Autosomal Dominant Polycystic Kidney Disease Using PKD1/PKD2 Mutations. *J Clin Med*, *9*(1). https://doi.org/10.3390/jcm9010146

Kim, E., Arnould, T., Sellin, L., Benzing, T., Comella, N., Kocher, O., Tsiokas, L., Sukhatme, V. P., & Walz, G. (1999). Interaction between RGS7 and polycystin. *Proc Natl Acad Sci U S A*, *96*(11), 6371-6376. https://doi.org/10.1073/pnas.96.11.6371

Kim, E., Arnould, T., Sellin, L. K., Benzing, T., Fan, M. J., Gruning, W., Sokol, S. Y., Drummond, I., & Walz, G. (1999). The polycystic kidney disease 1 gene product modulates Wnt signaling. *J Biol Chem*, *274*(8), 4947-4953. https://doi.org/10.1074/jbc.274.8.4947

Kip, S. N., Hunter, L. W., Ren, Q., Harris, P. C., Somlo, S., Torres, V. E., Sieck, G. C., & Qian, Q. (2005). [Ca2+]i reduction increases cellular proliferation and apoptosis in vascular smooth muscle cells: relevance to the ADPKD phenotype. *Circ Res*, *96*(8), 873-880. https://doi.org/10.1161/01.RES.0000163278.68142.8a

Klein, H., Abu-Arish, A., Trinh, N. T., Luo, Y., Wiseman, P. W., Hanrahan, J. W., Brochiero, E., & Sauve, R. (2016). Investigating CFTR and KCa3.1 Protein/Protein Interactions. *PLoS One*, *11*(4), e0153665. https://doi.org/10.1371/journal.pone.0153665

Klein, H., Garneau, L., Trinh, N. T., Prive, A., Dionne, F., Goupil, E., Thuringer, D., Parent, L., Brochiero, E., & Sauve, R. (2009). Inhibition of the KCa3.1 channels by AMP-activated protein kinase in human airway epithelial cells. *Am J Physiol Cell Physiol*, *296*(2), C285-295. https://doi.org/10.1152/ajpcell.00418.2008

Koptides, M., Hadjimichael, C., Koupepidou, P., Pierides, A., & Constantinou Deltas, C. (1999). Germinal and somatic mutations in the PKD2 gene of renal cysts in autosomal dominant polycystic kidney disease. *Hum Mol Genet*, *8*(3), 509-513. https://doi.org/10.1093/hmg/8.3.509

Koptides, M., Mean, R., Demetriou, K., Pierides, A., & Deltas, C. C. (2000). Genetic evidence for a trans-heterozygous model for cystogenesis in autosomal dominant polycystic kidney disease. *Hum Mol Genet*, *9*(3), 447-452. https://doi.org/10.1093/hmg/9.3.447

Koslowski, S., Latapy, C., Auvray, P., Blondel, M., & Meijer, L. (2020). An Overview of In Vivo and In Vitro Models for Autosomal Dominant Polycystic Kidney Disease: A Journey from 3D-Cysts to Mini-Pigs. *Int J Mol Sci*, *21*(12). https://doi.org/10.3390/ijms21124537

Koulen, P., Cai, Y., Geng, L., Maeda, Y., Nishimura, S., Witzgall, R., Ehrlich, B. E., & Somlo, S. (2002). Polycystin-2 is an intracellular calcium release channel. *Nat Cell Biol*, *4*(3), 191-197. https://doi.org/10.1038/ncb754

Kranzlin, B., Schieren, G., & Gretz, N. (1997). Azotemia and extrarenal manifestations in old female Han:SPRD (cy/+) rats. *Kidney Int*, *51*(4), 1160-1169. https://doi.org/10.1038/ki.1997.159

Kshatri, A. S., Gonzalez-Hernandez, A., & Giraldez, T. (2018). Physiological Roles and Therapeutic Potential of Ca(2+) Activated Potassium Channels in the Nervous System. *Front Mol Neurosci*, *11*, 258. https://doi.org/10.3389/fnmol.2018.00258

Kuang, Q., Purhonen, P., & Hebert, H. (2015). Structure of potassium channels. *Cell Mol Life Sci*, *72*(19), 3677-3693. https://doi.org/10.1007/s00018-015-1948-5

Kuehn, E. W., Park, K. M., Somlo, S., & Bonventre, J. V. (2002). Kidney injury molecule-1 expression in murine polycystic kidney disease. *Am J Physiol Renal Physiol*, *283*(6), F1326-1336. https://doi.org/10.1152/ajprenal.00166.2002

Kurbegovic, A., Cote, O., Couillard, M., Ward, C. J., Harris, P. C., & Trudel, M. (2010). Pkd1 transgenic mice: adult model of polycystic kidney disease with extrarenal and renal phenotypes. *Hum Mol Genet*, *19*(7), 1174-1189. https://doi.org/10.1093/hmg/ddp588

Kurbegovic, A., Kim, H., Xu, H., Yu, S., Cruanes, J., Maser, R. L., Boletta, A., Trudel, M., & Qian, F. (2014). Novel functional complexity of polycystin-1 by GPS cleavage in vivo: role in polycystic kidney disease. *Mol Cell Biol*, *34*(17), 3341-3353. https://doi.org/10.1128/MCB.00687-14

Kwon, T. H., Frokiaer, J., & Nielsen, S. (2013). Regulation of aquaporin-2 in the kidney: A molecular mechanism of body-water homeostasis. *Kidney Res Clin Pract*, *32*(3), 96-102. https://doi.org/10.1016/j.krcp.2013.07.005

Lager, D. J., Qian, Q., Bengal, R. J., Ishibashi, M., & Torres, V. E. (2001). The pck rat: a new model that resembles human autosomal dominant polycystic kidney and liver disease. *Kidney Int*, *59*(1), 126-136. https://doi.org/10.1046/j.1523-1755.2001.00473.x

Lakhia, R., Ramalingam, H., Chang, C. M., Cobo-Stark, P., Biggers, L., Flaten, A., Alvarez, J., Valencia, T., Wallace, D. P., Lee, E. C., & Patel, V. (2022). PKD1 and PKD2 mRNA cis-inhibition drives polycystic kidney disease progression. *Nat Commun*, *13*(1), 4765. https://doi.org/10.1038/s41467-022-32543-2

Lal, M., Song, X., Pluznick, J. L., Di Giovanni, V., Merrick, D. M., Rosenblum, N. D., Chauvet, V., Gottardi, C. J., Pei, Y., & Caplan, M. J. (2008). Polycystin-1 C-terminal tail associates with beta-catenin and inhibits canonical Wnt signaling. *Hum Mol Genet*, *17*(20), 3105-3117. https://doi.org/10.1093/hmg/ddn208

Lambert, P. P. (1947). Polycystic disease of the kidney; a review. *Arch Pathol (Chic)*, *44*(1), 34-58. https://www.ncbi.nlm.nih.gov/pubmed/20258281

Lancaster, M. A., & Gleeson, J. G. (2010). Cystic kidney disease: the role of Wnt signaling. *Trends Mol Med*, *16*(8), 349-360. https://doi.org/10.1016/j.molmed.2010.05.004

Lancaster, M. A., Schroth, J., & Gleeson, J. G. (2011). Subcellular spatial regulation of canonical Wnt signalling at the primary cilium. *Nat Cell Biol*, *13*(6), 700-707. https://doi.org/10.1038/ncb2259

Lanktree, M. B., Haghighi, A., di Bari, I., Song, X., & Pei, Y. (2021). Insights into Autosomal Dominant Polycystic Kidney Disease from Genetic Studies. *Clin J Am Soc Nephrol*, *16*(5), 790-799. https://doi.org/10.2215/CJN.02320220

Lantinga-van Leeuwen, I. S., Dauwerse, J. G., Baelde, H. J., Leonhard, W. N., van de Wal, A., Ward, C. J., Verbeek, S., Deruiter, M. C., Breuning, M. H., de Heer, E., & Peters, D. J. (2004). Lowering of Pkd1 expression is sufficient to cause polycystic kidney disease. *Hum Mol Genet*, *13*(24), 3069-3077. https://doi.org/10.1093/hmg/ddh336

Lantinga-van Leeuwen, I. S., Leonhard, W. N., van de Wal, A., Breuning, M. H., Verbeek, S., de Heer, E., & Peters, D. J. (2006). Transgenic mice expressing tamoxifen-inducible Cre for somatic gene modification in renal epithelial cells. *Genesis*, *44*(5), 225-232. https://doi.org/10.1002/dvg.20207

Lantinga-van Leeuwen, I. S., Leonhard, W. N., van der Wal, A., Breuning, M. H., de Heer, E., & Peters, D. J. (2007). Kidney-specific inactivation of the Pkd1 gene induces rapid cyst

formation in developing kidneys and a slow onset of disease in adult mice. *Hum Mol Genet*, *16*(24), 3188-3196. https://doi.org/10.1093/hmg/ddm299

Larsen, B. R., Assentoft, M., Cotrina, M. L., Hua, S. Z., Nedergaard, M., Kaila, K., Voipio, J., & MacAulay, N. (2014). Contributions of the Na(+)/K(+)-ATPase, NKCC1, and Kir4.1 to hippocampal K(+) clearance and volume responses. *Glia*, *62*(4), 608-622. https://doi.org/10.1002/glia.22629

Lebeau, C., Hanaoka, K., Moore-Hoon, M. L., Guggino, W. B., Beauwens, R., & Devuyst, O. (2002). Basolateral chloride transporters in autosomal dominant polycystic kidney disease. *Pflugers Arch*, *444*(6), 722-731. https://doi.org/10.1007/s00424-002-0880-3

Lee, S. H., & Somlo, S. (2014). Cyst growth, polycystins, and primary cilia in autosomal dominant polycystic kidney disease. *Kidney Res Clin Pract*, *33*(2), 73-78. https://doi.org/10.1016/j.krcp.2014.05.002

Lehman, J. M., Michaud, E. J., Schoeb, T. R., Aydin-Son, Y., Miller, M., & Yoder, B. K. (2008). The Oak Ridge Polycystic Kidney mouse: modeling ciliopathies of mice and men. *Dev Dyn*, *237*(8), 1960-1971. https://doi.org/10.1002/dvdy.21515

Leonhard, W. N., Song, X., Kanhai, A. A., Iliuta, I. A., Bozovic, A., Steinberg, G. R., Peters, D. J. M., & Pei, Y. (2019). Salsalate, but not metformin or canagliflozin, slows kidney cyst growth in an adult-onset mouse model of polycystic kidney disease. *EBioMedicine*, *47*, 436-445. https://doi.org/10.1016/j.ebiom.2019.08.041

Lin, F., Hiesberger, T., Cordes, K., Sinclair, A. M., Goldstein, L. S., Somlo, S., & Igarashi, P. (2003). Kidney-specific inactivation of the KIF3A subunit of kinesin-II inhibits renal ciliogenesis and produces polycystic kidney disease. *Proc Natl Acad Sci U S A*, *100*(9), 5286-5291. https://doi.org/10.1073/pnas.0836980100

Liu, S., Lu, W., Obara, T., Kuida, S., Lehoczky, J., Dewar, K., Drummond, I. A., & Beier, D. R. (2002). A defect in a novel Nek-family kinase causes cystic kidney disease in the mouse and in zebrafish. *Development*, *129*(24), 5839-5846. https://doi.org/10.1242/dev.00173

Liu, X., Vien, T., Duan, J., Sheu, S. H., DeCaen, P. G., & Clapham, D. E. (2018). Polycystin-2 is an essential ion channel subunit in the primary cilium of the renal collecting duct epithelium. *Elife*, *7*. https://doi.org/10.7554/eLife.33183

Liu, Y., Dai, B., Xu, C., Fu, L., Hua, Z., & Mei, C. (2011). Rosiglitazone inhibits transforming growth factor-beta1 mediated fibrogenesis in ADPKD cyst-lining epithelial cells. *PLoS One*, *6*(12), e28915. https://doi.org/10.1371/journal.pone.0028915

Losekoot, M., Meijer, E., Hagen, E. C., Belostotsky, V., de Borst, M., Tholens, A., Phylipsen, M., Pei, Y., Gansevoort, R. T., & Peters, D. J. M. (2020). Polycystic Kidney Disease Caused by Bilineal Inheritance of Truncating PKD1 as Well as PKD2 Mutations. *Kidney Int Rep*, *5*(10), 1828-1832. https://doi.org/10.1016/j.ekir.2020.07.006

Lozano-Gerona, J., Olivan-Viguera, A., Delgado-Wicke, P., Singh, V., Brown, B. M., Tapia-Casellas, E., Pueyo, E., Valero, M. S., Garcia-Otin, A. L., Giraldo, P., Abarca-Lachen, E., Surra, J. C., Osada, J., Hamilton, K. L., Raychaudhuri, S. P., Marigil, M., Juarranz, A., Wulff, H., Miura, H., . . . Kohler, R. (2020). Conditional KCa3.1-transgene induction in murine skin produces pruritic eczematous dermatitis with severe epidermal hyperplasia and hyperkeratosis. *PLoS One*, *15*(3), e0222619. https://doi.org/10.1371/journal.pone.0222619

Luciano, R. L., & Dahl, N. K. (2014). Extra-renal manifestations of autosomal dominant polycystic kidney disease (ADPKD): considerations for routine screening and management. *Nephrol Dial Transplant*, *29*(2), 247-254. https://doi.org/10.1093/ndt/gft437

Ma, M., Gallagher, A. R., & Somlo, S. (2017). Ciliary Mechanisms of Cyst Formation in Polycystic Kidney Disease. *Cold Spring Harb Perspect Biol*, *9*(11). https://doi.org/10.1101/cshperspect.a028209

Ma, M., Tian, X., Igarashi, P., Pazour, G. J., & Somlo, S. (2013). Loss of cilia suppresses cyst growth in genetic models of autosomal dominant polycystic kidney disease. *Nat Genet*, *45*(9), 1004-1012. https://doi.org/10.1038/ng.2715

Maezawa, I., Jenkins, D. P., Jin, B. E., & Wulff, H. (2012). Microglial KCa3.1 Channels as a Potential Therapeutic Target for Alzheimer's Disease. *Int J Alzheimers Dis*, *2012*, 868972. https://doi.org/10.1155/2012/868972

Magenheimer, B. S., St John, P. L., Isom, K. S., Abrahamson, D. R., De Lisle, R. C., Wallace, D. P., Maser, R. L., Grantham, J. J., & Calvet, J. P. (2006). Early embryonic renal tubules of wild-type and polycystic kidney disease kidneys respond to cAMP stimulation with cystic fibrosis transmembrane conductance regulator/Na(+),K(+),2Cl(-) Co-transporter-dependent cystic dilation. *J Am Soc Nephrol*, *17*(12), 3424-3437. https://doi.org/10.1681/ASN.2006030295

Makabe, S., Manabe, S., Kataoka, H., Akihisa, T., Yoshida, R., Ushio, Y., Sato, M., Tsuchiya, K., Mochizuki, T., & Nitta, K. (2021). Urinary Aquaporin 2 as a Potential Indicator Predicting Tolvaptan Response in Patients With ADPKD. *Kidney Int Rep*, *6*(9), 2436-2444. https://doi.org/10.1016/j.ekir.2021.06.033

Mangolini, A., de Stephanis, L., & Aguiari, G. (2016). Role of calcium in polycystic kidney disease: From signaling to pathology. *World J Nephrol*, *5*(1), 76-83. https://doi.org/10.5527/wjn.v5.i1.76

Mangoo-Karim, R., Uchic, M. E., Grant, M., Shumate, W. A., Calvet, J. P., Park, C. H., & Grantham, J. J. (1989). Renal epithelial fluid secretion and cyst growth: the role of cyclic AMP. *FASEB J*, *3*(14), 2629-2632. https://doi.org/10.1096/fasebj.3.14.2480260

Marose, T. D., Merkel, C. E., McMahon, A. P., & Carroll, T. J. (2008). Beta-catenin is necessary to keep cells of ureteric bud/Wolffian duct epithelium in a precursor state. *Dev Biol*, *314*(1), 112-126. https://doi.org/10.1016/j.ydbio.2007.11.016

Martin, G. M., Ogburn, C. E., Colgin, L. M., Gown, A. M., Edland, S. D., & Monnat, R. J., Jr. (1996). Somatic mutations are frequent and increase with age in human kidney epithelial cells. *Hum Mol Genet*, *5*(2), 215-221. https://doi.org/10.1093/hmg/5.2.215

Maser, R. L., & Calvet, J. P. (2020). Adhesion GPCRs as a paradigm for understanding polycystin-1 G protein regulation. *Cell Signal*, *72*, 109637. https://doi.org/10.1016/j.cellsig.2020.109637

Maser, R. L., Calvet, J. P., & Parnell, S. C. (2022). The GPCR properties of polycystin-1- A new paradigm. *Front Mol Biosci*, *9*, 1035507. https://doi.org/10.3389/fmolb.2022.1035507

Masyuk, T. V., Masyuk, A. I., Torres, V. E., Harris, P. C., & Larusso, N. F. (2007). Octreotide inhibits hepatic cystogenesis in a rodent model of polycystic liver disease by reducing cholangiocyte adenosine 3',5'-cyclic monophosphate. *Gastroenterology*, *132*(3), 1104-1116. https://doi.org/10.1053/j.gastro.2006.12.039

McAteer, J. A., Evan, A. P., & Gardner, K. D. (1987). Morphogenetic clonal growth of kidney epithelial cell line MDCK. *Anat Rec*, *217*(3), 229-239. https://doi.org/10.1002/ar.1092170303

Mengerink, K. J., Moy, G. W., & Vacquier, V. D. (2002). suREJ3, a polycystin-1 protein, is cleaved at the GPS domain and localizes to the acrosomal region of sea urchin sperm. *J Biol Chem*, *277*(2), 943-948. https://doi.org/10.1074/jbc.M109673200

Miller, C. (2000). An overview of the potassium channel family. *Genome Biol*, *1*(4), REVIEWS0004. https://doi.org/10.1186/gb-2000-1-4-reviews0004

Millership, J. E., Devor, D. C., Hamilton, K. L., Balut, C. M., Bruce, J. I., & Fearon, I. M. (2011). Calcium-activated K+ channels increase cell proliferation independent of K+ conductance. *Am J Physiol Cell Physiol*, *300*(4), C792-802. https://doi.org/10.1152/ajpcell.00274.2010

Miyazaki, T., Fujiki, H., Yamamura, Y., Nakamura, S., & Mori, T. (2007). Tolvaptan, an orally active vasopressin V(2)-receptor antagonist - pharmacology and clinical trials. *Cardiovasc Drug Rev*, *25*(1), 1-13. https://doi.org/10.1111/j.1527-3466.2007.00001.x

Mochizuki, T., Wu, G., Hayashi, T., Xenophontos, S. L., Veldhuisen, B., Saris, J. J., Reynolds, D. M., Cai, Y., Gabow, P. A., Pierides, A., Kimberling, W. J., Breuning, M. H., Deltas, C. C., Peters, D. J., & Somlo, S. (1996). PKD2, a gene for polycystic kidney disease that encodes an integral membrane protein. *Science*, *272*(5266), 1339-1342. https://doi.org/10.1126/science.272.5266.1339

Moy, G. W., Mendoza, L. M., Schulz, J. R., Swanson, W. J., Glabe, C. G., & Vacquier, V. D. (1996). The sea urchin sperm receptor for egg jelly is a modular protein with extensive homology to the human polycystic kidney disease protein, PKD1. *J Cell Biol*, *133*(4), 809-817. https://doi.org/10.1083/jcb.133.4.809

Moyer, J. H., Lee-Tischler, M. J., Kwon, H. Y., Schrick, J. J., Avner, E. D., Sweeney, W. E., Godfrey, V. L., Cacheiro, N. L., Wilkinson, J. E., & Woychik, R. P. (1994). Candidate gene associated with a mutation causing recessive polycystic kidney disease in mice. *Science*, *264*(5163), 1329-1333. https://doi.org/10.1126/science.8191288

Muller, R. U., Messchendorp, A. L., Birn, H., Capasso, G., Cornec-Le Gall, E., Devuyst, O., van Eerde, A., Guirchoun, P., Harris, T., Hoorn, E. J., Knoers, N., Korst, U., Mekahli, D., Le Meur, Y., Nijenhuis, T., Ong, A. C. M., Sayer, J. A., Schaefer, F., Servais, A., . . . Gansevoort, R. T. (2022). An update on the use of tolvaptan for autosomal dominant polycystic kidney disease: consensus statement on behalf of the ERA Working Group on Inherited Kidney Disorders, the European Rare Kidney Disease Reference Network and Polycystic Kidney Disease International. *Nephrol Dial Transplant*, *37*(5), 825-839. https://doi.org/10.1093/ndt/gfab312

Muto, Y., Dixon, E. E., Yoshimura, Y., Wu, H., Omachi, K., Ledru, N., Wilson, P. C., King, A. J., Eric Olson, N., Gunawan, M. G., Kuo, J. J., Cox, J. H., Miner, J. H., Seliger, S. L., Woodward, O. M., Welling, P. A., Watnick, T. J., & Humphreys, B. D. (2022). Defining cellular complexity in human autosomal dominant polycystic kidney disease by multimodal single cell analysis. *Nat Commun*, *13*(1), 6497. https://doi.org/10.1038/s41467-022-34255-z

Nagao, S., Morita, M., Kugita, M., Yoshihara, D., Yamaguchi, T., Kurahashi, H., Calvet, J. P., & Wallace, D. P. (2010). Polycystic kidney disease in Han:SPRD Cy rats is associated with

elevated expression and mislocalization of SamCystin. *Am J Physiol Renal Physiol*, *299*(5), F1078-1086. https://doi.org/10.1152/ajprenal.00504.2009

Nagao, S., Yamaguchi, T., Kusaka, M., Maser, R. L., Takahashi, H., Cowley, B. D., & Grantham, J. J. (2003). Renal activation of extracellular signal-regulated kinase in rats with autosomal-dominant polycystic kidney disease. *Kidney Int*, *63*(2), 427-437. https://doi.org/10.1046/j.1523-1755.2003.00755.x

Nakamura, T., Ushiyama, C., Suzuki, S., Ebihara, I., Shimada, N., & Koide, H. (2000). Elevation of serum levels of metalloproteinase-1, tissue inhibitor of metalloproteinase-1 and type IV collagen, and plasma levels of metalloproteinase-9 in polycystic kidney disease. *Am J Nephrol*, *20*(1), 32-36. https://doi.org/10.1159/000013552

Nakaya, M. A., Biris, K., Tsukiyama, T., Jaime, S., Rawls, J. A., & Yamaguchi, T. P. (2005). Wnt3a links left-right determination with segmentation and anteroposterior axis elongation. *Development*, *132*(24), 5425-5436. https://doi.org/10.1242/dev.02149

Nam, Y. W., Pala, R., El-Sayed, N. S., Larin-Henriquez, D., Amirrad, F., Yang, G., Rahman, M. A., Orfali, R., Downey, M., Parang, K., Nauli, S. M., & Zhang, M. (2022). Subtype-Selective Positive Modulation of K(Ca)2.3 Channels Increases Cilia Length. *ACS Chem Biol*, *17*(8), 2344-2354. https://doi.org/10.1021/acschembio.2c00469

Nauta, J., Ozawa, Y., Sweeney, W. E., Jr., Rutledge, J. C., & Avner, E. D. (1993). Renal and biliary abnormalities in a new murine model of autosomal recessive polycystic kidney disease. *Pediatr Nephrol*, *7*(2), 163-172. https://doi.org/10.1007/BF00864387

Nelson, M. T., & Quayle, J. M. (1995). Physiological roles and properties of potassium channels in arterial smooth muscle. *Am J Physiol*, *268*(4 Pt 1), C799-822. https://doi.org/10.1152/ajpcell.1995.268.4.C799

Neylon, C. B., D'Souza, T., & Reinhart, P. H. (2004). Protein kinase A inhibits intermediate conductance Ca2+-activated K+ channels expressed in Xenopus oocytes. *Pflugers Arch*, *448*(6), 613-620. https://doi.org/10.1007/s00424-004-1302-5

Nichols, A. S., Floyd, D. H., Bruinsma, S. P., Narzinski, K., & Baranski, T. J. (2013). Frizzled receptors signal through G proteins. *Cell Signal*, *25*(6), 1468-1475. https://doi.org/10.1016/j.cellsig.2013.03.009

Nobakht, N., Hanna, R. M., Al-Baghdadi, M., Ameen, K. M., Arman, F., Nobahkt, E., Kamgar, M., & Rastogi, A. (2020). Advances in Autosomal Dominant Polycystic Kidney Disease: A Clinical Review. *Kidney Med*, *2*(2), 196-208. https://doi.org/10.1016/j.xkme.2019.11.009

Norman, J. (2011). Fibrosis and progression of autosomal dominant polycystic kidney disease (ADPKD). *Biochim Biophys Acta*, *1812*(10), 1327-1336. https://doi.org/10.1016/j.bbadis.2011.06.012

Okada, H., Ban, S., Nagao, S., Takahashi, H., Suzuki, H., & Neilson, E. G. (2000). Progressive renal fibrosis in murine polycystic kidney disease: an immunohistochemical observation. *Kidney Int*, *58*(2), 587-597. https://doi.org/10.1046/j.1523-1755.2000.00205.x

Olbrich, H., Fliegauf, M., Hoefele, J., Kispert, A., Otto, E., Volz, A., Wolf, M. T., Sasmaz, G., Trauer, U., Reinhardt, R., Sudbrak, R., Antignac, C., Gretz, N., Walz, G., Schermer, B., Benzing, T., Hildebrandt, F., & Omran, H. (2003). Mutations in a novel gene, NPHP3, cause adolescent nephronophthisis, tapeto-retinal degeneration and hepatic fibrosis. *Nat Genet*, *34*(4), 455-459. https://doi.org/10.1038/ng1216

Omori, S., Hida, M., Fujita, H., Takahashi, H., Tanimura, S., Kohno, M., & Awazu, M. (2006). Extracellular signal-regulated kinase inhibition slows disease progression in mice with polycystic kidney disease. *J Am Soc Nephrol*, *17*(6), 1604-1614. https://doi.org/10.1681/ASN.2004090800

Ong, A. C., & Harris, P. C. (1997). Molecular basis of renal cyst formation--one hit or two? *Lancet*, *349*(9058), 1039-1040. https://doi.org/10.1016/S0140-6736(05)62286-6

Ong, A. C., & Harris, P. C. (2015). A polycystin-centric view of cyst formation and disease: the polycystins revisited. *Kidney Int*, *88*(4), 699-710. https://doi.org/10.1038/ki.2015.207

Ong, A. C., Harris, P. C., Davies, D. R., Pritchard, L., Rossetti, S., Biddolph, S., Vaux, D. J., Migone, N., & Ward, C. J. (1999). Polycystin-1 expression in PKD1, early-onset PKD1, and TSC2/PKD1 cystic tissue. *Kidney Int*, *56*(4), 1324-1333. https://doi.org/10.1046/j.1523-1755.1999.00659.x

Ordaz, B., Vaca, L., Franco, R., & Pasantes-Morales, H. (2004). Volume changes and whole cell membrane currents activated during gradual osmolarity decrease in C6 glioma cells: contribution of two types of K+ channels. *Am J Physiol Cell Physiol*, *286*(6), C1399-1409. https://doi.org/10.1152/ajpcell.00198.2003

Pagliarini, R., & Podrini, C. (2021). Metabolic Reprogramming and Reconstruction: Integration of Experimental and Computational Studies to Set the Path Forward in ADPKD. *Front Med (Lausanne)*, *8*, 740087. https://doi.org/10.3389/fmed.2021.740087

Paka, L., Smith, D. E., Jung, D., McCormack, S., Zhou, P., Duan, B., Li, J. S., Shi, J., Hao, Y. J., Jiang, K., Yamin, M., Goldberg, I. D., & Narayan, P. (2017). Anti-steatotic and anti-fibrotic effects of the KCa3.1 channel inhibitor, Senicapoc, in non-alcoholic liver disease. *World J Gastroenterol*, *23*(23), 4181-4190. https://doi.org/10.3748/wjg.v23.i23.4181

Pala, R., Alomari, N., & Nauli, S. M. (2017). Primary Cilium-Dependent Signaling Mechanisms. *Int J Mol Sci*, *18*(11). https://doi.org/10.3390/ijms18112272

Pang, C. J., Lemsaddek, W., Alhashem, Y. N., Bondzi, C., Redmond, L. C., Ah-Son, N., Dumur, C. I., Archer, K. J., Haar, J. L., Lloyd, J. A., & Trudel, M. (2012). Kruppel-like factor 1 (KLF1), KLF2, and Myc control a regulatory network essential for embryonic erythropoiesis. *Mol Cell Biol*, *32*(13), 2628-2644. https://doi.org/10.1128/MCB.00104-12

Parnell, S. C., Magenheimer, B. S., Maser, R. L., Rankin, C. A., Smine, A., Okamoto, T., & Calvet, J. P. (1998). The polycystic kidney disease-1 protein, polycystin-1, binds and activates heterotrimeric G-proteins in vitro. *Biochem Biophys Res Commun*, *251*(2), 625-631. https://doi.org/10.1006/bbrc.1998.9514

Parnell, S. C., Magenheimer, B. S., Maser, R. L., Zien, C. A., Frischauf, A. M., & Calvet, J. P. (2002). Polycystin-1 activation of c-Jun N-terminal kinase and AP-1 is mediated by heterotrimeric G proteins. *J Biol Chem*, *277*(22), 19566-19572. https://doi.org/10.1074/jbc.M201875200

Parrot, C., Kurbegovic, A., Yao, G., Couillard, M., Cote, O., & Trudel, M. (2019). c-Myc is a regulator of the PKD1 gene and PC1-induced pathogenesis. *Hum Mol Genet*, *28*(5), 751-763. https://doi.org/10.1093/hmg/ddy379

Pastor-Soler, N. M., Li, H., Pham, J., Rivera, D., Ho, P. Y., Mancino, V., Saitta, B., & Hallows, K. R. (2022). Metformin improves relevant disease parameters in an autosomal dominant polycystic kidney disease mouse model. *Am J Physiol Renal Physiol*, *322*(1), F27-F41. https://doi.org/10.1152/ajprenal.00298.2021

Patel, V., Li, L., Cobo-Stark, P., Shao, X., Somlo, S., Lin, F., & Igarashi, P. (2008). Acute kidney injury and aberrant planar cell polarity induce cyst formation in mice lacking renal cilia. *Hum Mol Genet*, *17*(11), 1578-1590. https://doi.org/10.1093/hmg/ddn045

Patera, F., Cudzich-Madry, A., Huang, Z., & Fragiadaki, M. (2019). Renal expression of JAK2 is high in polycystic kidney disease and its inhibition reduces cystogenesis. *Sci Rep*, *9*(1), 4491. https://doi.org/10.1038/s41598-019-41106-3

Paul, B. M., & Vanden Heuvel, G. B. (2014). Kidney: polycystic kidney disease. *Wiley Interdiscip Rev Dev Biol*, *3*(6), 465-487. https://doi.org/10.1002/wdev.152

Pavlov, T. S., Levchenko, V., Ilatovskaya, D. V., Palygin, O., & Staruschenko, A. (2015). Impaired epithelial Na+ channel activity contributes to cystogenesis and development of autosomal recessive polycystic kidney disease in PCK rats. *Pediatr Res*, *77*(1-1), 64-69. https://doi.org/10.1038/pr.2014.145

Pazour, G. J., Dickert, B. L., Vucica, Y., Seeley, E. S., Rosenbaum, J. L., Witman, G. B., & Cole, D. G. (2000). Chlamydomonas IFT88 and its mouse homologue, polycystic kidney disease gene tg737, are required for assembly of cilia and flagella. *J Cell Biol*, *151*(3), 709-718. https://doi.org/10.1083/jcb.151.3.709

Pearson, G. W., & Cobb, M. H. (2002). Cell condition-dependent regulation of ERK5 by cAMP. *J Biol Chem*, *277*(50), 48094-48098. https://doi.org/10.1074/jbc.M208535200

Pei, Y. (2001). A "two-hit" model of cystogenesis in autosomal dominant polycystic kidney disease? *Trends Mol Med*, *7*(4), 151-156. https://doi.org/10.1016/s1471-4914(01)01953-0

Pei, Y., Lan, Z., Wang, K., Garcia-Gonzalez, M., He, N., Dicks, E., Parfrey, P., Germino, G., & Watnick, T. (2012). A missense mutation in PKD1 attenuates the severity of renal disease. *Kidney Int*, *81*(4), 412-417. https://doi.org/10.1038/ki.2011.370

Pei, Y., Paterson, A. D., Wang, K. R., He, N., Hefferton, D., Watnick, T., Germino, G. G., Parfrey, P., Somlo, S., & St George-Hyslop, P. (2001). Bilineal disease and trans-heterozygotes in autosomal dominant polycystic kidney disease. *Am J Hum Genet*, *68*(2), 355-363. https://doi.org/10.1086/318188

Pei, Y., & Watnick, T. (2010). Autosomal dominant polycystic kidney disease. *Adv Chronic Kidney Dis*, *17*(2), 115-117. https://doi.org/10.1053/j.ackd.2009.12.002

Pei, Y., Watnick, T., He, N., Wang, K., Liang, Y., Parfrey, P., Germino, G., & St George-Hyslop, P. (1999). Somatic PKD2 mutations in individual kidney and liver cysts support a "two-hit" model of cystogenesis in type 2 autosomal dominant polycystic kidney disease. *J Am Soc Nephrol*, *10*(7), 1524-1529. https://doi.org/10.1681/ASN.V1071524

Pellegrino, M., & Pellegrini, M. (1998). Modulation of Ca2+-activated K+ channels of human erythrocytes by endogenous cAMP-dependent protein kinase. *Pflugers Arch*, *436*(5), 749-756. https://doi.org/10.1007/s004240050698

Pema, M., Drusian, L., Chiaravalli, M., Castelli, M., Yao, Q., Ricciardi, S., Somlo, S., Qian, F., Biffo, S., & Boletta, A. (2016). mTORC1-mediated inhibition of polycystin-1 expression drives renal cyst formation in tuberous sclerosis complex. *Nat Commun*, *7*, 10786. https://doi.org/10.1038/ncomms10786

Penna, A., & Stutzin, A. (2015). KCa3.1-Dependent Hyperpolarization Enhances Intracellular Ca2+ Signaling Induced by fMLF in Differentiated U937 Cells. *PLoS One*, *10*(9), e0139243. https://doi.org/10.1371/journal.pone.0139243

Philp, A. R., Riquelme, T. T., Millar-Buchner, P., Gonzalez, R., Sepulveda, F. V., Cid, L. P., & Flores, C. A. (2018). Kcnn4 is a modifier gene of intestinal cystic fibrosis preventing lethality in the Cftr-F508del mouse. *Sci Rep*, *8*(1), 9320. https://doi.org/10.1038/s41598-018-27465-3

Piontek, K., Menezes, L. F., Garcia-Gonzalez, M. A., Huso, D. L., & Germino, G. G. (2007). A critical developmental switch defines the kinetics of kidney cyst formation after loss of Pkd1. *Nat Med*, *13*(12), 1490-1495. https://doi.org/10.1038/nm1675

Piontek, K. B., Huso, D. L., Grinberg, A., Liu, L., Bedja, D., Zhao, H., Gabrielson, K., Qian, F., Mei, C., Westphal, H., & Germino, G. G. (2004). A functional floxed allele of Pkd1 that can be conditionally inactivated in vivo. *J Am Soc Nephrol*, *15*(12), 3035-3043. https://doi.org/10.1097/01.ASN.0000144204.01352.86

Pirson, Y. (2010). Extrarenal manifestations of autosomal dominant polycystic kidney disease. *Adv Chronic Kidney Dis*, *17*(2), 173-180. https://doi.org/10.1053/j.ackd.2010.01.003

Preminger, G. M., Koch, W. E., Fried, F. A., McFarland, E., Murphy, E. D., & Mandell, J. (1982). Murine congenital polycystic kidney disease: a model for studying development of cystic disease. *J Urol*, *127*(3), 556-560. https://doi.org/10.1016/s0022-5347(17)53911-7

Pritchard, L., Sloane-Stanley, J. A., Sharpe, J. A., Aspinwall, R., Lu, W., Buckle, V., Strmecki, L., Walker, D., Ward, C. J., Alpers, C. E., Zhou, J., Wood, W. G., & Harris, P. C. (2000). A human PKD1 transgene generates functional polycystin-1 in mice and is associated with a cystic phenotype. *Hum Mol Genet*, *9*(18), 2617-2627. https://doi.org/10.1093/hmg/9.18.2617

Qian, F., Watnick, T. J., Onuchic, L. F., & Germino, G. G. (1996). The molecular basis of focal cyst formation in human autosomal dominant polycystic kidney disease type I. *Cell*, *87*(6), 979-987. https://doi.org/10.1016/s0092-8674(00)81793-6

Qiu, W., Zhuang, S., von Lintig, F. C., Boss, G. R., & Pilz, R. B. (2000). Cell type-specific regulation of B-Raf kinase by cAMP and 14-3-3 proteins. *J Biol Chem*, *275*(41), 31921-31929. https://doi.org/10.1074/jbc.M003327200

Rader, R. K., Kahn, L. E., Anderson, G. D., Martin, C. L., Chinn, K. S., & Gregory, S. A. (1996). T cell activation is regulated by voltage-dependent and calcium-activated potassium channels. *J Immunol*, *156*(4), 1425-1430. https://www.ncbi.nlm.nih.gov/pubmed/8568243

Ramasubbu, K., Gretz, N., & Bachmann, S. (1998). Increased epithelial cell proliferation and abnormal extracellular matrix in rat polycystic kidney disease. *J Am Soc Nephrol*, *9*(6), 937-945. https://doi.org/10.1681/ASN.V96937

Rapetti-Mauss, R., Lacoste, C., Picard, V., Guitton, C., Lombard, E., Loosveld, M., Nivaggioni, V., Dasilva, N., Salgado, D., Desvignes, J. P., Beroud, C., Viout, P., Bernard, M., Soriani, O., Vinti, H., Lacroze, V., Feneant-Thibault, M., Thuret, I., Guizouarn, H., & Badens, C. (2015). A mutation in the Gardos channel is associated with hereditary xerocytosis. *Blood*, *126*(11), 1273-1280. https://doi.org/10.1182/blood-2015-04-642496

Raphael, K. L., Strait, K. A., Stricklett, P. K., Miller, R. L., Nelson, R. D., Piontek, K. B., Germino, G. G., & Kohan, D. E. (2009). Inactivation of Pkd1 in principal cells causes a more severe cystic kidney disease than in intercalated cells. *Kidney Int*, *75*(6), 626-633. https://doi.org/10.1038/ki.2008.659

Reif, G. A., & Wallace, D. P. (2019). ADPKD cell proliferation and Cl(-)-dependent fluid secretion. *Methods Cell Biol*, *153*, 69-92. https://doi.org/10.1016/bs.mcb.2019.06.001

Rio, D. C., Ares, M., Jr., Hannon, G. J., & Nilsen, T. W. (2010). Purification of RNA using TRIzol (TRI reagent). *Cold Spring Harb Protoc*, *2010*(6), pdb prot5439. https://doi.org/10.1101/pdb.prot5439

Roach, K. M., Feghali-Bostwick, C., Wulff, H., Amrani, Y., & Bradding, P. (2015). Human lung myofibroblast TGFbeta1-dependent Smad2/3 signalling is Ca(2+)-dependent and regulated by KCa3.1 K(+) channels. *Fibrogenesis Tissue Repair*, *8*, 5. https://doi.org/10.1186/s13069-015-0022-0

Robben, J. H., Knoers, N. V., & Deen, P. M. (2004). Regulation of the vasopressin V2 receptor by vasopressin in polarized renal collecting duct cells. *Mol Biol Cell*, *15*(12), 5693-5699. https://doi.org/10.1091/mbc.e04-04-0337

Rodova, M., Islam, M. R., Maser, R. L., & Calvet, J. P. (2002). The polycystic kidney disease-1 promoter is a target of the beta-catenin/T-cell factor pathway. *J Biol Chem*, *277*(33), 29577-29583. https://doi.org/10.1074/jbc.M203570200

Rohatgi, R., Milenkovic, L., & Scott, M. P. (2007). Patched1 regulates hedgehog signaling at the primary cilium. *Science*, *317*(5836), 372-376. https://doi.org/10.1126/science.1139740

Romao, E. A., Moyses Neto, M., Teixeira, S. R., Muglia, V. F., Vieira-Neto, O. M., & Dantas, M. (2006). Renal and extrarenal manifestations of autosomal dominant polycystic kidney disease. *Braz J Med Biol Res*, *39*(4), 533-538. https://doi.org/10.1590/s0100-879x2006000400014

Rossetti, S., Burton, S., Strmecki, L., Pond, G. R., San Millan, J. L., Zerres, K., Barratt, T. M., Ozen, S., Torres, V. E., Bergstralh, E. J., Winearls, C. G., & Harris, P. C. (2002). The position of the polycystic kidney disease 1 (PKD1) gene mutation correlates with the severity of renal disease. *J Am Soc Nephrol*, *13*(5), 1230-1237. https://doi.org/10.1097/01.asn.0000013300.11876.37

Rufo, P. A., Jiang, L., Moe, S. J., Brugnara, C., Alper, S. L., & Lencer, W. I. (1996). The antifungal antibiotic, clotrimazole, inhibits Cl- secretion by polarized monolayers of human colonic epithelial cells. *J Clin Invest*, *98*(9), 2066-2075. https://doi.org/10.1172/JCI119012

Saadi-Kheddouci, S., Berrebi, D., Romagnolo, B., Cluzeaud, F., Peuchmaur, M., Kahn, A., Vandewalle, A., & Perret, C. (2001). Early development of polycystic kidney disease in transgenic mice expressing an activated mutant of the beta-catenin gene. *Oncogene*, *20*(42), 5972-5981. https://doi.org/10.1038/sj.onc.1204825

Sandford, R., Sgotto, B., Aparicio, S., Brenner, S., Vaudin, M., Wilson, R. K., Chissoe, S., Pepin, K., Bateman, A., Chothia, C., Hughes, J., & Harris, P. (1997). Comparative analysis of the polycystic kidney disease 1 (PKD1) gene reveals an integral membrane glycoprotein with multiple evolutionary conserved domains. *Hum Mol Genet*, *6*(9), 1483-1489. https://doi.org/10.1093/hmg/6.9.1483

Sassone-Corsi, P. (2012). The cyclic AMP pathway. *Cold Spring Harb Perspect Biol*, *4*(12). https://doi.org/10.1101/cshperspect.a011148

Schaefer, L., Han, X., Gretz, N., Hafner, C., Meier, K., Matzkies, F., & Schaefer, R. M. (1996). Tubular gelatinase A (MMP-2) and its tissue inhibitors in polycystic kidney disease in the Han:SPRD rat. *Kidney Int*, *49*(1), 75-81. https://doi.org/10.1038/ki.1996.10

Schafer, K., Gretz, N., Bader, M., Oberbaumer, I., Eckardt, K. U., Kriz, W., & Bachmann, S. (1994). Characterization of the Han:SPRD rat model for hereditary polycystic kidney disease. *Kidney Int*, *46*(1), 134-152. https://doi.org/10.1038/ki.1994.253

Schilling, T., Stock, C., Schwab, A., & Eder, C. (2004). Functional importance of Ca2+-activated K+ channels for lysophosphatidic acid-induced microglial migration. *Eur J Neurosci*, *19*(6), 1469-1474. https://doi.org/10.1111/j.1460-9568.2004.03265.x

Schmitt, N., Grunnet, M., & Olesen, S. P. (2014). Cardiac potassium channel subtypes: new roles in repolarization and arrhythmia. *Physiol Rev*, *94*(2), 609-653. https://doi.org/10.1152/physrev.00022.2013

Schneider, C. A., Rasband, W. S., & Eliceiri, K. W. (2012). NIH Image to ImageJ: 25 years of image analysis. *Nat Methods*, *9*(7), 671-675. https://doi.org/10.1038/nmeth.2089

Schonauer, R., Baatz, S., Nemitz-Kliemchen, M., Frank, V., Petzold, F., Sewerin, S., Popp, B., Munch, J., Neuber, S., Bergmann, C., & Halbritter, J. (2020). Matching clinical and genetic diagnoses in autosomal dominant polycystic kidney disease reveals novel phenocopies and potential candidate genes. *Genet Med*, *22*(8), 1374-1383. https://doi.org/10.1038/s41436-020-0816-3

Schwab, A., Nechyporuk-Zloy, V., Gassner, B., Schulz, C., Kessler, W., Mally, S., Romer, M., & Stock, C. (2012). Dynamic redistribution of calcium sensitive potassium channels (hK(Ca)3.1) in migrating cells. *J Cell Physiol*, *227*(2), 686-696. https://doi.org/10.1002/jcp.22776

Sforna, L., Megaro, A., Pessia, M., Franciolini, F., & Catacuzzeno, L. (2018). Structure, Gating and Basic Functions of the Ca2+-activated K Channel of Intermediate Conductance. *Curr Neuropharmacol*, *16*(5), 608-617. https://doi.org/10.2174/1570159X15666170830122402

Shao, L., El-Jouni, W., Kong, F., Ramesh, J., Kumar, R. S., Shen, X., Ren, J., Devendra, S., Dorschel, A., Wu, M., Barrera, I., Tabari, A., Hu, K., Haque, N., Yambayev, I., Li, S., Kumar, A., Behera, T. R., McDonough, G., . . . Zhou, J. (2020). Genetic reduction of cilium length by targeting intraflagellar transport 88 protein impedes kidney and liver cyst formation in mouse models of autosomal polycystic kidney disease. *Kidney Int*, *98*(5), 1225-1241. https://doi.org/10.1016/j.kint.2020.05.049

Shao, X., Somlo, S., & Igarashi, P. (2002). Epithelial-specific Cre/lox recombination in the developing kidney and genitourinary tract. *J Am Soc Nephrol*, *13*(7), 1837-1846. https://doi.org/10.1097/01.asn.0000016444.90348.50

Sharma, N., Malarkey, E. B., Berbari, N. F., O'Connor, A. K., Vanden Heuvel, G. B., Mrug, M., & Yoder, B. K. (2013). Proximal tubule proliferation is insufficient to induce rapid cyst formation after cilia disruption. *J Am Soc Nephrol*, *24*(3), 456-464. https://doi.org/10.1681/ASN.2012020154

Shen, P. S., Yang, X., DeCaen, P. G., Liu, X., Bulkley, D., Clapham, D. E., & Cao, E. (2016). The Structure of the Polycystic Kidney Disease Channel PKD2 in Lipid Nanodiscs. *Cell*, *167*(3), 763-773 e711. https://doi.org/10.1016/j.cell.2016.09.048

Shibazaki, S., Yu, Z., Nishio, S., Tian, X., Thomson, R. B., Mitobe, M., Louvi, A., Velazquez, H., Ishibe, S., Cantley, L. G., Igarashi, P., & Somlo, S. (2008). Cyst formation and activation of the extracellular regulated kinase pathway after kidney specific inactivation of Pkd1. *Hum Mol Genet*, *17*(11), 1505-1516. https://doi.org/10.1093/hmg/ddn039

Shieh, C. C., Coghlan, M., Sullivan, J. P., & Gopalakrishnan, M. (2000). Potassium channels: molecular defects, diseases, and therapeutic opportunities. *Pharmacol Rev*, *52*(4), 557-594. https://www.ncbi.nlm.nih.gov/pubmed/11121510

Shillingford, J. M., Murcia, N. S., Larson, C. H., Low, S. H., Hedgepeth, R., Brown, N., Flask, C. A., Novick, A. C., Goldfarb, D. A., Kramer-Zucker, A., Walz, G., Piontek, K. B., Germino, G. G., & Weimbs, T. (2006). The mTOR pathway is regulated by polycystin-1, and its inhibition reverses renal cystogenesis in polycystic kidney disease. *Proc Natl Acad Sci U S A*, *103*(14), 5466-5471. https://doi.org/10.1073/pnas.0509694103

Shimizu, T., Mae, S. I., Araoka, T., Okita, K., Hotta, A., Yamagata, K., & Osafune, K. (2020). A novel ADPKD model using kidney organoids derived from disease-specific human iPSCs. *Biochem Biophys Res Commun*, *529*(4), 1186-1194. https://doi.org/10.1016/j.bbrc.2020.06.141

Shumilina, E., Lam, R. S., Wolbing, F., Matzner, N., Zemtsova, I. M., Sobiesiak, M., Mahmud, H., Sausbier, U., Biedermann, T., Ruth, P., Sausbier, M., & Lang, F. (2008). Blunted IgE-mediated activation of mast cells in mice lacking the Ca2+-activated K+ channel KCa3.1. *J Immunol*, *180*(12), 8040-8047. https://doi.org/10.4049/jimmunol.180.12.8040

Snyder, D. S., Tradtrantip, L., Yao, C., Kurth, M. J., & Verkman, A. S. (2011). Potent, metabolically stable benzopyrimido-pyrrolo-oxazine-dione (BPO) CFTR inhibitors for polycystic kidney disease. *J Med Chem*, *54*(15), 5468-5477. https://doi.org/10.1021/jm200505e

Sommardahl, C. S., Woychik, R. P., Sweeney, W. E., Avner, E. D., & Wilkinson, J. E. (1997). Efficacy of taxol in the orpk mouse model of polycystic kidney disease. *Pediatr Nephrol*, *11*(6), 728-733. https://doi.org/10.1007/s004670050376

Srivastava, S., Choudhury, P., Li, Z., Liu, G., Nadkarni, V., Ko, K., Coetzee, W. A., & Skolnik, E. Y. (2006). Phosphatidylinositol 3-phosphate indirectly activates KCa3.1 via 14 amino acids in the carboxy terminus of KCa3.1. *Mol Biol Cell*, *17*(1), 146-154. https://doi.org/10.1091/mbc.e05-08-0763

Srivastava, S., Li, Z., Lin, L., Liu, G., Ko, K., Coetzee, W. A., & Skolnik, E. Y. (2005). The phosphatidylinositol 3-phosphate phosphatase myotubularin- related protein 6 (MTMR6) is a negative regulator of the Ca2+-activated K+ channel KCa3.1. *Mol Cell Biol*, *25*(9), 3630-3638. https://doi.org/10.1128/MCB.25.9.3630-3638.2005

Steidl, M. E., Nigro, E. A., Nielsen, A. K., Pagliarini, R., Cassina, L., Lampis, M., Podrini, C., Chiaravalli, M., Mannella, V., Distefano, G., Yang, M., Aslanyan, M., Musco, G., Roepman, R., Frezza, C., & Boletta, A. (2023). Primary cilia sense glutamine availability and respond via asparagine synthetase. *Nat Metab*. https://doi.org/10.1038/s42255-023-00754-6

Stocker, J. W., De Franceschi, L., McNaughton-Smith, G. A., Corrocher, R., Beuzard, Y., & Brugnara, C. (2003). ICA-17043, a novel Gardos channel blocker, prevents sickled red blood cell dehydration in vitro and in vivo in SAD mice. *Blood*, *101*(6), 2412-2418. https://doi.org/10.1182/blood-2002-05-1433

Stokes, A. H., Kemp, D. C., Faiola, B., Jordan, H. L., Merrill, C. L., Hailey, J. R., Brown, R. E., & Bailey, D. W. (2013). Effects of Solutol (Kolliphor) and cremophor in polyethylene glycol 400 vehicle formulations in Sprague-Dawley rats and beagle dogs. *Int J Toxicol*, *32*(3), 189-197. https://doi.org/10.1177/1091581813485452

Strobaek, D., Brown, D. T., Jenkins, D. P., Chen, Y. J., Coleman, N., Ando, Y., Chiu, P., Jorgensen, S., Demnitz, J., Wulff, H., & Christophersen, P. (2013). NS6180, a new K(Ca) 3.1 channel inhibitor prevents T-cell activation and inflammation in a rat model of inflammatory

bowel disease. *Br J Pharmacol*, *168*(2), 432-444. https://doi.org/10.1111/j.1476-5381.2012.02143.x

Strobaek, D., Teuber, L., Jorgensen, T. D., Ahring, P. K., Kjaer, K., Hansen, R. S., Olesen, S. P., Christophersen, P., & Skaaning-Jensen, B. (2004). Activation of human IK and SK Ca2+ -activated K+ channels by NS309 (6,7-dichloro-1H-indole-2,3-dione 3-oxime). *Biochim Biophys Acta*, *1665*(1-2), 1-5. https://doi.org/10.1016/j.bbamem.2004.07.006

Strubl, S., Torres, J. A., Spindt, A. K., Pellegrini, H., Liebau, M. C., & Weimbs, T. (2020). STAT signaling in polycystic kidney disease. *Cell Signal*, *72*, 109639. https://doi.org/10.1016/j.cellsig.2020.109639

Su, L., Yuan, H., Zhang, H., Wang, R., Fu, K., Yin, L., Ren, Y., Liu, H., Fang, Q., Wang, J., & Guo, D. (2022). PF-06409577 inhibits renal cyst progression by concurrently inhibiting the mTOR pathway and CFTR channel activity. *FEBS Open Bio*, *12*(10), 1761-1770. https://doi.org/10.1002/2211-5463.13459

Su, Q., Hu, F., Ge, X., Lei, J., Yu, S., Wang, T., Zhou, Q., Mei, C., & Shi, Y. (2018). Structure of the human PKD1-PKD2 complex. *Science*, *361*(6406). https://doi.org/10.1126/science.aat9819

Sullivan, L. P., Wallace, D. P., & Grantham, J. J. (1998). Epithelial transport in polycystic kidney disease. *Physiol Rev*, *78*(4), 1165-1191. https://doi.org/10.1152/physrev.1998.78.4.1165

Sun, D., Gao, W., Hu, H., & Zhou, S. (2022). Why 90% of clinical drug development fails and how to improve it? *Acta Pharm Sin B*, *12*(7), 3049-3062. https://doi.org/10.1016/j.apsb.2022.02.002

Sun, Y., Zhou, H., & Yang, B. X. (2011). Drug discovery for polycystic kidney disease. *Acta Pharmacol Sin*, *32*(6), 805-816. https://doi.org/10.1038/aps.2011.29

Sundar, S. V., Zhou, J. X., Magenheimer, B. S., Reif, G. A., Wallace, D. P., Georg, G. I., Jakkaraj, S. R., Tash, J. S., Yu, A. S. L., Li, X., & Calvet, J. P. (2022). The lonidamine derivative H2-gamendazole reduces cyst formation in polycystic kidney disease. *Am J Physiol Renal Physiol*, *323*(4), F492-F506. https://doi.org/10.1152/ajprenal.00095.2022

Swenson-Fields, K. I., Vivian, C. J., Salah, S. M., Peda, J. D., Davis, B. M., van Rooijen, N., Wallace, D. P., & Fields, T. A. (2013). Macrophages promote polycystic kidney disease progression. *Kidney Int*, *83*(5), 855-864. https://doi.org/10.1038/ki.2012.446

Syme, C. A., Hamilton, K. L., Jones, H. M., Gerlach, A. C., Giltinan, L., Papworth, G. D., Watkins, S. C., Bradbury, N. A., & Devor, D. C. (2003). Trafficking of the Ca2+-activated K+ channel, hIK1, is dependent upon a C-terminal leucine zipper. *J Biol Chem*, *278*(10), 8476-8486. https://doi.org/10.1074/jbc.M210072200

Takahashi, H., Calvet, J. P., Dittemore-Hoover, D., Yoshida, K., Grantham, J. J., & Gattone, V. H., 2nd. (1991). A hereditary model of slowly progressive polycystic kidney disease in the mouse. *J Am Soc Nephrol*, *1*(7), 980-989. https://doi.org/10.1681/ASN.V17980

Takahashi, H., Honma, M., Miyauchi, Y., Nakamura, S., Ishida-Yamamoto, A., & Iizuka, H. (2004). Cyclic AMP differentially regulates cell proliferation of normal human keratinocytes through ERK activation depending on the expression pattern of B-Raf. *Arch Dermatol Res*, *296*(2), 74-82. https://doi.org/10.1007/s00403-004-0478-z

Takakura, A., Contrino, L., Zhou, X., Bonventre, J. V., Sun, Y., Humphreys, B. D., & Zhou, J. (2009). Renal injury is a third hit promoting rapid development of adult polycystic kidney disease. *Hum Mol Genet*, *18*(14), 2523-2531. https://doi.org/10.1093/hmg/ddp147

Takasato, M., Er, P. X., Chiu, H. S., Maier, B., Baillie, G. J., Ferguson, C., Parton, R. G., Wolvetang, E. J., Roost, M. S., Chuva de Sousa Lopes, S. M., & Little, M. H. (2015). Kidney organoids from human iPS cells contain multiple lineages and model human nephrogenesis. *Nature*, *526*(7574), 564-568. https://doi.org/10.1038/nature15695

Talbi, K., Cabrita, I., Kraus, A., Hofmann, S., Skoczynski, K., Kunzelmann, K., Buchholz, B., & Schreiber, R. (2021). The chloride channel CFTR is not required for cyst growth in an ADPKD mouse model. *FASEB J*, *35*(10), e21897. https://doi.org/10.1096/fj.202100843R

Tamargo, J., Caballero, R., Gomez, R., Valenzuela, C., & Delpon, E. (2004). Pharmacology of cardiac potassium channels. *Cardiovasc Res*, *62*(1), 9-33. https://doi.org/10.1016/j.cardiores.2003.12.026

Tamma, G., Di Mise, A., Ranieri, M., Geller, A., Tamma, R., Zallone, A., & Valenti, G. (2017). The V2 receptor antagonist tolvaptan raises cytosolic calcium and prevents AQP2 trafficking and function: an in vitro and in vivo assessment. *J Cell Mol Med*, *21*(9), 1767-1780. https://doi.org/10.1111/jcmm.13098

Tan, A. Y., Zhang, T., Michaeel, A., Blumenfeld, J., Liu, G., Zhang, W., Zhang, Z., Zhu, Y., Rennert, L., Martin, C., Xiang, J., Salvatore, S. P., Robinson, B. D., Kapur, S., Donahue, S., Bobb, W. O., & Rennert, H. (2018). Somatic Mutations in Renal Cyst Epithelium in Autosomal Dominant Polycystic Kidney Disease. *J Am Soc Nephrol*, *29*(8), 2139-2156. https://doi.org/10.1681/ASN.2017080878

Taub, M., Chuman, L., Saier, M. H., Jr., & Sato, G. (1979). Growth of Madin-Darby canine kidney epithelial cell (MDCK) line in hormone-supplemented, serum-free medium. *Proc Natl Acad Sci U S A*, *76*(7), 3338-3342. https://doi.org/10.1073/pnas.76.7.3338

Terryn, S., Ho, A., Beauwens, R., & Devuyst, O. (2011). Fluid transport and cystogenesis in autosomal dominant polycystic kidney disease. *Biochim Biophys Acta*, *1812*(10), 1314-1321. https://doi.org/10.1016/j.bbadis.2011.01.011

Tharp, D. L., Wamhoff, B. R., Turk, J. R., & Bowles, D. K. (2006). Upregulation of intermediate-conductance Ca2+-activated K+ channel (IKCa1) mediates phenotypic modulation of coronary smooth muscle. *Am J Physiol Heart Circ Physiol*, *291*(5), H2493-2503. https://doi.org/10.1152/ajpheart.01254.2005

Thivierge, C., Kurbegovic, A., Couillard, M., Guillaume, R., Cote, O., & Trudel, M. (2006). Overexpression of PKD1 causes polycystic kidney disease. *Mol Cell Biol*, *26*(4), 1538-1548. https://doi.org/10.1128/MCB.26.4.1538-1548.2006

Thompson, J., & Begenisich, T. (2009). Mechanistic details of BK channel inhibition by the intermediate conductance, Ca2+-activated K channel. *Channels (Austin)*, *3*(3), 194-204. https://doi.org/10.4161/chan.3.3.9043

Thomson, R. B., Mentone, S., Kim, R., Earle, K., Delpire, E., Somlo, S., & Aronson, P. S. (2003). Histopathological analysis of renal cystic epithelia in the Pkd2WS25/- mouse model of ADPKD. *Am J Physiol Renal Physiol*, *285*(5), F870-880. https://doi.org/10.1152/ajprenal.00153.2003

Tian, H., Feng, J., Li, J., Ho, T. V., Yuan, Y., Liu, Y., Brindopke, F., Figueiredo, J. C., Magee, W., 3rd, Sanchez-Lara, P. A., & Chai, Y. (2017). Intraflagellar transport 88 (IFT88) is crucial for craniofacial development in mice and is a candidate gene for human cleft lip and palate. *Hum Mol Genet*, *26*(5), 860-872. https://doi.org/10.1093/hmg/ddx002

Torres, J. A., Rezaei, M., Broderick, C., Lin, L., Wang, X., Hoppe, B., Cowley, B. D., Jr., Savica, V., Torres, V. E., Khan, S., Holmes, R. P., Mrug, M., & Weimbs, T. (2019). Crystal deposition triggers tubule dilation that accelerates cystogenesis in polycystic kidney disease. *J Clin Invest*, *129*(10), 4506-4522. https://doi.org/10.1172/JCI128503

Torres, V. E. (2004). Cyclic AMP, at the hub of the cystic cycle. *Kidney Int*, *66*(3), 1283-1285. https://doi.org/10.1111/j.1523-1755.2004.00945.x

Torres, V. E. (2005). Vasopressin antagonists in polycystic kidney disease. *Kidney Int*, *68*(5), 2405-2418. https://doi.org/10.1111/j.1523-1755.2005.00703.x

Torres, V. E., & Harris, P. C. (2009). Autosomal dominant polycystic kidney disease: the last 3 years. *Kidney Int*, *76*(2), 149-168. https://doi.org/10.1038/ki.2009.128

Torres, V. E., Harris, P. C., & Pirson, Y. (2007). Autosomal dominant polycystic kidney disease. *Lancet*, *369*(9569), 1287-1301. https://doi.org/10.1016/S0140-6736(07)60601-1

Torres, V. E., Higashihara, E., Devuyst, O., Chapman, A. B., Gansevoort, R. T., Grantham, J. J., Perrone, R. D., Ouyang, J., Blais, J. D., Czerwiec, F. S., & Investigators, T. T. (2016). Effect of Tolvaptan in Autosomal Dominant Polycystic Kidney Disease by CKD Stage: Results from the TEMPO 3:4 Trial. *Clin J Am Soc Nephrol*, *11*(5), 803-811. https://doi.org/10.2215/CJN.06300615

Torres, V. E., Wang, X., Qian, Q., Somlo, S., Harris, P. C., & Gattone, V. H., 2nd. (2004). Effective treatment of an orthologous model of autosomal dominant polycystic kidney disease. *Nat Med*, *10*(4), 363-364. https://doi.org/10.1038/nm1004

Tran, P. V., Haycraft, C. J., Besschetnova, T. Y., Turbe-Doan, A., Stottmann, R. W., Herron, B. J., Chesebro, A. L., Qiu, H., Scherz, P. J., Shah, J. V., Yoder, B. K., & Beier, D. R. (2008). THM1 negatively modulates mouse sonic hedgehog signal transduction and affects retrograde intraflagellar transport in cilia. *Nat Genet*, *40*(4), 403-410. https://doi.org/10.1038/ng.105

Trebak, M., & Kinet, J. P. (2019). Calcium signalling in T cells. *Nat Rev Immunol*, *19*(3), 154-169. https://doi.org/10.1038/s41577-018-0110-7

Trudel, M. (2015). c-Myc Signalling in the Genetic Mechanism of Polycystic Kidney Disease. In X. Li (Ed.), *Polycystic Kidney Disease*. https://doi.org/10.15586/codon.pkd.2015.ch10

Trudel, M., Barisoni, L., Lanoix, J., & D'Agati, V. (1998). Polycystic kidney disease in SBM transgenic mice: role of c-myc in disease induction and progression. *Am J Pathol*, *152*(1), 219-229. https://www.ncbi.nlm.nih.gov/pubmed/9422539

Trudel, M., Chretien, N., & D'Agati, V. (1994). Disappearance of polycystic kidney disease in revertant c-myc transgenic mice. *Mamm Genome*, *5*(3), 149-152. https://doi.org/10.1007/BF00352345

Trudel, M., D'Agati, V., & Costantini, F. (1991). C-myc as an inducer of polycystic kidney disease in transgenic mice. *Kidney Int*, *39*(4), 665-671. https://doi.org/10.1038/ki.1991.80

Trudel, M., Lanoix, J., Barisoni, L., Blouin, M. J., Desforges, M., L'Italien, C., & D'Agati, V. (1997). C-myc-induced apoptosis in polycystic kidney disease is Bcl-2 and p53 independent. *J Exp Med*, *186*(11), 1873-1884. https://doi.org/10.1084/jem.186.11.1873

Tubman, V. N., Mejia, P., Shmukler, B. E., Bei, A. K., Alper, S. L., Mitchell, J. R., Brugnara, C., & Duraisingh, M. T. (2016). The Clinically Tested Gardos Channel Inhibitor Senicapoc Exhibits Antimalarial Activity. *Antimicrob Agents Chemother*, *60*(1), 613-616. https://doi.org/10.1128/AAC.01668-15

University, A., Aarhus University, H., Odense University, H., Aalborg University, H., & Hvidovre University, H. (2021, April 24). *Senicapoc in COVID-19 Patients With Severe Respiratory Insufficiency*. https://ClinicalTrials.gov/show/NCT04594668

University of California, D. (2024, December). *Senicapoc in Alzheimer's Disease*. https://ClinicalTrials.gov/show/NCT04804241

Urrego, D., Tomczak, A. P., Zahed, F., Stuhmer, W., & Pardo, L. A. (2014). Potassium channels in cell cycle and cell proliferation. *Philos Trans R Soc Lond B Biol Sci*, *369*(1638), 20130094. https://doi.org/10.1098/rstb.2013.0094

Van Der Velden, J., Sum, G., Barker, D., Koumoundouros, E., Barcham, G., Wulff, H., Castle, N., Bradding, P., & Snibson, K. (2013). K(Ca)3.1 channel-blockade attenuates airway pathophysiology in a sheep model of chronic asthma. *PLoS One*, *8*(6), e66886. https://doi.org/10.1371/journal.pone.0066886

Vandorpe, D. H., Shmukler, B. E., Jiang, L., Lim, B., Maylie, J., Adelman, J. P., de Franceschi, L., Cappellini, M. D., Brugnara, C., & Alper, S. L. (1998). cDNA cloning and functional characterization of the mouse Ca2+-gated K+ channel, mIK1. Roles in regulatory volume decrease and erythroid differentiation. *J Biol Chem*, *273*(34), 21542-21553. https://doi.org/10.1074/jbc.273.34.21542

Veizis, E. I., Carlin, C. R., & Cotton, C. U. (2004). Decreased amiloride-sensitive Na+ absorption in collecting duct principal cells isolated from BPK ARPKD mice. *Am J Physiol Renal Physiol*, *286*(2), F244-254. https://doi.org/10.1152/ajprenal.00169.2003

Verani, R. R., & Silva, F. G. (1988). Histogenesis of the renal cysts in adult (autosomal dominant) polycystic kidney disease: a histochemical study. *Mod Pathol*, *1*(6), 457-463. https://www.ncbi.nlm.nih.gov/pubmed/3065782

Verghese, E., Zhuang, J., Saiti, D., Ricardo, S. D., & Deane, J. A. (2011). In vitro investigation of renal epithelial injury suggests that primary cilium length is regulated by hypoxia-inducible mechanisms. *Cell Biol Int*, *35*(9), 909-913. https://doi.org/10.1042/CBI20090154

Viau, A., Baaziz, M., Aka, A., Mazloum, M., Nguyen, C., Kuehn, E. W., Terzi, F., & Bienaime, F. (2020). Tubular STAT3 Limits Renal Inflammation in Autosomal Dominant Polycystic Kidney Disease. *J Am Soc Nephrol*, *31*(5), 1035-1049. https://doi.org/10.1681/ASN.2019090959

Viau, A., Bienaime, F., Lukas, K., Todkar, A. P., Knoll, M., Yakulov, T. A., Hofherr, A., Kretz, O., Helmstadter, M., Reichardt, W., Braeg, S., Aschman, T., Merkle, A., Pfeifer, D., Dumit, V. I., Gubler, M. C., Nitschke, R., Huber, T. B., Terzi, F., . . . Kuehn, E. W. (2018). Cilia-localized LKB1 regulates chemokine signaling, macrophage recruitment, and tissue homeostasis in the kidney. *EMBO J*, *37*(15). https://doi.org/10.15252/embj.201798615

Viau, A., Kotsis, F., Boehlke, C., Braeg, S., Klein, M., Nitschke, R., Walz, G., & Kuehn, E. W. (2020). Divergent function of polycystin 1 and polycystin 2 in cell size regulation. *Biochem Biophys Res Commun*, *521*(2), 290-295. https://doi.org/10.1016/j.bbrc.2019.10.074

Villa, C., & Combi, R. (2016). Potassium Channels and Human Epileptic Phenotypes: An Updated Overview. *Front Cell Neurosci*, *10*, 81. https://doi.org/10.3389/fncel.2016.00081

Vlad, A., Rohrs, S., Klein-Hitpass, L., & Muller, O. (2008). The first five years of the Wnt targetome. *Cell Signal*, *20*(5), 795-802. https://doi.org/10.1016/j.cellsig.2007.10.031

von Hahn, T., Thiele, I., Zingaro, L., Hamm, K., Garcia-Alzamora, M., Kottgen, M., Bleich, M., & Warth, R. (2001). Characterisation of the rat SK4/IK1 K(+) channel. *Cell Physiol Biochem*, *11*(4), 219-230. https://doi.org/10.1159/000051936

Vossler, M. R., Yao, H., York, R. D., Pan, M. G., Rim, C. S., & Stork, P. J. (1997). cAMP activates MAP kinase and Elk-1 through a B-Raf- and Rap1-dependent pathway. *Cell*, *89*(1), 73-82. https://doi.org/10.1016/s0092-8674(00)80184-1

Wallace, D. P. (2011). Cyclic AMP-mediated cyst expansion. *Biochim Biophys Acta*, *1812*(10), 1291-1300. https://doi.org/10.1016/j.bbadis.2010.11.005

Wallace, D. P., Hou, Y. P., Huang, Z. L., Nivens, E., Savinkova, L., Yamaguchi, T., & Bilgen, M. (2008). Tracking kidney volume in mice with polycystic kidney disease by magnetic resonance imaging. *Kidney Int*, *73*(6), 778-781. https://doi.org/10.1038/sj.ki.5002771

Wang, W., Jack, B. M., Wang, H. H., Kavanaugh, M. A., Maser, R. L., & Tran, P. V. (2021). Intraflagellar Transport Proteins as Regulators of Primary Cilia Length. *Front Cell Dev Biol*, *9*, 661350. https://doi.org/10.3389/fcell.2021.661350

Wang, W., Li, F., Sun, Y., Lei, L., Zhou, H., Lei, T., Xia, Y., Verkman, A. S., & Yang, B. (2015). Aquaporin-1 retards renal cyst development in polycystic kidney disease by inhibition of Wnt signaling. *FASEB J*, *29*(4), 1551-1563. https://doi.org/10.1096/fj.14-260828

Wang, W., Mei, C., Tang, B., Zhao, H., Xu, C., Li, Z., Shen, X., Fu, W., & Dai, B. (2006). Aberrant expression of SPARC and its impact on proliferation and apoptosis in ADPKD cyst-lining epithelia. *Nephrol Dial Transplant*, *21*(5), 1278-1288. https://doi.org/10.1093/ndt/gfk036

Wang, X., Gattone, V., 2nd, Harris, P. C., & Torres, V. E. (2005). Effectiveness of vasopressin V2 receptor antagonists OPC-31260 and OPC-41061 on polycystic kidney disease development in the PCK rat. *J Am Soc Nephrol*, *16*(4), 846-851. https://doi.org/10.1681/ASN.2004121090

Wang, X., Ward, C. J., Harris, P. C., & Torres, V. E. (2010). Cyclic nucleotide signaling in polycystic kidney disease. *Kidney Int*, *77*(2), 129-140. https://doi.org/10.1038/ki.2009.438

Wann, A. K., & Knight, M. M. (2012). Primary cilia elongation in response to interleukin-1 mediates the inflammatory response. *Cell Mol Life Sci*, *69*(17), 2967-2977. https://doi.org/10.1007/s00018-012-0980-y

Ward, C. J., Turley, H., Ong, A. C., Comley, M., Biddolph, S., Chetty, R., Ratcliffe, P. J., Gattner, K., & Harris, P. C. (1996). Polycystin, the polycystic kidney disease 1 protein, is expressed by epithelial cells in fetal, adult, and polycystic kidney. *Proc Natl Acad Sci U S A*, *93*(4), 1524-1528. https://doi.org/10.1073/pnas.93.4.1524

Watnick, T., He, N., Wang, K., Liang, Y., Parfrey, P., Hefferton, D., St George-Hyslop, P., Germino, G., & Pei, Y. (2000). Mutations of PKD1 in ADPKD2 cysts suggest a pathogenic effect of trans-heterozygous mutations. *Nat Genet*, *25*(2), 143-144. https://doi.org/10.1038/75981

Watnick, T. J., Torres, V. E., Gandolph, M. A., Qian, F., Onuchic, L. F., Klinger, K. W., Landes, G., & Germino, G. G. (1998). Somatic mutation in individual liver cysts supports a two-hit model of cystogenesis in autosomal dominant polycystic kidney disease. *Mol Cell*, *2*(2), 247-251. https://doi.org/10.1016/s1097-2765(00)80135-5

Wei, A. D., Gutman, G. A., Aldrich, R., Chandy, K. G., Grissmer, S., & Wulff, H. (2005). International Union of Pharmacology. LII. Nomenclature and molecular relationships of

calcium-activated potassium channels. *Pharmacol Rev*, *57*(4), 463-472. https://doi.org/10.1124/pr.57.4.9

Wei, W., Hackmann, K., Xu, H., Germino, G., & Qian, F. (2007). Characterization of cis-autoproteolysis of polycystin-1, the product of human polycystic kidney disease 1 gene. *J Biol Chem*, *282*(30), 21729-21737. https://doi.org/10.1074/jbc.M703218200

Wen, Y., Yan, H. R., Wang, B., & Liu, B. C. (2021). Macrophage Heterogeneity in Kidney Injury and Fibrosis. *Front Immunol*, *12*, 681748. https://doi.org/10.3389/fimmu.2021.681748

Wendt, M. K., Balanis, N., Carlin, C. R., & Schiemann, W. P. (2014). STAT3 and epithelial-mesenchymal transitions in carcinomas. *JAKSTAT*, *3*(1), e28975. https://doi.org/10.4161/jkst.28975

Weydert, C., Decuypere, J. P., De Smedt, H., Janssens, P., Vennekens, R., & Mekahli, D. (2019). Fundamental insights into autosomal dominant polycystic kidney disease from human-based cell models. *Pediatr Nephrol*, *34*(10), 1697-1715. https://doi.org/10.1007/s00467-018-4057-5

Whitby, D. J., & Ferguson, M. W. (1991). The extracellular matrix of lip wounds in fetal, neonatal and adult mice. *Development*, *112*(2), 651-668. https://doi.org/10.1242/dev.112.2.651

Wilkes, M., Madej, M. G., Kreuter, L., Rhinow, D., Heinz, V., De Sanctis, S., Ruppel, S., Richter, R. M., Joos, F., Grieben, M., Pike, A. C., Huiskonen, J. T., Carpenter, E. P., Kuhlbrandt, W., Witzgall, R., & Ziegler, C. (2017). Molecular insights into lipid-assisted Ca(2+) regulation of the TRP channel Polycystin-2. *Nat Struct Mol Biol*, *24*(2), 123-130. https://doi.org/10.1038/nsmb.3357

Wilson, J. L., Miranda, C. A., & Knepper, M. A. (2013). Vasopressin and the regulation of aquaporin-2. *Clin Exp Nephrol*, *17*(6), 751-764. https://doi.org/10.1007/s10157-013-0789-5

Wilson, P. D., Sherwood, A. C., Palla, K., Du, J., Watson, R., & Norman, J. T. (1991). Reversed polarity of Na(+) -K(+) -ATPase: mislocation to apical plasma membranes in polycystic kidney disease epithelia. *Am J Physiol*, *260*(3 Pt 2), F420-430. https://doi.org/10.1152/ajprenal.1991.260.3.F420

Wong, R., & Schlichter, L. C. (2014). PKA reduces the rat and human KCa3.1 current, CaM binding, and Ca2+ signaling, which requires Ser332/334 in the CaM-binding C terminus. *J Neurosci*, *34*(40), 13371-13383. https://doi.org/10.1523/JNEUROSCI.1008-14.2014

Woodward, O. M., Li, Y., Yu, S., Greenwell, P., Wodarczyk, C., Boletta, A., Guggino, W. B., & Qian, F. (2010). Identification of a polycystin-1 cleavage product, P100, that regulates store operated Ca entry through interactions with STIM1. *PLoS One*, *5*(8), e12305. https://doi.org/10.1371/journal.pone.0012305

Wu, G., D'Agati, V., Cai, Y., Markowitz, G., Park, J. H., Reynolds, D. M., Maeda, Y., Le, T. C., Hou, H., Jr., Kucherlapati, R., Edelmann, W., & Somlo, S. (1998). Somatic inactivation of Pkd2 results in polycystic kidney disease. *Cell*, *93*(2), 177-188. https://doi.org/10.1016/s0092-8674(00)81570-6

Wu, G., Tian, X., Nishimura, S., Markowitz, G. S., D'Agati, V., Park, J. H., Yao, L., Li, L., Geng, L., Zhao, H., Edelmann, W., & Somlo, S. (2002). Trans-heterozygous Pkd1 and Pkd2 mutations modify expression of polycystic kidney disease. *Hum Mol Genet*, *11*(16), 1845-1854. https://doi.org/10.1093/hmg/11.16.1845

Wu, H., Uchimura, K., Donnelly, E. L., Kirita, Y., Morris, S. A., & Humphreys, B. D. (2018). Comparative Analysis and Refinement of Human PSC-Derived Kidney Organoid Differentiation with Single-Cell Transcriptomics. *Cell Stem Cell*, *23*(6), 869-881 e868. https://doi.org/10.1016/j.stem.2018.10.010

Wulff, H., & Castle, N. A. (2010). Therapeutic potential of KCa3.1 blockers: recent advances and promising trends. *Expert Rev Clin Pharmacol*, *3*(3), 385-396. https://doi.org/10.1586/ecp.10.11

Wulff, H., Gutman, G. A., Cahalan, M. D., & Chandy, K. G. (2001). Delineation of the clotrimazole/TRAM-34 binding site on the intermediate conductance calcium-activated potassium channel, IKCa1. *J Biol Chem*, *276*(34), 32040-32045. https://doi.org/10.1074/jbc.M105231200

Wulff, H., Miller, M. J., Hansel, W., Grissmer, S., Cahalan, M. D., & Chandy, K. G. (2000). Design of a potent and selective inhibitor of the intermediate-conductance Ca2+-activated K+ channel, IKCa1: a potential immunosuppressant. *Proc Natl Acad Sci U S A*, *97*(14), 8151-8156. https://doi.org/10.1073/pnas.97.14.8151

Wulfmeyer, V. C., Auber, B., Haller, H., & Schmitt, R. (2019). Comparison of Different Selection Strategies for Tolvaptan Eligibility among Autosomal Dominant Polycystic Kidney Disease Patients. *Am J Nephrol*, *50*(4), 281-290. https://doi.org/10.1159/000502634

Xiao, Z., Zhang, S., Cao, L., Qiu, N., David, V., & Quarles, L. D. (2010). Conditional disruption of Pkd1 in osteoblasts results in osteopenia due to direct impairment of bone formation. *J Biol Chem*, *285*(2), 1177-1187. https://doi.org/10.1074/jbc.M109.050906

Xu, Y., Kuppe, C., Perales-Paton, J., Hayat, S., Kranz, J., Abdallah, A. T., Nagai, J., Li, Z., Peisker, F., Saritas, T., Halder, M., Menzel, S., Hoeft, K., Kenter, A., Kim, H., van Roeyen, C. R. C., Lehrke, M., Moellmann, J., Speer, T., . . . Kramann, R. (2022). Adult human kidney organoids originate from CD24(+) cells and represent an advanced model for adult polycystic kidney disease. *Nat Genet*, *54*(11), 1690-1701. https://doi.org/10.1038/s41588-022-01202-z

Yamaguchi, T., Hempson, S. J., Reif, G. A., Hedge, A. M., & Wallace, D. P. (2006). Calcium restores a normal proliferation phenotype in human polycystic kidney disease epithelial cells. *J Am Soc Nephrol*, *17*(1), 178-187. https://doi.org/10.1681/ASN.2005060645

Yamaguchi, T., Nagao, S., Kasahara, M., Takahashi, H., & Grantham, J. J. (1997). Renal accumulation and excretion of cyclic adenosine monophosphate in a murine model of slowly progressive polycystic kidney disease. *Am J Kidney Dis*, *30*(5), 703-709. https://doi.org/10.1016/s0272-6386(97)90496-0

Yamaguchi, T., Nagao, S., Wallace, D. P., Belibi, F. A., Cowley, B. D., Pelling, J. C., & Grantham, J. J. (2003). Cyclic AMP activates B-Raf and ERK in cyst epithelial cells from autosomal-dominant polycystic kidneys. *Kidney Int*, *63*(6), 1983-1994. https://doi.org/10.1046/j.1523-1755.2003.00023.x

Yamaguchi, T., Wallace, D. P., Magenheimer, B. S., Hempson, S. J., Grantham, J. J., & Calvet, J. P. (2004). Calcium restriction allows cAMP activation of the B-Raf/ERK pathway, switching cells to a cAMP-dependent growth-stimulated phenotype. *J Biol Chem*, *279*(39), 40419-40430. https://doi.org/10.1074/jbc.M405079200

Yanda, M. K., Cha, B., Cebotaru, C. V., & Cebotaru, L. (2019). Pharmacological reversal of renal cysts from secretion to absorption suggests a potential therapeutic strategy for

managing autosomal dominant polycystic kidney disease. *J Biol Chem*, *294*(45), 17090-17104. https://doi.org/10.1074/jbc.RA119.010320

Yang, B., Sonawane, N. D., Zhao, D., Somlo, S., & Verkman, A. S. (2008). Small-molecule CFTR inhibitors slow cyst growth in polycystic kidney disease. *J Am Soc Nephrol*, *19*(7), 1300-1310. https://doi.org/10.1681/ASN.2007070828

Yang, Y., & Ehrlich, B. E. (2016). Structural studies of the C-terminal tail of polycystin-2 (PC2) reveal insights into the mechanisms used for the functional regulation of PC2. *J Physiol*, *594*(15), 4141-4149. https://doi.org/10.1113/JP270933

Ye, M., Grant, M., Sharma, M., Elzinga, L., Swan, S., Torres, V. E., & Grantham, J. J. (1992). Cyst fluid from human autosomal dominant polycystic kidneys promotes cyst formation and expansion by renal epithelial cells in vitro. *J Am Soc Nephrol*, *3*(4), 984-994. https://doi.org/10.1681/ASN.V34984

Ye, M., & Grantham, J. J. (1993). The secretion of fluid by renal cysts from patients with autosomal dominant polycystic kidney disease. *N Engl J Med*, *329*(5), 310-313. https://doi.org/10.1056/NEJM199307293290503

Yoder, B. K. (2007). Role of primary cilia in the pathogenesis of polycystic kidney disease. *J Am Soc Nephrol*, *18*(5), 1381-1388. https://doi.org/10.1681/ASN.2006111215

Yoder, B. K., Hou, X., & Guay-Woodford, L. M. (2002). The polycystic kidney disease proteins, polycystin-1, polycystin-2, polaris, and cystin, are co-localized in renal cilia. *J Am Soc Nephrol*, *13*(10), 2508-2516. https://doi.org/10.1097/01.asn.0000029587.47950.25

Yu, S., Hackmann, K., Gao, J., He, X., Piontek, K., Garcia-Gonzalez, M. A., Menezes, L. F., Xu, H., Germino, G. G., Zuo, J., & Qian, F. (2007). Essential role of cleavage of Polycystin-1 at G protein-coupled receptor proteolytic site for kidney tubular structure. *Proc Natl Acad Sci U S A*, *104*(47), 18688-18693. https://doi.org/10.1073/pnas.0708217104

Yu, Y., Ulbrich, M. H., Li, M. H., Buraei, Z., Chen, X. Z., Ong, A. C., Tong, L., Isacoff, E. Y., & Yang, J. (2009). Structural and molecular basis of the assembly of the TRPP2/PKD1 complex. *Proc Natl Acad Sci U S A*, *106*(28), 11558-11563. https://doi.org/10.1073/pnas.0903684106

Yu, Z. H., Xu, J. R., Wang, Y. X., Xu, G. N., Xu, Z. P., Yang, K., Wu, D. Z., Cui, Y. Y., & Chen, H. Z. (2013). Targeted inhibition of KCa3.1 channel attenuates airway inflammation and remodeling in allergic asthma. *Am J Respir Cell Mol Biol*, *48*(6), 685-693. https://doi.org/10.1165/rcmb.2012-0236OC

Yuajit, C., Homvisasevongsa, S., Chatsudthipong, L., Soodvilai, S., Muanprasat, C., & Chatsudthipong, V. (2013). Steviol reduces MDCK Cyst formation and growth by inhibiting CFTR channel activity and promoting proteasome-mediated CFTR degradation. *PLoS One*, *8*(3), e58871. https://doi.org/10.1371/journal.pone.0058871

Yuajit, C., Muanprasat, C., Gallagher, A. R., Fedeles, S. V., Kittayaruksakul, S., Homvisasevongsa, S., Somlo, S., & Chatsudthipong, V. (2014). Steviol retards renal cyst growth through reduction of CFTR expression and inhibition of epithelial cell proliferation in a mouse model of polycystic kidney disease. *Biochem Pharmacol*, *88*(3), 412-421. https://doi.org/10.1016/j.bcp.2014.01.038

Zapata, R. C., Zhang, D., Chaudry, B., & Osborn, O. (2021). Self-Administration of Drugs in Mouse Models of Feeding and Obesity. *J Vis Exp*(172). https://doi.org/10.3791/62775

Zhang, H., Yan, W., Sun, Y., Yuan, H., Su, L., Cao, X., Wang, P., Xu, Z., Hu, Y., Wang, Z., Wang, Y., Fu, K., Sun, Y., Chen, Y., Cheng, J., & Guo, D. (2022). Long Residence Time at the

Vasopressin V(2) Receptor Translates into Superior Inhibitory Effects in Ex Vivo and In Vivo Models of Autosomal Dominant Polycystic Kidney Disease. *J Med Chem*, *65*(11), 7717-7728. https://doi.org/10.1021/acs.jmedchem.2c00011

Zhang, Y., Dai, Y., Raman, A., Daniel, E., Metcalf, J., Reif, G., Pierucci-Alves, F., & Wallace, D. P. (2020). Overexpression of TGF-beta1 induces renal fibrosis and accelerates the decline in kidney function in polycystic kidney disease. *Am J Physiol Renal Physiol*, *319*(6), F1135-F1148. https://doi.org/10.1152/ajprenal.00366.2020

Zhao, C., Wang, Q., Wang, B., Sun, Q., He, Z., Hong, J., Kuehn, F., Liu, E., & Zhang, Z. (2017). IGF-1 induces the epithelial-mesenchymal transition via Stat5 in hepatocellular carcinoma. *Oncotarget*, *8*(67), 111922-111930. https://doi.org/10.18632/oncotarget.22952

Zheleznova, N. N., Wilson, P. D., & Staruschenko, A. (2011). Epidermal growth factor-mediated proliferation and sodium transport in normal and PKD epithelial cells. *Biochim Biophys Acta*, *1812*(10), 1301-1313. https://doi.org/10.1016/j.bbadis.2010.10.004

Zheng, R., Zhang, Z., Lv, X., Fan, J., Chen, Y., Wang, Y., Tan, R., Liu, Y., & Zhou, Q. (2008). Polycystin-1 induced apoptosis and cell cycle arrest in G0/G1 phase in cancer cells. *Cell Biol Int*, *32*(4), 427-435. https://doi.org/10.1016/j.cellbi.2007.12.014

Zhu, Y., Teng, T., Wang, H., Guo, H., Du, L., Yang, B., Yin, X., & Sun, Y. (2018). Quercetin inhibits renal cyst growth in vitro and via parenteral injection in a polycystic kidney disease mouse model. *Food Funct*, *9*(1), 389-396. https://doi.org/10.1039/c7fo01253e

Zimmerman, K. A., Song, C. J., Li, Z., Lever, J. M., Crossman, D. K., Rains, A., Aloria, E. J., Gonzalez, N. M., Bassler, J. R., Zhou, J., Crowley, M. R., Revell, D. Z., Yan, Z., Shan, D., Benveniste, E. N., George, J. F., Mrug, M., & Yoder, B. K. (2019). Tissue-Resident Macrophages Promote Renal Cystic Disease. *J Am Soc Nephrol*, *30*(10), 1841-1856. https://doi.org/10.1681/ASN.2018080810

Zittema, D., Boertien, W. E., van Beek, A. P., Dullaart, R. P., Franssen, C. F., de Jong, P. E., Meijer, E., & Gansevoort, R. T. (2012). Vasopressin, copeptin, and renal concentrating capacity in patients with autosomal dominant polycystic kidney disease without renal impairment. *Clin J Am Soc Nephrol*, *7*(6), 906-913. https://doi.org/10.2215/CJN.11311111

APPENDIX

Fig. 2 End stage human autosomal polycystic kidneys are significantly enlarged compared to healthy human kidneys
Permission obtained on May 2, 2023 by RightsLink for Springer Nature
License: 5540880198296

Fig. 3 Schematic representation of structural domains in polycystin-1 and polycystin-2
Permission obtained on May 2, 2023 by RightsLink for Elsevier
License: 5540830406976

Fig. 4 Schematic representation of cyst initiation and progression in PKD
Permission obtained on October 4, 2023 by RightsLink for Elsevier
License: 5642120601830

Fig. 5 Schematic representation of ENaC localization and function in epithelial cells
Permission obtained on October 7, 2023 by RightsLink for Elsevier
License: 5643750976356

Fig. 6 Schematic representation of disrupted calcium and cAMP signaling in PKD
Permission obtained on October 7, 2023 by RightsLink for Elsevier
License: 5643820327341

Fig. 7 Schematic representation of MAPK/ERK signaling-mediated proliferation in NHK versus PKD cells
Permission obtained on October 7, 2023 by RightsLink for Wolters Kluwer Health, Inc.
License: 5643890338264